

# **Physiological underpinnings of healthy brain ageing**

by

Jodi Karlyn Watt, MSc, BSc



**University of  
Nottingham**  
UK | CHINA | MALAYSIA

Thesis submitted to The University of Nottingham for  
the degree of Doctor of Philosophy

September 2021

# Abstract

Changes in cerebral perfusion or metabolism can occur as a result of healthy ageing, and in conditions of impaired ageing such as mild cognitive impairment (MCI) or Alzheimer's disease (AD). Overarchingly, this thesis aimed to explore physiological magnetic resonance imaging (MRI) measures to study both cerebral perfusion and metabolism in the healthy ageing brain. Specifically, arterial spin labelling (ASL) and functional magnetic resonance spectroscopy ( $^1\text{H}$ -fMRS) were employed in the elucidation of healthy ageing.

Investigation of cerebral functionality is clinically important, enabling understanding of healthy ageing and disease pathology beyond that provided by structural measures. Given the necessity for tightly-regulated tissue perfusion in the delivery of oxygen to the brain, assessment of brain perfusion can enable elucidation of related brain health. Firstly, this thesis focused on changes in brain perfusion within a cross-sectional retrospective cohort of healthy subjects. This study aimed to assess the utility of univariate and multivariate pattern analysis (MVPA) techniques, and determine whether spatial coefficient of variation (sCoV) measures – which provide a method for inferring spatial heterogeneity of blood flow from single post-label delay (PLD) ASL data – are more significantly associated with age than standard perfusion metrics (ml/100g/min values). The impact of data processing steps on quantification of perfusion was initially assessed. Particularly, the influence of partial volume effect (PVE) correction and how this affected quantification of cerebral perfusion was of interest. The relationship between measures of cerebral perfusion – in regions of interest, vascular territories, and grey matter

– and age were assessed, before grey matter (GM) spatial covariance patterns were identified, with MVPA hypothesised to elucidate more subtle age-related change than univariate, voxel-wise methodology. The executive control network (ECN) was the only network exhibiting a significant decline in perfusion with age, after controlling for relevant covariates. Interestingly, whilst the PCA approach resulted in a pattern of both positive and negative associations with age across cerebral GM, the surviving clusters in voxel-wise approaches were deemed spurious. Five-fold cross validation of PCA findings was used to assess whether the resultant spatial covariance patterns were able to predict subject age. This prediction was successful, with related  $r^2$  values of between 0.5316 and 0.7297 ( $p < 0.001$  for all), however validation of these findings in an unseen dataset is required. The utility of the sCoV metric was also compared with standard tissue perfusion values, finding that sCoV may be more closely associated with ageing than ml/100g/min in certain regions. Particularly, a significant increase in whole GM sCoV with age was notable, given the absence of significant changes in perfusion with age in the same region.

Additionally, a MVPA approach was used to establish the complex unknown relationship between cerebral perfusion and the Montreal Cognitive Assessment (MoCA), before graph visualisation was used to further understand the regional relatedness of the spatial covariance pattern. PCA resulted in a model which provided a moderate explanation of the aforementioned relationship, but this may be improved by inclusion of additional covariates in subsequent work, such as those pertaining to genetic status, such as apolipoprotein E (APOE). This study also replicates an FDG-

PET cognitive resilience signature in an ASL cohort for the first time, with a trend towards declining perfusion with age found ( $p = .08$ ).

Lastly, as ageing is associated with metabolic failure in the brain, which is often investigated using methodology which employs ionising radiation, the final study was motivated to investigate possible metabolic markers of brain ageing which can be measured using MRI. Metabolic-functional coupling can be studied using functional stimulation, and functional magnetic resonance spectroscopy (fMRS) is perfectly poised to elucidate certain metabolic behaviour. Given the close relationship between glucose (Glc) – the key fuel for cerebral functionality – and lactate (Lac) metabolism, an optimised long echo time (TE) semi-localized by adiabatic selective refocusing (semi-LASER) sequence (TE=144ms) with optimised J-modulation selection at 7T was employed to assess the effects of age on the dynamic behaviour of Lac, and determine its absolute concentrations throughout the time course, whilst a visual stimulation paradigm was viewed. Successful quantification of metabolite concentrations – including Lac, tCr and tNAA – was achieved in both the young and old cohorts, and their Lac peaks clearly visually identifiable throughout the time course. A significant increase in Lac concentration was observed between rest and stimulation, but not stimulation and recovery, in the young cohort. No significant Lac time course changes were identified in the full old cohort.

This thesis concluded by summarising and contextualising the key findings herein, and discussion of possible directions for further associated research. The findings of this thesis broaden the field of knowledge around healthy

ageing, and therefore may contribute to subsequent translation efforts for both clinical diagnostics and treatment approaches.

**Keywords:** ageing, brain metabolism, cerebral perfusion, arterial spin labelling, multivariate pattern analysis, Montreal Cognitive Assessment, spatial coefficient of variation, magnetic resonance spectroscopy, lactate, visual stimulation

## Personal acknowledgements

Firstly, I would like to thank my supervisors, Professors Dorothee Auer and Peter Morris, and Drs Bernard Lanz and Sébastien Serres for your continuous support and encouragement. Working with you all has been incredibly rewarding, and I feel lucky to have experienced this PhD with your guidance. An important thank you too to all of the individuals who volunteered their time to have their brains scanned for this thesis – you have made an invaluable contribution to these studies, and I cannot thank you enough.

There are a large number of people who have helped me to feel at home in Nottingham over these past five years. Particularly everyone within Radiological Sciences and SPMIC-UP, without whom this experience would have not been nearly as great. Special thanks also to Will, Stefan and Chris, I will be forever grateful for your endless patience within my “stupid” questions, and your continued belief in my ability to finish this thing; and to Sarah Wilson, for her professional support, a listening ear when I needed to vent, and a shoulder to cry on when things got too much. And thank you too to Henry, who has had incredible patience with my incessant requests for printouts of my drafts.

It has been a highlight of my PhD to be asked to join the Equity, Diversity and Inclusion Task Force of ISMRM, through which I have worked with some amazing people. Regular meetings with Nikou Damestani and Dr Hamied Haroon fast became the highlight of my month during the write-up period, and

I will forever be indebted to Professor Karla Miller for her kindness, advice and belief in me.

Over my time at Nottingham, my life changed in ways I could never have anticipated, and I was met with bigger challenges than I have ever faced before. I owe huge gratitude to many friends, both old and new, for helping me through this period, but I would also like to explicitly thank a few more people, without whom this thesis would genuinely have never been completed. Sarah Wilson, Cheryl Ruse, Lynda Pycroft, Becky Palfrey, Jenna Bird, Sheetal Gosai and Dr Tiffany Hamilton have all provided invaluable support in navigating the complex extenuating circumstances that have arisen during my PhD. I would also like to thank my counsellor Adrienne, and the NHS, for bringing her into my life. Without our regular meetings, and your assurance that I was indeed making progress, I don't think I could have believed in myself. Thank you too, for your assurance that it was not only okay, but important to talk about mental health in academia, and that I was not alone in my feelings. Additional thanks are also owed to Thea, for being an absolute joy and one of the most beautiful souls I have ever met, and to Matt and his unwavering belief in me, which has existed since long before I even started on this PhD journey.

A special thank you to Andrew, who has gone from my mortal enemy, to best friend, to partner in global pandemic and in life. You are unlike anyone else I have ever met, and your love, support, and general nonsense over these past few years has kept me here and kept me sane. I'm also incredibly grateful for your restraint to not brag about how you finished your PhD first, and your well-timed anniversary gift of Hamish, a little furball of nonsense who has been

very good at confirming that a PhD isn't everything, sometimes relentlessly playing with the same pompoms for hours on end is more important.

Finally, to my family, both through blood and through choice. To Taylor, Hunter, Momma West and Mr John, thank you for your Southern hospitality, and for letting me add Chippewa Square, Jacksonville International Airport and Domino Park in Calle Ocho to the unusual list of places where I have had breakthroughs on my thesis. And to my mum, Fiona, and brother Finlay, I am eternally grateful for the love, support and enthusiasm you have always shown throughout my education, and for helping me through this final push, I could never have done it without you. I also want to thank my dad, George, who died in the third year of my PhD. Even in your death, you've probably managed to do more for science than I ever will, and you inspire me to be a better person every single day. I finished this for you.

***For anyone who might be reading through my thesis as they write up their own, I want to leave a list of mental health resources which may be able to help you as they helped me, if needed. You're not alone, and you can do this:***

- [www.giveusashout.org](http://www.giveusashout.org) (or text 85258 for 24 hour support)
- <https://www.nhs.uk/service-search/mental-health/find-an-urgent-mental-health-helpline>
- [www.mind.org.uk](http://www.mind.org.uk)
- [www.mentalhealth.org.uk](http://www.mentalhealth.org.uk)
- [www.samaritans.org](http://www.samaritans.org)
- The reddit site **r/MentalHealthUK** is incredibly supportive and has a constantly-updated list of resources.

***Or if you're just bored of the daily monotony of consistently writing and need some podcasts to listen to in the background, here are some that got me through my PhD:***

- Off Menu (James Acaster and Ed Gamble)
- James Acaster's Perfect Sounds
- The Taskmaster Podcast (Ed Gamble, previous contestants)
- My Dad Wrote a Porno (Alice Levine, Jamie Morton, James Cooper)
- Ologies (Alie Ward)
- No Such Thing as a Fish (The QI Elves)
- Drunk Women Solving Crime

**Good luck!**

## Study acknowledgements

During my PhD, I have been affiliated with Radiological Sciences in the Division of Clinical Neuroscience, and the Sir Peter Mansfield Imaging Centre (SPMIC), both part of the University of Nottingham. Funding for this PhD was predominantly provided by Life Cycle 5, the dementia/cognitive ageing-focused fifth iteration of Nottingham Life Cycle, a fundraising initiative at the University of Nottingham which has raised over £2.6 million for an array of life-changing research focuses since 2011 through sponsored cycles (<https://www.nottingham.ac.uk/impactcampaign/get-involved/lc/index.aspx/>).

Additional funding was provided by the University of Nottingham, School of Medicine. I would like to thank both Life Cycle 5 and the University of Nottingham for supporting me through this PhD, and enabling me to study and learn in such thought-provoking environments.

Chapter 4 also used data from the Alzheimer's Disease Neuroimaging Initiative. Data collection and sharing for this project was funded by the Alzheimer's Disease Neuroimaging Initiative (ADNI) (National Institutes of Health Grant U01 AG024904) and DOD ADNI (Department of Defense award number W81XWH-12-2-0012). ADNI is funded by the National Institute on Aging, the National Institute of Biomedical Imaging and Bioengineering, and through generous contributions from the following: AbbVie, Alzheimer's Association; Alzheimer's Drug Discovery Foundation; Araclon Biotech; BioClinica, Inc.; Biogen; Bristol-Myers Squibb Company; CereSpir, Inc.; Cogstate; Eisai Inc.; Elan Pharmaceuticals, Inc.; Eli Lilly and Company; EuroImmun; F. Hoffmann-La Roche Ltd and its affiliated company Genentech, Inc.; Fujirebio; GE Healthcare; IXICO Ltd.; Janssen Alzheimer Immunotherapy Research & Development, LLC.; Johnson & Johnson Pharmaceutical Research & Development LLC.; Lumosity; Lundbeck; Merck & Co., Inc.; Meso Scale Diagnostics, LLC.; NeuroRx Research; Neurotrack Technologies; Novartis Pharmaceuticals Corporation; Pfizer Inc.; Piramal Imaging; Servier; Takeda Pharmaceutical Company; and Transition Therapeutics. The Canadian Institutes of Health Research is providing funds to support ADNI clinical sites in Canada. Private sector contributions are facilitated by the Foundation for the National Institutes of Health ([www.fnih.org](http://www.fnih.org)). The grantee organization is the Northern California Institute for Research and Education, and the study is coordinated by the Alzheimer's Therapeutic Research Institute at the University of Southern California. ADNI data are disseminated by the Laboratory for Neuro Imaging at the University of Southern California.

Figures 2.5.5. and 2.5.6. in Chapter 2 contain a spectrum which was acquired and kindly provided by Dr Adam Berrington. Regarding the retrospective data

used in Chapters 3 and 4, explicit acknowledgement is due to the many individuals involved in the original studies. For PaMIR, Drs Yue Xing, Saadnah Naidu, Christopher Tench, Jonathan Evans, Gillian Sare, and Stefan Schwarz, alongside Mr Halim Abdul-Sapuan and Professor Dorothee Auer, are the main investigators. Mr Andrew Cooper and Dr Jan Alappadan Paul were responsible for scanning at the Nottingham site, with Dr Dewen Meng, Clair Mace, Jenny Wright, Maxine Kavanagh, Sarah Wilson, Andrea Junor and Linda Pycroft responsible for recruitment and administration. Thank you also to the research nurses and research coordinators in the Derby team - Kathleen Holding, Kay Hunt and Kathryn Walker.

ImPOA has been previously published (without MoCA data; Alshuft et al., 2016; Reckziegel et al., 2016; Cottam et al., 2016; Cottam et al., 2018). Key team members who contributed to this work were Drs William Cottam, Laura Condon, Hamza Alshuft, Diane Reckziegel, and Professor Dorothee Auer, with Dr Hamza Alshuft responsible for much of the work associated with the MoCA assessment. For INCOPE, the core study group included Drs William Cottam, Sarina Iwabuchi, and Marianne Drabek, as well as Dr Arman Tadjibaev and Professor Dorothee Auer. Recruitment for both ImPOA and INCOPE involved a wider team, including David Walsh, Ana Valdes, Michael Doherty, Weiya Zhang, Gwen Fernandes, Nadia Frowd, Bonnie Millar and Sarah Wilson. Mr Andrew Cooper was also involved in much of the scanning. For GSH-MRS, I was responsible for scanning alongside Mr Andrew Cooper and Dr Ben Babourina-Brooks. Sarah Wilson also provided support for subject recruitment. The main investigators for VeSPA-MS and BraNDy-MS were Dr Afaf Elsarraj, Dr Thomas Welton, Professor Rob Dineen, and Professor Cris Constantinescu.

Regarding the principal component analysis work (presented in Chapters 3 and 4) within this thesis, I would like to explicitly acknowledge the work of Drs Stefan Pszczolkowski and Yue Xing for the creation and modification of the MATLAB scripts used in this analysis. Additionally, Dr Christopher Tench helped with key theoretical implementations within these scripts. Dr Stefan Pszczolkowski also provided shell scripts which enabled data registration to MNI space. Thank you too to Dr Flora Kennedy McConnell, with whom I had many interesting discussions about arterial spin labelling and partial volume correction.

Dr Denis Schluppeck provided visual stimulation for the work in Chapter 5. Drs Adam Berrington and Jyothika Kumar also made theoretical contributions to the calculation of metabolite concentrations in Chapter 5. Throughout this thesis, Dr Christopher Tench and Dr Andrea Venn have also provided invaluable advice and thought-provoking discussion on relevant statistical approaches. Andrew Cooper and Dr Andrew Peters also provided technical support throughout this PhD.

## List of accepted conference abstracts

1. **Watt JK**, Psczolkowski S, Xing Y, Tench CR, Auer DP and the Alzheimer's Disease Neuroimaging Initiative. *Cerebral perfusion network analysis to understand cognition in old age: a principal component analysis of ASL-MRI*. ISMRM 29th Annual Meeting and Exhibition (Abstract 1302, Virtual. May 2021).
2. **Watt JK**, Berrington A, Kumar J, Auer DP and Morris PG. *Functional <sup>1</sup>H-MRS of cerebral lactate concentration changes during prolonged visual stimulation in young and old individuals*. British and Irish and Iberian Chapters of ISMRM, Postgraduate Meeting (Virtual. April 2021).
3. **Watt JK**, Babourina-Brooks B, Raschke F, Dineen R and Auer DP. *Feasibility of regional glutathione measurement in healthy older individuals using <sup>1</sup>H MEGA-PRESS MRS*. MRS Workshop on Metabolic Imaging (Utrecht, the Netherlands. October 2018).
4. **Watt JK**, Babourina-Brooks B, Raschke F, Dineen R and Auer DP. *Feasibility of regional glutathione measurement in healthy older individuals using <sup>1</sup>H MEGA-PRESS MRS*. British Chapter of ISMRM (Oxford, UK. September 2018).
5. **Watt JK**, Serres S, Morris PG and Auer DP. *Understanding metabolic failure in dementia*. East Midlands Doctoral Network Postgraduate

Research Conference (Nottingham, UK. September 2017) [Winner of Best Poster award].

# List of Tables

## CHAPTER 1

- 1.1.1. Summary characteristics of imaging modalities which can assess brain health.

## CHAPTER 2

- 2.5.1. Key metabolites detectable using  $^1\text{H-MRS}$ .

## CHAPTER 3

- 3.1.1. Summary of key voxel-wise studies which assess the relationship between healthy ageing and physiological brain changes.
- 3.3.1. Summary of differences in male and female GM perfusion values by merit of smoothing and PVE-correction.
- 3.3.2. Summary of the quantitative assessment of various GM masks, carried out on 94 PVE-corrected and smoothed cerebral perfusion maps.
- 3.5.1. P-values resulting from linear regressions assessing the relationship between age and cerebral perfusion within the GM.
- 3.5.2. P-values resulting from linear regressions assessing the relationship between age and perfusion within the whole GM by merit of PLD.
- 3.5.3. P-values resulting from linear regressions assessing the relationship between age and perfusion in various networks of interest.
- 3.6.1. Variance in age explained by each surviving component.
- 3.6.2. Summary demographics for PCA and validation cohorts used for five-fold validation.
- 3.7.1. P-values resulting from linear regressions assessing the relationship between age and sCoV within the GM.
- 3.7.2. P-values resulting from linear regressions assessing the relationship between age and sCoV within the whole GM by merit of PLD.
- 3.7.3. P-values resulting from linear regressions assessing the relationship between age and sCoV in networks of interest.
- 3.8.1. P-values resulting from linear regressions assessing the relationship between age and perfusion in various vascular territories.
- 3.8.2. P-values resulting from linear regressions assessing the relationship between age and sCoV in various vascular territories.

## **CHAPTER 4**

- 4.2.1. Summary of datasets considered for inclusion within this current study, the available data within each, and the rationale for subsequent inclusion or exclusion.
- 4.4.1. Summary demographics of the study cohort.
- 4.4.2. Key clusters identified within the PCA-derived spatial covariance pattern.
- 4.4.3. Unadjusted regional mean perfusion values in regions of interest within the full cohort.
- 4.4.4. Unadjusted regional 90th percentile mean perfusion values in regions of interest within the full cohort.
- 4.4.5. Summary of the results of linear regressions assessing the relationship between MoCA scores and mean cerebral blood flow in specific a-priori-defined regions, controlling for age, sex and GM volume.
- 4.4.6. Summary of the results of linear regressions assessing the relationship between MoCA scores and 90th percentile mean cerebral blood flow in specific a-priori-defined regions, controlling for age, sex and GM volume.
- 4.4.7. Summary of unadjusted mean perfusion values in selected networks.
- 4.4.8. Summary of the results of linear regressions assessing the relationship between MoCA scores and cerebral blood flow in specific a-priori-defined cognitive networks, when age, sex, and GM volume are included as additional covariates.
- 4.4.9. Demographics of female subjects with a MoCA score of 29.

## **CHAPTER 5**

- 5.1.1. Key papers which quantify “absolute” concentrations of lactate.
- 5.4.1. Summary of information used for calculation of saturation factors.
- 5.4.2. Summary of key values in the averaged spectra.
- 5.4.3. Summary of the tissue composition in spectroscopic voxels.
- 5.4.4. Summary of Lac concentrations in the averaged spectra, using various concentration calculation approaches.

# List of Figures

## CHAPTER 1

- 1.1.1. Summary diagram of key factors pertaining to healthy ageing.
- 1.1.2. Summary of brain ageing hallmarks.
- 1.1.3. Simplified summary of factors which cumulatively contribute to the signs and symptoms of healthy brain ageing, or neurodegenerative disease.
- 1.1.4. Schematic of the healthy ageing - mild cognitive impairment - AD continuum.
- 1.1.5. Temporal and spatial resolution of key imaging modalities.

## CHAPTER 2

- 2.1.1. Depiction of magnetic moments in (a) the absence of a magnetic field ( $B_0$ ) where they align in various directions, and (b) the presence of a magnetic field ( $B_0$ ) which causes the magnetic moments to align either parallel or anti-parallel.
- 2.1.2. Precession of a spin,  $\mu$ , about the z-axis inside a magnetic field.
- 2.1.3. Evolution of net magnetisation ( $M$ ) after  $B_1$  field application, in the (a) laboratory frame, and (b) rotating frame of reference.
- 2.2.1. Summary of the process of  $T_1$  relaxation.
- 2.2.2. The process of  $T_2$  relaxation.
- 2.2.3. The process of free induction decay.
- 2.3.1. The resonance frequencies of a given sample are altered by the magnetic field gradient  $G_z$ .
- 2.3.2. Summary of frequency and phase encoding.
- 2.3.3. Depiction of sagittal, axial and coronal imaging planes.
- 2.5.1. Summary schematic of certain blood vessel properties and how these change throughout the vasculature.
- 2.5.2. Generic schematic of the labelling process used for arterial spin labelling of the brain.

- 2.5.3. Summary of the differences in labelling strategies for CASL, PASL and PCASL.
- 2.5.4. Summary figure depicting (a) the free induction decay, with the red curve depicting the  $T_2^*$  envelope, and (b) and (c), real and imaginary components of the complex free induction decay signal, which have been Fourier Transformed.
- 2.5.5. Example spectrum acquired at 7T using a STEAM sequence in the posterior cingulate cortex, with TE = 14ms.
- 2.5.6. Schematic depicting the relationship between the Lac doublet (at 1.31ppm) and quartet (at 4.1ppm).
- 2.5.7. PRESS sequence pulse diagram.
- 2.5.8. Semi-LASER sequence pulse diagram.
- 2.5.9. Evolution of magnetisation into a steady state when using a  $90^\circ$  pulse.

### CHAPTER 3

- 3.1.1. Age-related changes in relative CBF in all participants from regression analysis in Zhang et al. (2018).
- 3.1.2. The network of CBF changes with aging identified by SSM/PCA from 50 healthy subjects, in Zhang et al. (2018).
- 3.3.1. Summary of the quality control, registration, preprocessing and analysis steps carried out within the current study.
- 3.3.2. Summary of registration and processing steps carried out within the present study.
- 3.3.3. Example axial slices of PVE-corrected and smoothed cerebral perfusion maps overlaid on a 2mm MNI template from (a) a 63 year-old male, (b) 78 year-old male, and (c) 67 year-old female, respectively.
- 3.3.4. Pearson's correlation coefficients between ASL-derived perfusion maps and an MNI GM probability map were calculated as an alternative to relying on visual assessment to assess registration quality. This was carried out for each subject within the full cohort, using two different registration approaches — MIRTk and SyN.
- 3.3.5. Example fit of the perfusion map of a 77 year-old male to a 2mm MNI template, using MIRTk and SyN for registration.
- 3.3.6. Selected GM mask, thresholded to exclude  $\leq 20\%$  GM, and  $\geq 30\%$  CSF, overlaid on the 2mm MNI152 template.

- 3.3.7. Cortical (red) and subcortical (yellow) masks overlaid on the MNI152 2mm template, and masked to the selected GM mask.
- 3.3.8. Summary of subject selection within ImPOA, PAMIR, GSH-MRS, INCOPE, BraNDy-MS and VeSPA-MS cohorts.
- 3.5.1. Key cohort results pertaining to age and whole, cortical and subcortical GM perfusion.
- 3.5.2. Comparison of perfusion measures in whole GM in (A) subjects with a PLD of 1525ms, and (B) subjects with a PLD of 2025ms.
- 3.5.3. Summary perfusion values in key networks.
- 3.6.1. Example GLM, with sex and GM volume as covariates, created using GLM Setup within FSL.
- 3.6.2. Depiction of the computation of principal components in the process of PCA, using normally-distributed dummy data.
- 3.6.3. Schematic of the assignment of subjects for five-fold cross-validation.
- 3.6.4. Significant positive cluster found after FSL-randomise analysis, using 5000 permutations, FWE-correction and TFCE, with sex and GM as covariates, overlaid on MNI152 2mm brain template.
- 3.6.5. Significant positive cluster found after FSL-randomise analysis, using 5000 permutations, FWE-correction and TFCE, with only sex as a covariate, overlaid on MNI152 2mm brain template.
- 3.6.6. The age-associated perfusion covariance pattern resulting from the combined surviving components (1-28) in the full cohort, overlaid on the MNI152 template with 2mm resolution.
- 3.6.7. The top five components (1-5) from the PCA-derived pattern of perfusion covariance, overlaid on the MNI152 2mm templated.
- 3.6.8. Results of the linear regressions carried out in the five-fold cross-validation analysis within validation cohorts (A) 1, (B) 2, (C) 3, (D) 4, and (E) 5, respectively.
- 3.6.9. Spatial covariance patterns in each of the five-fold validation cohorts (1-5), overlaid on the MNI152 2mm template.
- 3.6.10. The pattern resulting from PCA analysis within the male subcohort (n=36), comprising all surviving components.
- 3.6.11. The pattern resulting from PCA analysis within the female subcohort (n=58), comprising all surviving components.
- 3.7.1. GM perfusion maps in subjects with varying whole GM sCoV values.

- 3.7.2. Comparison of sCoV in whole GM in (A) subjects with a PLD of 1525ms, and (B) subjects with a PLD of 2025ms.
- 3.8.1. Schematic of the inferior surface of the brain, depicting key blood vessels and their position within the cerebrovasculature.
- 3.8.2. Selected vascular territory masks based on the Donahue Laboratory atlas, overlaid on an MNI152 2mm brain template.
- 3.8.3. Masks of vascular territories provided by Mutsaerts et al. (2015), overlaid on an MNI152 2mm brain template.
- 3.8.4. Summary of vascular territory perfusion values within the LICA, RICA, VBA, and left and right watershed regions of the brain.
- 3.8.5. Linear regressions between age and perfusion values (ml/100g/min) in (a) LICA, (b) RICA, (c) VBA, (d) the left watershed region and (e) the right watershed region.
- 3.8.6. Linear regressions between age and sCoV values (%) in (a) LICA, (b) RICA, (c) VBA, (d) the left watershed region and (e) the right watershed region.

## **CHAPTER 4**

- 4.2.1. Summary of key study steps, from conception to completion.
- 4.2.2. Summary of the process of subject selection within ADNI-3, ImPOA and PaMIR carried out in December 2019.
- 4.3.1. Mask of the resilience signature (based on Arenaza-Urquijo et al., 2019), comprising the bilateral ACC and anterior temporal pole, overlaid on the 2mm MNI template.
- 4.4.1. Summary of the spread of biological covariates within the healthy cohort used for PCA-ASL analysis.
- 4.4.2. Unthresholded combined surviving components (1, 4 and 42) for all 49 subjects, overlaid on the MNI152 template with 2mm resolution.
- 4.4.3. Investigation of voxel retention with decreasing  $r^2$ , from 100% - 5% of  $r^2$  retained.
- 4.4.4. Change in (a)  $r^2$  of the model and (b) voxel retention, by merit of threshold selection.
- 4.4.5. Combined surviving components (1, 4 and 42) for all 49 subjects, thresholded at 98%  $r^2$  retention and overlaid on the MNI152 template with 2mm resolution.

- 4.4.6. Trending linear regressions between MoCA scores and perfusion in (A) the resilience signature and (B) the anterior SN.
- 4.4.7. Colour-coded graph depicting the interrelatedness of any pairs of nodes.
- 4.4.8. Perfusion values associated with surviving components, visualised in perfusion space.
- 4.4.9. Correlations between MoCA scores and PCA-derived clusters that are (A) negatively and (B) positively associated with these scores.
- 4.4.10. Comparison of individual subject perfusion patterns in male subjects with MoCA scores of (A) 19 (n=1), and (B) 29 (n=1).
- 4.4.11. Individual perfusion patterns, shown in the same axial brain slice of subjects 1-8, females who scored identically in the MOCA.

## **CHAPTER 5**

- 5.1.1. Summary of the biochemical relationship between glucose and lactate, and their relationship to energy production.
- 5.1.2. Schematic representation of the biochemistry underlying the ANLS hypothesis.
- 5.3.1. Phantom used for investigation of possible echo times for semi-LASER investigation of Lac at 7T.
- 5.3.2. LCMoel fit of the Lac doublet in a phantom of the brain, using semi-LASER acquisition with 144ms TE, and 64 NSAs.
- 5.3.3. Evolution of the Lac doublet by merit of echo time during phantom investigation with semi-LASER acquisition.
- 5.3.4. Example outputs with TE of 288ms (a) and 40ms (b), in a phantom of the human brain, using semi-LASER acquisition at 7T.
- 5.3.5. Calcium titanate dielectric pads, which were placed strategically on the sides of the head.
- 5.3.6. Schematic of possible voxel positioning strategies.
- 5.3.7. Flashing (8Hz) checkerboard used for visual stimulation during fMRS measurement of lactate.
- 5.3.8. Summary of timings used in testing of the fMRI localiser and fMRS testing paradigm.
- 5.3.9. Outer volume suppression modules shown in blue during set-up for acquisition of a

spectrum in a 28-year-old female test subject.

5.3.10. Summary of the analysis pipeline for the pilot study.

5.3.11. LCMModel fit in a representative participant (33-year-old male)

5.3.12. Spectra acquired (a) before and (b) after changing the orientation of the Lac voxel in a 33-year-old male subject.

5.3.13. Representative example of a spectral artefact seen in a 69-year-old female test subject between 4.2-3.5ppm.

5.4.1. Summary of analysis approach used for in vivo investigations.

5.4.2. Schematics depicting (a) the rest/stimulation timings of sLASER acquisition, consisting of 360 NSAs. Each NSA is of ~4.75 secs duration, thus each kernel of 60 NSAs equates to ~285 secs, and a moving average is then utilised to ensure most accurate characterisation of the time course, and (b) the subsequent selection of kernels for inclusion.

5.4.3. Example averaged BOLD response (ON>OFF) of 5 older subjects during the fMRI acquisition for lactate voxel placement in the visual cortex (~3.5 minutes duration).

5.4.4. Representative example of a spectrum averaged across the entire time course, in a 32-year-old female.

5.4.5. Percentage change in Lac levels relative to first baseline measure in the young (orange) and old (purple) cohorts.

5.4.6. Gasparovic-corrected and scaled Lac concentrations throughout the time course of fMRS acquisition in (a) the young cohort and (b) the old cohort.

5.4.7. Histogram depicting Lac concentrations in the full cohort.

5.4.8. Comparison of Gasparovic-corrected and scaled concentrations of Lac, MM1, MM2 and MM3 over the time course.

## **CHAPTER 6**

6.3.1. The Ergospect pedal which would be used for sub-maximal exercise within the MRI scanner.

6.3.2. Summary of study visit timings.

6.3.3. Summary of DNP experimental protocol.

## List of Appendices

- A. Inclusion and exclusion criteria for the retrospective studies used in Chapter 3.
- B. Network masks as provided by FINDLab.
- C. Comparison of standardised beta values from linear regressions of perfusion and sCoV with age in investigated regions, with sex and GM volume as covariates.
- D. Inclusion and exclusion criteria for the studies used in Chapter 4.
- E. Key nodes and associated regions identified by graph visualisation.

## Abbreviations used in thesis

### A

ACC	anterior cingulate cortex
AC-PC	anterior commissure - posterior commissure
AD	Alzheimer's Disease
ADAS	Alzheimer's Disease Assessment Scale
ADAS-Cog	Alzheimer's Disease Assessment Scale - Cognitive Subscale
ADNI	Alzheimer's Disease Neuroimaging Initiative
ADNI-3	Alzheimer's Disease Neuroimaging Initiative (Third Iteration)
AFP	adiabatic full passage (refocusing pulses)
ANLS	astrocyte-neurone lactate shuttle
antCA	anterior cerebral arteries
ANTs	Advanced Normalization Tools
APOE	apolipoprotein-E
APOE- $\epsilon$ 4	apolipoprotein-E epsilon 4
ASL	arterial spin labelling
Asp	aspartate
ATP	adenosine triphosphate
ATT	arterial transit time

### B

BMI	body mass index
BOLD	blood-oxygen-level-dependent
BraNDy-MS	Brain Network Dysfunction in Multiple Sclerosis

### C

CASL	continuous arterial spin labelling
CBF	cerebral blood flow
Cho	choline
CI	Chief Investigator

CMRO <sub>2</sub>	cerebral metabolic rate of oxygen
CNR	contrast-to-noise ratio
Cr	creatine
CRLB(s)	Cramér-Rao lower bound(s)
CSF	cerebro-spinal fluid
CT	computed tomography
<b>D</b>	
DLPFC	dorsolateral prefrontal cortex
DMN	default mode network
DSM	Diagnostic and Statistical Manual of Mental Disorders
DSS	sodium trimethylsilylpropanesulfonate
DTI	Diffusion Tensor Imaging
DNP-MRI	dynamic nuclear polarisation magnetic resonance imaging
<b>E</b>	
ECN	executive control network
EPI	echo-planar imaging
EPISTAR	echo-planar MR imaging and signal targeting with alternating radiofrequency
<b>F</b>	
FA	flip angle
FAIR	flow-sensitive alternating inversion recovery
FASTMAP	fast, automatic shimming by mapping along projections
FDG-PET	fluorodeoxyglucose positron emission tomography
FID	free induction decay
FINDLab	Functional Imaging in Neuropsychiatric Disorders Laboratory
fMRI	functional magnetic resonance imaging
fMRS	functional magnetic resonance spectroscopy
FOV	field of view

FSL	FMRIB Software Library
FSPGR	fast spoiled gradient echo
FWE	family-wise error
FWHM	full width at half-maximum
<b>G</b>	
GABA	$\gamma$ -aminobutyric acid
GE	General Electric
GENFI	genetic frontotemporal dementia initiative
Glc	glucose
GLM	general linear model
Gln	glutamine
Glu	glutamate
Gly	glycine
GM	grey matter
GPC	glycerophosphocholine
GSH	glutathione
GSH-MRS	A comparison of potential regions of interest for glutathione MRS in the healthy adult brain
<b>H</b>	
HA-MCI-AD	healthy ageing – mild cognitive impairment – Alzheimer’s disease continuum
HMPAO-SPECT	hexamethyl propylenamine oxime single photon emission computed tomography
<b>I</b>	
ICA	Independent Component Analysis
ImPOA	Imaging to Understand Pain in Osteoarthritis
INCOPE	Imaging the Neural Correlates of Osteoarthritis Pain Phenotypes
ISIS	Image-Selected In Vivo Spectroscopy
<b>L</b>	
Lac	lactate

LDH-A	lactate dehydrogenase isoenzyme-A
LDH-B	lactate dehydrogenase isoenzyme-B
LICA	left internal carotid artery
<b>M</b>	
MALP-EM	Multi-Atlas Label Propagation with Expectation-Maximisation based refinement
MCI	mild cognitive impairment
MCT	monocarboxylate transporters
MET-AGE	Metabolic Brain Ageing
MET-AGED	Dynamic cerebral energy metabolism in healthy older individuals: <sup>1</sup> H-fMRS study at 7T
midCA	middle cerebral arteries
mIns	myo-inositol
MIRTK	Medical Image Registration ToolKit
ml/100g/min	millilitres per 100 grams of tissue per minute
mLTS	modified least-trimmed squares
MM	macromolecule
MMSE	Mini-Mental State Examination
MNI	Montreal Neurological Institute
MoCA	Montreal Cognitive Assessment
MP-RAGE	Magnetization Prepared - Rapid Gradient Echo
MRI	magnetic resonance imaging
MRS	magnetic resonance spectroscopy
mT	millitesla
MVPA	multivariate pattern analysis
<b>N</b>	
NAA	N-acetylaspartate
NAAG	N-acetylaspartylglutamate
NADH	nicotinamide adenine dinucleotide
Na <sub>2</sub> HPO <sub>4</sub>	disodium phosphate
NaH <sub>2</sub> PO <sub>4</sub>	monosodium phosphate
NaN <sub>3</sub>	sodium azide

NMR	nuclear magnetic resonance
NSA	number of signal averages
<b>O</b>	
OASIS	Open Access Series of Imaging Studies
OVS	outer volume suppression
<b>P</b>	
PaMIR	Parkinson's Magnetic Imaging Repository
PASL	pulsed arterial spin labelling
PCA	principal component analysis
PCASL	pseudo-continuous arterial spin labelling
PCC	posterior cingulate cortex
PCho	phosphocholine
PCr	phosphocreatine
PD	Parkinson's Disease
PET	positron emission tomography
PE	phosphorylethanolamine
PI	Principal Investigator
PLD	post-label delay
PNS	peripheral nerve stimulation
postCA	posterior cerebral arteries
ppm	parts per million
PRESS	point-resolved spectroscopy
pTFCE	probabilistic threshold-free cluster enhancement
PVE	partial volume effects
PVE-correction	partial volume correction
PW	perfusion-weighted
<b>R</b>	
RAPA	Rapid Assessment of Physical Activity
REST	regional saturation technique
RF	radiofrequency
RICA	right internal carotid artery

ROI(s)	region(s) of interest
RSN(s)	resting state network(s)
<b>S</b>	
SAR	specific absorption rate
SCI	subjective cognitive impairment
sCoV	spatial coefficient of variation
SE	spin echo
semi-LASER	semi-localized by adiabatic selective refocusing
SN	saliency network
SNR	signal-to-noise ratio
SPECT	single photon emission computed tomography
SPM	Statistical Parametric Mapping
SPMIC-QMC	Sir Peter Mansfield Imaging Centre - Queen's Medical Centre
SPMIC-UP	Sir Peter Mansfield Imaging Centre - University Park
SSM	Scaled Subprofile Model
STEAM	stimulated echo acquisition mode
SyN	symmetric image normalization

**T**

T	Tesla
Tau	taurine
TCA	tricarboxylic acid
tCho	total choline
tCr	total creatine
TE	echo time
TFCE	threshold-free cluster enhancement
TI	inversion time
TILDA	The Irish Longitudinal Study on Ageing
tNAA	total N-acetylaspartate
TR	repetition time

**V**

VAPOR	variable power and optimized relaxation delays scheme
VBA	vertebrobasilar artery
VE-ASL	vessel-encoded arterial spin labelling
VE-PCASL	vessel-encoded pseudo-continuous arterial spin labelling
VESPA	Versatile Simulation, Pulses, and Analysis
VeSPA-MS	Venous Stasis and Permeability Assessment in Multiple Sclerosis
VOI	volume of interest

## **W**

WM	white matter
WMH	white matter hyperintensities

## **Other**

$^1\text{H}$	hydrogen
$^{13}\text{C}$ -MRI	carbon-13 magnetic resonance imaging
$^{15}\text{O}$ ] $\text{H}_2\text{O}$	oxygen-15 labelled water
99mTC-ECD	technetium-99m-ethyl cysteinate diethylester

## Table of Contents

Abstract .....	ii
Personal acknowledgements .....	vi
Study acknowledgements .....	ix
List of accepted conference abstracts .....	xiii
List of Tables .....	xv
List of Figures .....	xvii
List of Appendices .....	xxiii
Abbreviations used in thesis .....	xxiv
1. General introduction .....	1
1.2. Problem statement .....	14
1.3. The scope of this thesis .....	15
2. Principles of Magnetic Resonance Imaging and Spectroscopy.....	18
2.1. Origin of the NMR signal .....	18
2.2. Relaxation .....	22
2.3. Formation of an image.....	25
2.3.1. Slice selection .....	25
2.3.2. Frequency encoding .....	26
2.3.3. Phase encoding.....	27
2.4. Magnetic field strength.....	30
2.5. Imaging approaches .....	31
2.5.1. Anatomical neuroimaging .....	31
2.5.2. Physiological brain measures using MRI .....	32
2.5.3. Magnetic resonance spectroscopy .....	47
2.6. General MR safety considerations.....	63
2.7. Summary .....	66
3. Brain perfusion changes in healthy ageing: on the role of pattern analysis and spatial coefficient of variation .....	67
3.1. Introduction.....	67
3.1.1. Aims and hypotheses .....	86
3.2. Dataset overview .....	87
3.2.1. Design and participants .....	87
3.2.2. Ethical approval and funding information .....	88
3.2.3. Subject recruitment approaches in original studies .....	89
3.2.4. MRI data acquisition .....	89
3.3. Data processing.....	91

3.3.1.	Methods .....	91
3.3.2.	Results .....	98
3.4.	Covariates pertinent to subsequent analysis.....	108
3.5.	Cerebral perfusion and ageing.....	108
3.5.1.	Methods .....	108
3.5.2.	Results .....	109
3.6.	Spatial covariance patterns of cerebral perfusion with age .....	115
3.6.1.	Methods .....	115
3.6.2.	Results .....	125
3.7.	Use of spatial coefficient of variation to understand brain perfusion changes .....	137
3.7.1.	Introduction.....	137
3.7.2.	Methods .....	138
3.7.3.	Results .....	139
3.8.	Cerebral perfusion and spatial coefficient of variation in vascular territories.....	143
3.8.1.	Introduction.....	143
3.8.2.	Methods .....	146
3.8.3.	Results .....	149
3.9.	Discussion .....	155
3.9.1.	Spatial covariance patterns of cerebral perfusion with age ....	155
3.9.2.	Cerebral perfusion and ageing.....	160
3.9.3.	Spatial coefficient of variation .....	162
3.9.4.	Data processing .....	169
3.9.5.	Limitations of the study.....	169
3.10.	Conclusions and future directions .....	175
4.	The relationship between brain perfusion patterns and cognitive testing: a spatial covariance analysis of arterial spin labelling MRI.....	178
4.1.	Introduction.....	178
4.1.1.	Aims and hypotheses .....	189
4.2.	Materials and methods .....	190
4.2.1.	Dataset selection .....	190
4.2.2.	Design and participants .....	197
4.3.	Analysis.....	201
4.3.1.	Image pre-processing.....	201
4.3.2.	Covariates for inclusion in whole-brain grey matter analyses.	202

4.3.3.	Voxel-wise analysis of cerebral blood flow data.....	202
4.3.4.	Principal component analysis of cerebral blood flow data.....	203
4.3.5.	Thresholding of ASL data .....	204
4.3.6.	Understanding perfusion covariance .....	205
4.4.	Results .....	208
4.4.1.	Voxel-wise analysis of cerebral blood flow data.....	212
4.4.2.	Principal component analysis of cerebral blood flow data.....	212
4.4.3.	Thresholding.....	213
4.4.4.	Understanding perfusion covariance .....	216
4.5.	Discussion .....	232
4.5.1.	General discussion .....	232
4.5.2.	Study limitations .....	238
4.6.	Conclusions and future directions.....	245
5.	Functional <sup>1</sup> H MRS of cerebral lactate concentration changes during prolonged visual stimulation.....	247
5.1.	Introduction .....	247
5.2.	Ethical approval and funding information.....	261
5.3.	Protocol development.....	261
5.3.1.	Introduction.....	261
5.3.2.	Echo time investigations .....	262
5.3.3.	Initial human studies .....	267
5.4.	Assessing cerebral lactate concentrations <i>in vivo</i> .....	286
5.4.1.	MRI measurements .....	286
5.4.2.	Implementation of protocol development findings.....	287
5.4.3.	Analysis.....	287
5.4.4.	Results .....	293
5.5.	Discussion.....	307
5.6.	Conclusions and future directions.....	317
6.	General conclusions and discussion.....	319
6.1.	Summary of results.....	319
6.2.	Limitations and methodological problems .....	321
6.3.	Future directions.....	325
6.3.1.	Furthering ASL investigation of cerebral perfusion.....	325
6.3.2.	Furthering MRS investigation of cerebral metabolism.....	326
6.4.	Conclusion.....	337
7.	References and appendices .....	339

7.1. References.....	339
7.2. Appendices.....	389

# 1. General introduction

Advancements in medicine, education, nutrition and living standards have rapidly increased human life expectancy (Oeppen and Vaupel, 2002; European Commission, 2012). The work of Oeppen and Vaupel (2002) evidences an increase of 2.5 years per decade since 1840, with the global number of people aged  $\geq 60$  years old expected to double between 2017 and 2050 (United Nations Population Division, 2017). However, this prolonged life expectancy is not matched by improvements in quality of life, with illnesses associated with increasing life expectancy never having been more prevalent. Generally, the final decade of life is spent in poor health, often characterised by physical health issues and cognitive decline (Brown, 2015). Ageing is the strongest risk factor for cognitive decline (Launer et al., 1999; Kawas et al., 2000), and around 54 million people are currently living with dementia globally, with around 10 million new cases diagnosed annually (Norton, Matthews and Brayne, 2013; Prince et al., 2013; Alzheimer's Association, 2019). The resultant socio-economic burden is huge, estimated at \$818 billion (USD) in 2015, an increase of  $\sim 35\%$  since 2010 (Wimo et al., 2016). To put this into perspective, this is 1.1% of global gross domestic product, and is only set to increase, with Wimo et al. (2016) predicting associated costs of around \$2 trillion (USD) by 2030. Such a mismatch between increasing life expectancy and prolonged quality of life is socio-economically unsustainable (Brayne, 2007; Brown, 2015), and thus research addressing this mismatch is timely and much-needed.

Whilst ageing is a dynamic process with a variable order of events in each individual (Bowling and Dieppe, 2005; Walhovd et al., 2005; Peters, 2006), for many the main concern with regards to increasing life expectancy is how brain health and cognitive abilities can be maintained. Brain health could be considered critical to our overall health, given its role in every aspect of our lives, yet a consensus definition of the term does not currently exist (Bowling and Dieppe, 2005; Jeste, Depp and Vahia, 2010; Lara et al., 2013; Wang, Pan and Li, 2020; Hachinski et al., 2021). However, Wang, Pan and Li (2020) define brain health as:

***“The preservation of optimal brain integrity and mental and cognitive function and the absence of overt neurological disorders,”***

a definition which is employed throughout this thesis.

The preservation of cognitive abilities is also closely linked to feelings of both independence and life satisfaction (Reichstadt et al., 2010; Halaweh et al., 2018). However, individual experiences of old age vary greatly. Whilst an array of factors may influence our brain health as we age – both modifiable and non-modifiable – the interplay between these is unique to every individual. This multi-faceted nature of brain health can make early cognitive decline particularly challenging to elucidate. Additionally, there is still much that is unknown with regards to modifiable factors improving brain health in old age, and how to devise preventative treatments and lifestyle recommendations. For example, there is a well-established link between exercise and brain health (Kramer, Erickson and Colcombe, 2006; Lustig, Shah, Seidler and Reuter-

Lorenz, 2009; Bherer, Erickson and Liu-Ambrose, 2013; Jackson et al., 2016; Baranowski et al., 2020), but there remains uncertainty as to the underlying physiological and metabolic mechanisms of this relationship. As such, the more that can be learned about the underlying physiology and metabolism of healthy ageing, the more such possible preventative measures and advantageous lifestyle changes can also be understood. A literature review by Lara et al. (2013) attempted to identify key features of the healthy ageing phenotype, and identified key domains including physiological and metabolic health, physical capability, cognitive function, and psychological and social well-being. *Figure 1.1.1.* summarises this work, and highlights the scope of this thesis within these domains.

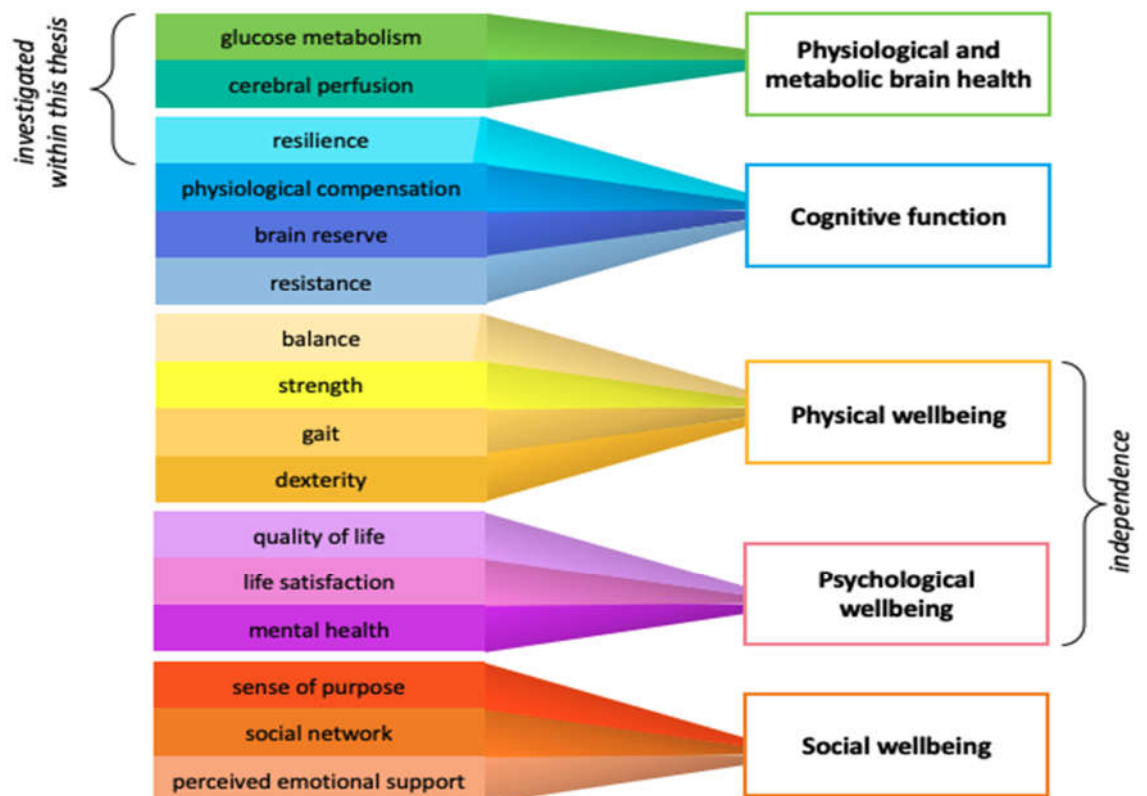


**Figure 1.1.1.:** Summary diagram of key factors pertaining to healthy ageing. Based on the work of Bowling and Dieppe (2005) and Lara et al. (2013).

Mattson and Arumugam (2018) highlight the complex interplay of brain ageing hallmarks – changes in the brain which are known to be strongly associated with the ageing process – and related bioenergetic changes, as summarised in *Figure 1.1.2.* Investigations of the brain have also highlighted that these ageing hallmarks are comparable to those seen in other bodily tissues (López-Otín et al., 2013).

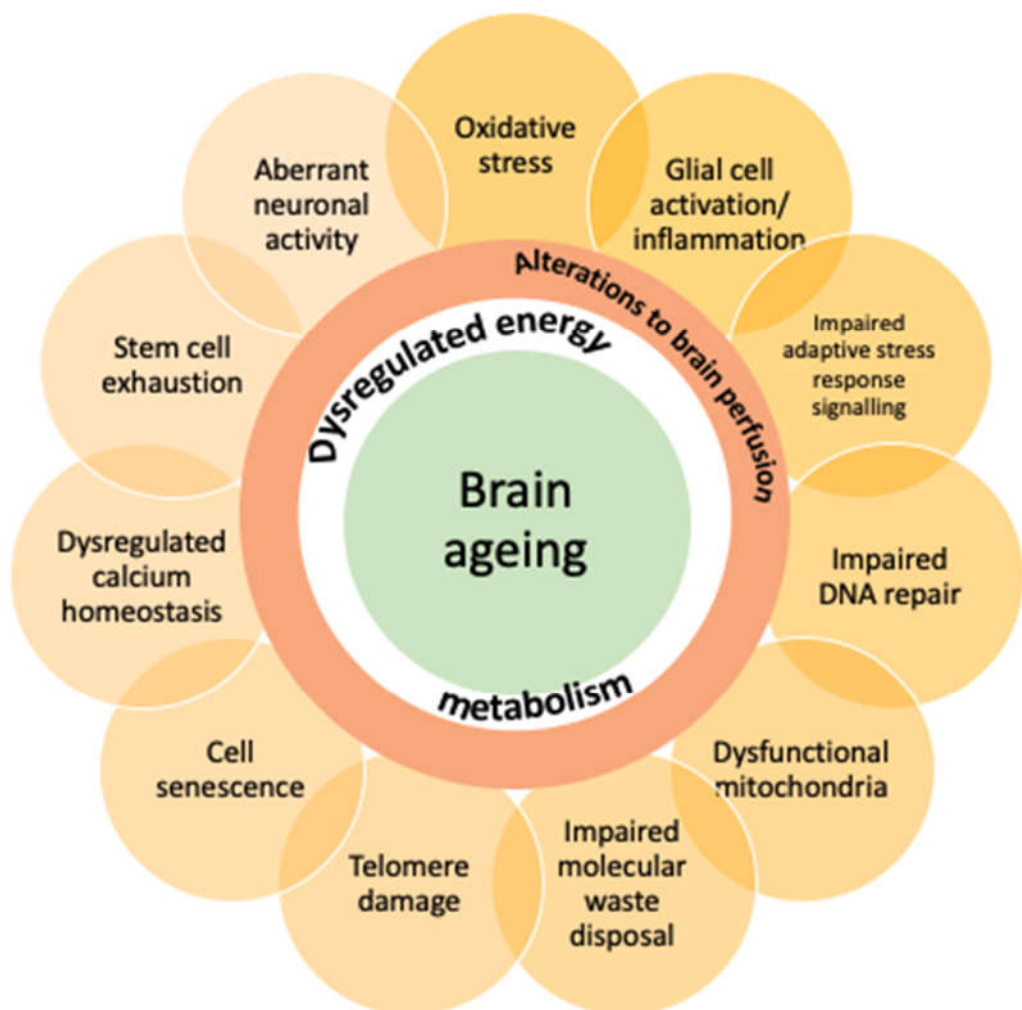


**Figure 1.1.2.:** *Summary of brain ageing hallmarks. All the hallmarks within the outer ring interact with dysregulated energy metabolism, and potentially also altered brain perfusion, as shown as the inner rings. It is notable that 'cell senescence' and 'telomere damage' are still to be established as hallmarks of brain ageing (figure based on the work of López-Otín et al., 2013, and Mattson and Arumugam, 2018).*

When considering brain ageing, both metabolic and perfusion changes are particularly pertinent, as both of these are tightly regulated under healthy conditions (Mergenthaler et al., 2013; Lin and Rothman, 2014; Watts, Pocock and Claudianos, 2018; Beishon et al., 2021). Adequate energy provision is critical for all cellular mechanisms to work properly. Glucose (Glc) is the predominant source of brain energy, particularly under normal physiological conditions, through the production of adenosine triphosphate (ATP) via glycolysis, the tricarboxylic acid (TCA) cycle, and oxidative phosphorylation. Thus, perturbations in Glc supply will have implications upon its catabolism, energy provisions, and any metabolic pathways linked to Glc, including those previously mentioned. Similarly, prolonged alterations in brain perfusion can damage the brain, which may be irreversible and affect brain integrity. For example, prolonged hypoperfusion is invariably damaging, and has been suggested to be a critical contributing factor in dementia pathogenesis and cognitive decline (Román, 2004; de la Torre, 2012; Kalback et al., 2013; Wolters et al., 2017). A review by de la Torre (2012) also indicates such brain hypoperfusion can in turn create a neuronal energy crisis, which may be related to protein synthesis abnormalities, and ultimately the formation of amyloid-beta plaques and neurofibrillary tangles, characteristic neurodegenerative lesions.

Compensatory mechanisms – systems which aim to address deviations from healthy homeostatic functionality by offsetting associated weaknesses – are

also important in healthy brain ageing. However, how successfully an individual can respond to perturbations in metabolic or physiological brain health can determine the signs and symptoms of brain ageing that they exhibit, or lack thereof. The interaction between protective, adverse, and mixed-effect factors contributes to brain ageing status – consider, for example, the protective effect of exercise (Baranowski et al., 2020; Bliss et al., 2021), and adverse effects of alcohol consumption (Topiwala et al., 2021) on the brain. Mixed effect factors are those which have a varying impact on a person’s brain ageing status, dependent on their capacity to respond to protective and adverse factors. Examples of such factors include brain reserve (anatomical brain aspects, excluding neuropathology; Stern et al., 2020), resistance (the absence or lower than expected presence of dementia-associate brain changes, based on characteristics and risk factors of the individual; Montine et al., 2019), resilience (normal cognition when dementia-associated pathology is present; Arenaza-Urquijo et al., 2019), and physiological compensation (the response following physiological injury to the brain; Montine et al., 2019). The relationship between these factors is summarised in *Figure 1.1.3.*

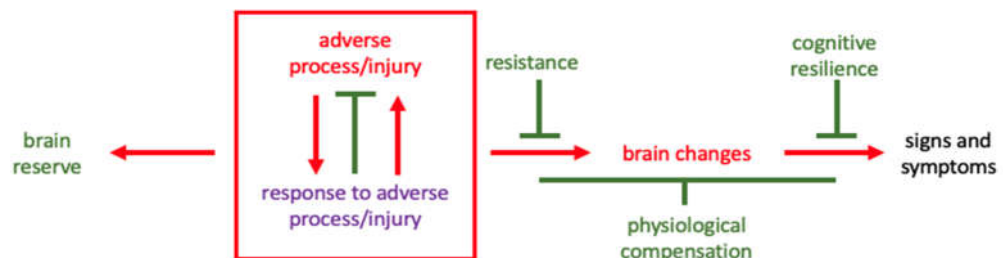


**Figure 1.1.3.:** Simplified summary of factors which cumulatively contribute to the signs and symptoms of healthy brain ageing, or neurodegenerative disease. Relationships are shown as protective (green), adverse (red), and mixed (purple). This figure is based on work by Montine et al. (2019).

Metabolic reprogramming – a change in energy generation and its subsequent utilisation – or physiological changes in brain ageing require investigation as they are imperative to the understanding of the complex interplay between causation, compensatory moderation, the resultant phenotypical and behavioural expression, and subsequent identification of early biomarkers of cognitive decline. Such metabolic and physiological changes are believed to occur well before established anatomical markers such as cerebral atrophy and increasing ventricle size in Alzheimer’s disease (AD, Drayer, 1988; Pini et al., 2016). It can be challenging to distinguish transient cognitive decline and related brain changes from those occurring due to early cognitive impairment, or from healthy brain ageing, given their existence on a continuum (Sperling et al., 2011; *Figure 1.1.4.*) and the individual expression of related symptomatology (Walhovd et al., 2005). This continuum is thought to occur due to the individual variance seen in brain ageing and associated cognitive decline, and the lack of a specific biomarker which links preclinical pathophysiology and cognitive decline, and subsequent transition to clinically-identifiable symptoms, and also includes a preclinical period which is thought to commence at least 10-20 years prior to clinical presentation (Sperling et al., 2011). A lack of mechanistic metabolic or physiological biomarkers of critical neurodegenerative events is also thought to contribute to the failure of clinical trials and prevention studies in AD – whilst many have been proposed, the associated evidence and result replication is limited (Yiannopoulou et al., 2019).

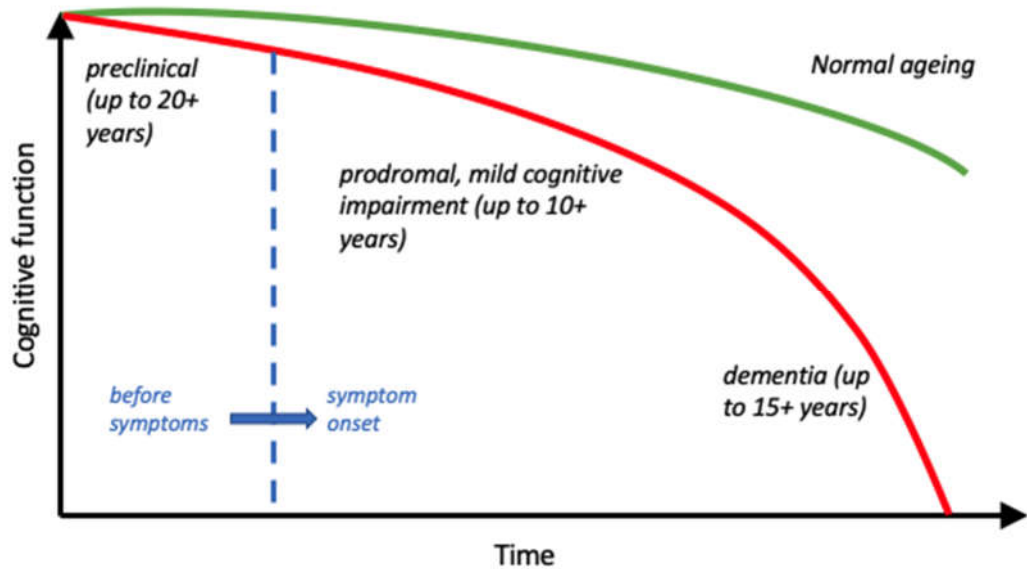


**Figure 1.1.4.:** Schematic of the healthy ageing-mild cognitive impairment-AD (HA-MCI-AD) continuum. Normal ageing is represented by the green line, and cognitive decline by the red. Taken from Sperling et al. (2011).

Research into pre-dementia states has suggested that there may be signs of future cognitive decline well before the symptoms commonly assessed by current diagnostic methods. A 2020 review of early non-cognitive markers of dementia carried out by the Canadian Consensus Conference on Diagnosis and Treatment of Dementia (Montero-Odasso et al., 2020) found that sleep measures, hearing loss, grip strength, frailty, neuropsychiatric symptoms, gait speed, and dual-task gait speed were all predictive of dementia, with changes in gait speed apparent up to 12 years prior to an MCI diagnosis (Buracchio et al, 2010). However, such changes are often attributed to other causes and, if they are identified as a possible prelude to dementia, can be difficult to address, as current drug targets predominantly focus upon the management of traditional clinical symptomatology.

Imaging-perceptible markers of metabolic and physiological characteristics of both healthy ageing and early cognitive impairment are required, as the majority of research efforts employing imaging for the elucidation of age-related brain changes focus on structural change. It is possible that structural changes represent late epiphenomena, rather than upstream drivers of healthy or impaired brain ageing changes, which metabolic or physiological alterations may be. Understanding the scope of healthy brain ageing can inform as to the early signs of an individual transitioning from healthy ageing to accelerated progression of cognitive decline, and may lead to identification of targets for preventative measures or additional modifiable risk factors. Specific metabolic and perfusion states may be identified as mechanistic drivers of cognitive decline, thus enabling tailored interventions to be designed to address this. For example, healthy metabolic reprogramming may be facilitated by nutritional supplementation, such as the use of ketogenic drinks to address inadequate cerebral Glc provisions (Fortier et al., 2021). Additionally, normative reference values will become increasingly important both within the research field, and clinically.

Various medical imaging techniques are readily available within research and clinical settings, and therefore would be pertinent to the assessment of brain health in ageing, with the potential for future clinical translation. However, not all techniques are suitable, due to the caveats of their use – as shown in Table 1.1.1. – or their spatial and temporal resolution, as depicted in *Figure 1.1.5.* These imaging techniques can also be used in combination with each other for a more holistic understanding of underlying brain health.

**Table 1.1.1.: Summary characteristics of imaging modalities which can assess brain health.** Abbreviations used within the table: MRI – magnetic resonance imaging; MRS – magnetic resonance spectroscopy; fMRS – functional magnetic resonance spectroscopy; PET – positron emission tomography; SPECT – single-photon emission computed tomography; EEG – electroencephalography; MEG – magnetoencephalography.

			Characteristics	
Imaging modality	Type of imaging	Biological feature probed	Positive	Negative
<b>MRI</b>	Structural, functional, molecular	Anatomy, physiology	<ul style="list-style-type: none"> <li>+ High spatial resolution</li> <li>+ High soft tissue contrast</li> <li>+ No ionising radiation</li> </ul>	<ul style="list-style-type: none"> <li>- Long scan duration</li> <li>- Expensive</li> <li>- Claustrophobia</li> <li>- Limited to the assessment of individuals who do not have MR-incompatible metal implants</li> </ul>
<b>(f)MRS</b>	Molecular, functional	Metabolism	<ul style="list-style-type: none"> <li>+ Large number of observable metabolites</li> <li>+ Non-invasive quantification of metabolism</li> <li>+ Can assess temporal dynamics</li> </ul>	<ul style="list-style-type: none"> <li>- Water resonance several orders of magnitude larger than metabolites</li> <li>- Limited spatial information</li> <li>- Poor spatial resolution</li> <li>- Narrow chemical shift range = overlapping resonances</li> <li>- Expensive</li> <li>- Vast range of approaches to acquisition, processing, quantification and reporting</li> <li>- Claustrophobia</li> <li>- Limited to the assessment of individuals who do not have MR-incompatible metal implants</li> </ul>

<b>PET/ SPECT</b>	Functional, molecular	Metabolism	<ul style="list-style-type: none"> <li>+ High sensitivity</li> <li>+ Fast</li> </ul>	<ul style="list-style-type: none"> <li>- Low spatial resolution</li> <li>- Ionising radiation</li> <li>- Cyclotron is expensive</li> </ul>
<b>EEG</b>	Functional	Neural oscillations	<ul style="list-style-type: none"> <li>+ Fast</li> <li>+ Cheap</li> <li>+ Hardware is mobile</li> <li>+ Silent</li> <li>+ Can have high temporal resolution</li> <li>+ Non-invasive</li> </ul>	<ul style="list-style-type: none"> <li>- Poor spatial resolution</li> <li>- Poor measurement of deeper neural activity</li> <li>- Time-consuming electrode placement</li> <li>- Poor signal-to-noise ratio</li> </ul>
<b>MEG</b>	Functional	Neural oscillations	<ul style="list-style-type: none"> <li>+ High temporal resolution</li> <li>+ Non-invasive</li> </ul>	<ul style="list-style-type: none"> <li>- Expensive</li> <li>- Requires shielded room</li> <li>- Signals of interest extremely small</li> <li>- Lower spatial resolution than fMRI</li> </ul>

---

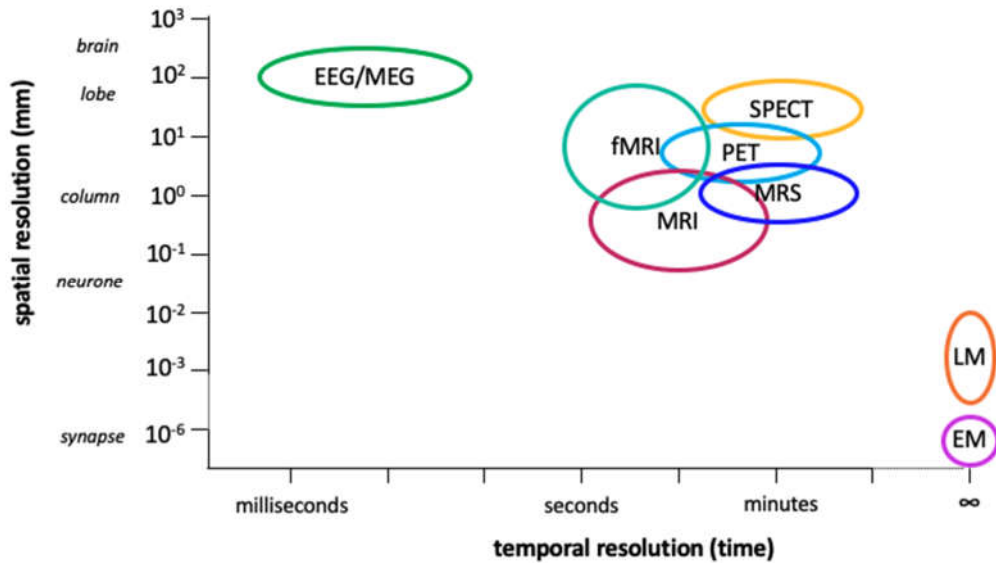


**Figure 1.1.5.:** Temporal and spatial resolution of key imaging modalities. Based on a figure by Pfister et al. (2012). Abbreviations used: EEG (electroencephalogram), MEG (magnetoencephalography), MRI (magnetic resonance imaging), fMRI (functional magnetic resonance imaging), PET (positron emission tomography), SPECT (single-photon emission computed tomography), LM (light microscopy), EM (electron microscopy).

Certain imaging techniques access different facets of pathology, such as the anatomy, biochemistry, metabolism and functional capacity, with all major neurodegenerative disorders exhibiting relatively specific imaging findings (Tartaglia, Rosen and Miller, 2011). Techniques such as positron emission tomography (PET), single-photon emission tomography (SPECT), and computed tomography (CT) exploit forms of ionising radiation in order to produce diagnostic images. These methods are useful, and have contributed extensively to the body of brain ageing research (Hoffman et al., 2000; Silverman, 2004; Yeo et al., 2013; Ishii, 2014; Valotassiou et al., 2018; Banerjee et al., 2020; Ferrando and Damian, 2021). However, concern has been raised over the use of such radiation, particularly in patient groups and cases where multiple scans are necessary (Lin, 2010; Lumbreras, Salinas and

Gonzalez-Alvarez, 2019; Ribeiro et al., 2020). Thus, MRI is well-placed as a safe imaging approach which can assess physiological and metabolic brain changes – beyond the neuronal processes which can be assessed by EEG or MEG – in both healthy and impaired ageing, as it does not necessitate exposure to ionising radiation.

A review by Elliott (2020) summarises the current state of the field when considering structural MRI-based biomarkers of accelerated ageing and dementia risk. This work clarifies the potential of grey (GM) and white matter (WM) metrics of cortical thickness, fractional anisotropy, mean diffusivity and white matter hyperintensities (WMH) as early biomarkers for the risk of cognitive decline, and concludes that these metrics have preliminary support as midlife biomarkers of accelerated ageing, but still require further development. Whilst multiple studies have shown such metrics to have moderate to high measurement reliability (Han et al., 2006; Vollmar et al., 2010; Iscan et al., 2015), it is notable that pathological changes in structure can be difficult to discern from healthy ageing, particularly in early disease stages. Additionally, the underlying physiological and molecular changes contributing to such pathologies is often unclear, such as for WMH (Alber et al., 2019), which can be found in more than 90% of individuals older than 65 (Schmidt et al., 2011). A recent shift in the research field towards combining multiple imaging metrics (Franke et al., 2010; Cole et al., 2017; Cole and Franke, 2017; Cole, 2017; Dickie et al., 2018; Rokicki et al., 2020) to improve their diagnostic potential also highlights that each of these metrics alone may be lacking in robust clinical validity.

Physiological and metabolic MRI approaches, such as arterial spin labelling (ASL) and magnetic resonance spectroscopy (MRS), can assess additional facets of healthy brain ageing, with ASL a comparable imaging metric to fluorodeoxyglucose positron emission tomography (FDG-PET) and hexamethyl propylenamine oxime single photon emission computed tomography (HMPAO-SPECT; Wintermark et al., 2005; Musiek et al., 2012; Cha et al., 2013; Takahashi et al., 2014; Zhang, 2016; Dolui et al., 2020). ASL enables the assessment of tissue perfusion, changes in which are thought to occur prior to brain atrophy (Jack et al., 2010; Sperling et al., 2011), whereas MRS is used to investigate brain metabolism, thereby providing a more comprehensive understanding of brain ageing beyond standard structural metrics (Kantarci, 2013; Chen, 2019). This is particularly reflected in a growing number of population imaging efforts which now include physiological measures in large cohorts, such as the Alzheimer’s Disease Neuroimaging Initiative (ADNI, <http://adni.loni.usc.edu>), Open Access Series of Imaging Studies (OASIS, [www.oasis-brains.org](http://www.oasis-brains.org)) and The Irish Longitudinal Study on Ageing (TILDA, <https://tilda.tcd.ie>).

## 1.2. Problem statement

Functional decline caused by brain ageing results in a huge socioeconomic and psychological burden for the affected individual, their caregivers, and the wider society. Historically, medical imaging has focused upon understanding later-stage disease, and current possible biomarkers of accelerated ageing are biased towards structural metrics. Elucidating the unknowns of metabolic reprogramming and physiological changes with ‘healthy brain ageing’ – and the interindividual variance which can occur under this umbrella term – may enable perfusion- and metabolism-related deviations to be pinpointed, thereby

identifying possible targets for future diagnostic biomarkers and treatments, and enabling researchers to develop interventions which may prolong optimal quality of life as we age. The MRI techniques of ASL and fMRS are uniquely positioned to clarify these very unknowns, and are also clinically viable. This aforementioned knowledge gap, and the potential for technique advancement, motivates the direction of this PhD thesis.

### 1.3. The scope of this thesis

The work herein took place at the University of Nottingham between October 2016 and June 2021, and investigated healthy brain physiology using functional metabolic and resting-state cerebral perfusion measures.

The current Chapter provides an introductory overview to the topic of healthy brain ageing, before Chapter 2 provides an overview of the physics pertinent to the understanding of magnetic resonance, with particular focus on ASL and functional MRS (fMRS).

Chapter 3 presents a study which utilises a retrospective cross-sectional ageing cohort to investigate age-related changes in perfusion as measured with ASL, using various techniques including principal component analysis (PCA), and spatial coefficient of variation (sCoV). Study conception, data acquisition, processing, analysis and interpretation are described. Here, the key experimental aims are as follows:

- To assess whether decreases in perfusion with ageing truly exist or are explicable by processing steps or underlying confounds;

- Identify PCA-derived spatial covariance patterns associated with age within a larger cohort than previously-published work;
- Assess the utility of spatial covariance patterns as predictors of age in a five-fold cross-validation PCA analysis;
- Compare the utility of ml/100g/min perfusion measures and sCoV as metrics for understanding perfusion variance across the brain with age, in various cortical and subcortical areas and vascular territories.

Chapter 4 describes a retrospective study which utilises PCA to assess the relationship between cerebral perfusion and Montreal Cognitive Assessment (MoCA) scores, using a healthy cohort comprising subjects from the Alzheimer's Disease Neuroimaging Initiative - third iteration (ADNI-3), and two internal cohorts from the University of Nottingham. The study design, acquisition of data, analysis, results and their interpretation, as well as future directions are described within this chapter. This study aims to:

- Identify a group-level perfusion pattern associated with the MoCA in cognitively intact older subjects using PCA;
- Describe the resultant pattern through assessment of key regions of interest (ROIs) and cognitive networks, and underlying cluster relatedness through graph visualisation;
- Compare the PCA spatial covariance pattern with a voxel-wise approach.
- Replicate an FDG-PET resilience signature (Arenaza-Urquijo et al., 2019) using ASL-derived perfusion maps, for the first time.

In Chapter 5, fMRS is employed to investigate cerebral lactate (Lac) behaviour in healthy young and old subjects, whilst a checkerboard visual stimulus is

viewed. The temporal changes in Lac were compared between young and old subjects, and absolute lactate concentrations quantified. The pilot study which optimised the protocol in both a brain phantom and human subjects is described, along with the main study in healthy subjects. The experimental aims were to:

- Determine the optimal protocol for subsequent *in vivo* experiments, in a brain phantom;
- Evaluate the feasibility of employing a long echo time (TE) fMRS sequence in the assessment of temporal dynamics in old subjects compared with young subjects;
- Quantify best-estimate 'absolute' concentrations of cerebral Lac throughout the time course.

Chapter 6 concludes the thesis with discussion of the results obtained throughout this work and the strengths and weaknesses of each study. The impact of the findings are considered, and directions for future research are also proposed.

## 2. Principles of Magnetic Resonance Imaging and Spectroscopy

This chapter provides a brief outline of nuclear magnetic resonance (NMR) principles and the origin of magnetic resonance imaging (MRI) and MRS, with particular focus on the techniques employed within this thesis. The basis of MRI, and the exploitation of tissue properties to achieve image contrast will be discussed, with the chapter concluding with discussion of the MRI techniques used in this thesis to assess both cerebral metabolism (i.e. MRS) and tissue perfusion (i.e. ASL).

### 2.1. Origin of the NMR signal

The basis of magnetic resonance is the interaction between nuclei that possess spin, and an external magnetic field. Protons ( $^1\text{H}$ ) possess spin (a fundamental property of nucleons) and also a magnetic moment ( $\mu$ ). These properties are related through the gyromagnetic ratio, which is the ratio of the magnetic moment to the angular momentum, denoted by  $\gamma$ , and as nuclei have a mass they generate spin angular momentum,  $\rho$ . The relationship between these properties are summarised in Equation 2.1..

$$\mu = \gamma\rho$$

[2.1]

Hydrogen ( $^1\text{H}$ ) is the most commonly investigated nucleus within the field of MRI, due to its natural abundance (99%) and biological abundance within the human body (63%), however it is possible to investigate other nuclei with net spin  $\frac{1}{2}$ , such as  $^{13}\text{C}$  and  $^{31}\text{P}$ .

Protons can classically be considered as spheres which are rotating about axes which are randomly orientated when there is no magnetic field (*Figure 2.1.1.a*). However, when introduced to a magnetic field, protons align parallel or anti-parallel to the magnetic field (*Figure 2.1.1.b*). The relationship between the frequency of the precession of the magnetic moment along the direction of the external field ( $\omega_0$ ) is proportional to a combination of the gyromagnetic ratio and magnetic field strength ( $B_0$ ), and is summarised mathematically by the Larmor equation (Equation 2.2):

$$\omega_0 = \gamma \cdot B_0$$

[2.2]

The gyromagnetic ratio of  $^1\text{H}$  is 42.58 MHz/T.

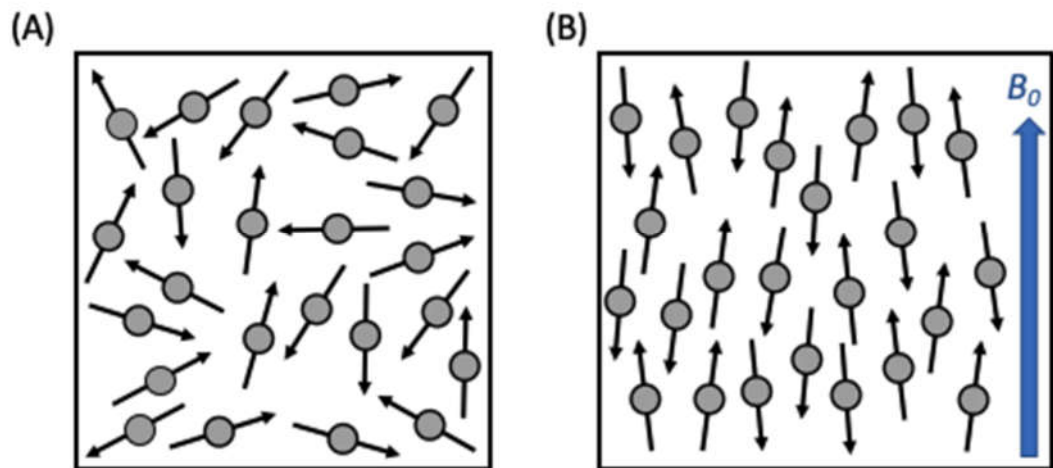


**Figure 2.1.1.:** Depiction of magnetic moments in (a) the absence of a magnetic field ( $B_0$ ), where they align in various directions, and (b) the presence of a magnetic field ( $B_0$ ), which causes the magnetic moments to align either parallel or anti-parallel.

We can define the direction of the external magnetic field as the z direction.

Spins precess about the z-axis (*Figure 2.1.2.*), and their precession can be exploited to create a signal.

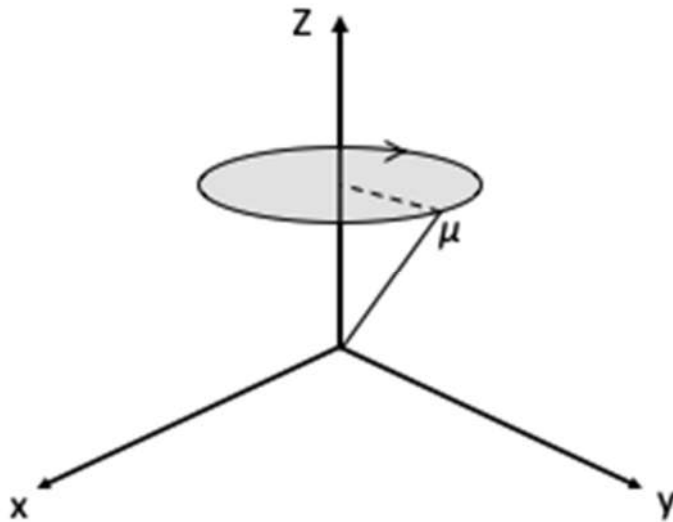


**Figure 2.1.2.:** Precession of a spin,  $\mu$ , about the z-axis inside a magnetic field.

A typical sample is comprised of many spins, which are averaged to create a net magnetisation vector. Application of an external second magnetic field in the xy-plane, for a given duration, will cause a change in direction of the net magnetic moment, tipping it through a nutation angle of a given degree. The theoretical basis for MRI relies upon such an applied secondary field, commonly known as the  $B_1$  field, which is produced by a radiofrequency (RF) pulse. Such RF pulses are generally on the order of micro-Tesla, whereas the  $B_0$  field is measured in Tesla.

When considering the laboratory frame of reference, application of the  $B_1$  field results in a spiralling of the net magnetisation towards the xy-plane. However, a more simplistic visualisation is generally used for NMR experiments,

whereby the frame of reference rotates at the Larmor frequency, known as the rotating frame (Rabi, Ramsey and Schwinger, 1954). These depictions of net magnetisation evolution are summarised in *Figure 2.1.3.*, with the angle at which this occurs dependent upon both the duration and magnitude of the applied  $B_1$  field.

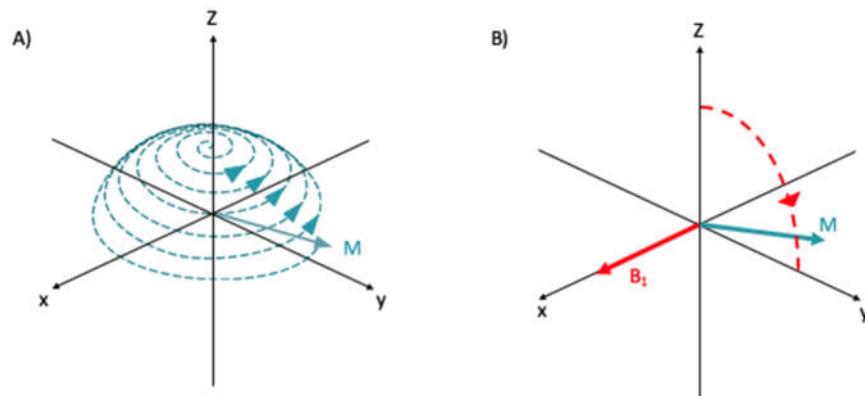


**Figure 2.1.3.:** Evolution of net magnetisation ( $M$ ) after  $B_1$  field application, in the (a) laboratory frame, and (b) rotating frame of reference.

## 2.2. Relaxation

Upon cessation of the RF pulse, the net magnetisation returns to its equilibrium value of  $M_0$  aligned with the static magnetic field,  $B_0$ . This occurs via two independent types of relaxation – longitudinal ( $T_1$ ) and transverse ( $T_2$  and  $T_2^*$ ). Longitudinal relaxation is where magnetisation returns to equilibrium after excitation in the xy direction and the time over which this occurs is defined by the time constant  $T_1$ . This varies between biological tissues and is a theoretical basis for tissue contrast in MRI images (*Figure 2.2.1.*).

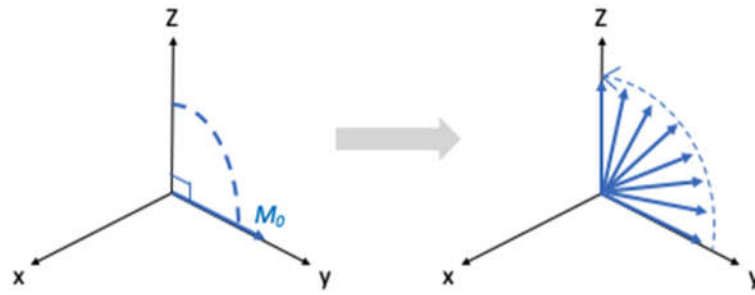


**Figure 2.2.1.:** Summary of the process of  $T_1$  relaxation. A  $90^\circ$  RF pulse knocks the magnetisation  $M_0$  – depicted in blue – into the  $xy$ -plane. Following this pulse, the magnetisation returns to equilibrium, in a duration governed by  $T_1$  relaxation time.

Transverse relaxation refers to the process by which spins lose coherence over time, becoming out of phase with each other after cessation of the RF pulse (*Figure 2.2.2.*) and returning to the equilibrium state. This decaying signal is referred to as the free induction decay (FID, *Figure 2.2.3.*). It is usually important that magnetisation recovers fully between each pulse application in order for pulses to behave as dictated within the sequence parameters, however this can lead to sequences which are very time-consuming in acquisition.

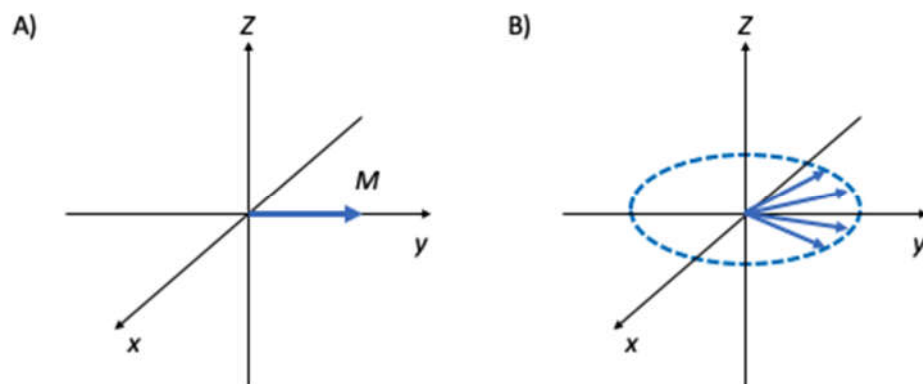


**Figure 2.2.2.:** The process of  $T_2$  relaxation, depicting (a) the magnetisation immediately after application of a  $90^\circ$  pulse, and (b) dephasing of spins after cessation of the pulse, in the rotating frame of reference.

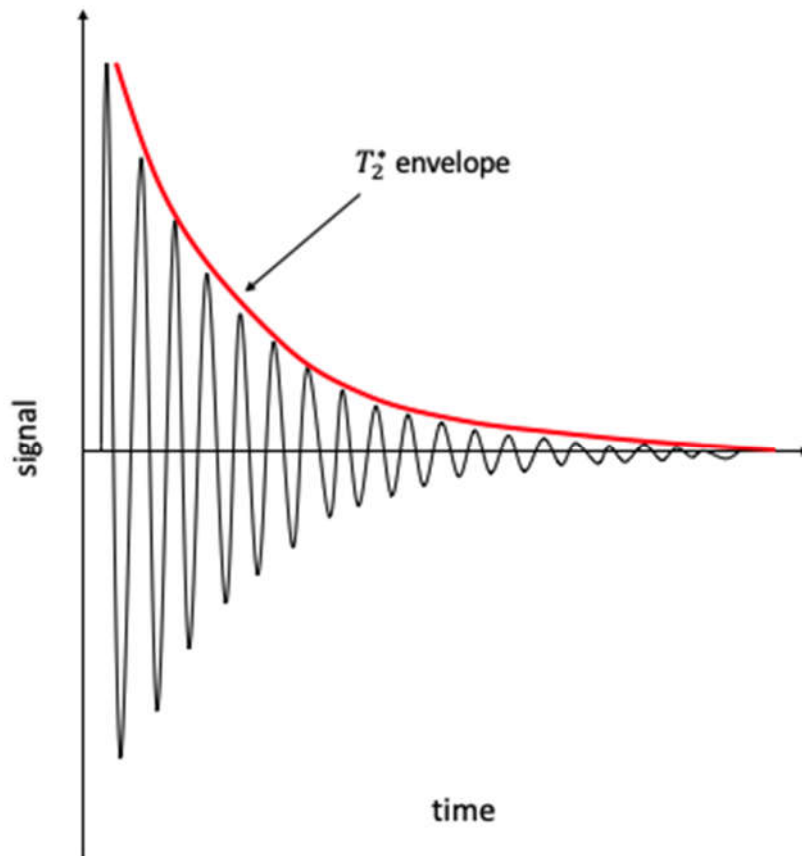


**Figure 2.2.3.:** The process of free induction decay. At the beginning, spins are all in phase, but over time they dephase as a function of  $T_2^*$ .

Phase coherence loss occurs faster than may be anticipated due to external inhomogeneities which affect the  $B_0$  field. This is known as the apparent transverse relaxation time, or  $T_2^*$ . External dephasing effects are significantly more prevalent at higher  $B_0$  field strengths which results in shorter  $T_2^*$ , presenting as distorted images, or signal loss.

The decay due to field inhomogeneity is reversible, if a  $180^\circ$  pulse is applied after an initial  $90^\circ$  pulse. Where application of one RF pulse creates an FID as above, two pulses occurring in succession results in a spin echo (SE), allowing retention of information which may otherwise be lost as the FID decayed. Application of a  $90^\circ$  pulse tips magnetisation to the transverse plane, albeit with some slight differences in the precession of spins relative to each other due to differing local fields. A subsequent  $180^\circ$  pulse is normally applied which flips the system, after which the spins that were precessing more quickly now have further to travel to catch up with slower spins. The term 'echo time' (TE) refers to the duration between the middle of the first RF pulse and the peak of the SE.

### 2.3. Formation of an image

There are three concepts which are critical to the understanding of image formation – slice selection, phase encoding and frequency encoding.

#### 2.3.1. Slice selection

Slice selection – also known as selective excitation – is the process through which three-dimensional information can be acquired by selecting spins in a specific two-dimensional plane. This limits the effect of the RF pulse to only nuclei which are rotating at a determined frequency within a given bandwidth, through application of an additional gradient. However, all spins within this frequency range will be excited by this given bandwidth, irrespective of their position. This is summarised in *Figure 2.3.1.* The thickness of the resultant slice is dependent on both the magnetic field gradient strength, and the RF pulse bandwidth.

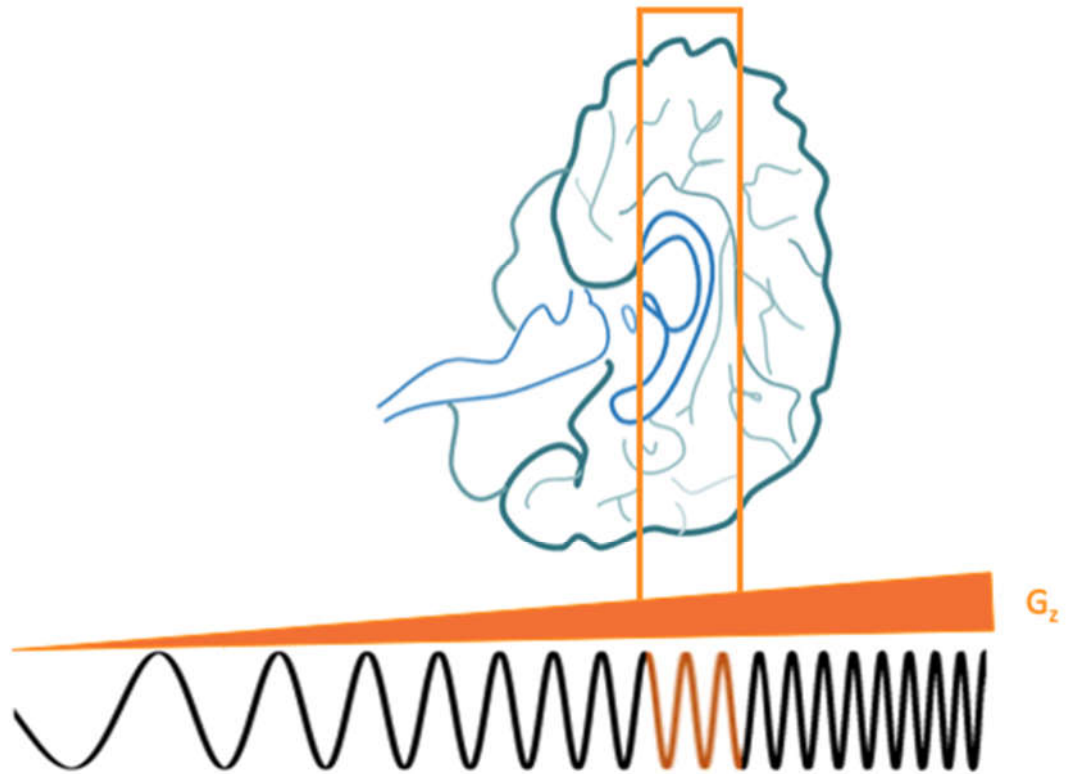


**Figure 2.3.1.:** The resonance frequencies of a given sample are altered by the magnetic field gradient  $G_z$ . RF pulses can be applied to excite a slice of the sample, with the frequency components of the RF pulse matching the frequency range of the target slice.

Stronger gradients can achieve thinner slabs of selective excitation, given the inversely proportional relationship between gradient strength and slice thickness (Garroway, Grannell and Mansfield, 1974). After localising to a slice, phase and frequency encoding enable the separation of signals from different voxels within the slice.

### 2.3.2. Frequency encoding

After slice selection, spatial encoding in the x- and y- directions is necessary for image production. Frequency encoding occurs along the x-direction, with application of an additional gradient (Mansfield and Maudsley, 1977). This

gradient alters the precession of excited spins, which will precess at a variety of frequencies that depend upon gradient strength, thereby varying resonance frequency as a function of position. This is depicted in *Figure 2.3.2.*

### 2.3.3. Phase encoding

Phase encoding is also required for spatial localisation, applied orthogonally to the frequency encoding gradient, commonly the y-direction. Phase encoding involves the application of a magnetic field gradient for a specified duration. This results in spins at different positions within a sample having precessed more or less relative to other spins, depending upon their position along the y-axis within a sample (*Figure 2.3.2.*).

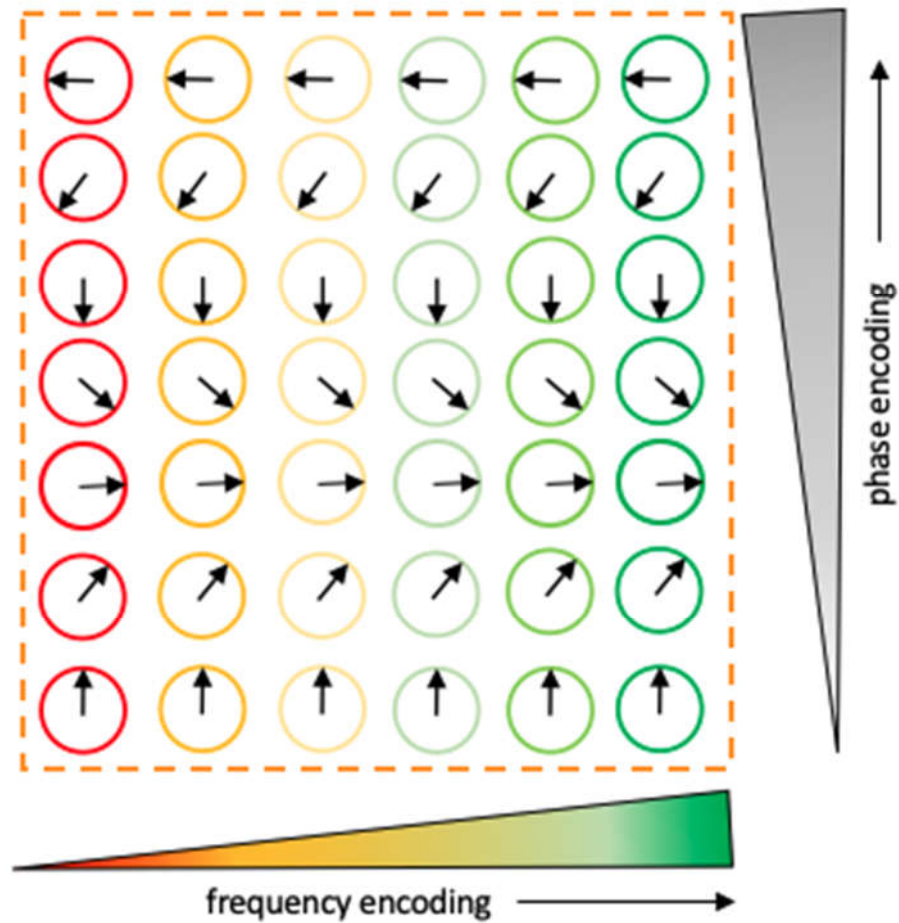


**Figure 2.3.2.:** Summary of frequency and phase encoding. The slice of interest – determined using slice selection as described in Section 2.3.1. – is depicted with the dashed orange line. Frequency encoding is represented by the red-green colour scale, and phase encoding by arrow position.

It should be noted that frequency and phase encoding gradients are not always used in the x- and y-directions, respectively, as poor selection of phase encoding direction may result in artefactual images. If the field of view (FOV) is smaller than the part of the body being imaged, aliasing can result, whereby information from outside the previously defined FOV is visible within the FOV, due to wrapping. Thus, the direction chosen for phase encoding is normally along the object's shortest dimension. In certain contexts, such as neuroimaging, it is commonplace to also select the directionality of the phase encoding gradient to avoid motion artefacts. An example of this is axial

neuroimaging, whereby phase encoding selection must consider eye motion and is therefore normally carried out in a left to right direction (Herrick et al., 1997).

The combination of slice selection and frequency and phase encoding results in a specified volume of interest. To understand these within a biological context, it is helpful to know the imaging planes of acquisition – sagittal, axial, and coronal – which are regularly referred to, in order to aid orientation within the body. The sagittal plane separates the left and right sides of the brain, through the corpus callosum, with the coronal plane separating the anterior and posterior, and the axial plane separating the superior and inferior parts of the brain. This is depicted in *Figure 2.3.3.*

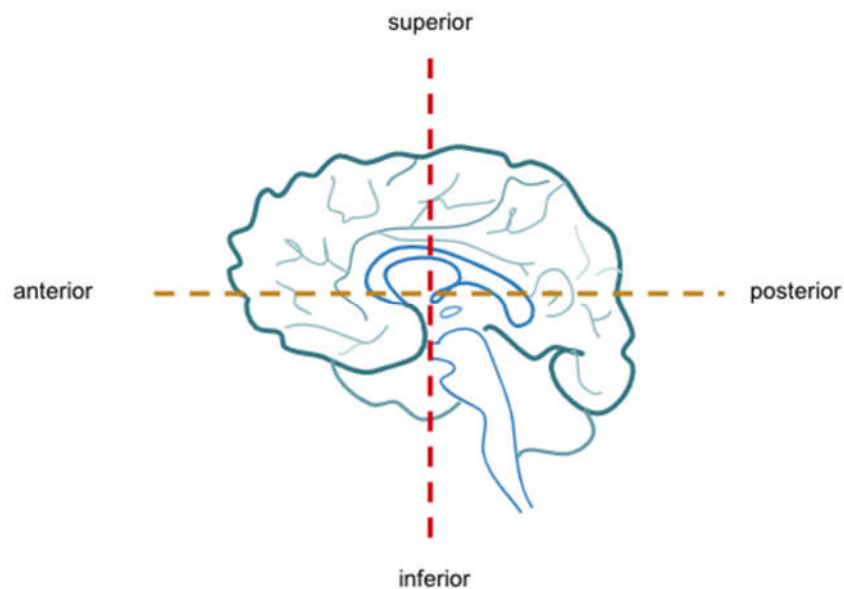


**Figure 2.3.3.:** *Depiction of sagittal, axial, and coronal imaging planes. The brain is shown in a sagittal view, with the coronal plane shown with a red line, and the axial shown in yellow.*

## 2.4. Magnetic field strength

The strength of the  $B_0$  field at which a scanner operates impacts the image that is produced. Commonly used field strengths vary from 0.5T to 7T, with 1.5 and 3T most often used in clinical settings, and 7T employed within research contexts, for various theoretical reasons. It is also more costly to run 7T MRI scanners, which can be prohibitive for health services. Research scanners are additionally available at 9.4, 11.7 and 14.1T, but there are only a few of these scanners globally, and thus are not used in most research work. Within this thesis, imaging was performed at both 3T and 7T.

When imaging at higher magnetic field strengths, signal-to-noise ratio (SNR) is improved due to magnetic moments being in proportionally higher alignment with the  $B_0$  field. Furthermore, contrast-to-noise ratio (CNR) is theoretically increased, given longer  $T_1$  relaxation and shorter  $T_2$  decay times exhibited by tissue at high field. Higher field strengths improve image quality and allow for identification of a greater number of spectral peaks in MRS (de Graaf, 2019), however as  $B_0$  increases, use of RF pulses of higher frequency is required to excite protons. As a result, specific absorption rate (SAR, a measure of RF power deposition within tissue) increases. As such, caution must be taken to ensure the safety of subjects and patients (see *Section 2.6.* for an in-depth discussion of appropriate considerations).

High field does offer benefits for MRS. Particularly, the strength of the applied field and chemical shift dispersion are linearly related, resulting in increased spectral resolution at higher field strengths. With these gains, metabolites are more clearly separated and more can be quantified than at lower field

strengths, including those implicated in various psychiatric conditions, such as glutamate (Glu), glutamine (Gln),  $\gamma$ -aminobutyric acid (GABA), glutathione (GSH), and Lac (Pradhan et al., 2015; Godlewska et al., 2017). However, they also result in a marked enhancement in chemical shift displacement, as well as issues arising from increased  $B_0$  and  $B_1$  inhomogeneity.

Shimming can be employed as a pre-scan measure and uses small electrical currents to achieve greater  $B_0$  homogeneity. However, a homogenous  $B_0$  field can be challenging to maintain at higher field strengths, with subjects within such fields introducing inhomogeneities. Poor homogeneity can cause an image to degrade, or introduce artefacts, and as such is of important consideration for patient groups. This is less likely to occur at lower field strengths, an advantage of using such scanners. Additionally, 1.5 and 3T scanners are readily available in hospitals and research institutions across the world, making findings from research studies employing these scanners more easily translated to clinical settings.

## 2.5. Imaging approaches

A number of different imaging schemes can be applied on the basis of the aforementioned underlying principles. The following sections overview those used in this thesis.

### 2.5.1. Anatomical neuroimaging

The acquisition of images which capture the anatomical structure is often critical to neuroimaging investigations, providing a basis for image registration.

These are commonly known as  $T_1$ -weighted images, as they exploit the process of  $T_1$  relaxation, whereby different tissues have different relaxation times, enabling brain structures to be viewed.

In  $T_1$ -weighted images, we shorten the sequence parameters TE and repetition time (TR), to create an image dominated by longitudinal relaxation. This aids tissue contrast due to differing times in which realignment of longitudinal magnetisation with  $B_0$  occurs, dependent on the tissue. For example, fat appears bright as longitudinal realignment with  $B_0$  occurs quickly, whereas this process is slower in water, resulting in a dark appearance due to low signal. If short TRs were not used, the resultant image would be of uniform intensity, as all protons will have recovered their alignment. Magnetisation prepared - rapid gradient echo (MP-RAGE, Mugler and Brookeman, 1990) and fast spoiled gradient echo (FSPGR, Bernstein, King and Zhou, 2004) are sequences which enable quick acquisition of  $T_1$  weighted images and are therefore useful in time-constrained clinical contexts. For the purposes of this thesis, anatomical images were used to support localisation of MRS and ASL acquisitions and enable calculation of tissue volumes.

#### 2.5.2. Physiological brain measures using MRI

Whilst the aforementioned structural imaging can be advantageous for anatomically focused diagnostics, such as the measurement of neurodegenerative atrophy, or localisation of brain changes, information is missed in its static nature. Investigation of cerebral functionality is clinically important, enabling further understanding of diseases and their effect upon patients.

Perfusion refers to the delivery of oxygenated blood to the tissue capillary network and is therefore a key measure of metabolic function and tissue health, as it enables constant provision of oxygen and nutrients to perfused regions. The anatomical construction of such capillary networks is optimised for this exchange, with the sheer number of capillaries and their small diameter (5-10 $\mu$ m) providing a large surface area across which this can occur, and waste products can be removed. Blood flow velocity also drops significantly in these vessels, which give increased time for such exchanges to occur. A summary schematic of key vessel properties and how they change throughout the vasculature is shown in *Figure 2.5.1*. Perfusion is expressed in units of cerebral blood flow in millilitres per 100 grams of tissue per minute (ml/100g/min), the typical values of which differ depending on the tissue of interest, with average GM perfusion varying between ~35 - 80 ml/100g/min, and WM perfusion ~20 ml/100g/min (Huang et al., 1983; Parkes et al., 2004; Leidhin et al., 2021). Inadequate perfusion to the brain can result in cerebral damage, which can have negative implications on brain integrity and cognition (Wolters et al., 2017).

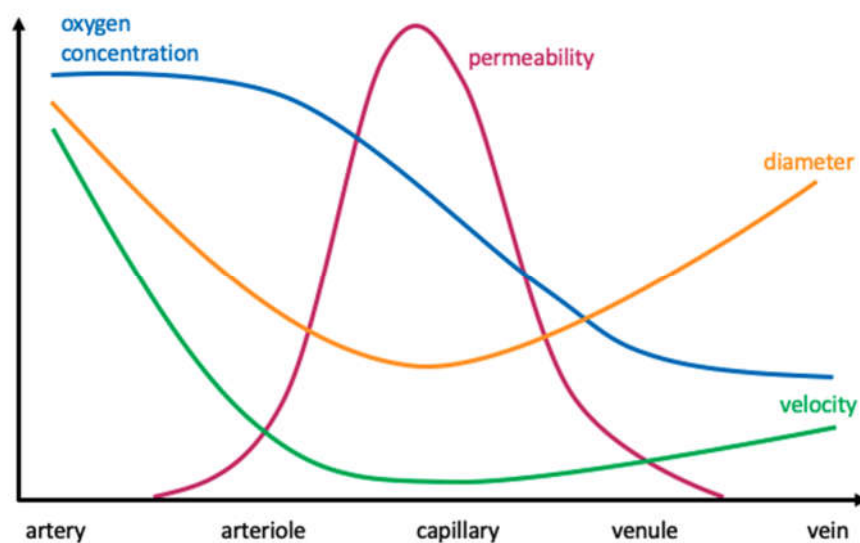


**Figure 2.5.1.:** Summary schematic of certain blood vessel properties and how these change throughout the vasculature, based on a figure by Parkes, 2003.

#### 2.5.2.1. Arterial spin labelling

ASL is one of the most commonly used types of physiological MRI, enabling the measurement of cerebral perfusion and allowing for clinical inferences to be drawn regarding energy use and neuronal activation within the brain (clinical applications of ASL are discussed further in Section 2.5.2.1.6., and Chapter 3).

Historically, MR investigations of perfusion employed established techniques used for angiography (Le Bihan et al., 1986). However, the tagging approach which underlies angiography necessitates water to be in motion across a long distance, whereas perfusion is defined by the flow of blood into a tissue, which can occur over distances that are far smaller than a typical voxel. The potential to exploit tracer kinetics through use of an MR-detectable tracer was then noted (Ackerman et al., 1987). Early studies using deuterium oxide as a tracer (Kim and Ackerman, 1988) were suggestive of the potential of water as an endogenous label for the measurement of tissue perfusion. Indeed, this potential was confirmed by the work of Detre et al., in 1992, through the magnetic labelling of water protons, which enables non-invasive, quantitative measurement of tissue perfusion. This is achieved by the application of RF and magnetic field gradients to 'label' the blood-water protons within target arteries through inversion of their spin. This labelling is followed into the imaging plane and is reflective of the perfusion of recipient tissues. This technique continues to be adapted for more accurate quantification through

hardware and sequence development, however this section will cover its modern implementation.

Theoretically, all ASL approaches are underpinned by the necessity to acquire two images, namely a label and control (*Figure 2.5.2.*). The labelling approach employed in ASL typically uses an off-resonance single adiabatic RF pulse, and the control image is collected when fully recovered after pulse application. These are subtracted to remove static background tissue and thereby produce a perfusion-weighted (PW) image, with the time between the labelling of inflowing blood and image acquisition referred to as the post-label delay (PLD, see Section 2.5.2.1.3.). ASL is an inherently low SNR imaging so typically several repeats of the imaging measurement are made with the same PLD, resulting in several label and control pairs, which are then averaged to gain improved SNR.

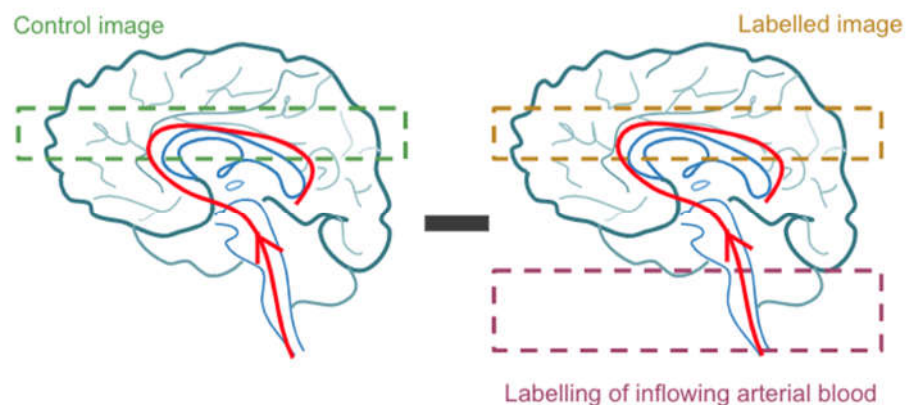


**Figure 2.5.2.:** *Generic schematic of the labelling process used for arterial spin labelling of the brain. Control and labelled images are acquired, with the labelled image acquired using an RF pulse to invert the spins of water protons within the target arteries - this labelling can then be imaged once the blood has had time to reach the capillary bed. The control image is collected without such a label, for fully recovered inflowing blood, and the images are then subtracted to form a perfusion-weighted image.*

#### 2.5.2.1.1. Variants of arterial spin labelling

The aforementioned difference between an image which has been labelled, and a control image with no labelling, is the basis of ASL. However, there are different ways in which this labelling and subsequent generation of the paired label/control images can occur, namely continuous ASL (CASL, Williams et al., 1992), pulsed ASL (PASL, Edelman et al., 1994; Kim, 1995; Wong, Buxton and Frank, 1998) and pseudo-continuous ASL (PCASL; Dai et al., 2008), which falls between CASL and PASL. Within this thesis, only PCASL is used, however understanding of both CASL and PASL informed the creation of PCASL, and thus all these methods are discussed below, with differences in acquisition summarised in *Figure 2.5.3.*

#### **Continuous ASL**

This approach involves the continuous excitement of blood, by merit of an RF pulse of low amplitude, in a single plane (Williams et al., 1992). This pulse is normally of a few seconds duration, in order to maximise the available signal. The CASL approach results in high SNR, however application of an RF pulse can result in the limits of SAR being reached, which has various implications, including significant tissue heating (see *Section 2.6.* for a summary).

Additionally, CASL can also be harder to achieve on scanner hardware due to the duration of the application of the RF pulse used. CASL acquisitions are not employed within this thesis.

#### **Pulsed ASL**

Pulsed ASL involves a slightly different approach to acquisition, with labelling occurring over a large slab surrounding or near the imaging plane, with a single, spatially-selective adiabatic inversion RF pulse applied. Where this labelling slab is positioned, and the pulse sequence which labels the blood, are what distinguish different PASL approaches, such as flow-sensitive alternating inversion recovery (FAIR, Kim, 1995), and echo-planar MR imaging and signal targeting with alternating radiofrequency (EPISTAR, Edelman et al., 1994). These are beyond the scope of this thesis, and as such will not be discussed further here.

### **Pseudo-continuous ASL**

PCASL was created to employ the basic theoretical underpinnings of CASL, with modifications to address its SAR limitations (Dai et al., 2008). The noticeable change in the technique is the use of repetitive short RF pulses, rather than a single, extended application. This train of short RF pulses is advantageous, as it mimics continuous excitation and delivers the SNR benefits of continuous labelling, whilst only necessitating a portion of the RF power. However, the limitations of SAR can still be reached quickly, and thus both CASL and PCASL approaches are principally suited for field strengths of up to 3T. PCASL is now the preferred acquisition for ASL imaging (Alsop et al., 2015), and with most clinical scanners having a  $B_0$  field strength of 1.5T, this is not a major limitation for clinically-translatable investigation.

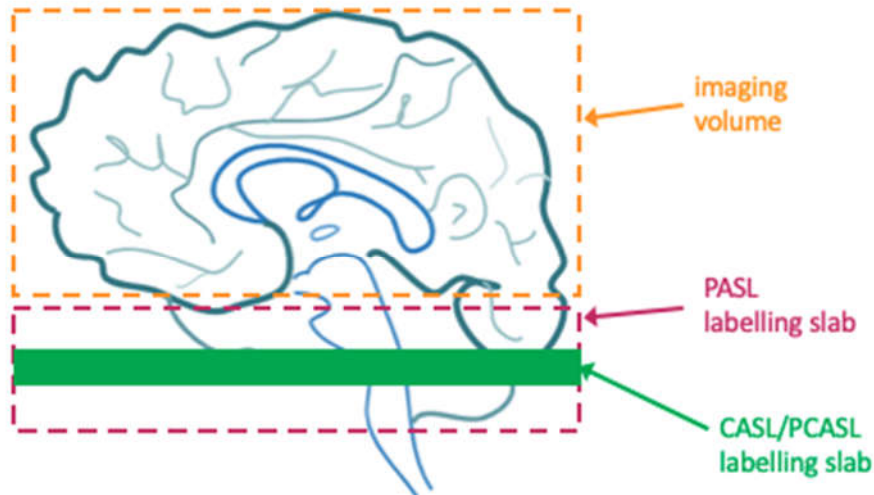


**Figure 2.5.3.:** Summary of the differences in labelling strategies for CASL, PASL, and PCASL.

#### 2.5.2.1.2. Labelling duration

The term ‘labelling duration’ is used differently when referring to PASL data, compared with CASL and PCASL. In PASL, the whole bolus is labelled at time  $t=0$  and occurs over a volume, and thus the bolus has a length,  $L$ , rather than a duration. Label and control images are subsequently acquired at time  $t=TI$ . However, for CASL and PCASL, blood is labelled as it flows through a thin plane, with all blood that passes through during a defined time – labelling duration,  $T$  – being labelled. Thus, the labelling duration of the bolus is defined in time, rather than space, as  $t=0$  to  $t=T$ . Label and control images are then acquired after a subsequent PLD.

#### 2.5.2.1.3. Post-label delay

The PLD of an ASL sequence refers to the time between labelling in the neck, and when the image is acquired within the imaging volume, summarised as

the time between time  $t=T$  and time  $t=(T+PLD)$ . Selection of this time is imperative, as if too short a duration is chosen then blood will not have reached the imaging volume, and if too long, the inverted magnetisation of the blood water protons will return to their non-inverted, unlabelled state. This is of particular relevance given the necessity to acquire pairs of images, and improper selection could result in tagged blood being present within the control image, and an absence of tagged blood within the “labelled” image. For PCASL imaging, the ASL white paper – a consensus paper which aims to provide guidance for clinical implementation of ASL – recommends a PLD of 1800ms for healthy adults <70 years old, 2000ms for 70 years old and above, and 2000ms for adult clinical patients (Alsop et al., 2015).

All early ASL experiments used a single PLD, estimating perfusion from the single time point data (Detre et al., 1992). However, this is not always ideal, as it can result in quantification errors due to lack of sampling throughout the signal curve and neglects the time at which the blood reaches the imaging slab, known as the arrival time. As such, some approaches implement multi-PLD acquisitions, whereby imaging measurements are repeated at multiple time points (PLDs) after labelling, thereby enabling more nuanced sampling of the ASL signal curve, and providing information regarding arrival time (Gunther, Bock and Schad, 2001). Despite the advantages of multi-PLD, the single-PLD approach is still often used today and is the consensus recommendation of the ASL white paper (Alsop et al., 2015).

#### 2.5.2.1.4. [Two-dimensional and three-dimensional approaches to ASL](#)

Early implementation of ASL imaging involved acquisition of information from a single slice. Naturally, this limits the information which can be gained, likely missing nuances of perfusion that occur elsewhere within the brain. As such, both two-dimensional (2D) and three-dimensional (3D) multi-slice methods became available.

A 2D multi-slice acquisition involves a readout where one slice is read out at a time, building up a 3D volume from these slices. This results in each slice having slightly different PLD, with the bottom slice acquired at the true PLD, and the subsequent slice acquired at a true PLD comprising the quoted PLD plus some multiple of the slice acquisition time. The resultant slice-to-slice signal variance and the differing relaxation effects in distal and proximal slices can be corrected by accounting for the slice-specific PLD when estimating voxel-wise perfusion in some instances, but encouraged the use of 3D approaches, where the PLD remains fixed over all slices (Alsop et al., 2015). Three-dimensional acquisition also results in higher SNR and greater spatial resolution, although can cause blurring in the inferior-superior direction (Chappell, MacIntosh and Okell, 2018).

#### 2.5.2.1.5. Quantification of cerebral perfusion

Simply subtracting the label and control from each other would generate an image which illustrates perfusion, however various pre-processing steps are often carried out to achieve greater accuracy in such analysis. These can be considered essential to perfusion quantification (such as calibration), or non-essential but theoretically advantageous to the research question, such as

motion correction, partial volume correction, and spatial smoothing, as described below.

### **Standard model for quantification of perfusion**

To aid interpretation of the ASL difference image, quantifying findings as generic ml/100g/min units can be additionally informative and aid in comparison of findings across the related literature. The standard model for quantification of perfusion in single-PLD ASL acquisitions is calculated as follows (Buxton et al., 1998; Alsop et al., 2015):

$$CBF = \frac{6000 \cdot \lambda \cdot (SI_{\text{control}} - SI_{\text{label}}) \cdot e^{-\frac{PLD}{T_{1,\text{blood}}}}}{2 \cdot \alpha \cdot T_{1,\text{blood}} \cdot SI_{PD} \cdot (1 - e^{-\frac{\tau}{T_{1,\text{blood}}}})} \text{ [ml/100g/min]}$$

[2.3]

Where  $\lambda$  refers to the partition coefficient of the brain/blood (ml/g), the time-averaged signal intensities in the control and label images are represented by  $SI_{\text{control}}$  and  $SI_{\text{label}}$ , respectively. Longitudinal relaxation time of blood (in seconds) is referred to by  $T_{1,\text{blood}}$ , and the efficiency of the label by  $\alpha$ . The duration of this label is represented by  $\tau$ , and the signal intensity of a proton density weighted image by  $SI_{PD}$ . PLD is defined earlier within this chapter. The factor of 6000 is included to align results with the norms of the literature, by changing the quantification units from ml/g/s to ml/100g/min.

Typical values for quantification of 3T PCASL are given in Alsop et al. (2015), as follows:

- $\lambda = 0.9$  ml/g (Herscovitch and Raichle, 1985)
- $T_{1,\text{blood}}$  at 3T = 1650ms (Lu et al., 2004)
- $\alpha$  for PCASL = 0.85 (Dai et al., 2008)

However, there are assumptions which underly this model and should be noted. Firstly, delivery of the full labelled bolus to the tissue of interest is assumed to have occurred. This relies on sensible selection of PLD time, and the arterial transit time (ATT, the time for the labelled bolus to travel to the volume of interest from the labelling plane) for that individual, which depends on their brain vasculature, but can be sensibly estimated based on age in healthy individuals. If this estimated ATT is not representative of the underlying anatomy of a given subject, this can affect perfusion quantification, leading to either over- or under-estimation of CBF. For example, very long ATT in an individual, whereby the labelled blood has not reached the imaging volume prior to readout, would lead to underestimated quantification. Hyperintense areas within the perfusion maps can occur when the labelled blood is within the imaging volume but has not yet reached the capillary bed. This results in over-estimation of perfusion values. Complete bolus delivery occurs when PLD is longer than ATT, and thus perfusion maps derived from a single-PLD subtraction image are only insensitive to ATT if the PLD is long enough.

Another assumption which underpins the quantification of perfusion is that T1 relaxation governs the decay of the blood label. There are errors that are introduced with this assumption, as blood and tissue T1 values differ, but these tend to be small.

### ***Calibration***

To achieve absolute units of perfusion, calibration is required. This process normalises the perfusion weighted image to the equilibrium magnetisation of blood, through collection of an  $M_0$  image, and results in a perfusion map. Such a map is a preferable description of perfusion, as a single value negates the variance in blood magnetisation which occurs due to  $B_1$  inhomogeneity, or coil sensitivity. Calibration can be an active pre-processing step, however within this thesis it is carried out as part of an automatic reconstruction process (Zaharchuk et al., 2010).

### **Additional processing steps**

#### ***Motion correction***

As with all MRI techniques, minimal movement is required to acquire good-quality ASL data. Given that ASL is a subtraction technique, this is particularly important to avoid, as movement of the head can result in misalignment of the label and control images which leads to imperfect subtraction of static background tissue signal. The process of motion correction realigns label/control pairs to a single image. It can be especially helpful when imaging patient groups who display symptoms relating to involuntary movement or have other challenges with remaining still within the scanner environment. Algorithms for motion correction of ASL may be computed automatically as part of data reconstruction (Zaharchuk et al., 2010), or carried out using tools such as FSL-MCFLIRT (Jenkinson and Smith, 2001; Jenkinson et al., 2002; Greve and Fischl, 2009).

### ***Partial volume correction***

Perfusion maps obtained from ASL acquisition will comprise data from a variety of tissue types, with a single voxel in the brain often containing cerebral GM, WM, and cerebrospinal fluid (CSF). This mixed tissue composition is a consequence of limited spatial resolution and the intrinsically low SNR of ASL, which necessitates use of larger voxels in order to acquire images with acceptable SNR. Due to this low resolution, partial volume effects (PVE) can occur, resulting in the perfusion value in any voxel comprising a weighted sum of the (potentially very different) perfusion values of the different tissues in that voxel – where the weights are the proportions of the voxel occupied by each tissue – such that:

$$voxel_{CBF} = PVE_{GM} * CBF_{GM} + PVE_{WM} * CBF_{WM} + PVE_{CSF} * CBF_{CSF}$$

[2.4]

where  $voxel_{CBF}$  is the cerebral blood flow within a given voxel,  $PVE_{GM}$ ,  $PVE_{WM}$ , and  $PVE_{CSF}$  are the partial volume estimations for GM, WM and CSF, and  $CBF_{GM}$ ,  $CBF_{WM}$  and  $CBF_{CSF}$  refer to the cerebral blood flow (CBF) within GM, WM and CSF, respectively.

The impact of the PVE on GM perfusion measures is more pronounced at GM/WM and GM/CSF boundaries, as well as with increasing voxel size, and decreasing tissue thickness such as that seen in GM atrophy (Chappell et al., 2021). For most investigations, the perfusion of only one type of tissue will be

of interest for analysis, and thus it is advantageous to separate these and distinguish the respective contributions of each, through partial volume correction (PVE-correction). Various strategies can be employed to achieve this. Many researchers choose to employ the linear regression method described in 2008 by Asllani, Borogovac and Brown. This method uses a kernel-based approach with the underlying assumption that GM perfusion in the voxel of interest is equal to that of the surrounding voxels within the kernel. Such kernels are usually  $5 \times 5 \times 1$  or  $7 \times 7 \times 1$  voxels large, resulting in a system of either 25 or 49 simultaneous versions of equation  $X$ , in which  $CBF_{GM}$  and  $CBF_{WM}$  are the only unknowns, and an approximate solution can then be achieved. However, these kernels are large, and therefore assume that perfusion in a specified voxel is affected by voxels that are situated far from it, resulting in image blurring. A more recent modified least-trimmed squares (mLTS) approach has been shown to improve PVE-correction for single-TI ASL (Liang, Connelly and Calamante, 2013), by reducing such blurring without demanding additional computational power. This method follows the same theoretical underpinnings, but the process of finding an approximate solution to the simultaneous equations differs. In this approach, the algorithm determines which voxels within the kernel are relevant and ignores contributions from voxels that it determines are irrelevant, thereby reducing blurring. This is the approach employed for PVE-correction within this thesis.

### ***Spatial smoothing***

Spatial smoothing of ASL perfusion maps involves averaging data points with neighbouring data points, resulting in the reduction of high signal frequencies, whilst enhancing low signals. Such an approach can improve the SNR and address inter-subject variance in neuronal organisation and functionality by

increasing the overlap of brain regions beyond that which is achieved by registration. Statistical power can also be improved as smoothing increases the normality of the error distribution. Various strategies exist for smoothing, with little consensus, but one common approach is to use a Gaussian filter (Bibic et al., 2010).

Smoothing will always reduce the spatial resolution of the data and can hide nuanced abnormalities in perfusion. As such, this should be approached carefully, using the minimum amount of smoothing that is appropriate to the needs of the dataset, as it can induce partial voluming, and over-smoothing may result in misleading edge artifacts which can suggest hypoactivity where there is none. However, under-smoothing will have little positive effect on the data, but will still result in reduced spatial resolution.

#### 2.5.2.1.6. [Clinical applications of ASL](#)

Continued development of ASL has enabled its utility to be expanded beyond neuroimaging. As such, it has a vast range of clinical applicability, ranging from various neurological conditions such as ageing and dementia (Zhang, Gordon and Goldberg, 2017), stroke (Chalela et al., 2000; Zaharchuk, 2014), brain tumour (Järnum et al., 2010; Kong et al., 2017; Hales et al., 2019), and epilepsy (Lim et al., 2008; Gaxiola-Valdez et al., 2017), to body imaging of organs such as the liver (Martirosian et al., 2019) and kidneys (Odudu et al., 2018).

ASL also produces results comparable to those of PET techniques (Dai et al., 2008; Xu et al., 2010; Weyts et al., 2017), and is preferable in many clinical populations as it does not require use of a radiotracer. However, despite growing clinical applicability, ASL is not used as an individual diagnostic tool, currently requiring complementary structural images to aid clinical interpretation.

### 2.5.3. Magnetic resonance spectroscopy

MRS can be highly complementary to ASL measures. Where ASL infers the manner in which energy is used throughout the brain by merit of perfusion, MRS is able to measure the concentration of various metabolites within a specific volume of interest (VOI). As with ASL, MRS expands on the basic principles of NMR and employs specialised approaches to enable such measurements. The theory underlying such acquisition is discussed at length in the following sections, focusing on  $^1\text{H}$  MRS, the nucleus of interest within this thesis.

#### 2.5.3.1. *The origin of the MRS signal*

When an RF pulse with a specified flip angle is applied, spins oscillate at a specific frequency, resulting in a measurable signal in the  $xy$  plane, the amplitude of which is reduced by the associated transverse relaxation effects. The magnetisation vector can be decomposed into two components, which can be measured individually using quadrature detection (see Glover et al., 1985), and recombined into an FID signal. In order to generate a spectrum, conversion from the time domain to the frequency domain is required, which is achieved by application of a Fourier Transform. Real and imaginary parts of

the spectrum can then be achieved – the real part is the absorption signal, and the imaginary part corresponds with the dispersion signal (see *Figure 2.5.4.*).

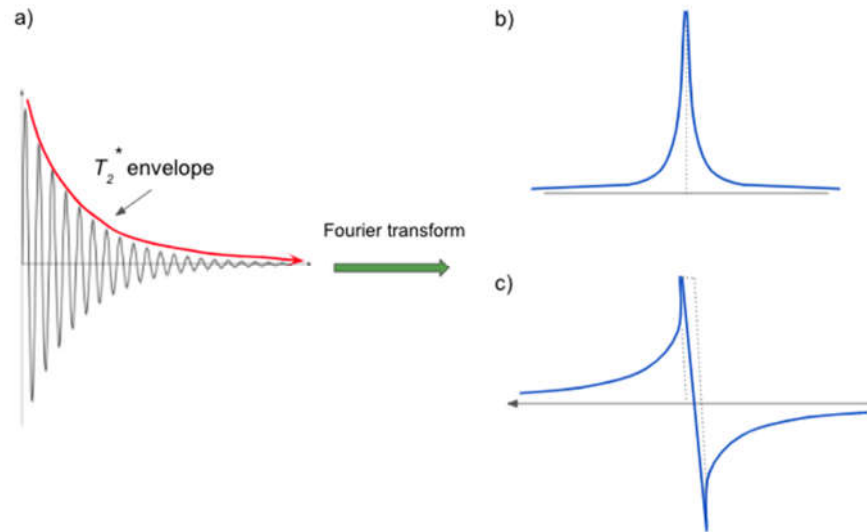


**Figure 2.5.4.:** Summary figure depicting (a) the free induction decay, with the red curve depicting the  $T_2^*$  envelope, and (b) and (c), real and imaginary components of the complex free induction decay signal, which have been Fourier Transformed.

The real part of an MRS spectrum is Lorentzian-shaped, which appears broader and of lower amplitude under conditions of shorter  $T_2^*$  relaxation, with the area under the peak remaining the same. This is important, as the area under the curve provides essential information about the spectrum, which is indicative of the number of protons within a sample. For MRS, the real part is most commonly used, as the imaginary spectrum is broader, thereby compromising the resolution of the spectra. FID acquisition parameters have a close relationship to spectral features, and directly affect the resolution of a resulting spectrum.

For example, in Chapter 5 the sequence used has a sample frequency of 4kHz, with 4096 sample points, resulting in an acquisition time of approximately 1 second.

#### 2.5.3.2. *Effect of spin interaction in MRS*

Spins can interact with the surrounding environment in various ways, and the way in which these interactions happen will result in different features within the spectrum, such as:

- Chemical shift
- J-coupling
- Dipolar coupling
- Quadripolar coupling
- Spin-rotation

Given the fast speed of molecular rotational motion in liquid, dipolar coupling averages to zero, and the contribution of spin-rotation interactions are also cancelled for the same reason. The effects of quadripolar coupling are not present for nuclei where  $I = \frac{1}{2}$  spins, such as  $^1\text{H}$ , and as such are beyond the scope of this thesis. Chemical shift and j-coupling most affect the signal achieved in *in vivo* MRS, and thus are discussed at length below.

##### 2.5.3.2.1. *Chemical shift*

A basic theoretical underpinning to the acquisition of an MRS spectrum is that the chemical environment in which a spin occurs affects its resonance frequency (Proctor and Yu, 1950). Molecules contain electrons, which

generate their own magnetic moment which either adds to or opposes the applied field, which is known as electron shielding. Spins with greater shielding experience a lower magnetic field and hence have a lower Larmor frequency. With each nucleus, the electron density surrounding it is also determined by both the type of nucleus and the bonds in the associated molecule. As a result, nuclei will vary in their frequency of resonance within different chemical environments. This difference in frequency dependent upon variation in distribution of electrons is known as the chemical shift, and the position and number of these shifts can be exploited for the identification of specific molecules, by merit of their structure. The chemical shift predominantly occurs intramolecularly, but intermolecular interactions also contribute significantly to this phenomenon (Levitt, 2013). It is also field-dependent, thus improved spectral resolution is achievable at higher field strengths, given the greater signal discrimination.

### **Chemical shift referencing**

The chemical shift can be referenced to identify the spectral position of peaks of interest. The scale used is normally expressed in parts per million (ppm, Harris et al., 2001, see *Figure 2.5.5*). Reference compounds are used, which must give a strong signal – often the highest peaks visible within the spectrum – whilst also being chemically inert and unaffected by changes in temperature and pH. N-acetylaspartate (NAA, 2.01 ppm) and total creatine (tCr) are commonly used as internal references within the brain, and sodium trimethylsilylpropanesulfonate (DSS) within aqueous solutions and phantoms (Wishart et al., 1995).

Despite these characteristics enabling the measurement of various metabolites, overlapping of metabolite resonances is common, due to the limited dispersion of the chemical shift. Most visible molecules have resonances which all occur within a narrow chemical shift range of approximately 10 ppm. By utilising higher field strengths, it is possible to achieve greater spectral separation, and thus make metabolites easier to identify and quantify.

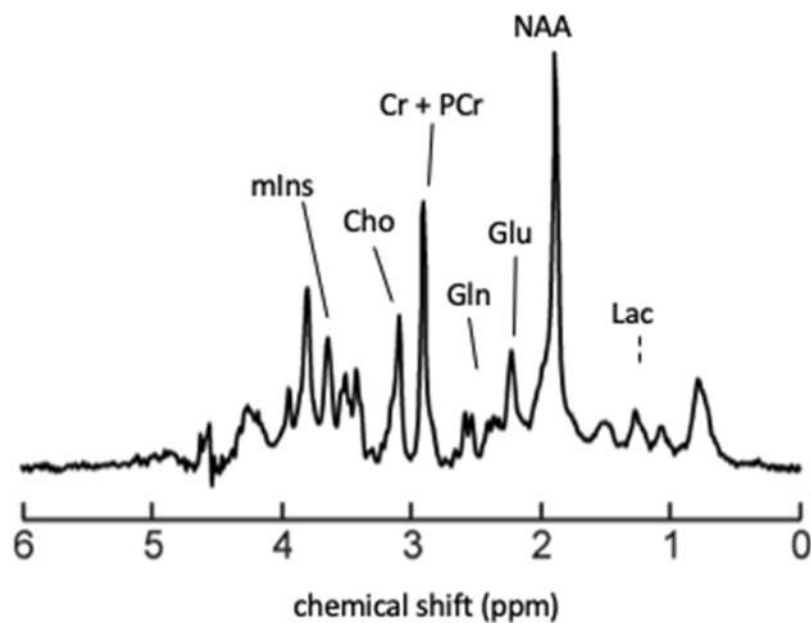


**Figure 2.5.5.:** Example spectrum acquired at 7T using a stimulated echo acquisition mode (STEAM) sequence in the posterior cingulate cortex, with TE = 14ms. Lactate appears at 1.31ppm but is not clearly evident within this spectrum due to contamination of macromolecules occurring at short TE.

### **Chemical shift displacement**

Chemical shift displacement is a type of artefact which can occur in MRS and is most challenging when using single voxel spectroscopy at ultra high-field,

as this increases with  $B_0$ . It is analogous to chemical shift artefacts which are common in conventional MRI, whereby spatial misregistration of cerebral fat and water molecules occurs. Given the necessity for precise localisation within MRS, in order to accurately identify metabolites of interest, chemical shift displacement is of great theoretical importance. It is of particular issue in coupled spin systems, where component parts may exhibit different behaviours due to their respective chemical shifts. This can lead to chemical shift displacement artefacts, by merit of associated compartmental evolution (Maudsley et al., 2005; Fernandes et al., 2021).

#### 2.5.3.2.2. J-coupling

J-coupling (also known as scalar coupling) is where neighbouring spins are linked together and influence each other through electron bonds. This creates a drift in the magnetic field between the two nuclei, modifying the magnetic field at the position of the coupled nucleus. J-coupling occurs on a solely intramolecular level (Levitt, 2013), and whilst it can reveal valuable information regarding the molecular structure, it can cause the signal intensity to be split across multiple coupled peaks, thus resulting in decreased SNR. For example, the effect of j-coupling interactions can be seen in the splitting of lactate – the lactate methyl ( $-\text{CH}_3$ ) resonance is split into a doublet, and the CH into a quartet (by the 3 protons of the ethyl group) (de Graaf, 2019). As such, j-coupling is an important consideration when determining the sequence of choice and associated parameters, with careful selection either compensating for or mitigating some of these effects. For example, a sequence with very short TE may be chosen so that j-coupling effects do not have time to evolve. Alternatively, a sequence may be designed to exploit the j-coupling, and

therefore maximise metabolite signal through use of a long TE, as in this thesis.

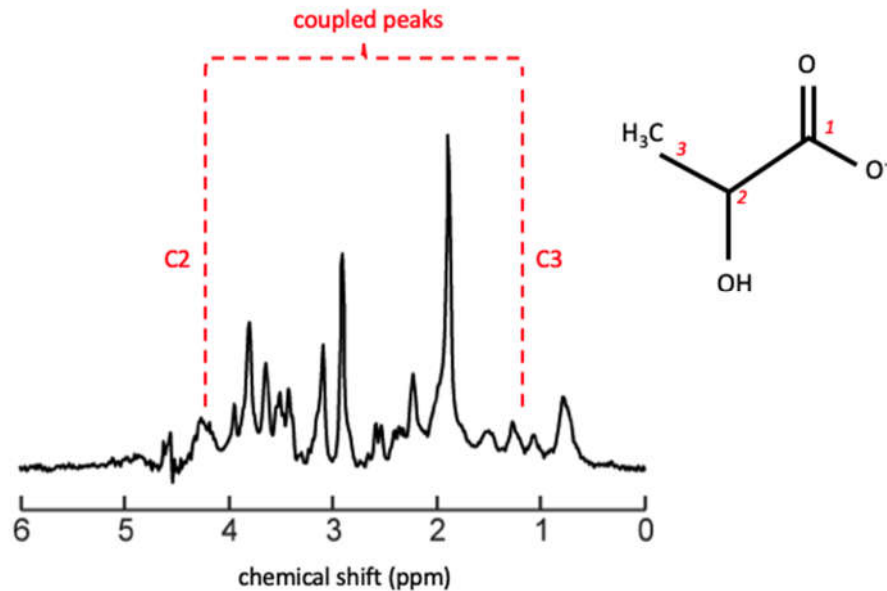


**Figure 2.5.6.:** Schematic depicting the relationship between the Lac doublet (at 1.31 ppm) and quartet (at 4.1 ppm).

### 2.5.3.3. Signal localisation in MRS

Single-voxel MRS methods also necessitate the application of field gradients for the determination of a specific volume within a sample, from which metabolites will be measured. By selectively exciting a small volume of tissue, the associated FID enables the production of a spectrum, with the concentration of each metabolite then reflected in the area of each peak.

#### 2.5.3.3.1. Sequences used for volume-localised spectroscopy

There are a few basic methods for volume-localised spectroscopy which are in general use, including STEAM (Stimulated Echo Acquisition Mode; Frahm,

Merboldt and Hänicke, 1969; Frahm et al., 1989), PRESS (Point-Resolved Spectroscopy; Bottomley, 1987) and ISIS (Image-Selected In Vivo Spectroscopy; Ordidge, Connelly and Lohman, 1986). Within this thesis, the semi-localized by adiabatic selective refocusing (semi-LASER) sequence is used (Scheenen et al., 2008). It is derived from the PRESS sequence and it is helpful to describe its operation before discussing the modifications to it which underpin the use of semi-LASER.

PRESS acquisition (*Figure 2.5.7.*) utilises a  $90^\circ$  excitation pulse to select a slice followed by two  $180^\circ$  refocusing pulses to isolate a VOI within the slice. Crusher gradients between these RF pulses dephase spurious signal originating from outside the specific VOI. A compensatory slice refocusing gradient ( $G_{sr}$ ) is employed after the  $90^\circ$  pulse to address phase dispersion which this pulse induces. Acquisition occurs at TE, comprising  $TE_1 + TE_2$ , or the combined time elapsing between the  $90^\circ$  pulse and first spin-echo, and first and second spin-echoes.

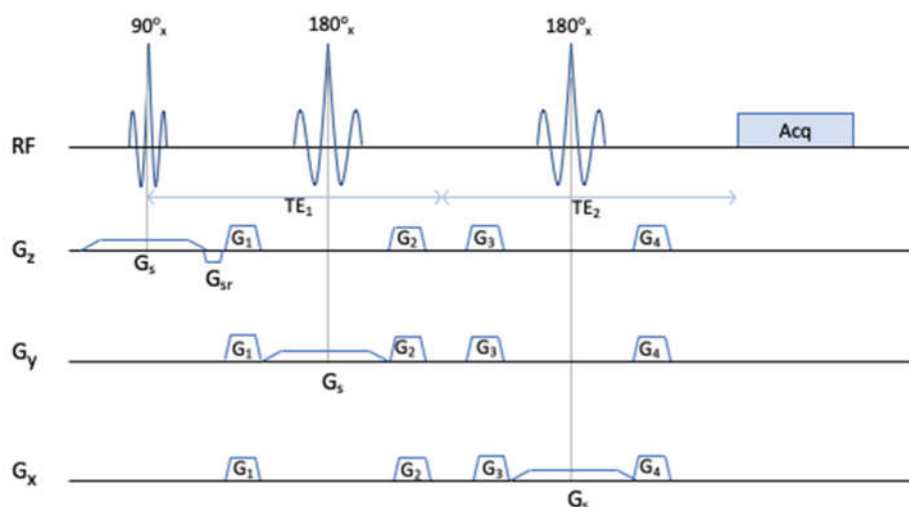


**Figure 2.5.7.:** PRESS sequence pulse diagram. The sequence consists of a  $90^\circ$  excitation pulse followed by two  $180^\circ$  refocusing pulses, generating a spin-echo at  $TE = TE_1 + TE_2$ . Slice selection gradients are represented as  $G_s$ , with  $G_{sr}$  the refocusing gradient, and  $G_{1,2,3,4}$  crusher gradients.

The semi-LASER technique comprises an excitation pulse followed by two pairs of adiabatic full passage (AFP) pulses. These pulses are independent of  $B_1$  (above a threshold) and mitigate the  $B_1$  inhomogeneity that occurs at high field. They are where semi-LASER differs from PRESS, and a summary diagram of the semi-LASER sequence is depicted in *Figure 2.5.8.* Where PRESS uses  $180^\circ$  pulses, these are substituted by pairs of AFP pulses in semi-LASER. The second AFP pulse in each pair enables refocusing of the nonlinear  $B_1$  and the phasing of the spins which was induced by the first pulse in the pair. Crusher gradients are also used between pulses, to eliminate signal from prior excitations, and a spin echo is generated at  $TE = 2(\tau_2 + \tau_4)$ , where  $\tau_2$  and  $\tau_4$  represent the time between the paired pulses for the first and second AFP pulse pair respectively.

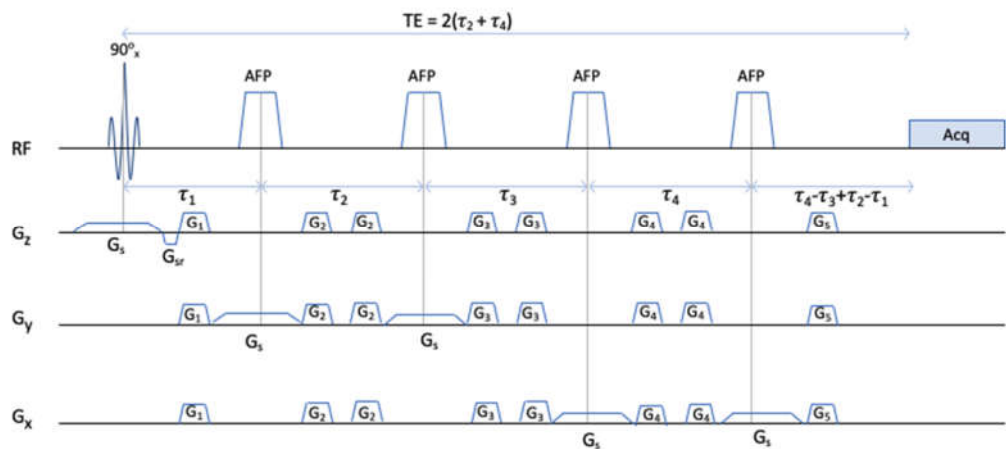


**Figure 2.5.8.:** Semi-LASER sequence pulse diagram. The sequence consists of a  $90^\circ$  pulse followed by two pairs of AFP pulses. Each AFP pulse is applied with a slice

*selection gradient  $G_s$ , the first of which is followed by a slice refocusing gradient,  $G_{sr}$ . Between the pulses, crusher gradients are also applied ( $G_{1,2,3,4,5}$ ) (Fernandes et al., 2020).*

Whilst PRESS is often used for Lac detection at clinical field strengths, the use of  $180^\circ$  pulses makes this sequence susceptible to chemical shift displacement artefacts. The use of  $90^\circ$  pulses within the STEAM sequence minimises these artefacts, due to the comparatively larger bandwidth. However, whilst not available with all scanner packages, semi-LASER is preferred at 7T, due to the improved spatial selection with use of AFP pulses. These pulses also help to address the problem of  $B_1$  inhomogeneity at high field, and sequence parameters can be designed such that the j-coupling of Lac is exploited, as is the case in this thesis.

#### *2.5.3.4. Saturation factors*

Within this thesis, saturation factors are a pertinent topic for consideration in the calculation of metabolite concentrations from spectra (see Chapter 5). When an RF pulse is applied, magnetisation tips into the  $xy$  plane, and is then allowed to recover for a time TR, after which a second RF pulse is applied. The TR is of a duration which does not allow the signal to fully relax, and the term 'saturation factor' refers to the amount by which the MR signal would be greater if this were allowed to happen (difference between  $M_0$  and  $M_{ss}$ , *Figure 2.5.9. B*). When applying multiple evenly-spaced RF pulses, magnetisation evolves into a steady state, whereby an equilibrium is reached at which the amount of recovery is the same each time, but is not full recovery to  $M_0$  (*Figure 2.5.9. A*).

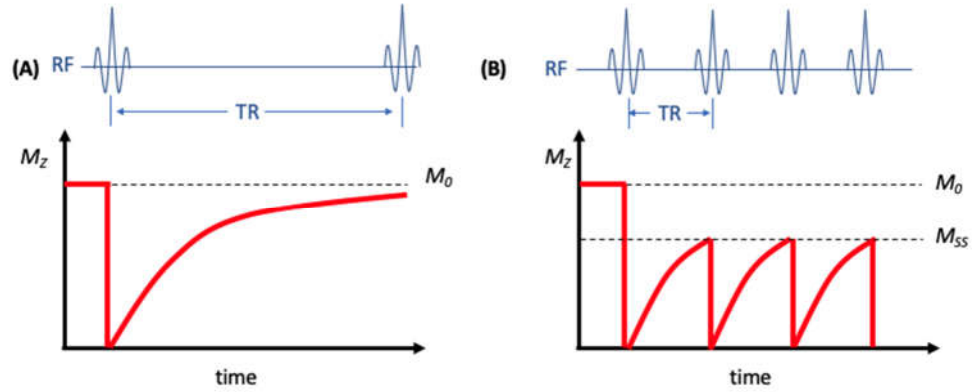


**Figure 2.5.9.:** Evolution of magnetisation into a steady state when using a  $90^\circ$  pulse. At a time  $t$ , an RF pulse is applied, tipping the magnetisation into the  $xy$  plane. In (A), the magnetisation is allowed to recover for a time TR, after which a second RF pulse is applied. When applying multiple evenly spaced RF pulses (B), the magnetisation will evolve into a steady state,  $M_{ss}$ . The ratio of  $M_0$  to  $M_{ss}$  is the saturation factor.

#### 2.5.3.5. Quantification of metabolites

To meaningfully understand the contribution of various metabolites within the spectrum, it is necessary to quantify them in an accurate and reliable manner. Peak extraction – whereby the area underneath a peak is measured – has previously been used but has been critiqued for its over-simplistic approach which ignores overlapping peaks within a spectrum (Landheer et al., 2020). Usually, metabolite quantification involves the use of basis sets, a combination of lineshapes which are created using experimental phantom measures or through simulation. For every metabolite relevant to a specific sequence, a  $^1\text{H}$  spectrum – measured or theoretically calculated – is included in the respective basis set. A measured spectrum is then fitted, with the assumption that it is a combination of the individual spectra within the basis set. The amount of each then gives the concentration of that metabolite. It is important for these to contain a complete set of relevant metabolites, as omission of metabolites from basis sets will result in biases in quantification (Hofman et al., 2002). It

may also be necessary to account for certain macromolecules within the basis set, as they may contaminate the peak of interest due to their proximity (see Fernandes et al., 2020), resulting in the misidentification, or over- or under-estimation of the peak of interest. They must also normally be tailored to the pulse sequence of choice and can be time-consuming to create.

Software is then used to quantify metabolites within the acquired spectrum. LCModel (Provencher, 1993) has long been the preferred software within the field and reports spectral quality with Cramér-Rao lower bounds (CRLB, Cavassila et al., 2001). CRLBs estimate the certainty (or lack thereof) of the metabolite concentrations, expressed as percentages, where a lower percentage suggests a more certain estimation. However, achieving low CRLB does not necessarily mean the fit of the spectrum to the basis set is “better”. CRLBs are higher with increased noise, and when there is more overlap of peaks. Thus, metabolites that are similar in structure and therefore appear at a similar location within a spectrum – such as creatine (Cr) and phosphocreatine (PCr), and NAA and N-acetylaspartylglutamate (NAAG) – can have high CRLBs when considered as individual compounds, but low CRLBs when summed (de Graaf, 2019). As such, they are often reported as combined pools. After completion of quantification, visual assessment is important, to ensure that metabolites have been accurately identified, and that the spectrum is of good general quality, i.e. there are no artefacts, metabolites of interest are clearly identified and fit well, and the spectrum is not too noisy.

It is important to note that absolute quantification of metabolites is challenging, and thus ratios of one metabolite relative to another are often reported. The

metabolite chosen for comparison is usually one which appears in high concentrations and is easily identified and unaffected by neurodegenerative disease. Cr has often been used for this, but as more accurate measurements are being made it is becoming clear that this is not a good idea, as Cr can vary significantly (Rackayova et al., 2017). As such, there has been a shift to attempting to determine absolute concentration, using water as a reference (Ernst, Kreis and Ross, 1993; Kreis, Ernst and Ross, 1993). To determine absolute concentrations, it is necessary to further account for subject variance in tissue composition, and saturation factors, to ensure that all subjects are on a comparable scale. A factor for  $T_2$  decay should also be included, particularly when using a long TE as in Chapter 5, given the differences in  $T_2$  by merit of tissue compartment.

#### *2.5.3.6. Functional magnetic resonance spectroscopy*

Functional MRS was developed to expand on the underlying principles of MRS. MRS is acquired at rest, and is therefore reflective of this state, with no information on how metabolism may vary temporally. fMRS furthers this by additionally assessing the temporal changes in brain metabolism, through acquisition of multiple spectra. To achieve adequate SNR and temporal resolution, higher magnetic field strengths are required. Such field strengths also have the advantage of improved spectral resolution, which enables detection of more metabolites and their associated dynamics.

Despite the information which can be gained using fMRS, it is a challenging technique, necessitating sophisticated approaches to acquisition and data quantification, as well as careful interpretation of findings. Not all metabolites

can be detected by fMRS or may require tailored sequences and parameter selection to measurement a specific peak of interest, such lactate at 7T using a long TE and a semi-LASER sequence (Fernandes et al., 2020). Currently, fMRS also requires a VOI of at least 1cm<sup>3</sup> and due to this limitation certain regions of the brain are either too small or close to CSF or ventricles or may be more likely to result in spectra containing contaminant signals from pericranial lipids. As such, many studies investigate a VOI within the visual cortex, where good MRS signal can be achieved.

#### *2.5.3.7. In vivo applications of MRS and fMRS*

MRS research has benefitted greatly from the increased spectral resolution and SNR available at ultra high-field, with ~17 different metabolites simultaneously detectable within the healthy brain at 7T, when considering <sup>1</sup>H-MRS (Melke et al., 2009). Pulse sequences are normally designed to focus on the measurement of specific metabolites, as these metabolites often have specialised functions within the brain. For example, Lac, Glc and tCr (comprising both Cr and PCr) are involved in cerebral metabolism (Béard and Braissant, 2010; Magistretti and Allaman, 2018), with NAA a neuronal marker, and total choline (tCho, comprising various choline-containing compounds) involved in membrane synthesis (Urenjak et al., 1993; Vion-Dury et al., 1994; Clark et al., 1998). Multiple metabolites are also involved in neurotransmission, including GABA, Glu, Gln, and aspartate (Asp) (Newsholme et al., 2003; Farooqui, Ong and Horrocks, 2008), astroglial marking (myo-inositol [mIns], Harris, Choi and Brooks, 2015) and anti-oxidative processes – GSH and taurine (Tau) (Dringen, 2000; Niu et al., 2018). *Table 2.5.1.* summarises these roles, alongside their expected

concentrations within the healthy brain (de Graaf, 2019), and their spectral position.

**Table 2.5.1.: Key metabolites detectable using <sup>1</sup>H-MRS, their metabolic roles within the brain, spectral position (Govindaraju, Young and Maudsley, 2000), and their expected concentrations within the healthy brain (de Graaf, 2019).**

<b>Metabolite</b>	<b>Role</b>	<b>Spectral position (ppm)</b>	<b>Concentration in healthy brain (mM)</b>
<b>Lactate</b>	Metabolite by-product of glycolysis	1.31, 4.10	0.2 - 1.0
<b>Glucose</b>	Main cerebral energy source	3.23 - 3.88	1.0 - 2.0
<b>NAA</b>	Marker of neuronal viability	2.01, 2.49, 2.67, 4.38	7.5 - 17.0
<b>Total creatine</b>	Crucial in energy metabolism, alongside ATP	3.03, 3.91	Cr (4.5 - 10.5) PCr (3.0 - 5.5)
<b>Glutamate</b>	Key excitatory neurotransmitter	2.04 - 2.35, 3.74	6.0 - 12.5
<b>Glutamine</b>	Involved in recycling of glutamate	2.11 - 2.45, 3.75	3.0 - 6.0
<b>GABA</b>	Key inhibitory neurotransmitter	1.89, 2.28, 3.01	1.0 - 2.0
<b>Myo-inositol</b>	Glial marker	3.27 - 3.61, 4.05	4.0 - 9.0
<b>Total choline</b>	Phospholipid synthesis/ degradation	3.19, 3.50 - 4.05, 4.28	0.5 - 2.5
<b>Glutathione</b>	Key antioxidant, which defends against oxidative stress	2.15, 2.51, 2.93, 3.77	1.5 - 3.0
<b>Aspartate</b>	Excitatory neurotransmitter	2.65, 2.80, 3.89	1.0 - 2.0
<b>Taurine</b>	Osmoregulation, and modulation of neurotransmission	3.25, 3.42	2.0 - 6.0

Clinically, <sup>1</sup>H-MRS has applicability as a tool for diagnosis, prognosis, and treatment response, however like ASL this is only used to complement structural imaging, rather than as a standalone technique. Despite this, it is a powerful tool which can probe cerebral neuroenergetics in healthy brains, as well as in various conditions, such as neurodegeneration (Martin, 2007), oncology (Murphy et al., 2002; Howe et al., 2003; Majós et al., 2003; Wilson et al., 2013), epilepsy (Connelly et al., 1994; Hammen and Kuzniecky, 2012), schizophrenia (Thakkar et al., 2017; Romeo et al., 2020), and depression (Auer et al., 2000; Hasler et al., 2007; Godlewska, Near and Cowen, 2015).

Whilst MRS has been used to assess a wide range of clinical conditions, fMRS tends to be used in research studies, which often compare healthy and patient populations. Key research using <sup>1</sup>H-fMRS within the brain has included the influence of visual stimulation on healthy brain metabolism (Mangia et al., 2007; Fernandes et al., 2020), colour-word Stroop tasks in patients with schizophrenia and major depressive disorder (Taylor et al., 2015), and verbal working memory tasks in patients with mild cognitive impairment (MCI) and healthy controls (Vijayakumari et al., 2020).

## 2.6. General MR safety considerations

MRI does not cause any known medical side effects, provided general safety is considered. This is highly advantageous when compared with other commonly used diagnostic imaging techniques which necessitate the use of x-

rays or other forms of ionising radiation, which can be inappropriate for use in certain patient groups (Lin, 2010).

Any subject who undergoes MR imaging must complete a safety screening prior to scanning and entering the scanner environment and must not be allowed beyond the 5 Gauss line (0.5 millitesla [mT]) if they have any contraindications or implants which can malfunction near magnetic fields, such as pacemakers, cochlear implants, or aneurism clips. Safety screening also minimises the risk of interactions with the RF field by merit of metallic objects, which can result in thermal burns. It is also imperative that any magnetic objects are not taken into the magnet hall, and MR-safe alternatives for items such as trolleys and fire extinguishers are used. Some items which researchers and subjects often carry are also magnetic (such as bank cards or coins), and thus these items must be removed when within the scanner vicinity. This is due to the risk of any such objects acting as projectiles, which will be attracted towards the bore at great force, risking damage to both the scanner and any individual who may be in the trajectory of the projectile.

Tissue heating is of great concern when considering MR safety, as in its severe form it can cause thermal burns, due to the absorption of RF radiation by the body. Tissue heating is defined by the SAR, a measure of the power absorbed per unit mass of tissue, given in watts per kilogram (W/kg).

Monitoring of this rate is imperative, and core body temperature should not increase by more than 1°C (Internal Commission on Non-ionising Radiation Protection guidelines, 2020), but proper subject screening should minimise this risk. Some risks can be more challenging to avoid, for example some

tattoos which have used older ink can also pose a risk of heating effects, due to the metal included within these dyes (Alsing et al., 2020). Additionally, certain crossed positions of body parts such as arms and feet, and the formation of current loops with items inside the scanner – such as emergency alarms and headphones – can result in the induction of currents, resulting in thermal burns, and should be avoided (Dempsey and Condon, 2001).

Particularly at ultra high-field strengths, a variety of uncomfortable physiological symptoms can temporarily occur whilst moving the subject through the static field to be positioned within the scanner bore. These can include – but are not limited to – nausea, a metallic taste in the mouth, claustrophobia, and dizziness (Versluis et al., 2013), and as such subjects should be moved into the bore slowly, to minimise these effects as much as possible. Peripheral nerve stimulation (PNS) is an additional uncomfortable sensation which subjects may experience, caused by rapid gradient switching. This is a twitching or numbness which is induced by currents within the nerves, and particularly affects the extremities. Minimisation of PNS effects can be largely aided by appropriate selection of a scan protocol. Additionally, a maximum slew rate is often set. The slew rate refers to the speed at which the gradient can be turned on and off, and as such can minimise such PNS effects.

Irrespective of the sequence used, MRI is associated with a lot of acoustic noise, due to rapid gradient coil switching, and ear protection must therefore be worn. This normally comprises a combination of earplugs, headphones and foam padding, depending on the space available within the coil. It is important

to acknowledge that MRI examination is often a cause of anxiety and claustrophobia for subjects, particularly those who are unfamiliar with the scanner environment (Katz, Wilson and Frazer, 1994; Munn and Jordan, 2011; van Minde, Klaming and Weda, 2014; Tazegul et al., 2015). As such, time should be taken to satiate such fears by answering any questions that subjects may have and providing reassurance where necessary. MR scanners are fitted with speaker systems to enable communication throughout the scan, and an emergency alarm for subject use if required. This alarm is tested prior to every scan, and if sounded during a session, the scanner operator will attempt to clarify the emergency using the speaker system and remove the subject from the scanner if necessary. If the reason for removal is an emergency, the trained first aider within the research group will take over, and the emergency services will be contacted. The scanner bed may be removed from the magnet room, if possible, but if it is necessary for emergency services to enter the magnet room, a staff member must ensure that no magnetic items are brought with them. Any such incidents or adverse effects must be documented on the scan record, which is completed after each scan. Serious incidents should be reported to the study lead or Principal Investigator, and to the funding body if required.

## 2.7. Summary

This chapter opened by exploring the theoretical principles which underpin NMR and MRI and are crucial to the understanding of the ASL and fMRS experiments carried out as part of this thesis. The theoretical nuances of ASL and fMRS approaches were then discussed, and these are applied in subsequent chapters of this thesis.

### 3. Brain perfusion changes in healthy ageing: on the role of pattern analysis and spatial coefficient of variation

#### 3.1. Introduction

There has been considerable interest in using neuroimaging to elucidate the brain changes seen in healthy ageing and age-associated health conditions. Assessment of cerebral perfusion is of particular interest, given its relationship with metabolic demand of the cerebral tissue (discussed further in Chapters 1 and 2) and thus its potential to indicate and differentiate metabolic alterations due to healthy and pathological brain ageing. Cerebral perfusion is tightly regulated to ensure the maintenance of healthy blood flow, as the implications of both hyperperfusion and ischaemia are serious, and can lead to permanent damage to the delicate tissues of the brain. Normal perfusion within the brain varies depending on tissue, with normative perfusion values of ~35-80 ml/100g/min in GM, and ~20 ml/100g/min in WM (Huang et al., 1983; Parkes et al., 2004; Alsop et al., 2015; Leidhin et al., 2021). Despite this tight regulation, both transient and prolonged physiological variance can occur. For example, transient localised increases in blood flow occur with brain activation, due to a coupling between cerebral activation and perfusion (Kuschinsky, 1991; Paulson, 2002), whereas prolonged decreases are thought to occur with age (Leenders et al., 1990; Bentourkia et al., 2000; Parkes et al., 2004; De Vis et al., 2015; Zhang, Gordon and Goldberg, 2017). However, these age-related changes still tend to remain within the aforementioned normative bounds when an individual is healthy (Leidhin et

al., 2021). Pathological changes in perfusion can be related to both hypo- and hyper-perfusion, and can result in ischemia, stroke and haemorrhage (Baron, 2001; Qureshi et al., 2002; Jordan and Powers, 2012; Prabhakaran and Naidech, 2012; Demeestere et al., 2020). The resultant damaged tissue can potentially be salvaged if appropriately re-perfused in a timely manner, as in the ischemic penumbra (Hakim, 1998; Fisher and Bastan, 2012), but will otherwise be permanently damaged. Ageing is a risk factor for both pathological cerebrovascular changes and neurodegeneration (Kelly-Hayes, 2010; Hou et al., 2019), with vascular dysregulation an early pathological event in the onset of AD (Iturria-Medina et al., 2016). As such, investigation of cerebral perfusion in healthy individuals across the adult age span would be desirable for the elucidation of a robust and sensitive method which can differentiate perfusion changes during healthy ageing from disease detection.

Many perfusion studies have reported that cerebral perfusion decreases with age, but details of the associations remain unclear. There is a challenging bidirectional association between cerebral perfusion and underlying brain atrophy, which can be difficult to disentangle, particularly given that both atrophy and CBF changes occur at differing rates throughout the brain (Terribilli et al., 2011; Romanowski and Wilkinson, 2011; Chen, Rosas and Salat, 2011). A study of 3,011 subjects followed up at 3.9 years, by Zonnewald et al. (2015), used phase-contrast MRI to investigate whether decreasing cerebral perfusion leads to atrophy or vice versa, and found that atrophy causes decreasing cerebral perfusion over time. However, Chen, Rosas and Salat (2011) found that significant regional tissue atrophy could be present alongside unaltered cerebral perfusion, suggesting that these changes are independent of one another. As such, control of brain atrophy

through use of an additional confounds such as GM volume or by correction for PVE is pertinent to the elucidation of true brain perfusion changes.

Multiple studies using both ASL and PET report CBF decline rates of around 0.37 - 0.5% per year (Leenders et al., 1990; Bentourkia et al., 2000; Parkes et al., 2004; De Vis et al., 2015). Such changes are seen especially within frontal, parietal and temporal lobes (Parkes et al., 2004). However, these studies do not account for PVE (see Chapter 2, Section 2.5.2.1.5.), meaning that the resultant perfusion values may be derived from voxels containing more than one type of tissue. Various studies argue that PVE-correction is imperative for elucidation of the true nature of cerebral perfusion changes which are due to age (Meltzer et al., 2000; Inoue et al., 2005; Curiati et al., 2011). Lu et al. (2011) account for PVE by correcting for GM and WM probability, and find a 0.14% decrease in global CBF per year. Asllani et al. (2009) found an age-related decrease of CBF of ~15% between their healthy young and healthy old cohorts (mean age difference = 43 years), after PVE-correction using a previously-developed algorithm, which is discussed in Section 2.5.2.1.5. of this thesis (Asllani, Borogovac and Brown, 2008). A recent large-scale, single-site study by Leidhin et al (2021) assessed variance in cerebral perfusion with age in a cohort of 468 healthy cognitively normal adults aged between 54 - 84 years. They thresholded GM at 70% to reduce the PVE, and found a decrease in CBF of 0.2ml/100g/min per year as age increased. However, their use of thick slices (8mm, with 1mm slice gap) for acquisition may have led to underestimations in CBF, given related PVE (Alsaedi et al., 2018). However, not all investigations using PVE-correction find significant decreases in CBF with age. Using oxygen-15 labelled water ( $[^{15}\text{O}]\text{H}_2\text{O}$ ) PET in healthy subjects, Meltzer et al. (2000) found apparent

significant differences in cortical CBF between young/midlife and elderly subjects no longer existed after PVE-correction using an MR-based algorithm which segmented brain and CSF through use of an optimal threshold value determined by fitting pixel signal intensities to Gaussian distributions.

The PVE has been shown to differ in males and females – in an ASL study by Allsani et al. (2009), the greatest contribution of PVE was found in the frontal lobe, and accounted for 10% (males) and 12% (females) of the age-related CBF differences, with an FDG-PET study by Ibáñez et al. (2004) evidencing a lack of significant reduction in males during ageing after PVE-correction. Multiple studies have also found that females have higher cerebral perfusion values than males. The largest single-site study using 3T PCASL-ASL within an elderly cohort (The Irish Longitudinal Study of Ageing [TILDA]; Leidhin et al. (2021)) found significantly higher average cerebral perfusion values in females than males (+3.1 ml/100g/min), although the aforementioned issues with slice thickness and PVE should be considered in the interpretation of these results. Another large-scale ASL study of 234 individuals within the Human Connectome Project - Ageing study also found significantly higher GM CBF values in females than males (Juttukonda et al., 2021), after PVE reduction through erosion of WM and subcortical GM masks. These findings are supported by multiple other studies, both with and without PVE-correction (Parkes et al., 2004; Liu et al., 2012; Soni, Jain and Kumar, 2016), however some have shown that these sex differences in cerebral perfusion do not occur in comparison of post-menopausal women and older males (Liu, Lou and Ma, 2016). Clearly, such findings highlight the necessity of PVE-correction in the elucidation of the relationship between brain perfusion and

age, particularly when investigating older individuals, however this processing step is currently under-utilised (Chappell et al., 2021).

Age-related brain changes do not occur uniformly across the brain, likely due to factors such as underlying differences in neuronal vulnerability. Particularly, oxidative stress is known to be implicated within this phenomena, due to the high oxygen requirements of the brain (Friedman, 2011) – whilst many neurones can compensate for changes in oxidative stress, there are certain neuronal populations which are more vulnerable. Such regions are usually the first to be implicated in ageing and neurodegeneration, and have been linked to conditions such as ischemia (Wang and Michaelis, 2010; Watts, Pocock and Claudianos, 2018). Additionally, inhibiting the effects of oxidative stress has been associated with healthy ageing (Vatner et al., 2020). Vulnerability to oxidative stress may therefore be associated with decreases in perfusion and metabolic changes (Castelli et al., 2019). Regional changes in perfusion might therefore be expected in age-related disease conditions, but have also been evidenced in healthy ageing. Chen, Rosas and Salat (2011) found age-related perfusion reductions in the superior-frontal, superior-parietal, middle-inferior temporal, orbitofrontal, lateral occipital, cingulate, precuneus, supramarginal and insular regions, and a relative sparing of subcortical tissue. Coupled with the aforementioned dissociation between CBF and structural changes they evidenced, which they suggest may be due to differential timings of physiological and structural changes, this highlights the utility of CBF in additionally informing on pathologic mechanisms of old age. However, the regionality of perfusion changes differs across studies, making robust regional perfusion biomarkers challenging to achieve. Lee et al. (2009) have shown that older individuals exhibit increased perfusion within the anterior cingulate

cortex (ACC), posterior cingulate cortex (PCC), amygdala and caudate, and decreases in perfusion in the precuneus, orbitofrontal and superior temporal regions in a PVE-corrected ASL cohort. Preibisch et al (2011) found age-related reductions in the cuneus, caudate and parietal cortex, alongside increases in the hippocampus, thalamus and calcarine gyrus. However, no statistically significant relationship between hippocampal perfusion and age has been found in other studies (Rusinek et al., 2011). Such findings are partially supported by the regionality shown in earlier PET and SPECT studies, with a PET study by Martin et al. (1991) evidencing age-related declines in the bilateral cingulate, medial frontal, parahippocampal, posterior parietal and superior temporal cortices, and left insular and posterior prefrontal cortex, and Nakano et al. (2000) used technetium-99m-ethyl cysteinate diethylester (99mTC-ECD) SPECT and found reductions in the ACC, prefrontal cortices, insular cortices and bilateral temporal poles. Pardo et al. (2007) also found reductions in the ACC and medial prefrontal cortex using FDG-PET. Many of the studies which investigate age-related perfusion changes are in fairly small cohorts, and regional findings are often challenged by other studies. Additionally, inter-subject perfusion variance in perfusion is large, up to 100% in subjects of the same sex and age (Parkes et al., 2004). Resultantly, conclusive perfusion changes with healthy brain ageing remain contentious.

The most compelling evidence of the relationship between ageing and regions of perfusion comes from longitudinal studies, and many of the aforementioned studies are limited by their cross-sectional design, which provides static insight into this relationship, rather than following the same subjects over time. However, some studies have assessed this relationship longitudinally, or

intend to do so in future. Many of the studies which assess longitudinal perfusion also look at metrics of cognitive health, and so these are discussed in Chapter 4 (Hanaoka et al., 2016; Benedictus et al., 2017; De Vis et al., 2018; Staffaroni et al., 2019). Both TILDA and the Calgary Normative Study intend to release longitudinal perfusion metrics in the near future (McCreary et al., 2020; Leidhin et al., 2021).

Some of the previously mentioned studies show regionality overlap with key networks such as the default mode network (DMN), which has been evidenced to exhibit altered metabolic processing in ageing and AD (Greicius et al., 2004; Chen, Rosas and Salat, 2011), and highlights the relationship between brain regions, and that physiological and metabolic brain ageing is unlikely to be a process occurring in distinct and independent brain structures. Thus, such findings suggest a regional relatedness which may underpin age-related perfusion changes.

Such regional brain perfusion changes over the age span may lend support to a physiological retrogenesis model of dementia and ageing. Proposed by Reisberg et al. (1999), this model suggests a pattern of reverse maturation, whereby brain regions which develop last degenerate first. This is supported by mirrored behavioural changes in childhood development and adult cognitive decline (Reisberg et al., 2002), with the regions which have been shown to myelinate last most vulnerable in AD (Papuć and Rejdak, 2020). Magnetisation transfer MRI measures have shown average global brain myelination to peak in the fourth decade (Carradus et al., 2020), with axonal degeneration implicated in both ageing and neurodegeneration (Salvadores,

Sanhueza and Manque, 2017). Particularly, Bouhrara et al. (2020) carried out the first study which examined associations between myelin integrity – assessed using myelin water fraction as a surrogate of myelin content – and regional perfusion in a cohort of 67 cognitively unimpaired subjects (39M, 28F; 24 - 88 years old, Mini-Mental State Examination [MMSE] =  $29 \pm 1.2$ ). They found that myelination decreases alongside perfusion in both the GM and WM of defined brain lobes (frontal, occipital, parietal and temporal), as well as the cerebellum and whole brain. This lends physiological support to the retrogenesis model of ageing and highlights a role which perfusion measures may play within this model.

Perfusion of key networks may also inform on the persistence of cognitive health with age, given established links between network function and cognitive performance. The DMN, a resting-state network (RSN) comprising the medial prefrontal cortex, angular gyrus, posterior cingulate cortex and precuneus, has been shown to be susceptible to normal ageing, with Damoiseaux et al. (2008) evidencing reduced activity in the DMN during rest, and others showing DMN disruption with cognitive impairment (Toussaint et al., 2014; Simic et al., 2014). The earliest accumulation of  $\beta$ -amyloid has been shown to occur in many of the key ROIs of the DMN, albeit without association to glucose hypometabolism (Palmqvist et al., 2017). However, resting-state fMRI has been used to evidence reduced connectivity throughout the DMN with age (Esposito et al., 2008; Biswal et al., 2010). The functional segregation of the DMN and executive control network (ECN), commonly described as comprising the prefrontal cortex, posterior parietal cortex, frontopolar cortex, and anterior cingulate cortex (Damoiseaux et al., 2006), has been observed to initially increase and then decrease with age (Ng et al.,

2016), which is interesting given the role of the ECN in cognitively-demanding processes (Seeley et al., 2007; Turner and Spreng, 2015). The salience network (SN) – which is composed of the anterior insula and dorsal anterior cingulate cortex – filters incoming stimuli and recruits the necessary functional networks (Menon and Uddin, 2010), thereby contributing to a multitude of complex brain functions. Interactions between these networks have been suggested to be important to elucidation of higher-level cognition and the ageing brain (Greicius and Kimmel, 2012). More recently, Gilmore, Nelson and McDermott (2015) proposed a parietal memory network, also known as the precuneus network, which lies adjacent to – and somewhat overlaps – the DMN (Yang et al., 2014; Hu et al., 2016). The precuneus network is composed of the precuneus, dorsal angular gyri, middle cingulate cortex and posterior inferior parietal lobule. Whilst the separation of this network from the DMN is still contentious, not doing so may bias the interpretation of studies pertaining to related brain function (Jones et al., 2016).

Other research has aimed to go beyond the assessment of pre-defined regions or networks by disregarding anatomical constraints of such analysis, through assessment of perfusion patterns which characterise the relationship between perfusion and healthy ageing. Univariate voxel-wise analysis evaluates variance on a voxel-by-voxel basis, whereas multivariate pattern analysis (MVPA) allows assessment of covariance across all voxels, thereby enabling underlying patterns to be characterised, and aiding the development of imaging-based biomarkers (Habeck and Stern, 2010; Linn et al., 2016; Weaverdyck, Lieberman and Parkinson, 2020).

Details of key studies employing voxel-wise approaches to the assessment of physiological brain changes with age are summarised in Table 3.1.1.. These studies were determined for inclusion after a search of the literature in October 2020. This included studies using any brain imaging modality and pertaining to the use of voxel-wise assessment of the relationship between brain perfusion and age. Studies were included within the table if they provided clear methodological descriptions, and also included older subjects (~50+ years old).

**Table 3.1.1.: Summary of key voxel-wise studies which assess the relationship between healthy ageing and physiological brain changes.** Ages include standard deviations where provided. Abbreviations used within the table: ↓ = decrease, ↑ = increase, R = right, L = left, CMRglc = cerebral metabolic rate of glucose, GLM = general linear model, GM = grey matter, PFC = prefrontal cortex, DLPFC = dorsolateral prefrontal cortex, MFG = middle frontal gyrus, IPL = inferior parietal lobule/IPC = inferior parietal cortex, PHG = (para)hippocampal gyrus, MTG = middle temporal gyrus, SFG = superior frontal gyrus, IFG = inferior frontal gyrus, ITG = inferior temporal gyrus, STG = superior temporal gyrus, SPL = superior parietal lobule, FG = fusiform gyrus, ACC = anterior cingulate cortex, SCC = superior cingulate cortex, PCC = posterior cingulate cortex, MCG = middle cingulate gyrus, CG = cingulate gyrus, MOF = middle orbital frontal region, SMA = supplementary motor area, SMG = supramarginal gyrus, MFC = medial frontal cortex, MC = motor cortex, FC = frontal cortex, TC = temporal cortex, IC = insular cortex, PC = parietal cortex, OL = occipital lobe, MCC = middle cingulate cortex, STP = superior temporal pole, OFC = orbitofrontal cortex, PSMC = primary sensorimotor cortex.

Author	Imaging modality	Subjects	PVC/ smoothing	Modelling approach	Covariates	Results
Martin et al., 1991	PET (unspecified)	30 (15M:15F, 62.4±15.4 years, range = 30-85)	Smoothed (Gaussian filter, 20mm FWHM)	Voxel-wise linear regression	Global CBF	No sign. relationship between global CBF and age. Regional ↓ in bilateral cingulate gyri, PHG, STG, MFC, posterior parietal cortex, and L posterior prefrontal cortex and insular.
Petit-Taboué et al. 1998	FDG-PET	24 (15M:9F, 20 - 70 years old)	Smoothed (isotropic Gaussian filter, 16mm)	Voxel-wise Pearson's correlations - global and adjusted CMRglc (SPM95, using voxels with CMRglc >80% of	-	Sign. ↓ in global CMRglc with age, of around 6% per decade. Peaks of CMRglc ↓ ( $p < 0.001$ ) are seen in MTG, orbitofrontal area, subgenual area, L pars orbitalis, L ITG, R STG, R angular gyrus, L SMG, R insula, L caudate, L putamen, thalamus, L DLPFC/pars opercularis, R cingulate

				mean). Normalised to grand mean.		cortex, R premotor cortex/SMA  <i>[Note - voxel-wise analysis did not assess entire brain tissue due to field width of PET device].</i>
Van Laere and Dierckx, 2001	<sup>99m</sup> Tc ECD SPECT	81 (40M:41F, mean = 44.2 years, range = 20-81)	Smoothed (anisotropic Gaussian kernel approximating SPECT spatial resolution)	Voxel-by-voxel comparison of VBM analysis of morphological data and perfusion data. Linear voxel-wise regression.	Age (squared values as covariate of interest, linear age as no-interest covariate), sex (covariates centred to mean values).	↓ with age in frontotemporal regions - primarily L insula, prefrontal and lateral frontal cortices, anterior and superior temporal cortices, anterior cingulate, caudate heads.  Largest ↓- bilateral insula, L caudate head. Males have significantly higher perfusion in L anterior TC and OFC. Females have higher perfusion in R IPC.
Willis et al. 2002	FDG-PET	66 (all R-handed, 38M [38.1±11.8 years, range = 24-69]: 28F [41.0±10.2 years, range = 20-65])	Smoothed (Gaussian low-pass filter - 10mm in-plane, 6mm axial [FWHM])	Voxel-wise Pearson's correlations within GLM, using SPM95 (M, F, and whole group). Z-threshold 1.96, cluster probability	Global CMRglc adjusted for (ANCOVA) when assessing normalised rCMRglc. Age adjusted for in sex comparisons (as mean ages differ)	<i>Absolute rCMRglc</i> - in whole group, FC, TC, IC, PC, and cingulate cortex, and bilateral (more L than R) putamen and globus pallida show sign. ↓, greatest ↓ in L inferior insula. 61% of GM voxels exhibit sign. ↓ metabolism. In females, greatest ↓ in L mid/superior temporal gyrus, and in males this was in a slightly more superior L temporal region. <i>Normalised rCMRglc</i> - ↓ remain prominent in L temporal/prefrontal

				threshold $p=0.05$ . Comparison of absolute and normalised rCMRglc between sexes used a voxel- wise t-test.		cortex (to insula), ACC to SCC. ↑ in (bilateral) cerebellum, PHG, and thalamus, and L PCC, cuneus and precuneus. Cerebellum and PCC ↑ appear to be due to males, thalamus and left cuneus to females.
Zuendorf et al., 2003	FDG-PET	74 (41M:33F, 56.6±12.8 years, range = 21-80)	Smoothed (Gaussian kernel, 8mm FWHM)	No details given - compared to Petit-Taboué et al. 1998	<i>Unclear for voxel- wise analysis</i>	Sign. ↓ metabolism in FC (particularly medial and dorsolateral prefrontal association cortex), posterior parietal cortex, PCC and caudate nuclei.  <i>(Comparator for PCA [PCA components 1 and 2 show almost exactly the same regions]).</i>
Allsani et al. 2009	1.5T MRI, CASL	30 old (16M, 69±6 years, range = 62- 86)  26 young (8M, 26±3, range = 21- 31)	PVE-correction as per Allsani et al., 2008	Old vs young, M and F separately, fixed effect model. Corrected for multiple comparisons (cluster level of 50 voxels,	<i>unclear</i>	Age-difference contrast CBF ↓ - in males in bilateral ACC, caudate, CG, precuneus, SFG and PFC, and L cuneus, MFG, IFG and insula. In females, in R MFG, L hypothalamus, and bilateral amygdala and hippocampus. ↓ was asymmetric in both males and females.

threshold t-value  
= 3.84  
( $p < 0.005$ )).

Kalpouzos et al. 2009	FDG-PET	45 (21M, 49.4±18 years, range = 20-83)	PVE-correction (Quarantelli et al., 2004). Smoothed (14mm isotropic Gaussian filter)	Voxel-wise correlations. Absolute values divided by global mean for analysis.	Age	Relative ↓ in <sup>18</sup> FDG uptake in bilateral superior MFC, MC, ACC, MCC, supramarginal, superior and inferior parietal cortices. The STP (approaching insular) and OFC particularly affected.
Aanerud et al. 2012	H <sub>2</sub> <sup>15</sup> O PET	66 (46M, 21-81 years). Only 65 included in CBF analysis - <i>details not given.</i>	Smoothed (FWHM 6mm)	Voxel-wise linear regression, fMRI stat assigned t-value in each voxel.	<i>unclear</i>	Largest ↓ of CBF in ACC and medial SFG. Further ↓ in regions of thalamus, pons, medulla oblongata, cerebellum, OL, and the superior PSMC
Zhang et al. 2018	3T MRI, pCASL	50 (22M, 45.8±18.5 years, range = 21-85). Split into young and	Smoothed (10mm Gaussian kernel)	Multiple regression model, identification of clusters >200 voxel (when no	Global CBF adjusted for using ANCOVA, sex included as covariate in regression model	<i>No adjustment</i> - negative correlation between absolute CBF and age in R MFG (to middle cingulate) L IPL, R MTG, bilateral thalamus, caudate body, and cerebellum. In older group, bilateral STG, R MFG, R STG, bilateral caudate, and

		old groups for comparison at median (41.8 years)		covariates), >100 after adjustment for global values		cerebellum were ↓ compared to younger group. No sign. ↑.  <i>Adjustment</i> - relative CBF in bilateral SFG, IPL, and cerebellum, L SPL, R MFG, R STG and R caudate body ↓ with age. ↑ CBF in bilateral putamen, FG and MCG, L ACC, L insula, L STG, and L MOF. No sex differences in sample regions (R MFG, L IPL, and R MCG).
MacDonald et al. 2020	3T MRI, pCASL	146 (58M, 18-87 years)	PVE-correction, as per Zhao et al., 2017	Voxel-wise regression	<i>unclear</i>	Results presented as voxel-wise regression maps. CBF ↓ consistently with age across cortical grey matter. Rate of ↓ higher in cortical GM and lower in subcortical GM.

---

The most comparable methodology to our own was used by Zhang et al. (2018), and their regression map is shown below in *Figure 3.1.1*.

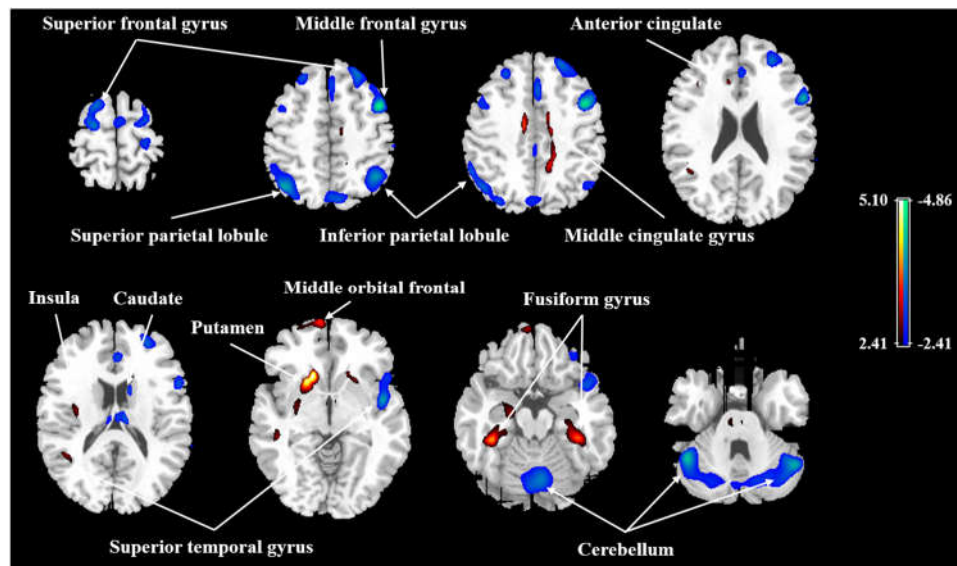


**Figure 3.1.1:** Age-related changes in relative CBF in all participants from regression analysis in Zhang et al. (2018). Cold colour indicates regions in which CBF negatively correlated with age, and warm colour indicates regions in which CBF positively correlated with age. A threshold of 2.41 ( $p < 0.01$ ) was used to overlay Statistical Parametric Mapping (SPM) maps onto a standard MNI brain template. [Figure and caption taken from Zhang et al., 2018].

When compared with voxel-wise methodology, multivariate approaches such as PCA have been shown to elucidate more subtle differences, and therefore more superior pattern expression (Asllani et al., 2008). Particularly, they can assess the co-relationships between brain regions and across subjects, known as covariance. One such MVPA technique is PCA (Pearson, 1901; Hotelling, 1933), a powerful analytical tool which is normally employed for the reduction of data dimensionality, making a dataset more computationally and statistically manageable with less multiple test correction needs, and enabling

detection of patterns across a population, often between healthy and disease cohorts. It is an adaptive method of analysis, as components are defined by the data itself, rather than *a-priori* by the researcher, and considers covariance calculated across all voxels, rather than in individual voxels, as in voxel-wise analysis. It is one of the oldest such methods, having first been evidenced in scientific literature in two key studies – Pearson (1901), which looked at the representation of systems in multi-dimensional space, and Hotelling (1933), who conveyed statistical variables as principal components.

PCA has been previously utilised in the discrimination between groups of the healthy ageing-MCI-AD continuum (Scarmeas et al., 2004; Fripp et al., 2008; Habeck et al., 2008; Nobili et al., 2008; Pagani et al., 2009; Cho et al., 2017), and other conditions associated with ageing, such as Parkinson's Disease (PD; Spetsieris et al., 2009; Melzer et al., 2011; Teune et al., 2014). Siedlecki et al. (2009) used H<sub>2</sub><sup>15</sup>O PET to identify an age-derived covariance pattern which discriminated between young and old subjects, and a separate pattern distinguishing old healthy subjects and those with mild AD. These two patterns were dissimilar, and the age-related pattern could not differentiate well between healthy older individuals and those with probable AD. Some studies focused exclusively on healthy ageing, with Moeller et al. (1996) showed reproducible covariation in healthy ageing using FDG-PET, characterised by relative frontal hypometabolism and increases within the basal ganglia, cerebellum and mid-brain. Pagani et al. (2002) used PCA to investigate 50 subjects (31-78 years old, 25M:25F) who underwent HMPAO-SPECT scans, finding 81% of variance was explained by 12 components, and significantly higher CBF on the right side of the brain than the left. Significant regional decrease with age was found in the left frontotemporal cortex and

temporocingulate cortex, as well as the brain vertex, however when sex was accounted for, the only significant difference was a reduction in posterior temporal cortex perfusion in males. Zuendorf et al. (2003) used PCA of FDG-PET on a cohort of 74 healthy and unmedicated subjects (21-80 years old, 41M:33F). The first component explained 10% of data variance, but was only reduced in subjects aged 55+, and reflective of age-related atrophy and increasing size of CSF-filled spaces, with signal loss in/adjacent to ventricles and basal cisterns. Component 2 correlated most with age, explained 8% of variance, and contained high loadings within the prefrontal, posterior parietal, and posterior cingulate cortices. These findings are in-line with known age-related declines in cerebral glucose consumption. Zhang et al. (2018) were the first to use ASL data to derive an age-related pattern of CBF in a cohort of 50 subjects (21-85 years old, 22M:28F) using Scaled Subprofile Model (SSM) PCA (Moeller et al., 1987). They identified a pattern which accounted for ~35% of the variance seen in CBF with age, which included positive relationships in the cuneus and calcarine as well as temporal areas, and negative relationship in the ACC, precuneus, thalamus, cerebellum, middle cingulate cortex, and the superior, middle and inferior frontal cortices (*Figure 3.1.2.*). However, this study is limited by its small sample size and the lack of PVE-correction employed. Additionally, they did not attempt to elucidate sex-specific PCA-derived spatial covariance patterns. No subsequent work has addressed this using ASL data, and such investigation is warranted to understand how this perfusion pattern varies when these aspects are considered.

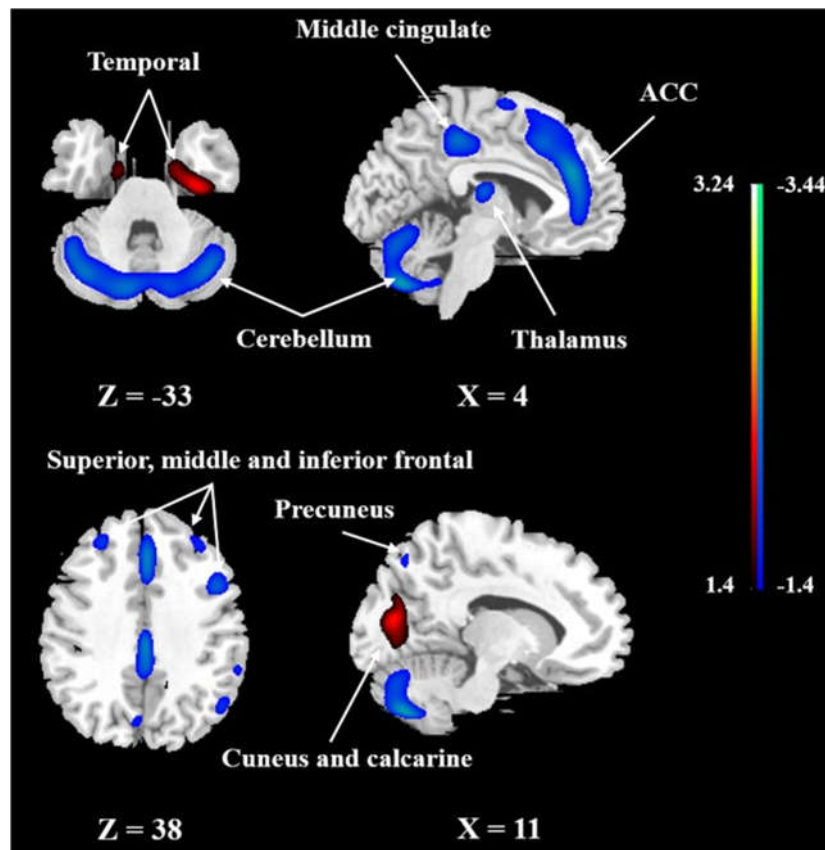


**Figure 3.1.2.:** The network of CBF changes with aging identified by SSM/PCA from 50 healthy subjects, in Zhang et al. (2018). Cold colour indicates regions loading negatively correlated with age, and warm colour indicates regions loading positively correlated with age. The pattern was overlaid onto a standard MRI brain template to display voxels that were reliable at  $p < 0.05$  based on the bootstrapping algorithm [Figure and caption taken from Zhang et al., 2018].

Theoretically, a pattern derived from MVPA techniques can subsequently be used to predict the variable of interest, for example an age-associated spatial covariance pattern could be used to predict age. Age prediction is of great research interest currently, as the variance between predicted brain age and actual brain age is thought to be reflective of advancing or delayed brain ageing (Franke and Gaser, 2019). Cole et al. (2017) have shown the potential for such a metric as a biomarker of brain ageing using  $T_1$ -weighted MR images, showing high reproducibility of brain-predicted age. Gaser et al. (2013) have shown the ability of brain age to discriminate between MCI and

AD, with an accuracy of up to 81%. However, much is yet to be elucidated in the field of brain-predicted age, given its relative infancy as a potential metric. Much of the research has focused on structural or multimodal metrics (Cole and Franke, 2017; Smith et al., 2019; Niu et al., 2020; Bashyam et al., 2020). MacDonald et al (2020) have shown that including CBF data within such models shows a marginal improvement in age estimation. Amen et al. (2018) used 99mTc-HMPAO SPECT to assess 128 brain regions for the prediction of patient age, in a study of 31,227 subjects aged between 9 months to 105 years old. Their results suggest that subject age can be predicted on the basis of CBF patterns, with clinical diagnoses and addictions linked to increased age prediction. However, the utility of perfusion data in the prediction of age is under-researched, and determining how successfully any PCA-derived perfusion pattern is able to predict age would add to the understanding of the wider utility and robustness of the pattern.

### 3.1.1. Aims and hypotheses

The purpose of this study was to use voxel-wise and MVPA (PCA) approaches to assess cerebral perfusion in a cross-sectional cohort of adult subjects. Specifically, this study aimed to (1) elucidate the PCA-derived spatial covariance patterns associated with age in a PVE-corrected cohort, (2) use five-fold cross-validation analysis to assess the utility of the PCA-derived perfusion patterns in the prediction of age, and (3) determine individual PCA-derived spatial covariance patterns in male and female subjects. The study also aimed to (4) assess whether decreases in perfusion with ageing truly exist or are explicable by the impact of pre-processing steps or underlying confounds.

It was hypothesised that the surviving components of PCA analysis would result in a spatial covariance pattern comprising regions of previously reported perfusion change, including the ACC, precuneus and thalamus, and parts of networks thought to be important in healthy ageing, such as the ECN and SN. PCA-derived spatial covariance patterns were hypothesised to be more sensitive to age effects than univariate, voxel-wise findings. Additionally, it was hypothesised that multivariate spatial covariance patterns would differ between males and females, given sex differences in perfusion literature, however, sex effects on PVE-correction were not expected to significantly differ.

## 3.2. Dataset overview

### 3.2.1. Design and participants

This was a cross-sectional retrospective study which used healthy control data collected as part of several studies at the University of Nottingham between 2011 and 2020. Subject inclusion criteria stated that healthy control subjects must be aged 18 or over, MRI-safe, free from any major medical, neurological and psychiatric comorbidities, and able to give consent to participation. Study-specific inclusion and exclusion criteria are summarised in Appendix A.

The cohort used within this study contains healthy control subjects from ImPOA (Imaging to Understand Pain in Osteoarthritis), INCOPE (Imaging the Neural Correlates of Osteoarthritis Pain Phenotypes), PaMIR (Parkinson's Magnetic Imaging Repository), GSH-MRS (A comparison of potential regions of interest for glutathione MRS in the health adult brain), BraNDy-MS (Brain

Network Dysfunction in Multiple Sclerosis) and VeSPA-MS (Venous Stasis and Permeability Assessment in Multiple Sclerosis). I was the key researcher involved in GSH-MRS, responsible for literature searching, study design, data acquisition, analysis, write-up of related abstracts, and subsequent conference presentation. The final dataset consisted of 94 healthy subjects (36M:58F, mean age = 54.017 [SD = 15.204, range = 23 - 78]).

### 3.2.2. Ethical approval and funding information

All studies from which data was retrospectively used within this study were granted ethical approval prior to commencement. Approval for ImPOA and INCOPE was granted by Nottingham Research Ethics Committee 2 (Ref: 10/H0408/115), and they were funded by Versus Arthritis UK (formerly Arthritis Research UK, Grant 18769). Professor Dorothee Auer was the Chief Investigator (CI) for both studies. GSH-MRS received approval under an overarching ethics within the University of Nottingham which covers studies for protocol development (Ref: B12012012-53). This study was also supervised by CI Professor Dorothee Auer, and was funded by the National Institute for Health Research (NIHR) Nottingham Biomedical Research Centre and University of Nottingham, School of Medicine.

PaMIR is overseen by CI Professor Dorothee Auer, and is funded by Parkinson's UK (Grant J-1204), with ethical approval from the National Health Service (NHS) Research Committee (Ref: 14/EM/0061). VeSPA-MS and BraNDy-MS were both granted ethical approval by the NHS Health Research Authority. They were overseen by Professor Rob Dineen, and led by Dr Afaf Elsarraj (VeSPA-MS, Ref: 10/H0408/37) and Dr Thomas Welton (BraNDy-MS, Ref: 14/EM/0064). Funding was provided by the University of Nottingham

Early Career and Knowledge Transfer Award, and a grant from the Multiple Sclerosis Society (Ref: 988), for VeSPA-MS and BrANdy-MS, respectively. All studies allow for the sharing of data within the Centre for further analyses, and all data was anonymised at the point of acquisition, with only age and sex recorded.

### 3.2.3. Subject recruitment approaches in original studies

Recruitment for these studies occurred through various pathways. ImPOA, INCOPE, PaMIR, BrANdy-MS and VeSPA-MS all used poster advertisements with ethical approval within the University of Nottingham, School of Medicine, and specific hospital areas where appropriate (for example, studies which recruited MS patients also used poster advertisements in areas where associated treatments take place). ImPOA, INCOPE, PaMIR and GSH-MRS recruited subjects who had previously been involved in similar studies and were interested in being contacted about future research. PaMIR also specifically sought to recruit the partners of patients involved in the study.

### 3.2.4. MRI data acquisition

All subjects were scanned on a 3T Discovery MR750 (GE Healthcare, Chicago, IL) with 32-channel head coil (MR Instruments Inc., Hopkins, MN) between 2011 and 2020. In all studies, T1-weighted images were acquired for the purposes of image registration, with CBF assessed using a pseudo-continuous ASL sequence with 3D spiral readout. T1-weighted images were acquired parallel to the anterior commissure - posterior commissure (AC-PC) line, and the bottom of ASL images positioned below the cerebellum, to enable imaging of the whole brain.

The INCOPE, PaMIR and GSH-MRS studies used the same parameters for both 3D FSPGR and 3D PCASL acquisitions. These were as follows - 3D FSPGR: TE/TR = 3.164/8.132 ms, inversion time (TI) = 450 ms, slice gap = 1mm, FOV = 256, matrix = 256x256, flip angle (FA) = 12°, voxel resolution = 1 mm<sup>3</sup>. ASL: tag/control image pairs = 72, FA = 111°, TE/TR = 10.536/4844 ms, labelling duration = 1450 ms, PLD = 2025 ms, FOV = 240 ms, slice thickness = 4 mm, slice gap = 4 mm, number of slices = 36, echo train length = 1, number of excitations = 3, matrix = 128 x 128, voxel resolution = 1.875 x 1.875 x 4 mm. BrANDy-MS parameters for ASL acquisition were identical, but FSPGR acquisition differed with respect to TE/TR/TI (3.172/8.148/900 ms). For ImPOA, 3D FSPGR acquisition used different TE/TR (3.172/8.148 ms) values, and 3D PCASL used the following altered parameters: PLD = 1525 ms, and TR = 4632ms, when compared with INCOPE, PAMIR and GSH-MRS parameters. VeSPA-MS acquisition parameters for FSPGR were the same as BrANDy-MS, but differed in ASL acquisition, with TE/TR = 10.536/4632 ms, and PLD = 1525ms. Background suppression was employed and an  $M_0$  image used for calibration, as recommended in the ASL white paper (Alsop et al., 2015). However, it is notable that PLD and labelling durations in these studies do not align with those given in this white paper, due to the commencement of five of these studies prior to its release.

### 3.3. Data processing

#### 3.3.1. Methods

Cerebral perfusion maps were created directly on the scanner, using an automated reconstruction script, as described by Zaharchuk et al. (2010). Various processing steps were then taken, to ensure the data is comparable across studies and enable subsequent analysis of the data. There is no established gold standard for the processing of ASL data, which can result in quality issues across studies. As such, the best-available implementation at the time of this study was employed, with use of PVE-correction and smoothing as justified in Chapter 2. Data processing steps are described in the following sections, and the full process summarised in *Figure 3.3.1.* below.

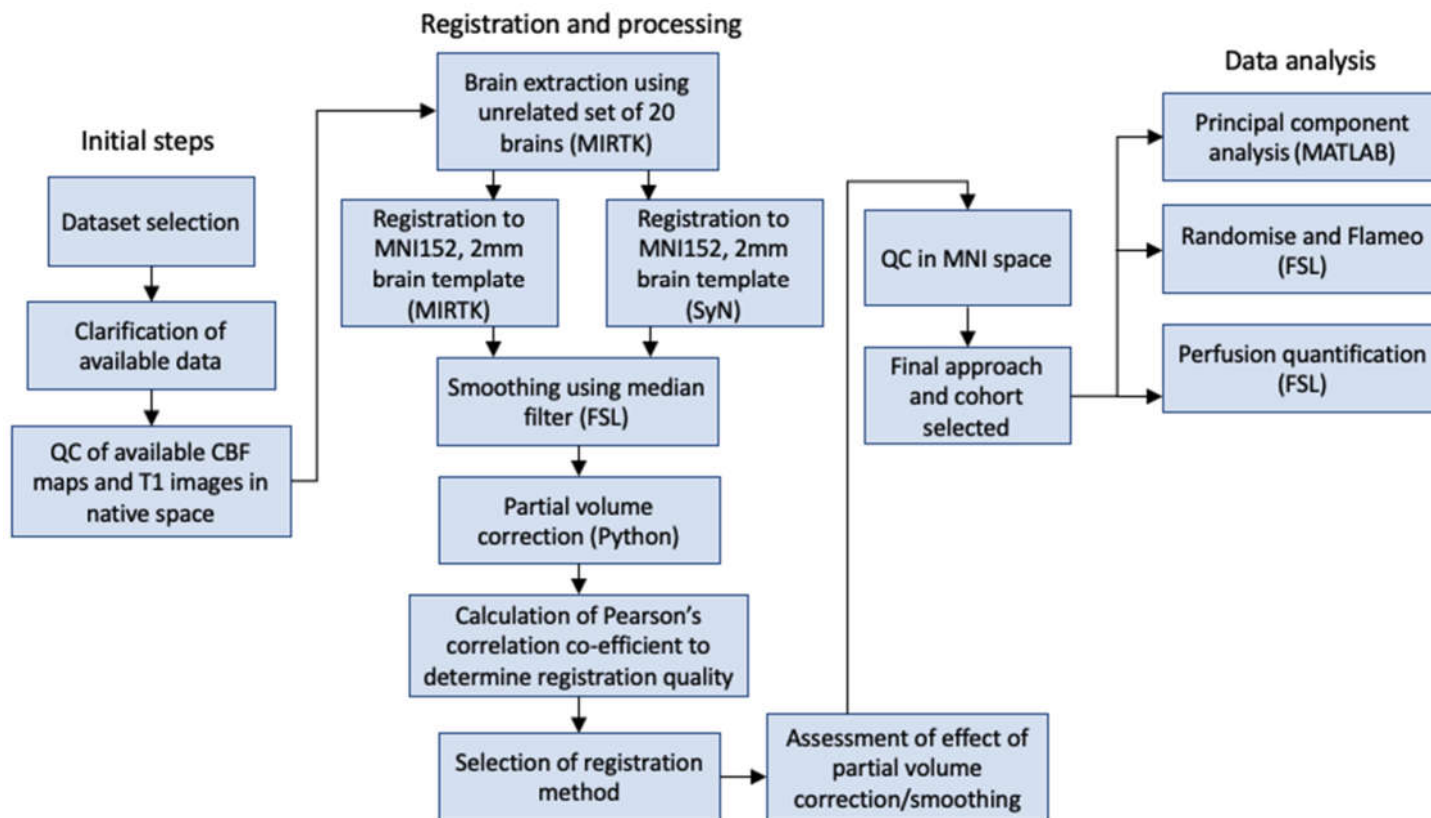


**Figure 3.3.1.:** Summary of the quality control, registration, preprocessing and analysis steps carried out within the current study.

#### 3.3.1.1. Registration to MNI space

Two different approaches were trialled for registration to MNI space, to determine which resulted in more accurate registration to MNI space. Both carried out initial brain extraction using the Medical Imaging Registration Toolkit (MIRTK, Rueckert et al., 1999, <https://github.com/BioMedIA/MIRTK>), whereby an additional dataset of twenty unrelated brains ([www.brain-development.org](http://www.brain-development.org), Hammers et al., 2003; Heckemann et al., 2006; Heckemann et al., 2010) were used as individual templates to determine which voxels did and did not include brain tissue. This employed a majority strategy, with the status of each voxel determined by the definition of that voxel in most of the twenty brain templates.

Subsequent registration was carried out using either MIRTK, or symmetric image normalization (SyN) within the Advanced Normalization Tools (ANTs, Avants et al., 2008) toolkit. First, perfusion maps were linearly registered to individual subjects' T<sub>1</sub>-weighted images, and then non-linear registration of T<sub>1</sub>-weighted images — and co-registered perfusion maps — to 2mm isotropic MNI space (T<sub>1</sub>-weighted brain averaged over 152 subjects; Montreal Neurological Institute, Montreal, QC, Canada; (Mazziotta et al., 1995; Mazziotta et al., 2001a; 2001b). Non-linear registration with MIRTK employs a cubic B-spline function, utilising the free-form deformations given by its associated parameters, whereas SyN non-linear registration uses diffeomorphic mapping to preserve topology (Bartel et al., 2019). The registration selection process is summarised in *Figure 3.3.2.*

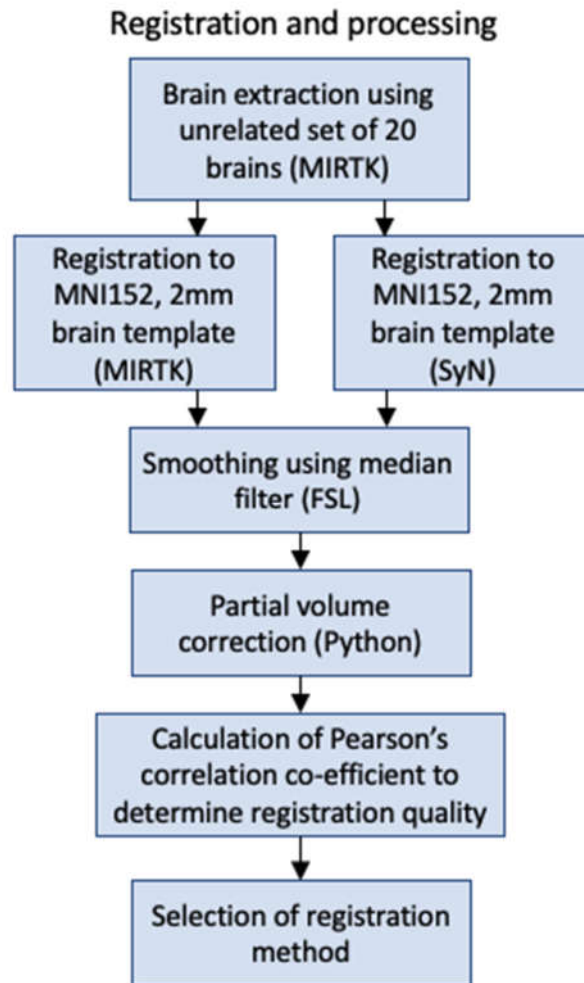


**Figure 3.3.2.:** Summary of registration and processing steps carried out within the present study.

The registration quality of both methods was initially assessed visually, however this has been shown to be an unreliable method of assessment which is unable to distinguish accurate and inaccurate registrations (Rohlfing, 2011). As such, based on the work of Mutsaerts et al. (2018) in the genetic frontotemporal dementia initiative (GENFI) cohort, Pearson's correlation coefficients were then calculated for the outputs of both MIRTK and SyN registration, in each subject. These were calculated between the perfusion

map and an MNI GM probability map, using fslcc within FMRIB Software Library (FSL; Smith et al., 2004; Woolrich et al., 2009; Jenkinson et al., 2012).

#### *3.3.1.2. Partial volume correction and spatial smoothing*

Partial volume correction was carried out using the mLTS approach by Liang, Connelly and Calamante (2013), which is discussed at length in Section 2.5.2.1.5.. This was carried out in Python (Python Software Foundation, Version 3.6. Available at <http://www.python.org>) and was run over ten iterations. Perfusion maps were then smoothed using a median filter with 3x3x3 kernel.

Perfusion values were assessed in whole GM, cortical GM and subcortical GM using FSLstats. Whole GM was defined as discussed in Section 3.3.2.3., with cortical and subcortical regions determined using the Harvard-Oxford atlas (Frazier et al., 2005; Desikan et al., 2006; Makris et al., 2006; Goldstein et al., 2007). Each region was assessed in perfusion maps that were 1) both PVE-corrected and smoothed, 2) only PVE-corrected, and 3) neither PVE-corrected nor smoothed. Subsequent statistical analysis was carried out in SPSS to quantify the effect of these processing steps in male and female subjects and determine whether there was a statistically significant difference between the sexes. Determination of whether PVE-correction and smoothing were to be subsequently used was based on a combination of theory and resultant findings.

### *3.3.1.3. Grey matter mask selection*

Various GM masks were trialled for use in subsequent analyses, as defining GM accurately is important for the interpretation of subsequent results, and avoidance of contamination by WM and CSF. The original GM mask was provided by Statistical Parametric Mapping (SPM; Rex, Ma and Toga, 2003), and a variety of different thresholds of this mask were trialled (here, 0% would refer to the most liberal definition of GM). Masks were thresholded at increments of 10%, between 20 - 50%, a range which was justified by visual assessment of the mask overlaid on the Montreal Neurological Institute (MNI) 152 2mm brain template (Mazziotta et al., 1995; Mazziotta et al., 2001a; 2001b). Additionally, a 42% thresholded mask created by Dr Yue (Lily) Xing for the PaMIR study was assessed, with this threshold chosen for preservation of the basal ganglia. All the aforementioned masks were binarised using FSL (Smith et al., 2004; Woolrich et al., 2009; Jenkinson et al., 2012). A dual-probability mask, thresholded to exclude  $\leq 20\%$  GM, and  $\geq 30\%$  CSF and used by the team working on INCOPE and ImPOA (Cottam et al., 2016), was also trialled. The aim was to find a mask which is liberal enough to include as much GM as possible, whilst being conservative enough to exclude blood flow information from other tissue compartments. This was assessed in all individuals who survived quality control, by merit of ml/100g/min values, in combination with visual assessment, additional regionality guidance using WM and CSF masks, and confirmation of the number of voxels included within each GM mask. The brainstem was removed from the selected mask, given there is little GM within it. The brainstem mask was created using Multi-Atlas Label Propagation with Expectation-Maximisation based refinement (MALP-EM; Ledig et al., 2015), and kindly provided by Dr Stefan Pszczolkowski. It was then subtracted from the selected mask using FSL (Smith et al., 2004; Woolrich et al., 2009; Jenkinson et al., 2012). It was expected that masks with

more conservative thresholds would have higher perfusion values, given that they should be more reflective of true GM. However, the more thresholded the mask, the smaller the extent of GM capture, which may lead to inaccuracies in findings.

#### 3.3.1.4. *Quality control*

The approach to quality control was guided by the ASL white paper (Alsop et al., 2015) and established practice in the research laboratory. Each image underwent a visual assessment of quality, including possible artefacts that may result from motion, or poor labelling, defined as values of <20 ml/100g/min in the occipital regions of the brain, comparatively to the rest of the cortex. The overall GM perfusion value was also checked to ensure it was physiologically plausible. In instances of ambiguity, the quality control process was repeated and the imaging data assessed again. If the quality was still unclear, the results of the quality control carried out at earlier stages (if applicable) were assessed again, to determine if there was an issue in the processing of the subject. If still of ambiguous quality, or the underlying issue could not be determined and corrected, the subject was excluded from the study. Quality control was carried out at various stages in the analysis process (see *Figure 3.3.1.*) to ensure there were no issues with any registration and processing steps. An example of perfusion map quality control after PVE-correction and smoothing is shown in *Figure 3.3.3.* Visual assessment of the original T<sub>1</sub> images and subsequent brain extracted images was also carried out, with a focus on scan coverage and any artefacts.

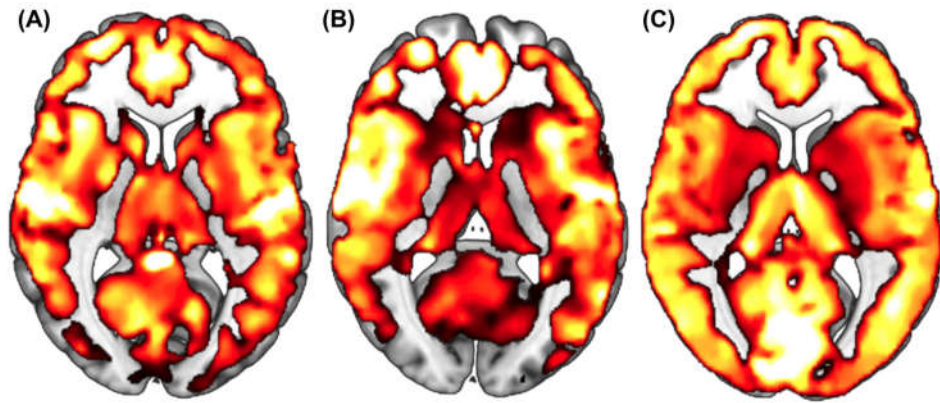


**Figure 3.3.3.:** Example axial slices of PVE-corrected and smoothed cerebral perfusion maps overlaid on a 2mm MNI template from (a) a 63 year-old male, (b) 78 year-old male, and (c) 67 year-old female, respectively. Subjects (a) and (b) show posterior labelling issues, and were excluded on this basis.

### 3.3.2. Results

#### 3.3.2.1. Registration to MNI space

Assessment of MIRTk and SyN approaches to registration of perfusion maps to MNI space using Pearson's correlation coefficient calculated between the perfusion map and an MNI GM probability map gave results of  $\rho = 0.5256$  and  $\rho = 0.5167$  for MIRTk and SyN, respectively. There was no significant difference between registration methods, as tested by a two-tailed Wilcoxon matched-pairs signed rank test ( $p = 0.0547$ ). This is summarised in *Figure 3.3.4.*

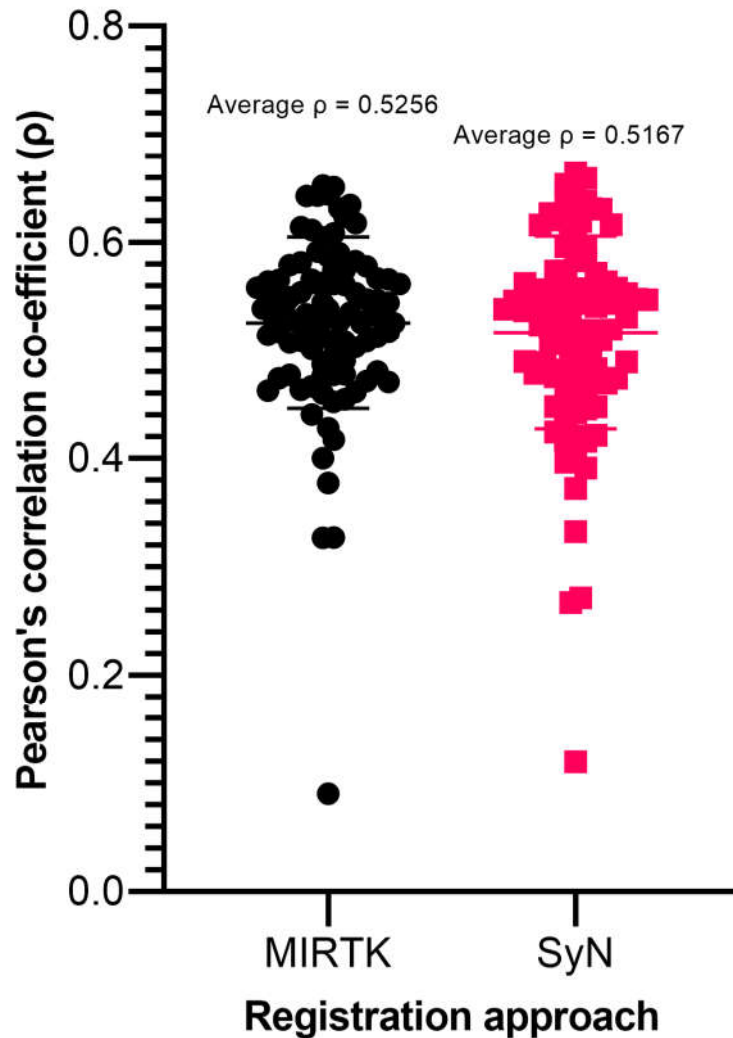


**Figure 3.3.4.:** *Pearson's correlation coefficients between ASL-derived perfusion maps and an MNI GM probability map were calculated as an alternative to relying exclusively on visual assessment to assess registration quality. This was carried out for each subject within the full cohort, using two different registration approaches — MIRTK and SyN. The average  $\rho$  for MIRTK was 0.5256, and for SyN was 0.5167.*

Analysis highlighted an outlier subject (identical outlier subject in both MIRTK and SyN analysis) with comparatively poor registration. Whilst this outlier subject remained in the subsequent study, a sensitivity test which involved removing the subject and carrying out a two-tailed paired samples t-test was done, as the distribution of the remaining values was confirmed as Gaussian. This evidenced a significantly higher Pearson's correlation coefficient using MIRTK registration methods ( $p = 0.0049$ ).

Post-hoc outlier analysis of the 65-year-old female subject from the PaMIR cohort who had the lowest Pearson's correlation coefficient was carried out, to determine why this might be. This subject had slightly above group average GM volume of 617.49 cm<sup>3</sup> and below group average CBF of 51.25 ml/100g/min, and is discussed further in Section 3.7.3..

Visual assessment of the registered perfusion maps to the MNI 2mm T1 template was also carried out. Perfusion maps which were registered using MIRTk generally appeared to fit better to the template, when considering the fit to the edge of the template and around the ventricles. An example of this is shown in *Figure 3.3.5.*

As a result of both registration quality assessments, MIRTk registration was employed throughout all subsequent analyses.

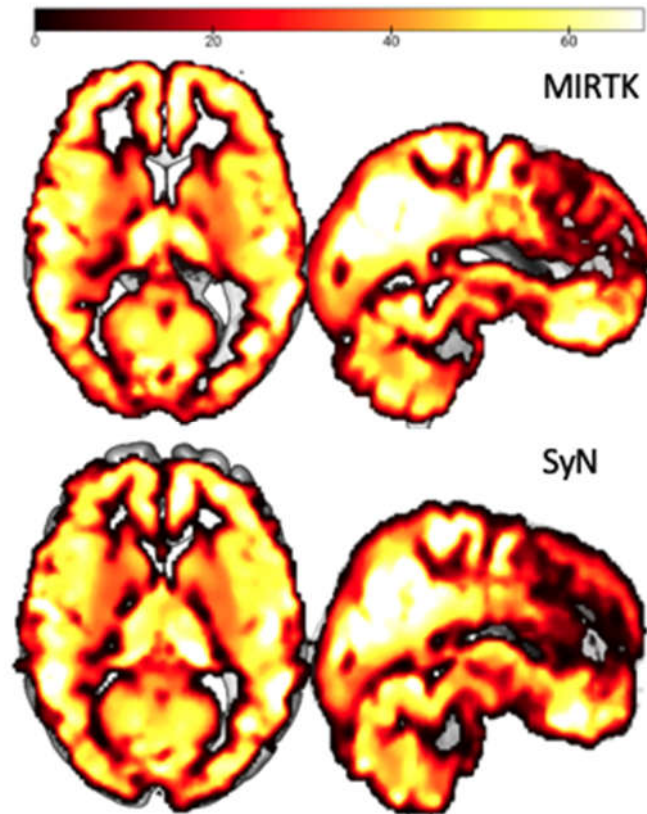


**Figure 3.3.5.:** Example fit of the perfusion map of a 77-year-old male to a 2mm MNI template, using MIRTk and SyN for registration.

### 3.3.2.2. *Partial volume correction and spatial smoothing*

The influence of smoothing using a median filter with 3x3x3 kernel, and PVE-correction with an mLTS approach (Liang, Connelly and Calamante, 2013) on perfusion measures was assessed in the whole GM, and cortical and subcortical GM, to determine how this differed between tissue regions. Sex differences were also assessed to determine whether the effect of these processing steps was significantly different between males and females. Results are summarised in Table 3.3.1..

**Table 3.3.1.: Summary of differences in male and female GM perfusion values by merit of smoothing and PVE-correction.**

		Region	Range (ml/100g/min)	Mean [ $\pm$ SD] (ml/100g/min)
<b>Males</b>	<b>PVE-corrected and smoothed</b>	<b>whole GM</b>	43.5 - 72.5	54.9 [ $\pm$ 6]
		<b>cortical GM</b>	46.2 - 78.2	58.4 [ $\pm$ 6.6]
		<b>subcortical GM</b>	36 - 63.6	45.7 [ $\pm$ 5.6]
	<b>Only PVE-corrected</b>	<b>whole GM</b>	43.4 - 72.2	54.6 [ $\pm$ 6.1]
		<b>cortical GM</b>	46.7 - 79	59 [ $\pm$ 6.7]
		<b>subcortical GM</b>	36.5 - 64.1	46.1 [ $\pm$ 5.6]
	<b>Neither PVE-corrected or smoothed</b>	<b>whole GM</b>	39.7 - 65	49.1 [ $\pm$ 5.5]
		<b>cortical GM</b>	39.5 - 66.6	50.1 [ $\pm$ 5.9]
		<b>subcortical GM</b>	38 - 62.7	46.7 [ $\pm$ 5.4]
<b>Females</b>	<b>PVE-corrected and smoothed</b>	<b>whole GM</b>	47.7 - 81.6	61.6 [ $\pm$ 8.6]
		<b>cortical GM</b>	51.1 - 87.2	66.5 [ $\pm$ 9.4]
		<b>subcortical GM</b>	37.7 - 71.3	51.4 [ $\pm$ 7.2]
	<b>Only PVE-corrected</b>	<b>whole GM</b>	47.5 - 81.1	61.3 [ $\pm$ 8.5]
		<b>cortical GM</b>	51.6 - 88	67.2 [ $\pm$ 9.5]
		<b>subcortical GM</b>	38.2 - 71.6	51.8 [ $\pm$ 7.3]
	<b>Neither PVE-corrected or smoothed</b>	<b>whole GM</b>	42.6 - 72.6	55.5 [ $\pm$ 7.6]
		<b>cortical GM</b>	43.7 - 74.7	57.1 [ $\pm$ 8.2]
		<b>subcortical GM</b>	37.9 - 69.6	51.2 [ $\pm$ 6.8]

Paired t-tests were used to determine the significance of perfusion value differences by merit of the aforementioned processing steps. In male subjects, PVE-correction resulted in an average increase in perfusion values of 11.2% ( $p < 0.0001$ ) in whole GM and 17.9% ( $p < 0.0001$ ) in cortical GM. The use of PVE-correction in the subcortical GM decreased tissue perfusion estimates by 1.3% ( $p < 0.05$ ). The subsequent use of smoothing increased perfusion values by 0.6% ( $p < 0.0001$ ) in whole GM. For female subjects, PVE-correction increased perfusion values by 10.4% ( $p < 0.0001$ ) in whole GM, 17.9% ( $p < 0.0001$ ) in cortical GM, and 1.1% ( $p < 0.01$ ) in subcortical GM. When smoothing was additionally applied, whole GM perfusion increased by a further 0.5% ( $p < 0.0001$ ). Ultimately, PVE-corrected and smoothed perfusion maps were used for subsequent analysis, due the similarity of the impact of these processing steps across the sexes, and the theoretical advantages of both (see Section 2.5.2.1.5.).

#### *3.3.2.3. Grey matter mask selection*

The quantitative results of GM mask selection are summarised in Table 3.3.2. below. Masks were thresholded from the original SPM toolbox GM mask, using FSL (Smith et al., 2004; Woolrich et al., 2009; Jenkinson et al., 2012). The original mask consisted of 255093 voxels, and the number of voxels retained after thresholding was calculated.

**Table 3.3.2.: Summary of the quantitative assessment of various GM masks, carried out on 94 PVE-corrected and smoothed cerebral perfusion maps.**

<b>Mask (% threshold)</b>	<b>Voxels retained</b>	<b>Mean CBF [SD] (ml/100g/min)</b>	<b>Range (ml/100g/min)</b>
<b>20</b>	195144	56.257 [ $\pm 8.237$ ]	40.6 - 78
<b>Dual tissue probability mask</b> <i>(excluding <math>\leq 20</math> GM, <math>\geq 30</math> CSF, brainstem included)</i>	166123	58.354 [ $\pm 8.237$ ]	43.1 - 80.6
<b>Dual tissue probability mask</b> <i>(excluding <math>\leq 20</math> GM, <math>\geq 30</math> CSF, brainstem excluded)</i>	163072	59.04 [ $\pm 8.237$ ]	43.1 - 80.6
<b>30</b>	177684	58.952 [ $\pm 8.603$ ]	42.5 - 81.5
<b>40</b>	157904	61.559 [ $\pm 8.983$ ]	44.4 - 84.9
<b>42</b>	152496	62.148 [ $\pm 9.069$ ]	44.8 - 85.7
<b>50</b>	130992	64.024 [ $\pm 9.336$ ]	46.1 - 88.4

Visual assessment of the various masks overlaid on the MNI152 2mm template (Mazziotta et al., 1995; Mazziotta et al., 2001a; 2001b) and the whole-brain perfusion maps of each subject was carried out in template space. For the most part, higher perfusion values were found in more tightly-thresholded masks, as anticipated. The original GM mask from the SPM toolbox was deemed too liberal, due to the inclusion of some voxels of WM

and CSF, and the 20 and 30% masks excluded due to possible inclusion of CSF voxels. The 50% threshold was very conservative, and excluded some voxels which were unequivocally GM, as did the 40 and 42% masks. Ultimately, the mask which thresholded both GM and CSF was chosen for use in subsequent analyses, due to its comparative balancing of liberality and conservation when considering GM, as well as accounting for CSF. The resultant mask is shown in *Figure 3.3.6.*

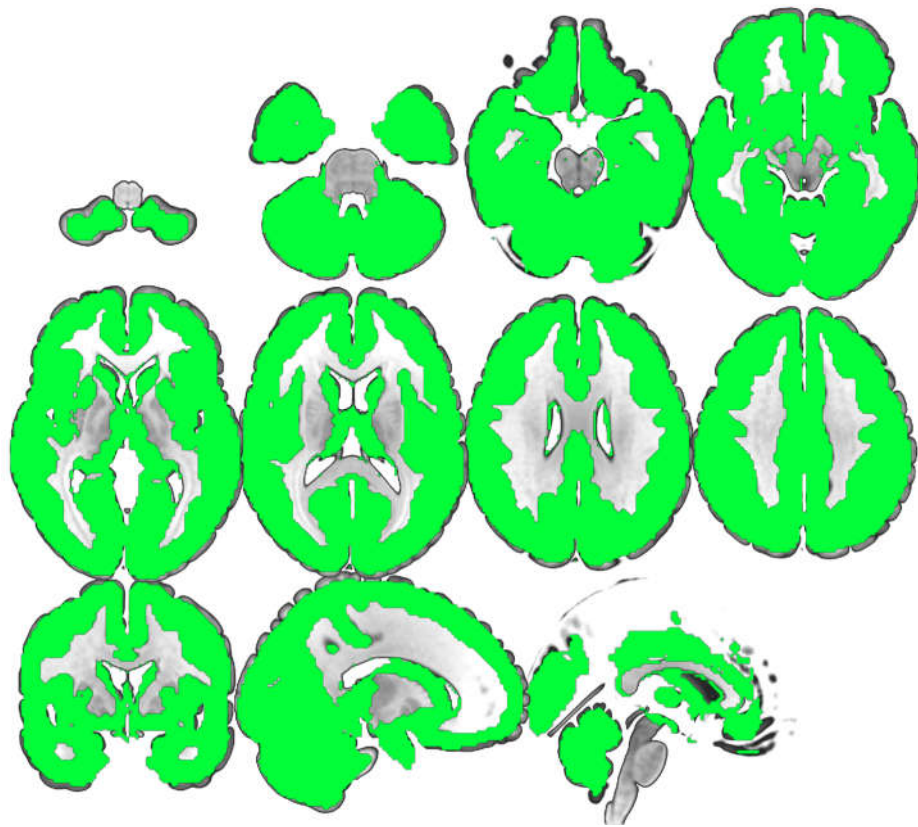


**Figure 3.3.6.:** Selected GM mask, thresholded to exclude  $\leq 20\%$  GM, and  $\geq 30\%$  CSF, overlaid on the 2mm MNI152 template.

For cortical and subcortical analysis, masks were created by combining and binarising regional masks from the Harvard-Oxford atlas (Frazier et al., 2005; Desikan et al., 2006; Makris et al., 2006; Goldstein et al., 2007), then limiting to the GM mask area as defined above. The cortical mask comprises the left and right cortical masks, and the subcortical mask the left and right caudate, hippocampus, pallidum, putamen and thalamus. These masks are shown in *Figure 3.3.7.*

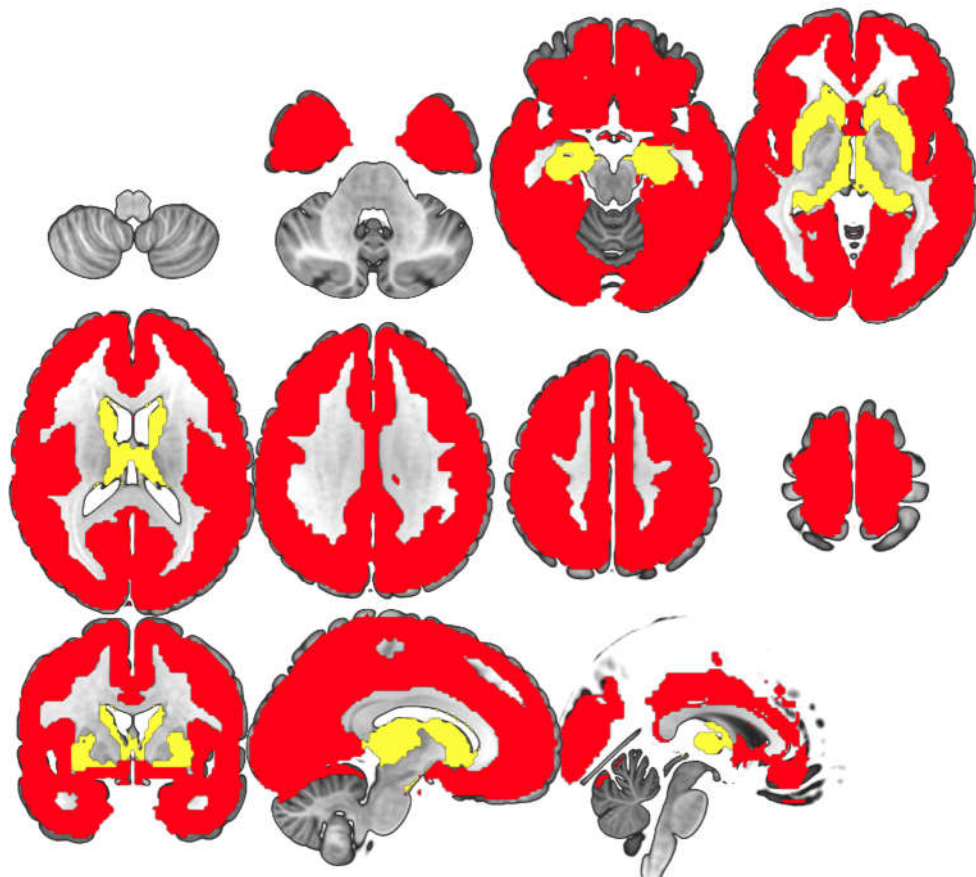


**Figure 3.3.7.:** Cortical (red) and subcortical (yellow) masks overlaid on the MNI152 2mm template, and masked to the selected GM mask.

### 3.3.2.4. Quality control

Quality control was guided by the Alsop et al. (2015) white paper. The results of quality control assessments are summarised in *Figure 3.3.8.* This quality control approach revealed a high attrition rate within these datasets, with 174 individuals prior to quality control, but only 106 of these surviving image quality control and suitable for subsequent use. However, 12 of these subjects crossed over between cohorts, due to the nature of retrospective data use in cohorts which shared participant contact lists, leaving a final cohort comprising 94 subjects. This represents an attrition rate of 39.1%, based on image quality alone.

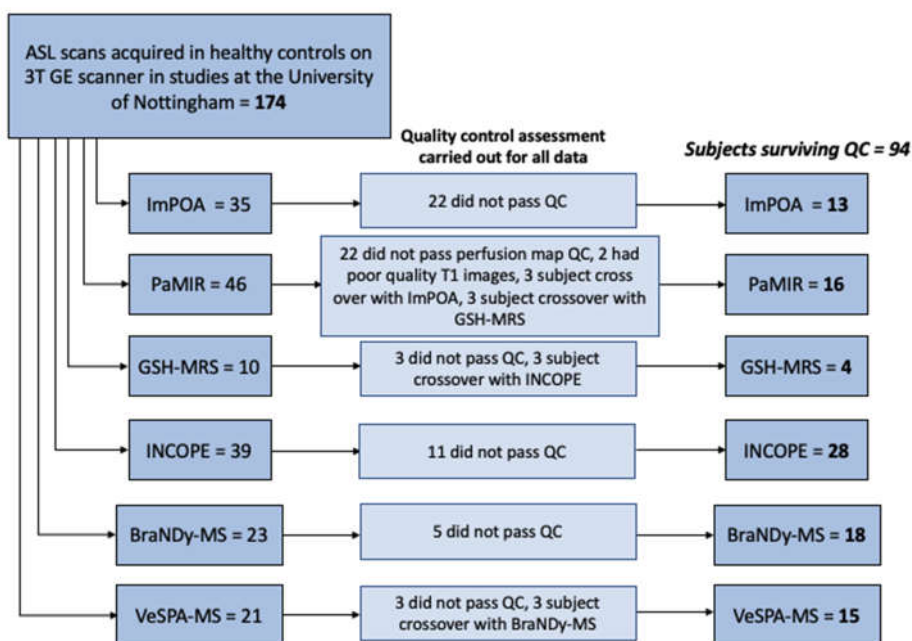


**Figure 3.3.8.:** Summary of subject selection within ImPOA, PAMIR, GSH-MRS, INCOPE, BraNDy-MS and VeSPA-MS cohorts.

### 3.4. Covariates pertinent to subsequent analysis

Much of the subsequent analysis uses covariates to control for additional inter-subject variances. Sex was included as a covariate due to significant differences in male and female perfusion within the brain (Parkes et al., 2004; Liu et al., 2012; Soni, Jain and Kumar, 2016; Juttakonda et al., 2021; Leidhin et al., 2021). GM volume was also included due to differences in male and female brain and GM volumes (Lüders et al., 2009; Ritchie et al., 2018; Sanchis-Segura et al., 2019; Lotze et al., 2019), and apparent distinction of structural and physiological changes in brain ageing (Peters, 2006; Fjell and Walhovd, 2010; Chen, Rosas and Salat, 2011). GM volume was calculated using GM PVE files output as part of the PVE-correction process. They contained information on the amount of GM within each voxel, with the sum of all voxels giving GM volume. GM perfusion was included as a covariate in certain analyses, to control for inter-subject perfusion differences of no interest.

### 3.5. Cerebral perfusion and ageing

#### 3.5.1. Methods

FSLstats (Smith et al., 2004; Woolrich et al., 2009; Jenkinson et al., 2012) was used to assess whole GM, cortical GM and subcortical GM, as per *Figure 3.3.6.* and *Figure 3.3.7.*. To further understand the subject variance in cerebral perfusion with age, perfusion analysis was carried out in key networks associated with ageing, namely the ECN, SN, DMN and precuneus network. Binarised masks of these networks were taken from the Stanford University Functional Imaging In Neuropsychiatric Disorders Laboratory (FINDLab; <https://findlab.stanford.edu>), from their atlas of ninety functional ROIs (Shirer et al., 2012; see Appendix B). SPSS (*IBM SPSS Statistics for Windows*,

Version 26, Armonk, NY) was used to carry out linear regressions exploring these relationships.

### 3.5.2. Results

Perfusion values were assessed in whole GM, and cortical and subcortical GM. In the full cohort of 94 subjects, mean whole GM perfusion was 59.04 ml/100g/min (SD = 8.36, range = 43.5 - 81.6 ml/100g/min), cortical GM perfusion was 64.44 ml/100g/min (SD = 9.3, range = 46.2 - 87.2 ml/100g/min), and subcortical GM perfusion values of 49.23 ml/100g/min (SD = 7.17, range = 35.96 - 71.3 ml/100g/min).

Linear regressions were used to assess whether there was a decline in perfusion with increasing age. Before inclusion of covariates, whole GM perfusion decrease with age only approached significance ( $\beta = -.105$ , 95% CI:  $-.217$  to  $.007$ ,  $p = .065$ ), whereas the decrease in both cortical GM CBF ( $\beta = -.155$ , 95% CI:  $-.277$  to  $-.032$ ,  $p = .014$ ) and subcortical GM CBF ( $\beta = -.111$ , 95% CI:  $-2.06$  to  $-.016$ ,  $p = .022$ ) was significant. How this decrease varies when covariates are included is summarised in Table 3.5.1..

**Table 3.5.1.: P-values resulting from linear regressions assessing the relationship between age and cerebral perfusion within the GM. Significant p-values are highlighted (\*).**

Region	No adjustment	Sex-adjusted	Sex- and GM volume-adjusted	Sex-, GM volume- and whole GM CBF-adjusted
<b>Whole GM</b>	.065	.094	.255	N/A
<b>Cortical GM</b>	.014*	.019*	.079	.000*
<b>Subcortical GM</b>	.022*	.031*	.069	.063

It is notable that whole GM perfusion was significant after sex and GM volume covariate inclusion, when assessed in the original perfusion maps which had not undergone PVE-correction or smoothing ( $\beta = -.097$ , 95% CI:  $-.191$  to  $-.002$ ,  $p = .044$ ).

This original cohort was split by sex into two sub-cohorts. The male cohort consisted of 36 subjects (mean age = 55.52 [SD = 15.8], range = 23-77 years), and the female cohort was comprised of 58 subjects (mean age = 53.1 [SD = 14.9], range = 26-78). A two-tailed t-test with Welch's correction revealed no significant difference in the age of male and female subjects within this cohort, although the mean age of males is slightly higher (difference in means: 2.43 years, 95% CI:  $-4.11$  to  $8.97$ ,  $p = 0.461$ ). When GM volume (as defined using the PVE-correction outputs) was considered using a two-tailed t-test with Welch's correction, the male cohort had significantly greater volumes of GM within their brains when compared with the female cohort (difference in means =  $50.75 \text{ cm}^3$ , 95% CI:  $22.65$  to  $78.85$ ,  $p < 0.001$ ).

In male subjects, mean perfusion values were 54.9 ml/100g/min (SD = 6.04, range = 43.5 - 72.5 ml/100g/min) for whole GM, 58.4 ml/100g/min (SD = 6.61, range = 46.2 - 78.2 ml/100g/min) for cortical GM, and 45.73 ml/100g/min (SD = 5.6, range = 35.96 - 63.62 ml/100g/min) for subcortical GM. In the female cohort, mean whole GM perfusion was 61.6 ml/100g/min (SD = 8.6, range = 47.74 - 81.65 ml/100g/min), mean cortical GM perfusion was 66.55 ml/100g/min (SD = 9.42, range = 51.14 - 87.17 ml/100g/min), and mean subcortical GM perfusion was 51.4 (SD = 7.2, range = 37.7 - 71.32 ml/100g/min). This is summarised in *Figure 3.5.1.*

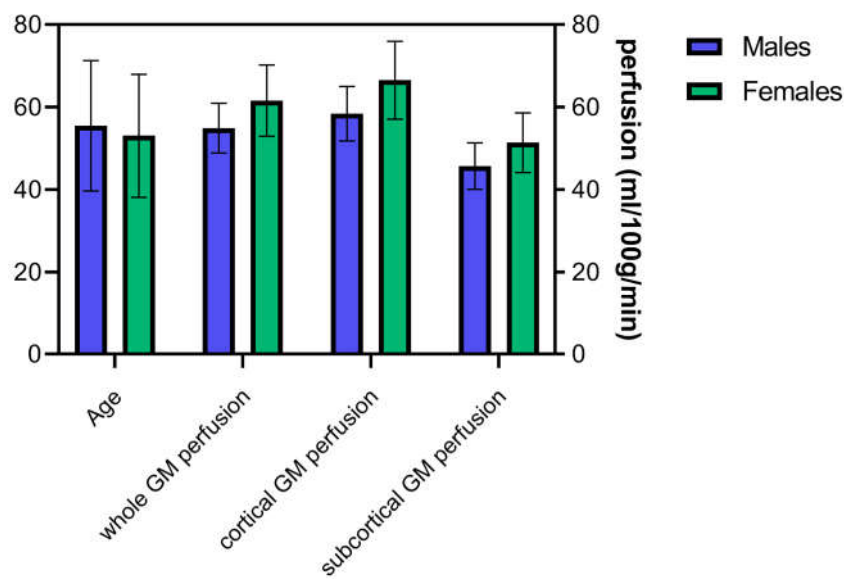


**Figure 3.5.1.:** Key cohort results pertaining to age and whole, cortical and subcortical GM perfusion. Males are depicted in blue and females in red.

When comparing male and female subjects using two-tailed independent samples t-tests with Welch's corrections, whole GM perfusion is significantly

higher in female subjects (difference in means = 6.69 ml/100g/min, 95% CI: 3.68 to 9.69,  $p < 0.0001$ ). The same test revealed that this was also significantly higher in females when considering cortical (difference in means = 8.1 ml/100g/min, 95% CI: 4.81 to 11.39,  $p < 0.0001$ ) and subcortical (difference in means = 5.67 ml/100g/min, 95% CI: 3.03 to 8.32,  $p < 0.0001$ ) measures separately.

Whole GM perfusion measures were also compared with age on the basis of PLD (*Figure 3.5.2.*, *Table 3.5.2.*). The resultant cohorts were as follows:

- PLD = 1525ms - 8M:20F, age range = 23 - 69 years ( $45.4 \pm 13.5$ ), GM volume = 424.15 - 743.78 cm<sup>3</sup> ( $603.45 \pm 81.27$ )
- PLD = 2025ms - 28M:38F, age range = 26 - 78 years ( $57.9 \pm 14.5$ ), GM volume = 408.41 - 766.38 cm<sup>3</sup> ( $597.86 \pm 67.98$ )

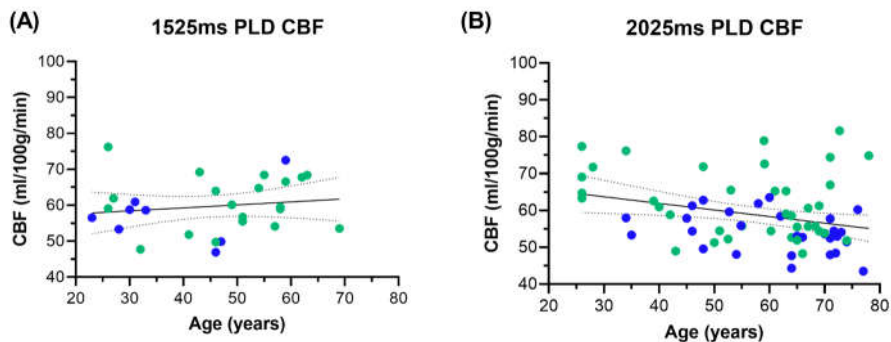


**Figure 3.5.2.:** Comparison of perfusion measures in whole GM in (A) subjects with a PLD of 1525ms, and (B) subjects with a PLD of 2025ms. Female data points are depicted in green, males in blue.

**Table 3.5.2.: P-values resulting from linear regressions assessing the relationship between age and perfusion within the whole GM by merit of PLD. Significant p-values are highlighted (\*).**

PLD	No adjustment	Sex- adjusted	Sex- and GM- volume- adjusted
1525	.452	.722	.480
2025	.015*	.049*	.094

An age-matched subset of subjects with PLD = 2025ms (7 females, aged 49±16.2 years) and with PLD = 1525ms (7 females, aged 49±16.2 years) was analysed to determine whether PLD affected cerebral perfusion measures within this cohort. No male subjects were compared due to limitations of cohort size. Average whole GM perfusion in subjects with a PLD of 2025ms was 64.6 ± 7.8 ml/100g/min, whereas for a PLD of 1525ms this was 61.5 ± 8 ml/100g/min. A two-tailed unpaired t-test with Welch's correction revealed no significant difference in perfusion due to PLD ( $p = 0.45$ ). Given that this finding was in a subcohort representing a limited subset of the full cohort, and only females, it was corroborated using two-tailed unpaired t-tests with Welch's correction to compare GM perfusion in all males with PLD = 1525ms and PLD = 2025ms, and an identical analysis in the female cohort. No significant differences in GM perfusion values by merit of PLD were found in male or female subjects ( $p = 0.35$  and  $p = 0.55$ , respectively). Thus, PLD was not included as a covariate in subsequent analyses.

Network perfusion values were investigated within the ECN, SN, DMN and precuneus network. In the full cohort, associated perfusion values were 60.2

(SD = 10.3), 67.7 (SD = 10), 68.4 (SD = 9.7) and 69.1 (SD = 11.5) ml/100g/min, respectively. In all networks, perfusion was significantly higher in females, as analysed through two-tailed independent t-tests with Welch's correction ( $p < 0.001$  for all, *Figure 3.5.3.*).

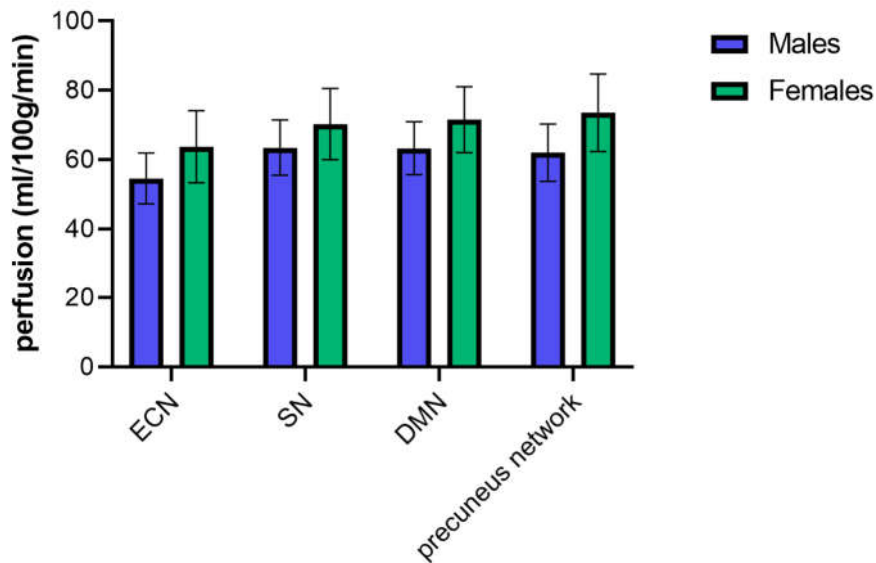


**Figure 3.5.3.:** Summary perfusion values in key networks. Males are depicted in blue and females in green.

Cerebral perfusion within key networks of interest significantly decreases with age before covariates are considered. However, after the covariates of sex, GM volume and whole GM CBF (to account for additional perfusion variance of no interest) are included, only perfusion within the ECN significantly declines with increasing age ( $\beta = -.073$ , 95% CI:  $-.120$  to  $-.026$ ,  $p = .003$ ). These findings are summarised in Table 3.5.3..

**Table 3.5.3.: P-values resulting from linear regressions assessing the relationship between age and perfusion in various networks of interest. Significant p-values are highlighted (\*).**

Network	No adjustment	Sex-adjusted	Sex- and GM volume-adjusted	Sex-, GM volume- and whole GM CBF-adjusted
<b>ECN</b>	.004*	.004*	.044*	.003*
<b>SN</b>	.018*	.026*	.287	.925
<b>DMN</b>	.049*	.069	.262	.940
<b>Precuneus network</b>	.044*	.061	.107	.191

### 3.6. Spatial covariance patterns of cerebral perfusion with age

#### 3.6.1. Methods

##### 3.6.1.1. Voxel-wise analysis of cerebral perfusion

Voxel-wise analysis of the cerebral blood flow data was carried out prior to PCA, to compare resultant perfusion patterns. A general linear model (GLM; *Figure 3.6.1.*) was constructed using GLM Setup within FSL (Jenkinson et al., 2012), with either sex only, or sex and GM volume as additional covariates, and two contrasts for age (positive and negative). GM perfusion maps were included as a concatenated image. Data was demeaned prior to GLM inclusion – a well-established approach in linear modelling – and the Harvard-Oxford atlas tool within FSLview (Smith et al., 2004; Woolrich et al., 2009; Jenkinson et al., 2012) used to localise any significant findings.

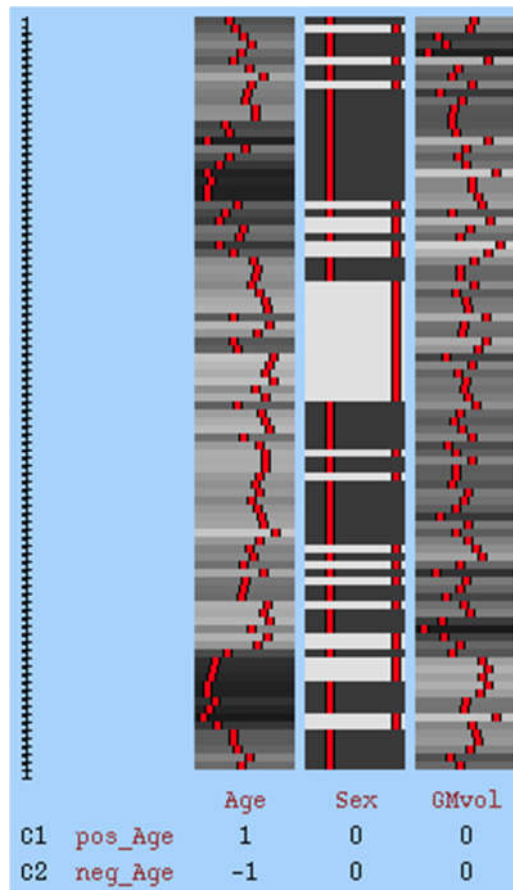


**Figure 3.6.1.:** Example GLM, with sex and GM volume as covariates, created using GLM Setup within FSL.

### **FSL-randomise**

FSL-randomise (Winkler et al., 2014) was used to carry out non-parametric permutation testing to correct for multiple comparisons (5000 permutations), defining significance as  $p < 0.05$  family-wise error (FWE)-corrected using threshold-free cluster enhancement (TFCE; Nichols and Holmes, 2002; Smith and Nichols, 2009). This analysis was done twice, using sex and GM volume as covariates, and using sex only as a covariate for sensitivity testing.

## **FSL-flameo**

Post-hoc comparison to FSL-randomise results was carried out using FSL-flameo and probabilistic TFCE (pTFCE; Spisák et al., 2019; Github code: <https://spisakt.github.io/pTFCE>), with application of the relevant  $p < 0.05$  FWE threshold that was calculated as part of this code. Identical GLMs were used here as for FSL-randomise analysis. This FSL-flameo analysis was carried out due to the surprising results of FSL-randomise analysis.

### *3.6.1.2. Principal component analysis*

PCA computes principal components, which can be thought of as fitting an ellipsoid of  $p$ -dimensions to the given data. Each axis of this ellipsoid represents a principal component, with the first component explaining the greatest variance in data, and the second explaining the next greatest variance, perpendicularly. Thus, features are selected based on the output variance they are responsible for. This is described pictorially in *Figure 3.6.2.* below.

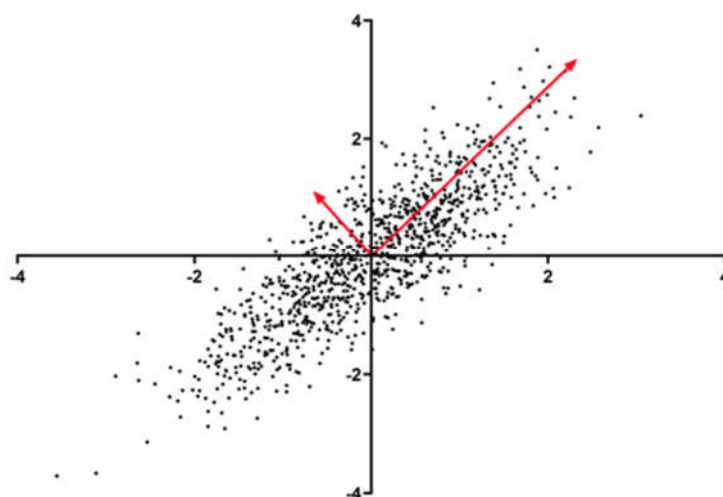


**Figure 3.6.2.:** *Depiction of the computation of principal components in the process of PCA, using normally-distributed dummy data. The components are depicted in red, showing the greatest variance in data as the first component, with the second capturing the greatest variance perpendicular to the first.*

A PCA-based ASL linear regression model was used to assess the relationship between cerebral perfusion and subject age, and the associated pattern of spatial covariance derived within the aforementioned dataset. The MATLAB script used for PCA analysis was loosely based on the theoretical methods of Spetsieris et al (2009) and Melzer et al. (2011), without the use of group differentiation. The original script was provided by Dr Yue (Lily) Xing and employed group differentiation and was rewritten by Dr Stefan Psczolkowski. Theoretical discussion regarding code development involved myself, Dr Stefan Psczolkowski and Dr Christopher Tench.

The PCA process reduces the dimensionality of the data when run on the transpose of  $I$ , where  $I$  is a  $V$  by  $N$  matrix, with columns corresponding to log-transformed ASL measures of  $N$  subjects over  $V$  grey matter voxels, which has been mean-centred both row-wise and column-wise. Resultantly, the following matrix decomposition is yielded:

$$I^T = L \cdot C^T$$

[3.1]

where  $L$  is an  $N$  by  $N-1$  matrix of  $N-1$  loadings, and  $C$  a  $V$  by  $N-1$  matrix of  $N-1$  orthonormal voxel components (eigenvectors). Given the orthonormality of the columns of  $C$ ,  $C^T C$  is the  $N-1$  by  $N-1$  identity matrix. Thus, right multiplication of  $C$  on both sides of Equation 3.1, the following is obtained:

$$I^T \cdot C = L$$

[3.2]

Given that the columns of  $L$  and  $C$  are ordered according to the amount of variance they explain, it is possible to remove “spurious” components and their corresponding loadings from these matrices. To achieve this, the Kaiser-Gutmann criterion (Jackson, 1993) was used. This method selects the first  $K$  components such that their corresponding eigenvalue – as computed by PCA – is greater than the mean of all eigenvalues. In consequence, and for the rest of this chapter,  $L$  will correspond to an  $N$  by  $K$  matrix,  $C$  will correspond to a  $V$  by  $K$  matrix, and Equations 3.1. and 3.2. will correspond to approximations, rather than equalities.

A regression model was then employed, whereby the columns of matrix  $L$  (or the loading vectors) were utilised as independent variables, with age in years as the dependent variable. As such, the regression model of age can be expressed as:

$$S \approx L^{cov} \cdot w + w_0$$

[3.3]

Here,  $S$  represented an  $N$  by  $1$  vector of subject age values (one value per subject),  $w$  is an  $N-2$  by  $1$  vector of regression coefficients (or ‘weights’),  $w_0$  is an  $N$  by  $1$  vector with the repeated regression intercept value, and  $L^{cov}$  is an  $N$  by  $P+K$  matrix which is constructed by appending  $P$  vectors of  $N$  covariate values to  $L$ , as such:

$$L^{cov} = [cov^{(1)} cov^{(2)} \dots cov^{(P)} L]$$

[3.4]

It is important to note that any covariate which is categorical in nature, such as sex, must undergo binary “dummyfication” with one-hot encoding – whereby for example ‘male’ and ‘female’ are represented by the numbers 0 and 1 – prior to inclusion within  $L^{cov}$ . However, this is not necessary for numerical covariates such as age and GM volume. Resultantly, all categorical covariates with  $M$  categories will span  $M-1$  columns of  $L^{cov}$ . As such,  $P$  does not necessarily represent the number of covariates, rather the total number of columns which are spanned by the covariate set after this “dummyfication” process. Note that if the resulting number of columns in  $L^{cov}$  is greater than  $N$ , additional columns from  $C$  and  $L$  would have to be removed to ensure that the least squares solution can be computed. Nevertheless, this was not the case in this study. The regression coefficients vector –  $w$  – can then be expressed as:

$$w = \begin{bmatrix} W_{cov(1)} \\ W_{cov(2)} \\ \vdots \\ W_{cov(P)} \\ W_{L_1} \\ W_{L_2} \\ \vdots \\ W_{L_k} \end{bmatrix}$$

[3.5]

The “optimal” C components (with  $C \leq P+K$ ) are then selected by use of a backwards selection approach, in which the script removes a component with each interaction, such that the residual variance increases the least. This process repeats until the residual variance of the regression model described in Equation 3.3. is just above the expected error variance of the subject age. As subject ages had to be included within the script as integer values, this was set to 0.5 (6 months) to account for rounding to the closest integer year. Resultantly, only C of the P+K regression coefficients associated with L have non-zero values.

After the regression is performed, the resulting regression coefficients can be used to create a V by 1 vector of linearly-combined voxel loadings  $C^{comb}$  such that:

$$c^{comb} = C \cdot \begin{bmatrix} W_{L_1} \\ W_{L_2} \\ \vdots \\ W_{L_k} \end{bmatrix}$$

This linearly-combined voxel component corresponds to an image which characterises the association between the amount of perfusion in each voxel, and the subject age.

### **Five-fold validation of the PCA process**

The intention of this validation process was to test the model in an unseen cohort. However, such a cohort was not available, and validation was instead carried out using a five-fold validation approach within the same cohort. Subjects from the full cohort were randomly assigned to five validation groups. One of these groups was set aside, and the PCA script was run again on the remaining four groups (combined as one cohort). This process is summarised in *Figure 3.6.3.*

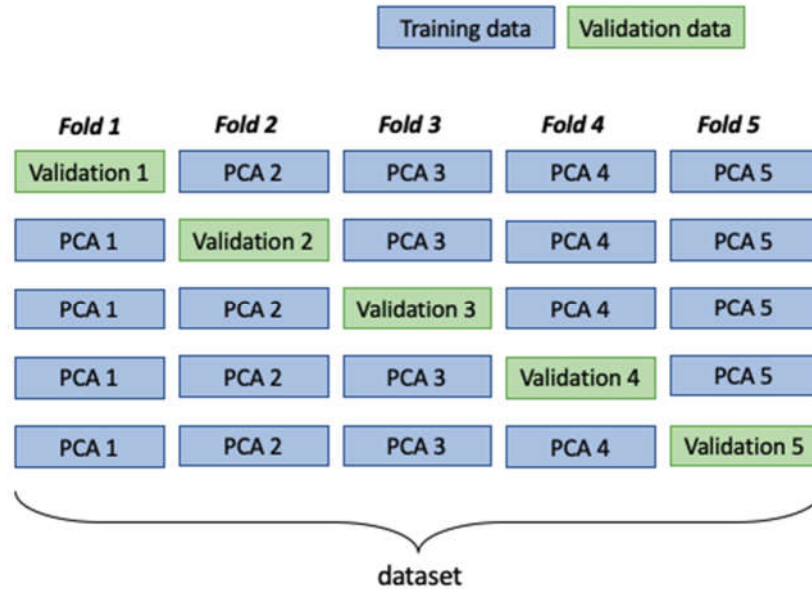


**Figure 3.6.3.:** Schematic of the assignment of subjects for five-fold cross-validation. Training groups are depicted in blue, and validation groups in green.

The following validation approach was then used to predict age within the validation cohort that was set aside, and this was repeated five times, once on each validation cohort.

Validation involved the construction of a new  $V$  by  $M$  matrix,  $I_{new}$ , from ASL data from  $M$  testing subjects. By utilising Equation 3.2, it is possible to then compute an estimation of their associated coefficient vectors –  $L_{new}$  – as:

$$L_{new} = I_{new}^T \cdot C$$

[3.7]

where  $C$  refers to the training voxel matrix described previously. Age estimations were then computed by combining Equations (3.3), (3.4) and (3.7) as such:

$$S_{estim} = \left[ cov_{new}^{(1)} \quad cov_{new}^{(2)} \quad \dots \quad cov_{new}^{(P)} (I_{new}^T \cdot C) \right] \cdot w + w_{0_{new}}$$

[3.8]

Here,  $cov_{new}^{(i)}$  corresponds to the  $P$  covariate vectors (of size  $M$  by  $1$ ) of the new data, and  $w_{0_{new}}$  to an  $M$  by  $1$  vector with the repeated regression intercept value. By use of Equation 3.5, Equation 3.8. can be rewritten thusly:

$$S_{estim} = \left[ cov_{new}^{(1)} \quad cov_{new}^{(2)} \quad \dots \quad cov_{new}^{(P)} \right] \cdot \begin{bmatrix} w_{cov^{(1)}} \\ w_{cov^{(2)}} \\ \vdots \\ w_{cov^{(P)}} \end{bmatrix} + I_{new}^T \cdot C \cdot \begin{bmatrix} w_{L1} \\ w_{L2} \\ \vdots \\ w_{LN-P-2} \end{bmatrix} + w_{0_{new}}$$

[3.9]

which is equivalent to the following when employing Equation 3.6.:

$$S_{estim} = \begin{bmatrix} cov_{new}^{(1)} & cov_{new}^{(2)} & \dots & cov_{new}^{(P)} \end{bmatrix} \cdot \begin{bmatrix} W_{cov^{(1)}} \\ W_{cov^{(2)}} \\ \vdots \\ W_{cov^{(P)}} \end{bmatrix} + I_{new}^T \cdot c^{comb} + w_{0_{new}}$$

[3.10]

The resultant output of Equation 3.10 was then compared with the actual ages of the M testing subjects, and simple linear regression computed using these estimations to assess the model's success and generalisability.

### 3.6.2. Results

#### 3.6.2.1. Voxel-wise analysis of cerebral perfusion

#### **FSL-randomise**

FSL-randomise analysis with 5000 permutations and sex and GM volume as covariates found a significant cluster (after TFCE and FWE-correction) that was positively related with age, comprising parts of the angular gyrus, middle temporal gyrus and lateral occipital cortex (*Figure 3.6.4.*).

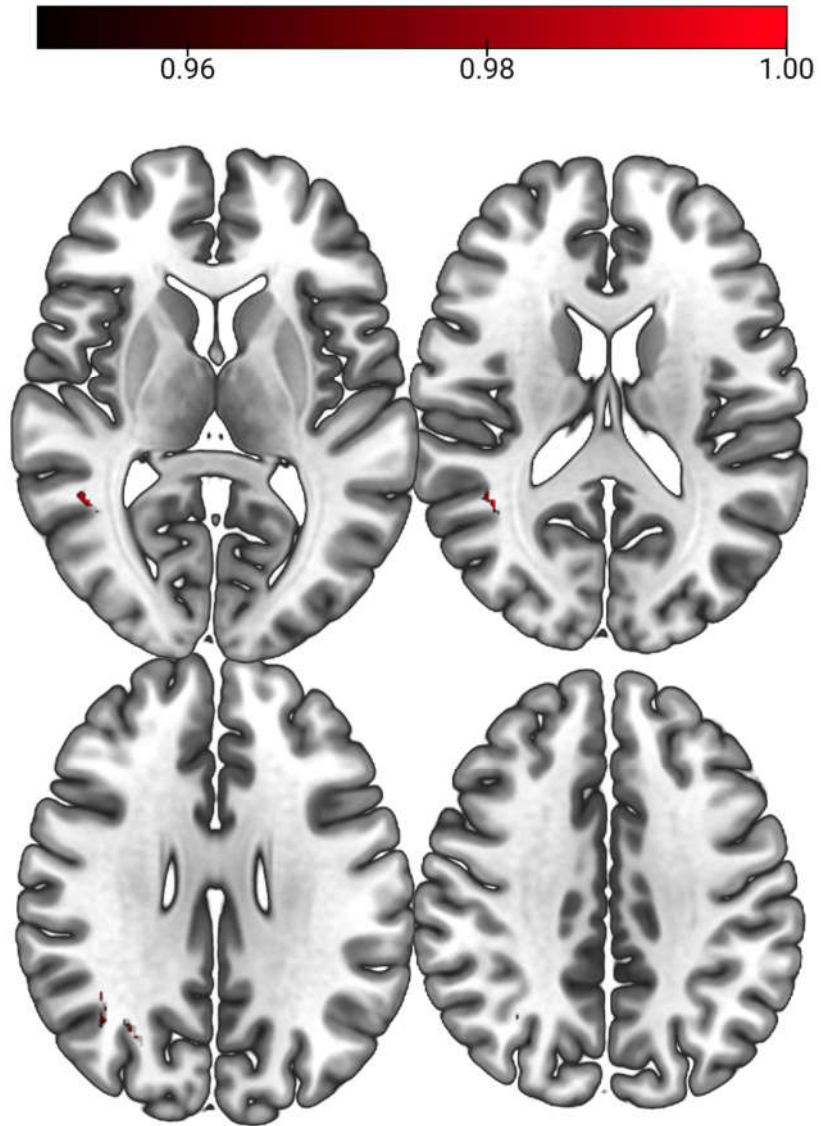


**Figure 3.6.4.:** Significant positive cluster found after FSL-randomise analysis, using 5000 permutations, FWE-correction and TFCE, with sex and GM volume as covariates, overlaid on MNI152 2mm brain template.

When only sex was used as a covariate for sensitivity analysis, a larger significant cluster with a positive relationship to age was found in the same location (*Figure 3.6.5.*).

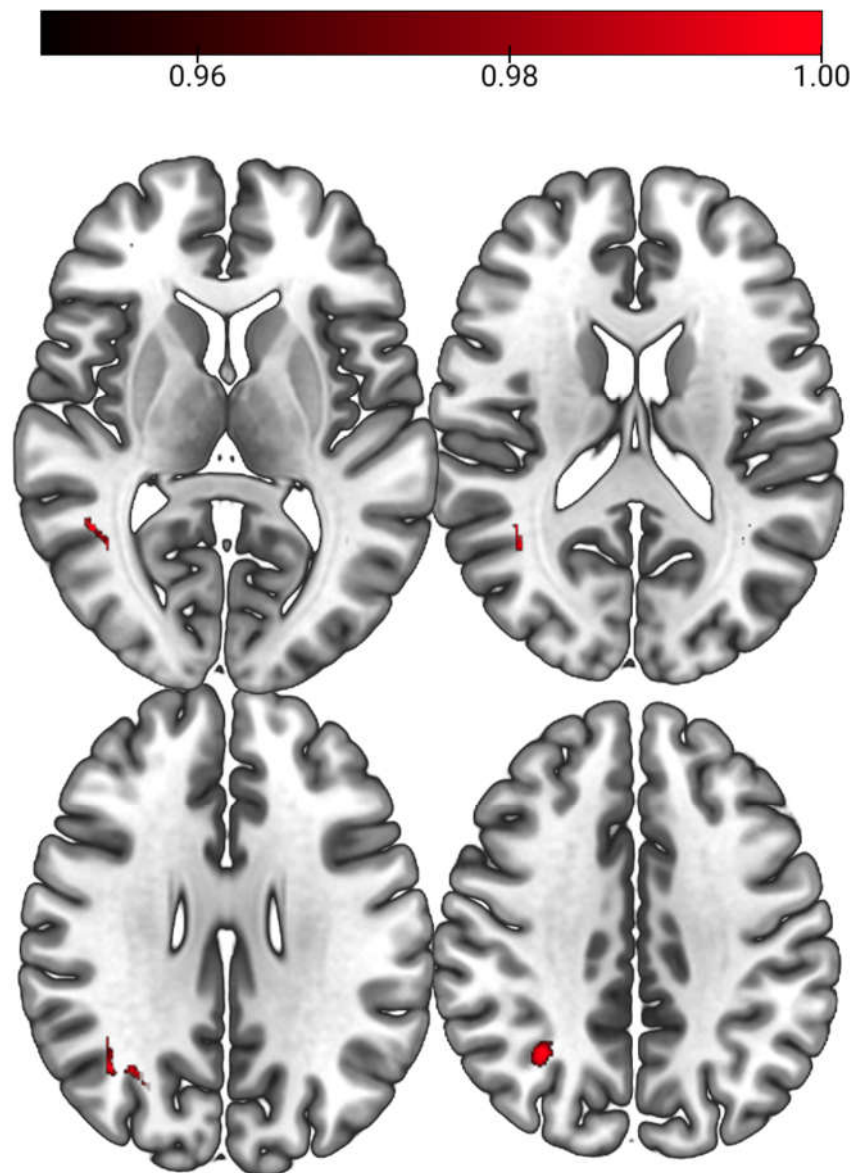


**Figure 3.6.5.:** Significant positive cluster found after FSL-randomise analysis, using 5000 permutations, FWE-correction and TFCE, with only sex as a covariate, overlaid on MNI152 2mm brain template.

### **FSL-flameo**

FSL-flameo with pTFCE was carried out *post-hoc* to compare with the results of FSL-randomise but found no significant clusters when using sex only as a covariate, or sex and GM volume as covariates.

### 3.6.2.2. Principal component analysis

A PCA-based linear regression model was used to assess the relationship between cerebral perfusion and subject age and derive an associated pattern of spatial covariance. This was carried out for the full cohort, a five-fold validation cohort, and male and female subcohorts separately.

#### **PCA-derived perfusion pattern in full cohort**

The PCA model considered 28 components – components 1-28. The overall model had an  $r^2$  of 0.8292 when the covariates of sex, GM volume and whole GM CBF were considered, but this reduced to  $r^2 = 0.779$  when sex was the only additional covariate of interest. The 28 surviving components explained 55.1% of the variance in age. The visual output for these combined components is exhibited below in *Figure 3.6.6.*, and the variance resulting from each of these components summarised in Table 3.6.1..

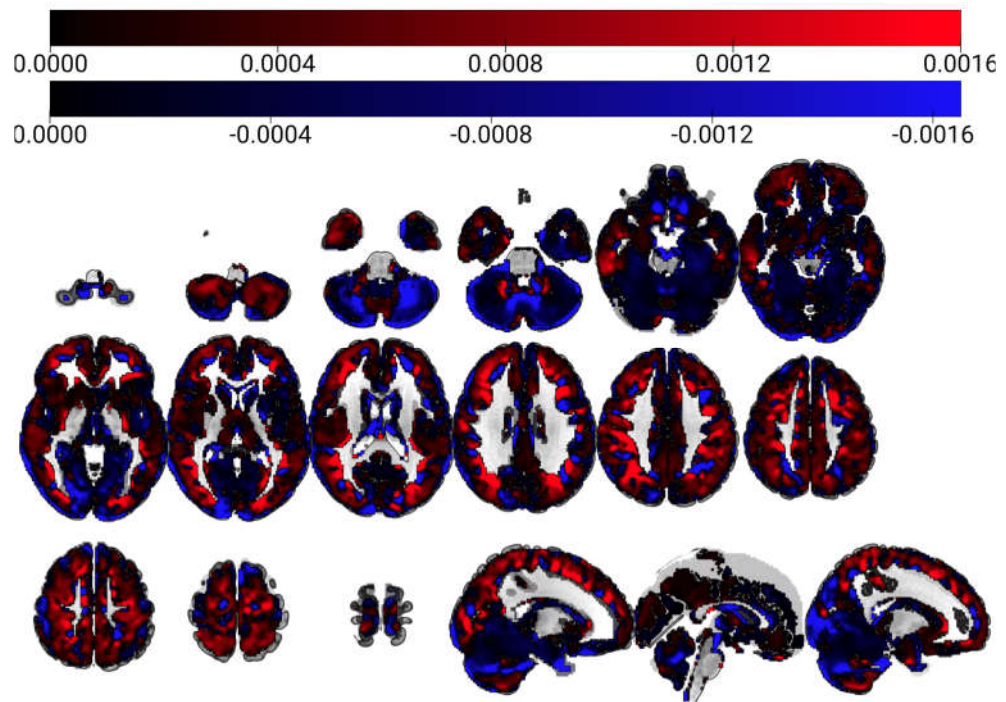


**Figure 3.6.6.:** *The age-associated perfusion covariance pattern resulting from the combined surviving components (1-28) in the full cohort, overlaid on the MNI152 template with 2mm resolution. The associated scale is in arbitrary units, but perfusion values in the blue regions are negatively associated with age, and perfusion values in the red regions are positively associated with age.*

This pattern is characterised by positive associations with age in parts of the cerebellum, cuneus, precuneus, occipital cortex, temporal and frontal poles, frontal, angular, postcentral, temporal cingulate, paracingulate, anterior and posterior supramarginal gyrus, and superior parietal lobule. Negative associations were found in parts of regions including the cerebellum, occipital cortex, frontal pole, frontal, temporal and anterior parahippocampal gyri, subcallosal cortex and the left and right thalami.

**Table 3.6.1.: Variance in age explained by each surviving component.**

<b>Component number</b>	<b>Variance (%)</b>
1	7.56
2	5.02
3	3.68
4	2.89
5	2.56
6	2.4
7	2.12
8	1.93
9	1.79
10	1.71
11	1.57
12	1.52
13	1.5
14	1.45
15	1.42
16	1.38
17	1.35
18	1.33
19	1.32
20	1.3
21	1.24

22	1.22
23	1.2
24	1.18
25	1.14
26	1.13
27	1.11
28	1.08

---

The top five components are depicted in *Figure 3.6.7.* below.

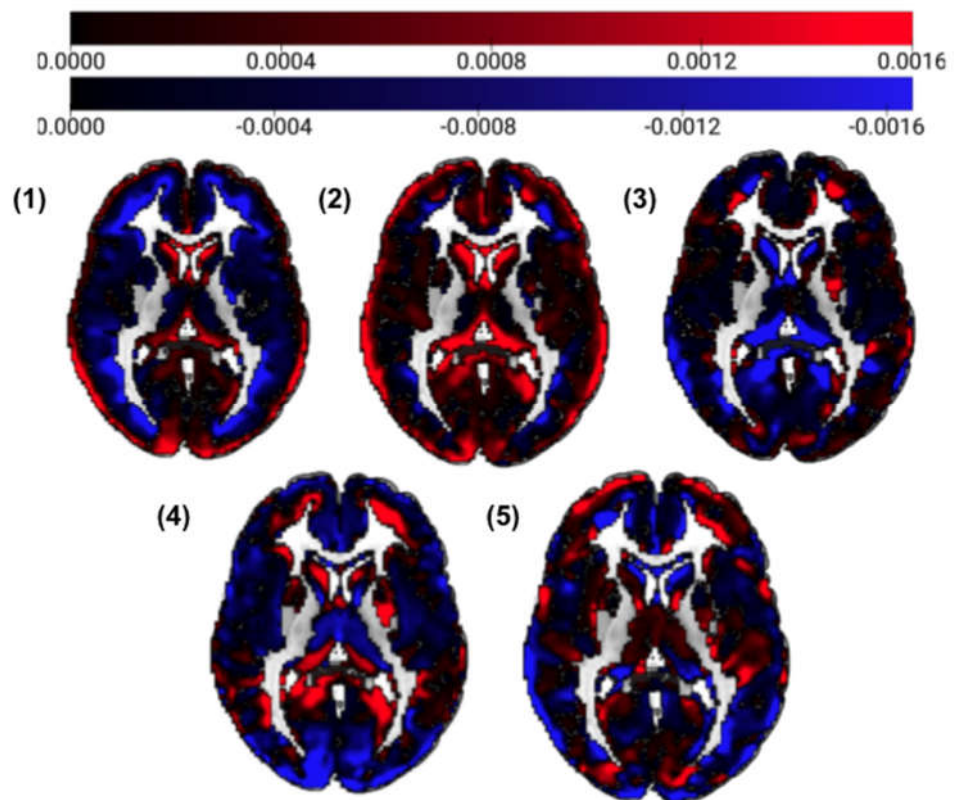


**Figure 3.6.7.:** The top five components (1-5) from the PCA-derived pattern of perfusion covariance, overlaid on the MNI152 2mm template. Perfusion values within blue regions are negatively associated with age, and vice-versa for red regions.

### Five-fold validation - age prediction

The quality of the age prediction was assessed using linear regressions which determined the relationship between actual age and predicted age, resulting in  $r^2$  values of between 0.5316 to 0.7297 ( $p < 0.001$  for all). The fits of these regressions are shown in *Figure 3.6.8.*, and the demographics of each validation group in *Table 3.6.2.* Spatial covariance patterns from each of the five PCA cohorts were compared, and are shown in *Figure 3.6.9.* No clear regional difference was seen within the resultant patterns.

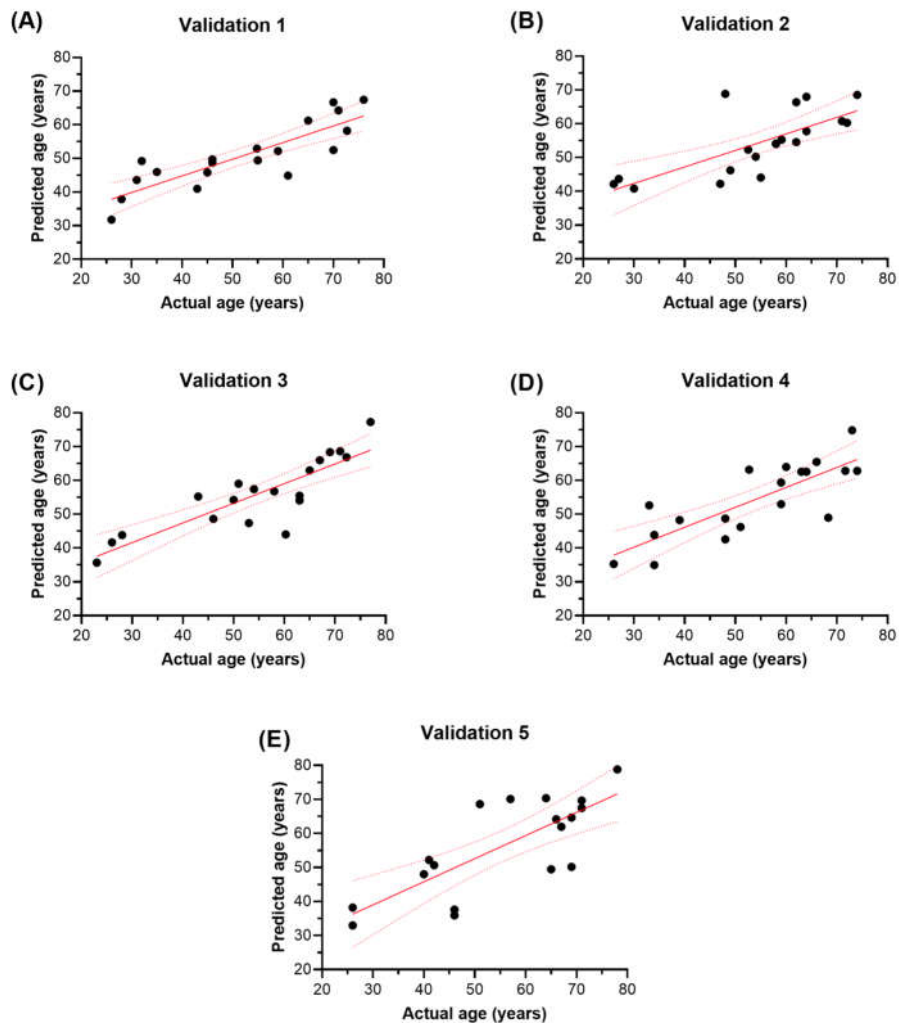


**Figure 3.6.8.:** Results of the linear regressions carried out in the five-fold cross-validation analysis within validation cohorts (A) 1, (B) 2, (C) 3, (D) 4, and (E) 5, respectively. The line of best fit is in red, and the dotted red lines represent the 95% confidence bands of the best fit lines.

**Table 3.6.2.:** Summary demographics for PCA and validation cohorts used for five-fold validation.

<b>Cohort</b>	<b>Number of subjects</b>	<b>Sex</b>	<b>Age (years, <math>\pm</math> SD [range])</b>
<b>PCA 1</b>	75	29 M: 46 F	54.55 $\pm$ 14.92 [23-78]
<b>Validation 1</b>	19	7 M: 12 F	51.93 $\pm$ 16.52 [26-76]
<b>PCA 2</b>	75	29 M: 46 F	53.93 $\pm$ 15.55 [23-78]
<b>Validation 2</b>	19	7 M: 12 F	54.35 $\pm$ 14.14 [26-74]
<b>PCA 3</b>	75	29 M: 46 F	53.84 $\pm$ 15.15 [26-78]
<b>Validation 3</b>	19	7 M: 12 F	54.71 $\pm$ 15.83 [23-77]

<b>PCA 4</b>	75	26 M: 49 F	$54.05 \pm 15.37$ [23-78]
<b>Validation 4</b>	19	10 M: 9 F	$53.88 \pm 14.95$ [26-74]
<b>PCA 5</b>	76	31 M: 45 F	$53.72 \pm 15.11$ [23-77]
<b>Validation 5</b>	18	5 M: 13 F	$55.28 \pm 15.96$ [26-78]

---

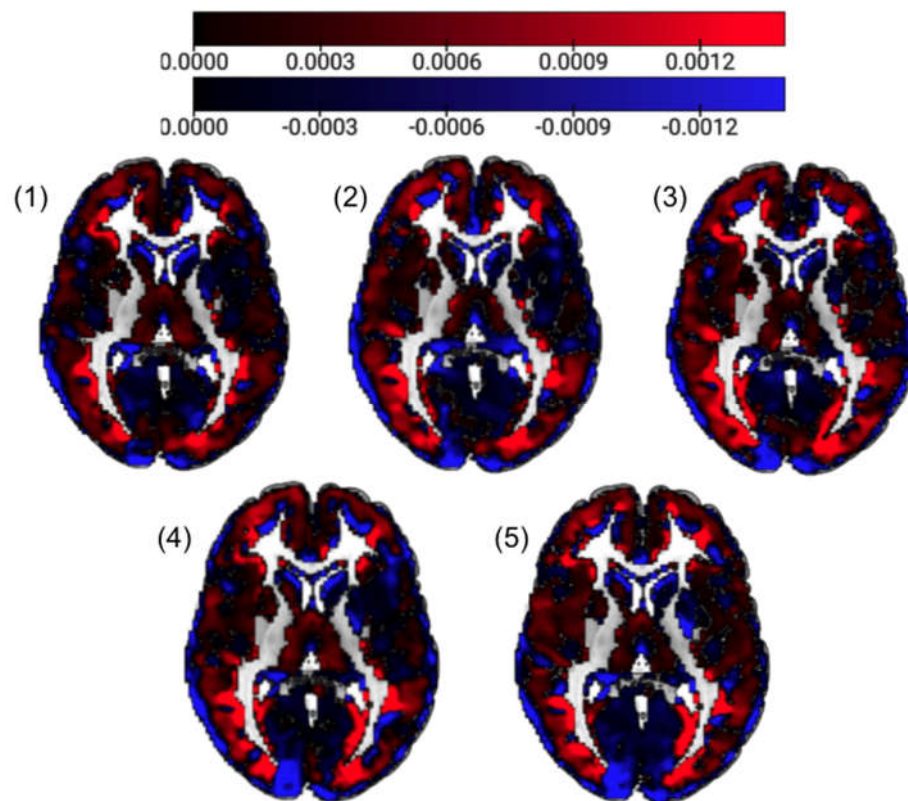


**Figure 3.6.9.:** Spatial covariance patterns in each of the five-fold validation cohorts (1-5), overlaid on the MNI152 2mm template. Perfusion values within blue regions are negatively associated with age, and vice-versa for red regions.

### **PCA-derived perfusion pattern in male subjects**

The same PCA analysis was run again on only male subjects. This analysis considered 10 components (components 1-10). The overall model quality was  $r^2 = 0.8348$ , and the surviving components explained 54.3% of the variance in age. The resultant pattern is shown in *Figure 3.6.10*.

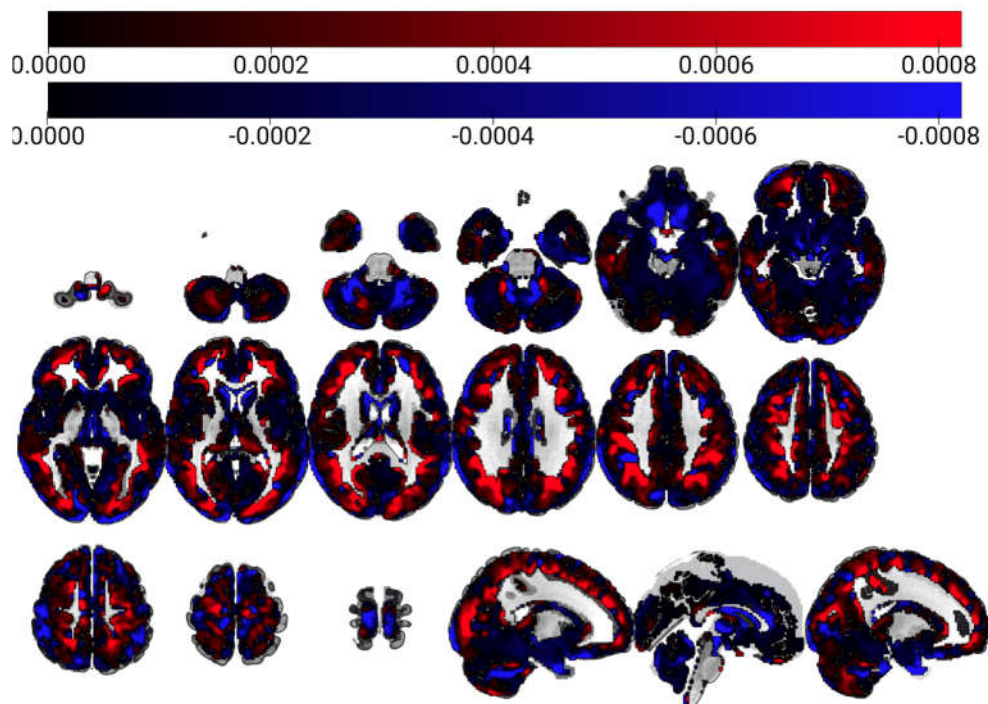


**Figure 3.6.10:** The pattern resulting from PCA analysis within the male sub-cohort ( $n=36$ ), comprising all surviving components. Higher perfusion values in blue regions will reduce the estimation of age, and higher perfusion values in red regions will increase this estimation.

### **PCA-derived perfusion pattern in female subjects**

PCA analysis was run on the female sub-cohort, with the model considering twenty components (components 1-20). The resultant model quality was  $r^2 =$

0.8334, and 53.81% of the variance was explained by the surviving components. The resultant spatial covariance pattern is shown in *Figure 3.6.11.*

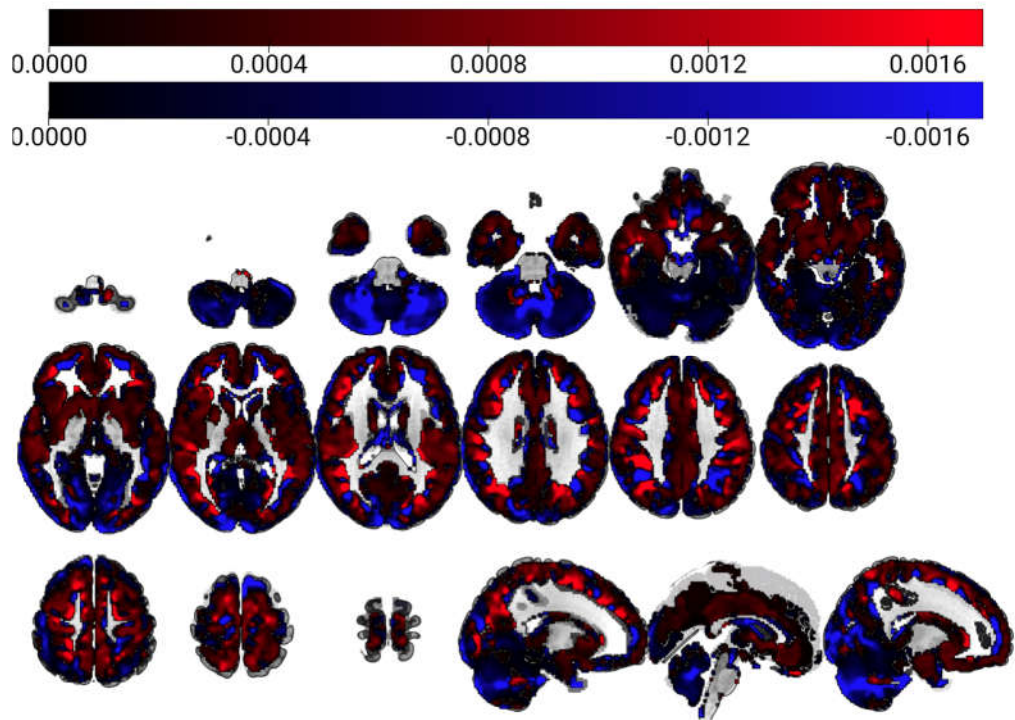


**Figure 3.6.11.:** *The pattern resulting from PCA analysis within the female sub-cohort (n=58), comprising all surviving components. Higher perfusion values in blue regions will reduce the estimation of age, and higher perfusion values in red regions will increase the estimated age.*

The male and female spatial covariance patterns do slightly vary, with females exhibiting a greater preponderance of negative regional association in the cerebellum and occipital regions.

### 3.7. Use of spatial coefficient of variation to understand brain perfusion changes

#### 3.7.1. Introduction

The way in which blood flow differs within a defined region is of interest in understanding the heterogeneity of perfusion changes in the brain that are apparent with ageing. Assessment of ATT – the time required for the labelled blood to travel to the ROI – is often employed to glean further information regarding the haemodynamic status of cerebral tissue, enabling accurate calculation of absolute CBF values. ATT has been shown to be significantly longer in elderly subjects (Dai et al., 2017), and implicated in AD, correlating negatively with MMSE scores (Mak et al., 2012). However, ATT can only be derived from multi-PLD data, but sCoV measures provide a method for inferring spatial heterogeneity of blood flow from single-PLD data (Mutsaerts et al., 2017), by assessing perfusion variance on the basis of the relationship between the standard deviation and mean of perfusion values within the ROI. Physiologically, this metric assumes that an intra-vascular labelling delay is reflected in ASL signal variance. This can in turn inform on underlying vasculature and related disease conditions. Given this technique has only been proposed relatively recently, there is a limited number of studies which employ it. Mutsaerts et al (2020) showed that sCoV could be used to determine the occluded side of the brain in patients with carotid occlusive disease with a sensitivity rate of 96.4%, whereas the same assessment with CBF measures revealed a sensitivity rate of 71.4%. A study by Ibaraki et al. (2019) looked at steno-occlusive disease and found sCoV measures were significantly positively correlated with ATT. Theoretically, arrival of the label differently affects sCoV and CBF, with sCoV only requiring the label to have arrived within an imaging voxel, compared with the necessity for tissue arrival

in CBF measures, and may therefore provide an interesting and clinically-useful metric, particularly for investigation of those with cerebrovascular pathology, or in ageing when cerebral blood vessels are known to become more tortuous (Brown and Thore, 2011).

Few sCoV studies investigating ageing have been carried out. Shirzadi et al. (2019) use this as a discriminatory technique which can aid the distinction of individuals into different cognitive groups, particularly cognitively healthy and cognitively impaired, finding sCoV was higher in AD and MCI patients than healthy controls. Additionally, memory clinic patients with cortical microinfarcts have been shown to have 22% higher sCoV measures than those without (Ferro et al., 2020). As of yet, sCoV has not been studied across the healthy age span, nor in vascular territories within such a cohort. Both are needed to enable a fuller understanding of the utility of this metric in such a cohort.

The aim of this additional sub-study was to determine the usefulness of sCoV as a metric for understanding perfusion changes across the brain with age, and how this compares with traditional cerebral perfusion measures. It was hypothesised that associations between age and sCoV would be stronger than those of age and perfusion, in both GM and key networks.

### 3.7.2. Methods

The mean and standard deviation of perfusion values were determined in GM, key networks of interest, and vascular territories, using FSL (Jenkinson et al., 2012). sCoV was calculated as follows:

$$sCoV_{ROI} = \frac{\sigma(CBF_{ROI})}{\mu(CBF_{ROI})} \cdot 100\%$$

[3.12]

Where  $\sigma$  is the standard deviation of CBF, and  $\mu$  is the mean CBF, within a given ROI.

Linear regressions were then carried out using SPSS to assess the relationship between mean perfusion/sCov values, and age, and how these varied by merit of PLD.

### 3.7.3. Results

Spatial coefficient of variation was assessed in GM (whole, cortical and subcortical) and key networks.

#### **sCoV within GM**

Linear regressions between sCoV measures and age revealed were significant when considering the whole GM ( $\beta = .072$ , 95% CI: .039 to .104,  $p = .000$ ), cortical GM ( $\beta = .177$ , 95% CI: .127 to .228,  $p = .000$ ), and subcortical GM ( $\beta = .093$ , 95% CI: .038 to .149,  $p = .001$ ). Table 3.7.1. summarises how

these results are altered after controlling for covariates, and *Figure 3.7.1.* shows GM perfusion maps in subjects with a range of sCoV values.

**Table 3.7.1.: P-values resulting from linear regressions assessing the relationship between age and sCoV within the GM. Significant p-values are highlighted (\*).**

Region	No adjustment	Sex-adjusted	Sex- and GM volume-adjusted
Whole GM	.000*	.000*	.000*
Cortical GM	.000*	.000*	.000*
Subcortical GM	.001*	.002*	.026*

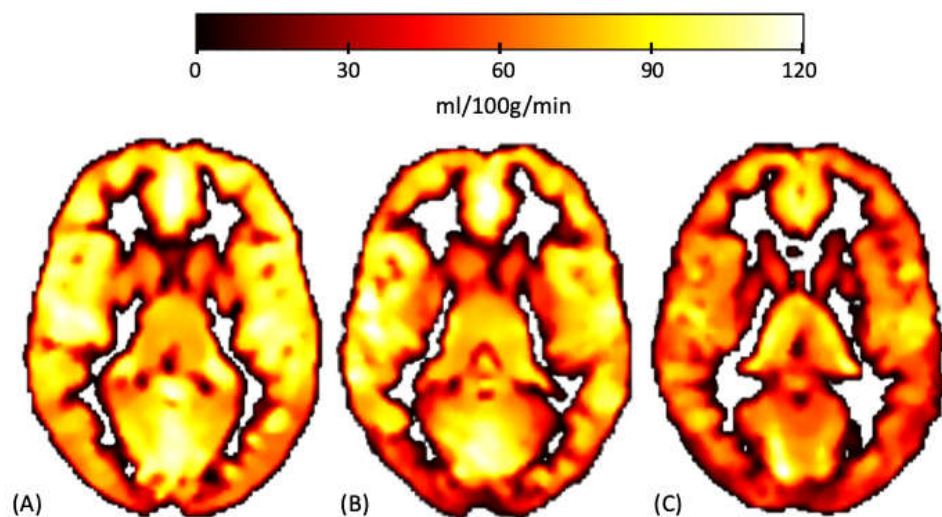


**Figure 3.7.1.: GM perfusion maps (ml/100g/min) in subjects with varying whole GM sCoV measures. (A) shows the subject with lowest sCoV score, a 26-year-old female [sCoV = 29.77%], (B) a 62-year-old female with intermediate sCoV score [sCoV = 37.41%], and (C) the highest sCoV score, in a 65-year-old female [sCoV = 45.3%].**

It is also notable that the registration outlier subject (see Section 3.3.2.1.) has the highest sCoV value within their whole GM (45.3%).

Whole GM sCoV measures were also compared with age on the basis of PLD. Results are depicted in *Figure 3.7.2.* Table 3.7.2. summarises how these findings vary when additional covariates are accounted for. Two-tailed unpaired t-tests with Welch's correction revealed no significant difference in sCoV due to PLD in either males or females ( $p > 0.05$  for both).

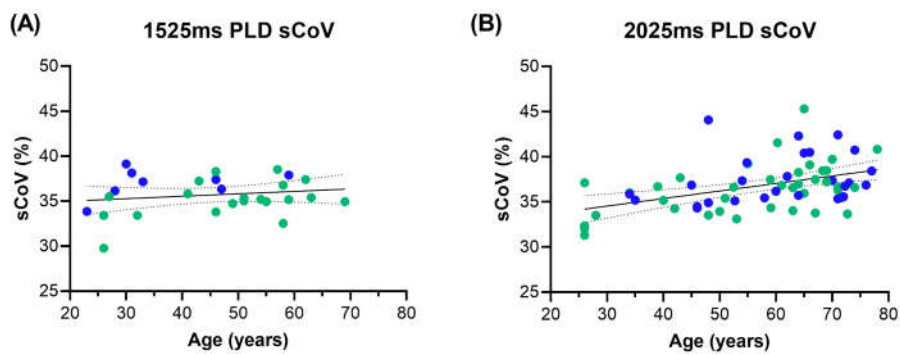


**Figure 3.7.2.:** Comparison of sCoV in whole GM in (A) subjects with a PLD of 1525ms, and (B) subjects with a PLD of 2025ms. Female data points are depicted in green, males in blue.

**Table 3.7.2.: P-values resulting from linear regressions assessing the relationship between age and sCoV within the whole GM by merit of PLD. Significant p-values are highlighted (\*).**

PLD	No adjustment	Sex- adjusted	Sex- and GM- volume-adjusted
1525	.369	.037*	.130
2025	.000*	.001*	.000*

When linear regressions for males and females were carried out separately for PLD = 1525ms – without adjustment, including GM volume as a covariate, and including GM volume and whole GM CBF as covariates – no significant results were found ( $p > 0.05$  for all). The same analysis for PLD = 2025ms found no significant results for male subjects ( $p > 0.05$ ), but significant results for females in all conditions ( $p < 0.01$  for all).

### **sCoV within key brain networks**

The ECN, SN, DMN and precuenus network sCoV measures were compared with age, using linear regressions. These were significant in all networks of interest ( $p < 0.01$  for all), prior to any corrections. Table 3.7.3. shows the results of these regressions after controlling for covariates.

**Table 3.7.3.: P-values resulting from linear regressions assessing the relationship between age and sCoV in networks of interest. Significant p-values are highlighted (\*).**

<b>Network</b>	<b>No adjustment</b>	<b>Sex-adjusted</b>	<b>Sex- and GM volume-adjusted</b>
<b>ECN</b>	.000*	.000*	.000*
<b>SN</b>	.000*	.000*	.003*
<b>DMN</b>	.003*	.003*	.008*
<b>Precuneus network</b>	.000*	.000*	.000*

sCoV measures in GM and networks of interest were generally found to be more significantly associated with age than perfusion measures in the same regions, when standardised linear regression betas were compared (Appendix C).

### 3.8. Cerebral perfusion and spatial coefficient of variation in vascular territories

#### 3.8.1. Introduction

The brain is perfused by blood supplied by multiple arteries (Tatu et al., 1998), with each supplying a specific tissue territory. These vascular territories can be informative in cerebrovascular diagnostics, through determination of the likely vessel supply for haemodynamically-disrupted regions, and can be independently assessed to understand perfusion variance across the brain in

healthy ageing or age-associated health conditions. Particularly, watershed regions of the brain – the regions which are considered to be border-zone regions, as they are supplied by branching ends of the arteries, and resultantly may have a decreased blood supply (Torvik, 1984; Momjian-Mayor and Baron, 2005) – may be of great interest as they are the first deprived of sufficient blood flow under conditions of cerebral hypoperfusion (Suter et al., 2002), and infarcts within these regions are thought to contribute to declining cognitive abilities in AD (Miklossy, 2003).

However, the boundaries of these territories are highly variable and individual anatomy can vary markedly (Hendrikse et al., 2008; Shi, 2016), particularly when considering the watershed regions, making comparisons across studies challenging. Generally, the brain is split into regions which are contributed to by key vessels, including the left (LICA) and right (RICA) internal carotid, and vertebrobasilar arteries (VBA) (*Figure 3.8.1.*). The anatomy of the core territories of these three vessels is very consistent between subjects – the LICA and RICA supply much of their respective cerebral hemisphere, and in most instances the VBA supplies blood to the cerebellum, brainstem, occipital lobes and thalamus. Asymmetry of the VBA is also common (Ghandehari and Ghandehari, 2012).

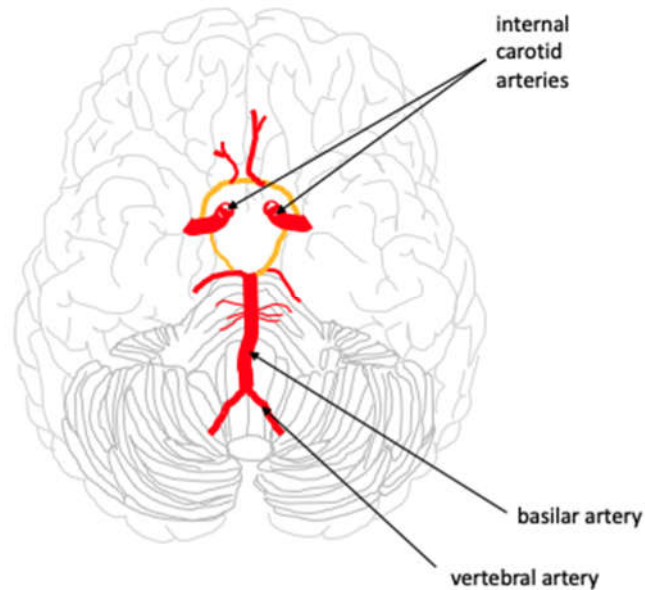


**Figure 3.8.1.:** Schematic of the inferior surface of the brain, depicting key blood vessels and their position within the cerebrovasculature. The vertebral, basilar and internal carotid arteries are shown, with the Circle of Willis depicted in orange.

Previous work assessing vascular territories has predominantly been carried out by vessel-encoded ASL (VE-ASL), given methodological specificity to the assessment of blood vessels, whereby vessels can be labelled separately, and then the origin artery of blood for each voxel determined through a set of simultaneous equations (Wong, 2007; Okell et al., 2010). Direct assessment of vascular territories is only possible using the aforementioned VE-ASL method, or angiography, however multi-PLD acquisition can provide an indirect index of watershed regions by merit of label arrival times. Single-PLD ASL assessment of vascular territories is not often carried out due to the inability to identify signal contributions from a given vessel, or indirectly infer on their integrity. However, given the consistency of core territories of the LICA, RICA and VBA across individuals, assessing these territories using appropriate masks can still inform about the perfusion variance across the

brain. Blood flow measures may highlight any perfusion issues within tissue which is perfused via a specific vessel, particularly in distal vasculature, whereas sCoV may provide additional information pertaining to vessel health and asymmetries on the basis of signal dispersion. Indeed, ATT has been shown to increase in watershed regions (Hendrikse et al., 2008), and sCoV findings may be similar, given the potential of sCoV as a proxy for ATT. As such, blood flow and sCoV metrics may be of interest in combination.

This sub-study aimed to use the aforementioned cohort (Section 3.2) to assess age-related variance in cerebral perfusion and sCoV with the LICA, RICA and VBA, as well as watershed regions. It was hypothesised that territory perfusion would decrease significantly with age, and sCoV would significantly increase with age. Additionally, it was hypothesised that both perfusion and sCoV measures may vary between different territories, due to the respective distance from the labelling plane and possible age-related vasculature changes. The most significant relationship between both perfusion and age, and sCoV and age was expected to be within watershed regions. sCoV measures were expected to be highest in the watershed regions.

### 3.8.2. Methods

Within the literature, two vascular territory maps were identified for possible use. The first originated from the Vanderbilt University Medical Centre, specifically the Vanderbilt Brain Institute Donahue Laboratory (<https://www.vumc.org/donahue-lab/software>), and the second from work in a hypertensive elderly cohort by Mutsaerts et al. (2015), based on territories defined by Tatu et al. (1998), and deposited by the author on FigShare (<http://dx.doi.org/10.6084/m9.figshare.1488674>).

The Donahue Laboratory atlas is a flow territory probability atlas, comprising maps of the LICA and RICA and created using a cohort of 158 adult subjects using vessel-encoded PCASL (VE-PCASL, Wong, 2007). An algorithm was then applied to combine the resultant images into the three aforementioned flow territories. This algorithm does not distinguish between GM and WM but involves an SNR threshold which effectively does this. The probability refers to the likelihood of a specific voxel being fed by a vessel of interest, across all subjects.

Communications with Professor Donahue clarified that the territory maps originate from a pathological cohort (intracranial vasculopathy – either arteriosclerotic or non-arteriosclerotic moyamoya-like vasculopathy), information which was not provided at the point of download and may explain the asymmetries that were seen in initial processing. There was therefore no suitable healthy vascular territory atlas available. As such, modifications were made to these masks using FSL (Jenkinson et al., 2012). The original RICA mask was flipped and defined as the new LICA mask, and the original VBM mask duplicated and flipped, then the newly-created mask combined with the original to create a symmetrical VBM mask with posterior watershed regions (*Figure 3.8.2.*). Doing this ensured each voxel was only assigned to one of the LICA, RICA or VBA. The Mutsaerts et al. (2015) territory maps were assessed without modifications but were provided as a single file and therefore separated into individual masks in FSL (Jenkinson et al., 2012). This atlas is separated as the anterior (antCA), middle (midCA), and posterior cerebral arteries (postCA) (*Figure 3.8.3.*).

With the help of an expert in both radiology and neuroimaging (Professor Dorothee P Auer), these possible territory masks were visually compared. The modified Dohanue Laboratory territory maps were chosen to use for subsequent analysis, as this map included the precuneus and basal ganglia and was determined by D.P.A. to be more realistic, given her soft experience. The Mutsaerts et al. (2015) maps also appear overly strict in their territory definitions, given inter-subject variation.

The selected masks were limited to the GM mask as previously defined, using *fslmaths* (Jenkinson et al., 2012), and the watershed region maps checked slice-by-slice in ITK-SNAP v3.8.0 ([www.itksnap.org](http://www.itksnap.org), Yushkevich et al., 2006), and then separated by hemisphere in FSL (Jenkinson et al., 2012). SPSS (*IBM SPSS Statistics for Windows*, Version 26, Armonk, NY) was used to assess relationships between sCoV/perfusion and age in these vascular territories, using linear regressions.

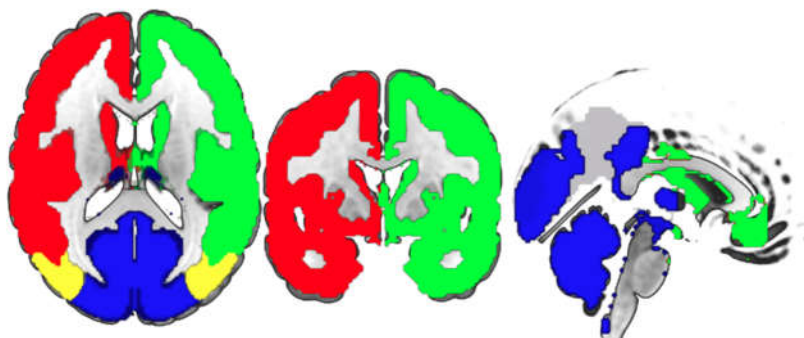


**Figure 3.8.2.:** Selected vascular territory masks based on the Donahue Laboratory atlas, overlaid on an MNI152 2mm brain template. The RICA is depicted in red, the LICA in green, the VBA in blue, with the posterior watershed region in yellow. Shown in radiological convention.

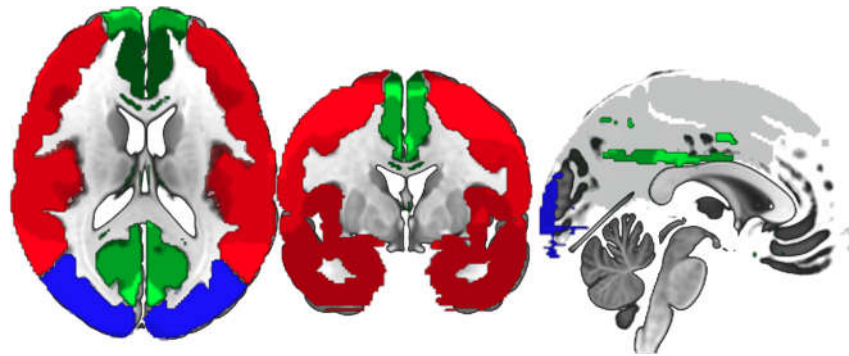


**Figure 3.8.3.:** Masks of vascular territories provided by Mutsaerts et al. (2015), overlaid on an MNI152 2mm brain template. The antCA is depicted in green, the midCA in red, and the postCA in blue.

### 3.8.3. Results

#### 3.8.3.1. Vascular territory perfusion

Summary raw perfusion values for each vascular territory in both males and females are shown in *Figure 3.8.4.*. For all territories, perfusion values which were uncorrected for additional covariates were significantly higher in females ( $p < 0.01$  for all).

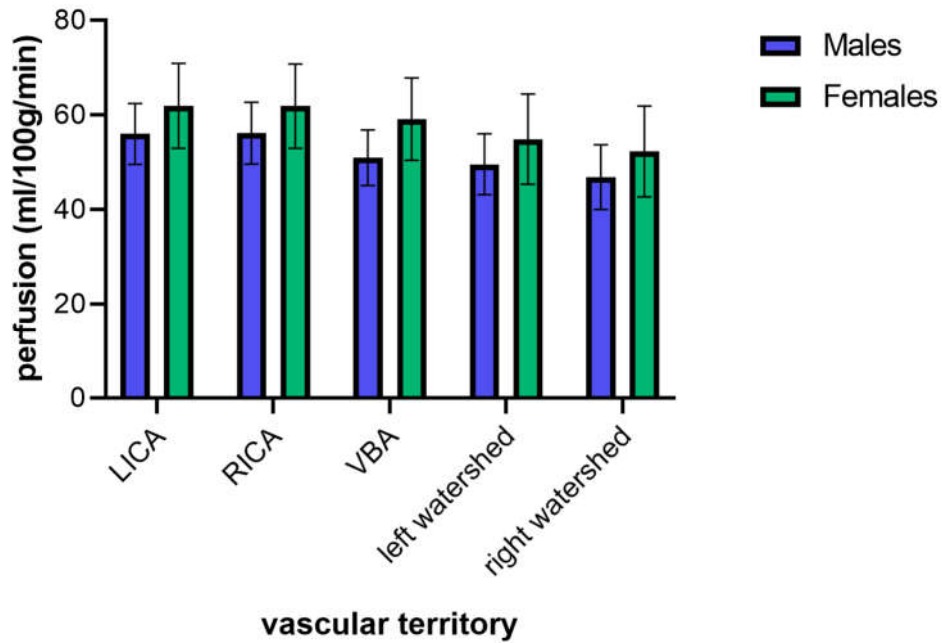


**Figure 3.8.4.:** Summary of vascular territory perfusion values within the LICA, RICA, VBA, and left and right watershed regions of the brain. Males are depicted in blue, and females in green. Error bars represent SD.

The relationships between age and the LICA, RICA, VBA, left watershed and right watershed were investigated to determine whether the relationship varied by vascular territory. The relationship between age and vascular territory CBF declined significantly when considering the LICA ( $\beta = -.128$ , 95% CI:  $-.241$  to  $-.014$ ,  $p = .028$ ) and VBA ( $\beta = -.129$ , 95% CI:  $-.244$  to  $-.014$ ,  $p = .028$ ), prior to correction for additional covariates. This relationship was not significant in the RICA and left and right watershed regions before correction (*Figure 3.8.5.*). Results after inclusion of additional covariates are given in *Table 3.8.1.*

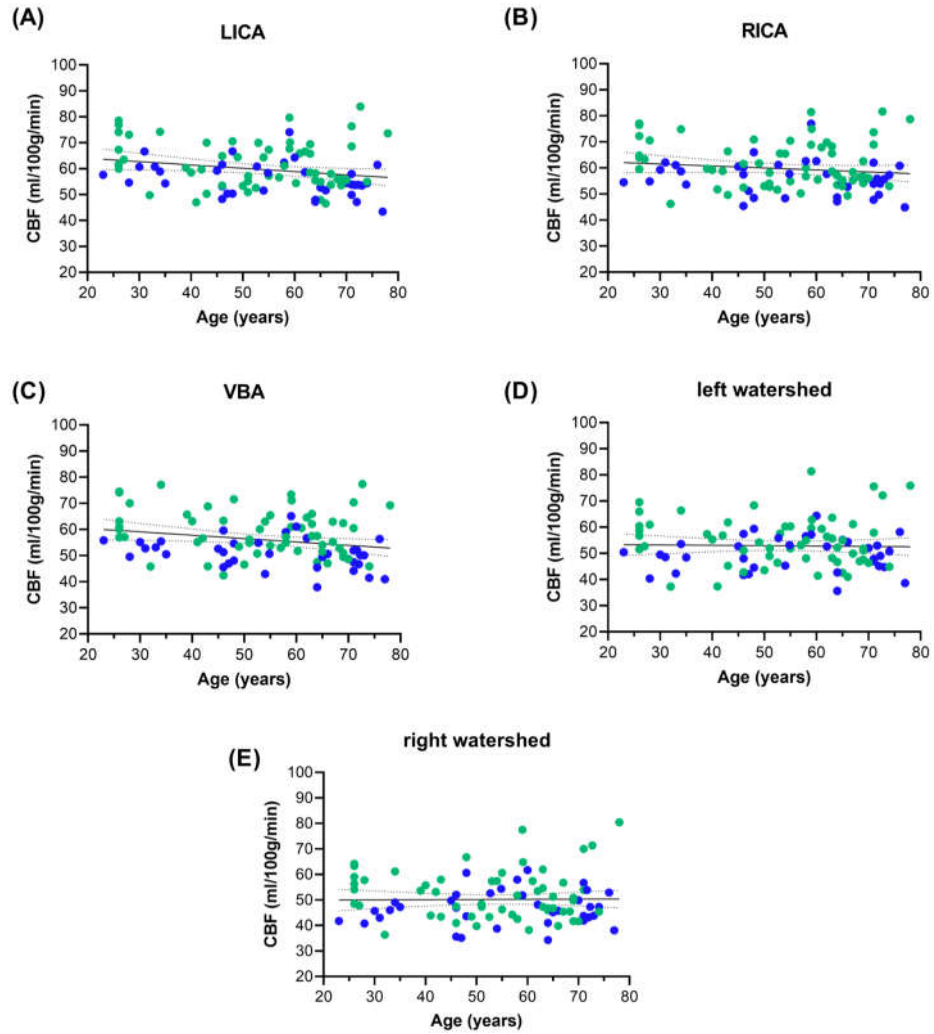


**Figure 3.8.5.:** Linear regressions between age and perfusion values (ml/100g/min) in (a) LICA, (b) RICA, (c) VBA, (d) the left watershed region and (e) the right watershed region. Females are depicted in green, males in blue, the line of best fit is depicted in black and the dotted lines represent the 95% confidence bands of the best fit line.

**Table 3.8.1.:** P-values resulting from linear regressions assessing the relationship between age and perfusion in various vascular territories. Significant p-values are highlighted (\*).

Vascular territory	No adjustment	Sex-adjusted	Sex- and GM volume-adjusted	Sex-, GM volume- and whole GM CBF-adjusted
LICA	.028*	.040*	.275	.949

<b>RICA</b>	.191	.263	.682	.001*
<b>VBA</b>	.028*	.038*	.037*	.001*
<b>Left watershed</b>	.811	.984	.870	.011*
<b>Right watershed</b>	.909	.728	.732	.005*

---

### 3.8.3.2. *Spatial coefficient of variation*

Linear regressions revealed significant relationships between age and sCoV within the LICA ( $\beta = .084$ , 95% CI: .049 to .118,  $p = .000$ ), RICA ( $\beta = .050$ , 95% CI: .019 to .082,  $p = .002$ ) and VBA ( $\beta = .140$ , 95% CI: .096 to .185,  $p = .000$ ) prior to correction for covariates of no interest (*Figure 3.8.6*). The effect of additional covariate inclusion within these linear regressions is summarised in Table 3.8.2..

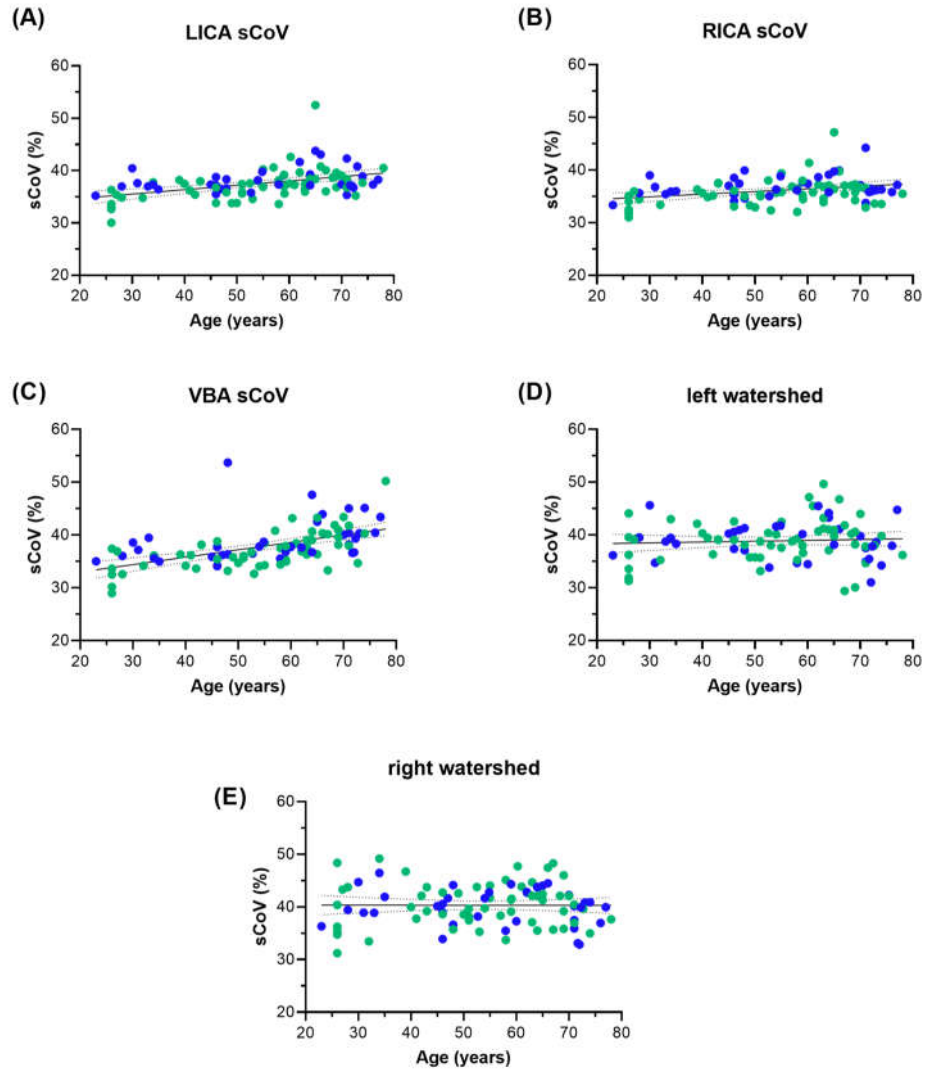


**Figure 3.8.6.:** Linear regressions between age and sCoV values (%) in (a) LICA, (b) RICA, (c) VBA, (d) the left watershed region and (e) the right watershed region. Females are depicted in green, males in blue, the line of best fit is depicted in black and the dotted lines represent the 95% confidence bands of the best fit line.

**Table 3.8.2.: P-values resulting from linear regressions assessing the relationship between age and sCoV in various vascular territories. Significant p-values are highlighted (\*).**

<b>Vascular territory</b>	<b>No adjustment</b>	<b>Sex-adjusted</b>	<b>Sex- and GM volume-adjusted</b>
<b>LICA</b>	.000*	.000*	.000*
<b>RICA</b>	.002*	.003*	.008*
<b>VBA</b>	.000*	.000*	.000*
<b>Left watershed</b>	.534	.529	.174
<b>Right watershed</b>	.972	.994	.913

sCoV measures in vascular territories were generally found to be more significantly associated with age than perfusion measures in the same regions, when standardised linear regression betas were compared (Appendix C). However, the right watershed was more significantly associated with perfusion than sCoV measures.

### 3.9. Discussion

In the present study, variance in cerebral perfusion with age was assessed using a variety of different metrics. Specifically, the study aimed to address whether apparent age- and sex-related changes in perfusion truly exist or can be explained by underlying confounds such as partial volume effects, tissue volume, or sCoV, and assess the age-associated voxel-based and multivariate spatial patterns of perfusion using FSL-randomise, FSL-flameo, and PCA. Key results include three PCA-derived spatial covariance patterns within the whole cohort, and males and females separately, which explain 55.1%, 54.3%, and 53.8% of the variance in age, respectively. A five-fold validation within the full cohort which compared actual age and predicted age with linear regressions resulted in  $r^2$  values between 0.5316 and 0.7297 ( $p < 0.001$  for all). The results of the sCoV sub-study indicate that this metric is more sensitive to age than more traditional perfusion metrics (ml/100g/min), throughout the GM and specified brain networks and vascular territories.

#### 3.9.1. Spatial covariance patterns of cerebral perfusion with age

##### 3.9.1.1. *Principal component analysis*

PCA was used as a MVPA technique to assess covariance across all voxels within the GM, within the full cohort and male and female sub-cohorts separately. The motivation for this study was to elucidate the spatial covariance patterns associated with age in a PVE-corrected cohort, and to use five-fold cross-validation analysis to assess the utility of the PCA-derived perfusion patterns in the prediction of age in the full cohort. The full cohort findings were then compared with univariate, voxel-wise methods.

Within the full cohort, the overall model had an  $r^2$  of 0.8292 when sex, GM volume and GM CBF were considered as covariates, and the subsequent surviving components explained 55.1% of the variance in age. The resultant pattern (*Figure 3.6.6.*) was characterised by positive associations with age in parts of the cerebellum, cuneus, precuneus, occipital cortex, temporal and frontal poles, frontal, angular, postcentral, temporal, cingulate, paracingulate, anterior and posterior supramarginal gyri, and superior parietal lobule. Of particular interest were the associations in the precuneus, an area of complex processing linked to memory (Cavanna and Trimble, 2006), in which perfusion has been shown to significantly decrease with age in previous ASL studies (Lee et al., 2009; Chen, Rosas and Salat, 2011; Preibisch et al., 2011; Zhang et al., 2018). This contrasts with the findings of the current study, which suggests that the perfusion within the precuneus is related to an increased prediction of age and may thus infer increasing perfusion of this region with age.

Negative associations with age estimation were found in regions including parts of the cerebellum, occipital cortex, frontal pole, frontal gyrus, temporal gyrus, anterior parahippocampal gyrus, sub-callosal cortex, and both the left and right thalami. This negative age association within the thalamus is interesting, given its functional connectivity with the hippocampus, and role in working memory (Fama and Sullivan, 2015; Wolff and Vann, 2019). Perfusion of the thalamus has been shown to be positively associated with executive function (Staffaroni et al., 2019), and additionally shown to exhibit both increases and decreases in perfusion with age (Preibisch et al., 2011; Zhang et al., 2018). The current study suggests that perfusion within the thalamus is

negatively associated with age prediction, which supports some of the aforementioned findings.

Whilst the inference which can be drawn from the current study and that of Zhang et al. (2018) differs slightly – their pattern relates to increases or decreases in regional CBF, whereas ours relates to the increase or decrease of the age estimation – there are some key pattern commonalities. Their age-related CBF pattern is characterised by relative increases in temporal and occipital CBF, and decreases in frontal, parietal and cerebellar areas, particularly the thalamus, precuneus, and anterior cingulate gyrus. The PCA pattern in the current study showed that negative clusters within the thalamus was related to a decrease in the estimation of age. Zhang et al. (2018) found decreased perfusion within this region with age, potentially supporting this finding. It is notable that they found perfusion decreases in the precuneus with age, whereas the current study found that perfusion within this region would increase the estimation of age. Whilst the findings of these studies cannot be directly compared, this suggests a key regional discrepancy between both studies which warrants further investigation. It is worth noting that the cohort within the work of Zhang et al. (2018) covered a different age range than the current study and does not use PVE-correction, which may provide some explanation for discrepancies between our findings.

Consideration of the top five components within the whole cohort PCA pattern holds little validity for regional assessment, given that there are a total of 28 components which survive PCA and are thus relevant to the relationship between age and cerebral perfusion. Nevertheless, the outer ring of apparent

positive association (red) in the posterior regions of component 1 is suggestive of possible CSF contamination, however the selected GM mask should control for this possibility. As such, this warrants further investigation within an unseen validation cohort, to determine if this is still seen in the resultant pattern.

The spatial covariance pattern does vary when males and females are considered separately (see *Figure 3.6.10.* and *Figure 3.6.11.*). Females exhibit a greater preponderance of negative regional association in the cerebellum and occipital regions. Notably, there is a high negative association in the orbitofrontal cortex of males which is not seen in female subjects and is implicated in emotion and cognition (Beer et al., 2006).

The findings of the current study highlight that whole GM age-related spatial covariance is not specific to certain ROIs or networks and is a whole-brain process. It is possible that such patterns are driven by perfusion retrogenesis, and related axonal degradation and decreasing myelin in underlying neuronal populations (Salvadores, Sanhueza and Manque, 2017; Bouhrara et al., 2020). The five-fold validation approach suggested that the pattern and model are fairly robust, with  $r^2$  values between 0.5316 to 0.7297 ( $p < 0.001$  for all), although this is a tentative conclusion without validation in an unseen cohort. The lack of notable differences in perfusion pattern between the five PCA validation cohorts is not surprising, due to the vast majority of subjects being shared across these cohorts, given the nature of cross-validation. Future work should aim to determine differences in pattern between the original cohort and an independent validation cohort, however. Nevertheless, this work supports

the assertion that MVPA techniques such as PCA are more sensitive to subtle changes with age than univariate, voxel-wise analysis approaches, resulting in superior pattern expression (Asllani et al., 2008). Independent component analysis (ICA; Jutten and Héroult, 1991) may be an interesting comparator to this work in future studies, with ICA-derived components shown to exhibit similarity with RSNs in healthy subjects (Pirastru et al., 2020).

#### *3.9.1.2. Voxel-wise analysis of cerebral perfusion*

Voxel-wise analysis carried out using FSL-randomise and TFCE, with sex, GM volume and whole GM CBF as covariates, revealed a significant cluster of voxels positively related with age, comprising parts of the angular gyrus, middle temporal gyrus, and lateral occipital cortex. No significant negative associations were found. However, the significant cluster is small enough that it may be considered spurious, and indeed the results of comparative analysis with FSL-flameo and pTFCE, and sense-checking with fewer permutations support this assertion. When only sex is used as a covariate, no negative clusters are found but this positive significant cluster is more pronounced, however FSL-flameo and pTFCE still find no significant clusters. The absence of significant findings using pTFCE is somewhat surprising as the intention of pTFCE is, in part, to improve the sensitivity of cluster identification (Spisák et al., 2019). However, given that FSL-randomise findings could be regarded as spurious, this FSL-flameo result was feasible, particularly after sensitivity testing with covariate removal and repeat analysis to ensure accuracy of data input.

These results are also unexpected when compared with key papers in the field (summarised in Table 3.1.1.). Generally, these papers showed far more expansive coverage of GM with significant clusters, with Willis et al. (2002) finding that 61% of voxels exhibited decreasing metabolism in their FDG-PET study, hence the additional post-hoc analysis using FSL-flameo and pTFCE to confirm these findings. Whilst the current study employed more covariates than some included within the aforementioned table, Zhang et al. (2018) still found negative associations with age in multiple regions including the bilateral thalamus, middle frontal gyrus, caudate body and cerebellum, when only sex is included as a covariate, the sensitivity analysis condition of the current study. It is notable that some of these studies do find consistent GM perfusion decrease with age (Petit-Taboué et al., 1998), which was only found in cortical GM here, after inclusion of additional covariates. This current work employs a larger cohort than the majority of similar studies and employs PVE-correction but given the inter-subject variance which can be seen (Parkes et al., 2004) and that the reason for the current findings is unclear, future replication of this analysis in a larger cohort with acquisition parameters that align with the ASL white paper recommendations (Alsop et al., 2015) is warranted.

### 3.9.2. Cerebral perfusion and ageing

When considering sex differences in underlying measures brain composition which may influence perfusion, there was no significant difference in age between male and female subjects. GM volume was significantly greater in male subjects ( $p < 0.001$ ). There was no significant difference in whole GM perfusion values due to PLD duration in either males or females ( $p > 0.05$  for both).

Further assessment of the full cohort using linear regression revealed no trend in whole GM perfusion with increasing age. This contrasts with studies both with and without PVE-correction. In the largest single-site study which also employs 3D PCASL acquisition and PVE-correction – albeit with a different approach to PVE-correction – Leidhin et al. (2021) found a decrease of 0.2 ml/100g/min per year. Other studies reported decreases of 0.37 - 0.5% per year (Leenders et al., 1990; Bentourkia et al., 2000; Parkes et al., 2004; De Vis et al., 2015), but did not employ PVE-correction, and thus are not directly comparable to the results of the current study. It is notable however that whole GM perfusion was significant after sex and GM volume covariate inclusion, when assessed in the original perfusion maps which had not undergone PVE-correction or smoothing ( $p = .044$ ), highlighting the influence of these processing steps. In the current study, decreases in cortical GM were significant after adjustment for sex, GM volume and whole GM CBF (to address additional variance in perfusion of no interest), which is in contrast with the findings of Meltzer et al. (2000).

Cerebral perfusion within the GM was significantly lower in male subjects, in-line with the findings of various studies (Parkes et al., 2004; Liu et al., 2012; Juttakonda et al., 2021; Leidhin et al., 2021). The mean whole GM perfusion values – 54.9 ml/100g/min and 61.6 ml/100g/min for males and females, respectively – were in-keeping with previous studies using various imaging methods (Huang et al., 1983; Parkes et al., 2004; Alsop et al., 2015; Leidhin et al., 2021).

Perfusion in networks of interest found a significant decline with age after covariate adjustment in only the ECN, which is involved in cognitively demanding processes (Seeley et al., 2007; Turner and Spreng, 2015). The significant decline with age seen in the ECN has previously been identified in the literature (Ng et al., 2016). As such, this network is also investigated in Chapter 4. The lack of significant covariate-corrected changes in perfusion with age in the SN, DMN and precuneus network of this healthy cohort is not surprising, given their important roles in cognitive functionality and rest (Greicius and Kimmel, 2012; Chand et al., 2017; Smallwood et al., 2021).

When sex, GM volume and whole GM perfusion values are adjusted for, only the LICA does not significantly decline with age. This is a surprising finding given the declines in all other territories of interest, and combined with the significant decrease in RICA perfusion, warrants further investigation to elucidate whether this represents an unknown asymmetry, on a subject-by-subject basis.

### 3.9.3. Spatial coefficient of variation

The sCoV metric was used to infer spatial heterogeneity of blood flow, underpinned by the physiological assumption that an intra-vascular labelling delay is reflected in ASL signal variance. Described by Mutsaerts et al. (2017) as a potential proxy for ATT in single-PLD ASL acquisitions, sCoV was employed within the current study to determine its utility in understanding perfusion changes in the brain with age, in comparison to standard ml/100g/min values. sCoV was generally found to be more significantly associated with age than cerebral perfusion measures when standardised

linear regression betas were compared, as hypothesised (see Appendix C). Whilst the relationship between whole GM perfusion and age was not significant, increases in whole GM sCoV with age remained significant, even when additional covariates were included (see Table 3.7.1.). The range of sCoV measures within the whole GM was 29.77 - 45.3%. Notably, the highest GM sCoV value was in the subject who was also the outlier subject during registration quality assessment which, combined with their below average GM perfusion and above average GM volume, may be suggestive of impairments in cerebrovasculature.

Limited comparisons can be drawn with other studies in the literature due to the relative recency of the metric itself. These results are broadly comparable to the findings of Shirzadi et al. (2019) within the lower end of the range of their cognitively unimpaired group (GM sCoV mean = 73.4%, range = 41.3 - 207.6%), however this group used subjects (n = 67) ranging from 56.3 - 87.6 years, notably older and with fewer subjects than the current cohort, and assessed different ROIs to the current study, particularly brain lobes. They also employed 2D PASL ASL techniques, limiting direct comparison. The findings of their study may suggest that the sCoV values within the current study are lower than anticipated, and thus warrants further investigation, particularly in a cohort with identical PLD for all subjects. However, without established normative reference values, it is also possible that the findings of both the current study and Shirzadi et al. (2019) are within normal sCoV limits for healthy individuals.

Within the current cohort, cortical and subcortical sCoV measures also remained significantly associated with age after controlling for GM volume and sex, ROIs which had insignificant results when considering their perfusion. In the vascular territories, sCoV was assessed to determine variances in sCoV within tissues and watershed regions perfused by different vessels. Linear regressions defining the relationship between sCoV and age found significant increases with age in the LICA, RICA and VBA after correcting for sex and GM volume, but not in the left and right watershed regions. The insignificant findings in the watershed regions may be due to the small size of these ROIs and the challenge to define them. The watershed regions were expected to have higher associated sCoV values, and this was broadly the case in subjects up to ~40 years old (*Figure 3.8.6*).

The original sCoV paper by Mutsaerts et al. (2017) also investigated vascular territories, albeit in a hypertensive cohort, and with differently defined vascular territories (anterior, middle and posterior carotid artery territories; Tatu et al., 1998). Whilst the authors did not share explicit sCoV results for these territories, they found that there was lower reliability in the prediction of ATT using sCoV within this region. Although comparisons cannot be drawn here due to differing territory definitions and the lack of comparative multi-PLD data, it is of note to current findings, particularly given that the posterior vasculature can exhibit greater tortuosity with age, and issues with labelling efficiency (Nowinski et al., 2011; Chen, Wang and Detre, 2012). The atlas used by Mutsaerts et al. (2017) has been published (see Mutsaerts et al., 2015), and was considered as an atlas for this study, but this was ultimately not used due to concerns about boundary definitions and inclusion of specific brain structures. When considering vascular territories, it is important to note

that these territory boundaries can vary dramatically between subjects, and any interpretation is cautionary due to the necessity to validate our atlas in a cohort of much greater size.

Linear regressions of sCoV with age within key networks of interest (the ECN, SN, DMN and precuneus network) found significant increases with age, even after correction for sex, GM volume and whole GM perfusion ( $p < 0.05$  for all). When considering cerebral perfusion in these networks, the only significant relationship with age after covariate adjustment was a decrease in the ECN, evidencing more robust age associations with sCoV than cerebral perfusion when considering brain networks. This is interesting, given its role in cognition regulation, working memory, and integration of sensory information, and disruption in cognitive decline (Seeley et al., 2007; Turner and Spreng, 2015). Investigation of such networks is important to inform understanding of subsequent spatial covariance patterns.

The general finding of more robust associations with age using the sCoV metric over cerebral perfusion measures is perhaps not surprising, given the theoretical underpinnings. The sCoV metric does not necessitate the label arriving in the tissue compartment, as in single-PLD ASL, but just the imaging voxel (Alsop et al., 2010; Mutsaerts et al., 2017). Lacking the requirement to specify between vascular and tissue compartments can be advantageous in those who have changes in cerebrovasculature due to ageing, and the normalisation of sCoV to mean GM perfusion may make it more robust to fluctuations that are seen in perfusion, or by merit of discrepancies in quantification parameters across subjects (Mutsaerts et al., 2017). Indeed,

population variation in sCoV was smaller than that of cerebral perfusion. sCoV has been suggested as a proxy of ATT (Mutsaerts et al., 2017), with ATT used to understand cerebral haemodynamics and achieve absolute measures of cerebral perfusion. ATT has been shown to increase with advancing age ( $p < 0.01$ ; Liu et al., 2012), and correlated negatively with MMSE, but positively with the Alzheimer's Disease Assessment Scale - Cognitive Subscale (ADAS-Cog; Mak et al., 2012), and it is important to note that whilst sCoV has been shown to share >70% covariance with ATT (Mutsaerts et al. 2017), various further sources may contribute to the very spatial heterogeneity which it measures. For example, PVEs can result in different tissue contributions to the spatial heterogeneity, if PVE-correction is not carried out, and thus PVE-correction is particularly recommended for future sCoV studies. Smoothing would theoretically lessen the spatial heterogeneity, and thus requires further investigation in future studies of the sCoV metric. However, this was rationalised in the current study given that all subjects had undergone smoothing as a pre-processing step. Head motion, susceptibility distortion, and labelling asymmetry could also contribute to sCoV findings, however adequate quality control and preprocessing metrics can account for some of this. Additionally, the ratio nature of the sCoV metric may minimise some such issues, if present. It is also possible that macrovascular contamination may be driving sCoV, where the label is still on its way to a tissue, and the perfusion values are resultantly overestimated, and is of concern in multi-PLD acquisitions where some PLDs are short (Chappell et al., 2010). This is generally relevant to sCoV as it is calculated in relation to perfusion values, but is also of concern with shorter PLDs such as the 1525ms used for some subjects within this cohort. In the current study there was no significant difference in whole GM sCoV due to PLD in males or females ( $p > 0.05$  for both), although additional investigation into sCoV variance with differing PLDs

is warranted. More accurate definitions of cerebral vasculature on a subject-by-subject basis would also support understanding of sCoV within different territories. It is also important to note, however, that sCoV may simply reflect regional heterogeneity in metabolism or cerebral perfusion and may not show future utility as an ATT proxy.

*Post-hoc* comparison of perfusion and sCoV in whole GM at both 1525 and 2025ms was carried out, and the results of PLD = 1525ms revealed no significant results when assessing the relationship between perfusion and age, even after adjustment for covariates. For sCoV in this cohort, results were only significant after adjustment for sex, but this significance was not retained after inclusion of GM volume as an additional covariate. Separating this cohort by sex revealed no significant results in either males or females, suggesting that this initial finding of significance was driven by the covariates which were subsequently included. These results should be considered with caution, not only due to the limited cohort size, but given that the PLD does not meet white paper recommendations, particularly for older subjects (Alsop et al., 2015). Identical analysis of data acquired at a PLD of 2025ms found significant relationships between age and sCoV when all covariates are considered. CBF and age were significantly related when adjusted for sex and GM volume independently, but not when adjusted for both covariates, highlighting the necessity for inclusion of any covariates which may be relevant, if possible. When separated by sex, no significant relationships between age and whole GM perfusion are found. The relationship between sCoV and age in males are insignificant in all conditions, whereas they are significant in all covariate conditions in females, suggesting that the group results are driven by females, although this is to be expected due to the

difference in subject numbers between males and females. Ultimately, such analysis would benefit from further study in a larger cohort, with PLDs shorter and longer than the recommended PLD tested in the same subjects. It would also be recommended to test this in subjects of various age groups comprising subjects with very similar ages, to better understand the variance in sCoV at a given age. The recommended PLD is either 1800ms (<70 years old) or 2000ms (>70 years old), and therefore the current parameters used for some subjects (1525ms) may be too short to enable adequate arrival of labelled blood in the imaging plane and may explain some of the subject attrition seen in this study. The implications of these sub-optimal parameters will vary by subject however and can be affected by their individual anatomy and vasculature. The utility of the sCoV measures described within this study is limited, as they are yet to be compared in a study directly with ATT, which would enable determination of its validity. Further investigation is also required to assess the variance in sCoV with inclusion of other covariates which may affect vessel length. It also may be of interest to compare the utility of sCoV with more advanced metrics such as signal histogram analysis (Emblem et al., 2008). It should be noted however that this metric is excellent in its simplicity and lack of requirement for additional acquisition or further costs, and resultantly may prove clinically useful with further validation. sCoV also may have potential utility in WM (Mutsaerts et al., 2017), a tissue in which perfusion measures can be challenging (Skurdal et al., 2015). As the results of the current study indicated that signal dispersion is more sensitive to age than average perfusion values, sCoV has additional value to studies of disrupted brain vasculature, such as stroke (Lo, Dalkara and Moskowitz, 2003), cerebral small vessel disease (Pantoni, 2010), and vascular dementia (O'Brien and Thomas, 2015).

#### 3.9.4. Data processing

Registration quality is generally difficult to assess, however the Pearson's cross-correlation strategy, which involves calculation of this metric between a subject's perfusion map and a GM probability map, provides a quick and quantifiable approach which is comparable to other strategies suggested in the literature (Mutsaerts et al., 2018). Whilst this approach to registration quality assessment would have been more accurate if the ASL image pairs or  $M_0$  image for each subject were utilised — as these would enable the quality of registration to be evaluated pair-by-pair, and account for calibration within the registration assessment — these were unavailable in this study, and thus a single, noisy perfusion map had to be used. Future use of this metric for image registration quality assessment should make use of these additional image types where possible. It would also be interesting to trial pairwise Pearson's cross-correlation between all CBF maps in future, as a measure of consistency. The influence of PVE-correction significantly affected the resultant perfusion values, which is supported by other studies within the field (Ibáñez et al. 2004; Allsani et al., 2009), and the work of Chappell et al. (2021) argues for combined reporting of PVE-corrected and uncorrected values, which the findings of the current study support.

#### 3.9.5. Limitations of the study

The most significant limitation of this study is a lack of longitudinal data. Such data would allow for evaluation of changes in brain perfusion, spatial covariance patterns, and sCoV over time, providing additional information as to their utility in understanding how brain physiology changes with age which

is not available with cross-sectional study design. Additionally, there are no published studies employing the mLTS PVE-correction approach (Liang, Connelly and Calamante, 2013) in ageing-focused studies, making comparison and interpretation of results caveated by methodological discrepancies. It should also be noted that whilst Bonferroni correction was considered within this chapter, such multiple test corrections put undue significance on an arbitrary threshold (Rothman, 1990; Perneger, 1998; Morgan, 2007), and as such the discussion and interpretation focuses on the original p-values, whilst acknowledging that multiple tests have occurred.

The high attrition rate within this cohort also limited the data available for analysis. Whilst the white paper (Alsop et al., 2015) guidance was followed for the most part, the use of an exclusion criterion of  $\leq 20$  ml/100g/min perfusion in occipital regions of the brain was employed due to historical quality control norms within the University of Nottingham. It is notable that this criterion was often responsible for subject exclusion in the current study (although rarely exclusively). However, the validity of this approach — rationalised as evidence of improper labelling — is uncertain and may inappropriately exclude subjects who simply have lower perfusion values occipitally. As such, this approach potentially biases the sample towards subjects with higher perfusion values. Whilst global coverage is necessary for the complex MVPA methodology, as justified in the current study, this may be less appropriate for more simple univariate analyses. Ideally, the quality control approach would have utilised the acquired label-control pairs for more robust inclusion and exclusion criteria, but this was not possible in the current study.

Demographic and lifestyle information for cohort characterisation available within these retrospective cohorts was sub-optimal for the purposes of investigating physiological change. Whilst all subjects in these original studies were recruited as 'healthy controls' and had no major medical conditions, it is possible that they may have had preclinical conditions or lifestyle choices which may have affected the results of the study. Additionally, given the demographics of the local population from which subjects in the current study were recruited, they are likely predominantly, if not exclusively, Caucasian individuals (this information was not retrospectively available).

Whilst the current study covers a broad age range, it is important to consider that significant decreases in cerebral perfusion with age may occur prior to the oft-investigated adult age groups, perhaps around as early as ~16 years (Biagi et al., 2007). Given the individual variance which can be seen with perfusion values (Parkes et al., 2004), the cohort size is small, however it is broadly in-line with similar studies in the field. Inclusion of socio-economic factors is also warranted, given the association between socio-economic inequality indicators and poor health outcomes (Grundy and Sloggett, 2003).

Given the reliance on visual assessment to determine the most appropriate GM mask, there was some concern about possible WM contamination in the chosen GM mask, however this was alleviated by use of CBF maps which included contributions from only voxels which contain some GM, as a result of the PVE-correction process – essentially a GM contribution map. Given that the PVE-correction process assumes that the contribution of CSF is zero, the chosen mask accounts for possible associated contamination. Nevertheless,

exploration of different GM masks with tighter definitions of GM would be interesting, to see if any findings exist only because of the GM mask definition.

Methodologically, it is important to note that PCA components can be challenging to interpret due to the conversion from the original image features to principal components, and thus subsequent validation is imperative. Additionally, a larger cohort would allow for elucidation of a more accurate spatial covariance pattern, with PCA often used on datasets comprising thousands of subjects. The components which do not survive selection due to low variance are also still relevant to the model, but are treated as noise by PCA, which may not be the case.

Future investigation of sCoV requires both direct comparison with ATT and determination of a normative range of healthy values to enable greater interpretability of results and validation of sCoV as a proxy of ATT.

Assessment of vascular territories within the current study is biased due to not accounting for individual territory variance but doing so would necessitate a time-intensive approach employing VE-ASL, and thus was not feasible within the current work.

An additional key limitation of the analysis within this chapter is the lack of availability of further covariates which may provide partial additional explanation for some of the results seen here. This is of particular importance for the FSL-randomise, FSL-FLAMEO and PCA models, and may improve the overall explanatory power of these models and subsequent age prediction. However, the analysis pathways used here can easily accommodate

additional covariates in future. Whilst finding such datasets was challenging in the duration of this PhD, this is becoming more feasible with the scale of information available through huge studies such as UK Biobank ([www.ukbiobank.ac.uk](http://www.ukbiobank.ac.uk), Sudlow et al., 2015) or TILDA ([www.tilda.tcd.ie](http://www.tilda.tcd.ie), Kearney et al., 2011). Additionally, CBF has not yet been used in the context of large dataset age prediction but could be of interest in explaining some of the chronological deviations from predicted age, similarly to the 99mTc HMPAO SPECT study of Amen et al. (2018).

Genetically, the apolipoprotein-E (APOE) pathological phenotype, APOE epsilon 4 (APOE- $\epsilon$ 4), and presenilin-1 gene mutations may be important additions to subsequent models. APOE is the best-known genetic risk factor for AD across various ethnic groups (Sadigh-Eteghad, Talebi and Farhoudi, 2012; Belloy, Napolioni and Greicius, 2019), and APOE- $\epsilon$ 4 has been linked to an increase in amyloid- $\beta$  with age (Morris et al., 2010), and may be indicative of future risk in healthy older individuals (Mormino and Papp, 2018). Mutations in the presenilin-1 gene have been linked to familial risk, and carriers with this mutation have shown hypometabolic perfusion patterns which are consistent with typical patterns in AD (Mosconi et al., 2006). Hematocrit levels should also be accounted for where possible, as using a singular fixed value, such as the 43.5% value recommended in the ASL white paper (Alsop et al., 2015) can result in over-estimations of perfusion values in women, non-Europeans, and those with diabetes (Smith et al., 2019). Vascular risk factors, such as diabetes, hypertension and atherosclerosis should also be accounted for as they have been shown to be implicated in cerebrovascular health (Vemuri et al., 2018). Furthermore, activity profiles would be a critical covariate for

inclusion, given the discrepancy in cerebrovascular health between sedentary and active individuals (Sugawara et al., 2020; Dunstan et al., 2021).

Various medications affect cerebral perfusion and are often in common use within older age groups, particularly due to the commonality of polypharmacy within this group (Veehof et al., 2000; Mintzer and Burns, 2000; Hajjar, Cafiero and Hanlon, 2007; Maher, Hanlon and Hajjar, 2014). Depression is common across the adult lifespan (Brody, Pratt and Hughes, 2018) and anti-depressant use has been shown to be associated with CBF increases in certain regions, such as the middle and posterior cingulate (Wei et al., 2018). The vascular depression hypothesis of late-life depression also suggests cerebrovascular disease either perpetuates or predisposes geriatric depression (Taylor, Aizenstein and Alexopoulos, 2013). Additionally, WMH in late-life depression have been linked to slower cognitive processing (Respino et al., 2019), and thought to be indicative of increased risk of stroke, dementia and death (Debette and Markus, 2010), and T2-weighted or FLAIR acquisitions which allow for these to be captured should therefore be considered as an additional imaging modalities to be included within subsequent models.

For all subjects used in this study, there was no information regarding their consumption of stimulants such as caffeine, which may have been in their system at the time of ASL acquisition. Caffeine consumption has been shown to reduce CBF by between 20-30%, using both ASL and PET (Cameron, Modell and Hariharan, 1990; Addicott et al., 2009; Vidyasagar et al., 2013), whilst increasing resting brain atrophy (Chang et al., 2018). This mismatch between cerebral perfusion and neuronal activation as a result of caffeine

consumption somewhat contradicts the theoretical assumptions of ASL. As such, the psychoactive nature of its consumption, coupled with its widespread consumption, makes control of its use within such studies of cerebral perfusion imperative. Smoking status should also be considered, as being an ex-smoker, as well as a current smoker, has been shown to influence cerebral perfusion, with a return to baseline CBF values after smoking cessation shown to take nine years (Yamashita, Kobayashi and Yamaguchi (2000). Cigarette smoking has additionally been linked to increasing stroke risk, with a meta-analysis of 14 studies – including 303,134 subjects – evidencing a statistically-significant relationship between any type of stroke and smoking status (Pan et al., 2019). Clearly cigarette smoking status is an important covariate for inclusion, and in large-scale studies may provide interesting sub-cohort differentiation for further investigation.

### 3.10. Conclusions and future directions

The use of PCA within this specific cohort results in a model which explains the association between whole GM perfusion and age well, and begins to define the complexity of this relationship, whilst also highlighting its methodological advantage over network perfusion measures. Whilst validation in an unseen cohort is required, five-fold cross validation by age prediction suggests this model is a good first step. Inclusion of further relevant covariates is also highly important to ensure model accuracy, and the analysis process is designed such that these additional covariate changes can be easily implemented. This PCA approach showed an advantage over FSL-randomise and FSL-flameo, however the minimal findings in these analyses are surprising and warrant further investigation. ICA may also provide an interesting comparative metric for future work.

In the main study, no significant correlation with whole GM perfusion and age was found after accounting for covariates. This is at odds with much of the literature, and highlights that the presence of a decrease in CBF with age remains contentious. Network perfusion decreases were only significant in the ECN after addition of sex, GM volume and whole GM CBF as covariates. Given its role in cognitively demanding processes, this may be indicative of preserved cognition in a healthily-ageing cohort. As such, this is investigated alongside the MoCA in Chapter 4.

This study was the first to carry out sCoV analysis across a healthy age span, and within key cognitive networks. As a relatively new metric, further investigation is needed – particularly in direct comparison to ATT – but the current results suggest that this may be more closely related with age than cerebral perfusion is, calling for the study of sCoV in age-related diseases. Additional investigation in vascular territories would also be of interest but requires such territories to be more consistently defined.

This chapter also proposes a metric for assessment of registration quality in GE 3D pCASL acquisition and evidences the influence of PVE-correction and smoothing on cerebral perfusion values. It is recommended that the Pearson's cross-correlation metric is used over visual assessment to ascertain the quality of image registration, and that reporting of the impact of PVE-correction and smoothing should be normalised within the field.

This chapter provides many avenues for future work. Of particular interest is the further development of the sCoV measure, as well as PCA spatial covariance pattern validation within a larger unseen cohort. The results of the current study suggest that both these metrics explore distributions which are more sensitive than commonly used ml/100g/min values and may have future value in elucidating the relationship between cerebral perfusion and age, and in the promotion of cerebral health in the elderly, as well as in clinical contexts. The advent of huge, accessible datasets such as the UK Biobank (Sudlow et al., 2015) – who are starting to collect ASL data as part of their imaging protocol – may provide future opportunities to further investigate the findings of this study.

## 4. The relationship between brain perfusion patterns and cognitive testing: a spatial covariance analysis of arterial spin labelling MRI

### 4.1. Introduction

Maintenance of brain health and cognitive function with ageing is of paramount importance to many, and has been directly related to quality of life in older people (Stites et al., 2018; Christiansen et al., 2019; Hussenoeder et al., 2020). Age is the strongest risk factor for cognitive decline (Norton, Matthews and Brayne, 2013), particularly when considering MCI and AD (see Keller, 2006 for a review). Understanding of critical neurodegenerative events may be facilitated by elucidation of brain correlates of age-related cognitive decline, and using ASL to identify perfusion-related pathomechanisms could open new avenues for the effective treatment of cognitive decline.

A biomarker of the processes underlying brain ageing and functional decline is yet to be elucidated, but would be desirable to better understand the detrimental and protective process associated with ageing, in order to promote cognitive health for the elderly. When considering conditions of impaired brain ageing, it is imperative that such a possible biomarker is reproducible and simple so that it can be widely used by clinicians and researchers, whilst additionally being capable of discerning fundamental features of the

associated pathology (Biomarkers Definitions Working Group, 2001). Taking a first step towards such a biomarker pertaining to cerebral perfusion necessitates understanding of perfusion variance within a healthy cohort.

Understanding how cognitive functionality can be retained requires a clear distinction of contributing factors – broadly resistance, reserve, and resilience – as the general consensus of the field of cognitive decline and dementia shifts away from that of a single disease and towards an idiosyncratic combination of age-related brain changes and disease processes. Montine et al. (2019) proposed operational definitions for these concepts. ‘Resistance’ refers to the presence of low or absent brain injury, relative to that expected by merit of the person’s age, genetics or other characteristics known to impact brain health. ‘Reserve’ is the structural or physiological capacity prior to any morbidity, and disruptions to which can be inferred through the performance of individuals during cognitive tests, even before the onset of cognitive decline. The term ‘cognitive resilience’ stems from the ability of an individual to overcome negative stressors on cognitive functionality (Staal and Bolton, 2008), further operationalised as an observed disconnect between observed cognitive functionality and underlying pathology (Montine et al., 2019; Arenaza-Urquijo et al., 2019). Given the accumulation of life experience and life stressors as we age, it follows that older people exhibiting healthy cognitive functionality may provide an opportunity to assess cognitive resilience, and subsequent cognitive decline. Recent work by Arenaza-Urquijo et al. (2019) proposed an FDG-PET biomarker of cognitive resilience in a cohort of subjects aged 80+ with stable cognition, termed the ‘resilience signature’, which comprises the bilateral anterior cingulate cortex and the anterior temporal pole, and provides an interesting metric for the investigation

of retained cognitive functionality with age. This resilience signature is yet to be replicated, and doing so in a non-ionising modality would be desirable for wider utility.

True understanding of these contributing aspects of cognitive functionality necessitates investigation prior to any cognitive disruption, to enable accurate understanding as to the impact of cognitive impairment. However, the actuality of the majority of current patient experience is that cognitive functionality is only assessed when already in subjective decline and the extent of brain injury and resilience capacity of the individual is unknown. Such assessments employ cognitive tests which do not focus upon these broad aspects of cognitive functionality, but are either domain-specific, or assess multiple domains or 'global' cognition. Much of the research field is focused on perfusion of the GM or specific regions, with the assessment of cognition commonly occurring through the use of the MMSE (Folstein, Folstein and McHugh, 1975; Folstein, Robins and Helzer, 1983), one of three oft-used tests of multiple cognitive domains – the MMSE, ADAS-Cog (Rosen, Mohs and Davis, 1984), and the MoCA (Nasreddine et al., 2005). The MMSE has been used extensively in both large clinical trials and day-to-day within the clinic, due to the ease and speed of its administration. However, whilst it is considered to be satisfactory in its validity and reliability (Tombaugh and McIntyre, 1992), it has been critiqued for its lack of sensitivity, failing to adequately discriminate between healthy individuals and those with mild dementia, MCI and subjective cognitive impairment (SCI), as well as limited capacity for the detection of hemisphere- or domain-specific impairments (Tombaugh et al., 1996), with various systematic reviews showing there to be no evidence to support it as a standalone test for AD development (Arevalo-

Rodriguez et al., 2015). ADAS-Cog (Rosen, Mohs and Davis, 1984) is regularly used for clinical trials (Cano et al., 2010), as it is considered to be the 'gold standard' for treatments which aim to halt or reverse dementia aetiology (Kueper, Speechly and Montero-Odasso, 2018), and has been expanded to improve detection of MCI-related changes (Skinner et al., 2012). A review by Kueper, Speechly and Montero-Odasso (2018) found 31 modified versions of the ADAS-Cog. Whilst ADAS and its expansions have been repeatedly shown to have well-considered conceptual and neurophysiological underpinnings (Cano et al., 2010), the average 30-35 minute administration length is challenging given the overwhelming number of people at risk for, or at the cusp of, cognitive decline, and the healthcare provisions required to ensure their prompt assessment. Furthermore, Kueper, Speechly and Montero-Odasso (2018) evidence that this test is less effective for the assessment of individuals with less severe cognitive impairments, although it does outperform the MMSE here (Lezak et al., 2004).

In many clinical contexts, the MMSE has been superseded by the MoCA, the most widely-used test with reasonable administration time for the assessment of global cognition (Nasreddine et al., 2005), developed for earlier detection of cognitive impairments, with the aim of quicker diagnosis and optimal patient care. A 30-point test which assesses language, abstract reasoning, memory recall, visuospatial abilities, orientation in time and place, and abstract reasoning and executive function, this test includes tasks which are adapted from other tests which assess a singular cognitive domain such as the Trail Making Test (Partington and Leiter, 1949). In a systematic review of 34 articles, Pinto et al. (2019) found that in >80% of these articles, the use of MoCA to discriminate between MCI and healthy cognition was superior to

MMSE. The MoCA also assesses multiple cognitive components which the MMSE does not. It has also been shown to have greater ability to predictively diagnose dementia than MMSE, following the Diagnostic and Statistical Manual of Mental Disorders (DSM) criteria (Hsu et al., 2015). Although the MoCA was developed for English-speaking populations, it has been adapted and validated for other languages, and is available in nearly 200 countries. When considering MoCA scoring, a score of 26+ is considered to be cognitively normal, however the work of Ihle-Hansen et al. (2017) suggests this may be too high to distinguish normal functionality from MCI, given 49% of the cohort of 3,413 individuals (aged 63-65 years old, living in Akershus Country, Norway) scored under the 26 point cut-off, and less than 5% scored 30. Indeed, a meta-analysis of nine studies (Carson, Leach and Murphy, 2018) focused on the differentiation of healthy ageing and MCI found that a cut-off score of 23 may yield greater diagnostic accuracy. Whilst sensitivity was lower at a MoCA score of 23 (.86) than at 26 (.94), the associated specificity was higher (.88 compared with .66). Youden indices also revealed a better balance between positive and false positive findings using a cut-off score of 23 (Youden index = .71) than at 26 (Youden index = .59), and independent proportion analysis showed significantly higher classification accuracy of subjects at 23 (86% correctly classified), than at 26, where 78% correctly classified ( $z=3.12$ ,  $p=.002$ ). Nevertheless, it remains an informative test for not only cognitive impairment associated with dementias, but also other neurological diseases such as glioma (Olson, Chhanabhai and McKenzie, 2008), PD (Hoops et al., 2009; Dalrymple-Alford et al., 2010) and vascular cognitive impairment (Wong et al., 2009).

As well as ageing (discussed at length in Chapter 3), cerebral perfusion is known to be related to both brain health – through the provision of oxygen and restoration of substrates such as Glc that are involved in cerebral metabolism (Sierra-Marcos, 2017; de la Torre, 2017) – and cognition (Benedictus et al., 2017). Despite a critical reliance upon cardiovascular supply of blood to the brain, much variance in healthy perfusion values occurs (Aanerud et al., 2012), and this coupled relationship between neuronal activation and perfusion can become altered due to various brain changes, including ageing and disease. As mentioned previously within this thesis (Chapters 2 and 3), healthy brain perfusion occurs in an autoregulated state of homeostasis – as does neuronal activation – and deviation from this regulation can damage the brain. Cerebral activation is accompanied by changes in cerebral perfusion, and these tend to be minor and localised, based on local neuronal demand (Kuschinsky, 1991; Paulson, 2002), and return to their tightly-regulated homeostatic state after cessation of the local activity. However, neuronal homeostasis can be disrupted by age-related vascular impairments (de la Torre, 2004), which impede cerebral perfusion and associated neuronal activity. Furthermore, pathological variation in cerebral perfusion exacerbates such impairment and can lead to permanent damage to the cerebrovasculature and tissues of the brain (Kunz and Iadecola, 2008; Toth et al., 2017). Resultantly, it may be impossible for cerebral metabolic requirements in afflicted individuals to be met.

Lacking the capacity to achieve cerebral metabolic requirements is strongly associated with dementia, due to inadequate provisions of metabolic substrates (Alexander et al., 2002). HMPAO-SPECT and FDG-PET provide an opportunity to assess brain health in relation to cerebral perfusion.

HMPAO-SPECT allows for assessment of cerebral perfusion through the labelling of white blood cells, which can be followed in the tissue using a gamma camera, whereas FDG-PET infers blood flow by merit of relative uptake of fluorodeoxyglucose, a glucose analog, by cells which consume glucose. FDG-PET studies have confirmed temporo-parietal hypometabolism as a classic biomarker of AD (Hoffman et al., 2000), and highlighted the challenging hypometabolic heterogeneity of MCI (Mosconi et al., 2008), the interpretation of which can be complicated by the underlying compensatory mechanisms which may contribute, such as the resilience signature proposed by Arenaza-Urquijo et al. (2019), or genetic characteristics, like carrying AD-susceptibility gene APOE- $\epsilon$ 4 (Wierenga et al., 2013). HMPAO-SPECT has been shown to be able to discriminate MCI patients from those with subjective cognitive complaints (Rossini et al., 2019), and utility in the discrimination of early- and late-onset dementia (Kemp et al., 2003), although is less reliable in the detection of AD in patients assessed for general cognitive impairment (Nadebaum et al., 2020). However, both HMPAO-SPECT and FDG-PET involve the use of ionising radiation, which is of concern in patient populations who may require multiple imaging or therapy sessions. The cerebral hypoperfusion seen in AD and MCI as measured using ASL is comparable to findings of FDG-PET and HMPAO-SPECT (Wintermark et al., 2005; Musiek et al., 2012; Cha et al., 2013; Takahashi et al., 2014; Zhang, 2016; Dolui et al., 2020), and provides a patient-safe alternative.

Understanding the relationship between frequently-used measures of such cognitive decline and imaging-derived metrics such as cerebral perfusion may be highly beneficial, by informing upon how these important clinical measures relate to underlying physiology. There is evidence for region-specific brain

ageing which has been shown by patterns of atrophy and perfusion change (Whitwell et al., 2007; Bergfield et al., 2010; Ding et al., 2014; Huang et al., 2018; Zhang et al., 2018), although these structural and physiological MR measures have been shown to be distinct from one another (Chen, Rosas and Salat, 2011). Exact perfusion patterns associated with the HA-MCI-AD continuum also remain controversial, with heterogeneous patient demographics making precise comparisons difficult.

Reduced CBF has been linked to neurodegeneration (Vernooij et al., 2008), with findings of hypoperfusion in regions across the brain (Sandson et al., 1996; Alsop, Detre and Grossman, 2000; Johnson et al., 2005; Dai et al., 2009; Yoshiura et al., 2009), and GM as a whole (Asllani et al., 2008) in AD. Recent work by Benedictus and colleagues (2017) has highlighted the prognostic value of cerebral perfusion, associating decreased CBF with cognitive decline by use of linear mixed models. This finding is supported by a multitude of studies and reviews (Hays, Zlatar and Wierenga, 2016; Zhang, Gordon and Goldberg, 2017; Wolters et al., 2017; Leeuwis et al., 2017; Leeuwis et al., 2018), including a recent meta-analysis of 60 ROIs by Zhang et al. (2021). This work assessed 13,644 subjects across 244 studies, and suggests that the hypoperfusion pattern which characterises progression through the healthy ageing-MCI-AD continuum affects the PCC, precuneus, and temporo-parietal regions. However, many such investigations have utilised the Mini-Mental State Examination (MMSE, Folstein, Robins and Helzer, 1983), despite the extensive critique this battery has faced due to its lack of sensitivity (Tombaugh et al., 1996).

Whilst hypoperfusion is generally accepted and thought to be associated with faster cognitive decline (Benedictus et al., 2017), several studies have also evidenced cerebral hyperperfusion within the PCC, precuneus, bilateral parietal and temporal lobes (Alsop, Detre and Grossman, 2000; Asllani et al., 2008; Dai et al., 2009; Ding et al., 2014), and the hippocampus (Alsop et al., 2008) throughout the HA-MCI-AD continuum. However, such findings can be contentious, with Camargo, Wang and the Alzheimer's Disease Neuroimaging Initiative (2021) finding that longitudinal reductions in hippocampal perfusion throughout the continuum were independent of disease status. Nevertheless, the most consistent regional finding throughout the continuum is a hypoperfusion of the PCC, which may be considered the closest finding thus far to a functional biomarker of AD-pathology underlying cognitive decline (Sierra-Marcos, 2017). However, how successful this is as a biomarker of processes which explain physiological age-related changes is less clear.

Well-established networks such as the DMN (Vidal-Piñeiro et al., 2014) and ECN (see Chapter 3; Damoiseaux et al., 2006; Seeley et al., 2007; Turner and Spreng, 2015; Ng et al., 2016) have also been linked to cognitive decline across the continuum (Greicius et al., 2004; Mevel et al., 2011; Chen, Rosas and Salat, 2011; Cai et al., 2017; Zhao et al., 2018), particularly within hub regions (Dai et al., 2015). Whilst the existence of a HA-MCI-AD continuum is generally accepted, further investigation is needed as to the additional compensatory mechanisms which may be involved, such as the aforementioned resilience signature (Arenaza-Urquijo et al., 2019), the perfusion underpinnings of which remain unclear. It is notable that these networks work flexibly in response to demand, integrating or working in segregation to adapt to the specific cognitive needs (Cohen and D'Esposito,

2016), and it is possible that such compensatory regions as those proposed in the resilience signature may also collaborate in this network performance in ageing. Such collaboration with possible compensatory physiology may be represented in a unique pattern of selective segregation and binding of sub-regions of multiple networks. As such, MVPA may provide an optimal approach to understand the complexity of cognition-related brain perfusion.

Many studies which attempt to elucidate the relationship between cognitive decline and cerebral perfusion by employing univariate, voxel-wise or region-of-interest methods lack the sensitivity required to capture subtle effects (Allsani et al., 2008; Pagani et al., 2009). Whilst voxel-wise analysis can detect regionally specific changes in brain function, it usually ignores the functional correlations between anatomical structures of interest. However, when multivariate approaches are employed, we start to understand the brain's functional architecture and the related dynamic functional networks which underpin this. The segregation and binding of such networks has been linked to cognitive abilities, with a functional balance between both in the resting state associated with better memory (Wang et al., 2021). Galiano et al. (2020) have evidenced a reduction in this coupling between functional connectivity and cerebral blood flow in healthy ageing. A 2016 study by Cohen and D'Esposito highlights the utility of graph theory in clarifying the dynamics of functional reconfiguration, finding that between-network communication is critical for working memory.

Allsani et al. (2008) and Habeck et al. (2008) evidenced increased sensitivity of multivariate analysis when compared with univariate approaches in the

discrimination of healthy controls and AD patients using ASL and FDG-PET, respectively, with Habeck et al. (2008) evidencing a sensitivity of 0.5 with a univariate approach, and 0.85 with a multivariate one. Such a finding is supported by further studies of AD, even when localised CBF changes and the resultant progressive spread is largely known (Scarmeas et al., 2004).

Steffener et al (2013) used PCA (see Chapter 3) to elucidate whether CBF and GM volume were better predictors of cognition than age alone, when considering cognition in three domains – memory, fluid ability, and speed/attention – in 35 healthy young (14M:21F, mean age = 24.34, SD = 3.19) and 23 old subjects (9M:14F, mean age = 66.39, SD = 4.11). They found that both CBF and GM volumes account for unique aspects of the composite cognitive scores, and both contribute more variance to the model than age. Actual cognitive scores were compared with predicted scores, using individual covariance pattern expressions, with the resultant correlation coefficients significant at the  $p < 0.001$  level in 43 of the 45 correlation assessments. Specific perfusion covariance patterns related to the memory composite score included relative increase in the cerebellum and middle orbital frontal lobe, and decreases in the hippocampus, postcentral gyrus and temporal cortex. However, this pattern varied for both the fluid ability and speed/attention domains. Fluid ability was characterised by increased prefrontal and anterior cingulate perfusion and decreased perfusion in the precentral regions and putamen, whereas the speed/attention pattern included increased perfusion in the middle, superior frontal, parietal and cerebellar regions, as well as the calcarine sulcus, and relative decreases in the occipital cortex, putamen and temporal gyri. It follows that cerebral perfusion patterns derived from domain-specific cognitive tests may differ from those related to global cognition. Such PCA-based investigation of cerebral perfusion data provides a data-driven approach to extract features of brain activity relevant to

cognition and to my knowledge, such PCA analysis and subsequent assessment of score prediction has not yet been done using a commonly-used clinical metric for multi-domain assessment in a cohort of exclusively healthy older subjects.

#### 4.1.1. Aims and hypotheses

This study aimed to address the unknown relationship between cerebral perfusion and MoCA scores in a cohort of healthy subjects. This was done by using a PCA approach to (1) identify a group-level perfusion pattern associated with this cognitive test in cognitively intact older subjects (2) describe the resultant pattern through assessment of key ROIs, cognitive networks, and graph visualisation, and (3) compare the PCA output with a voxel-wise approach. Additionally, aim (4) was to replicate an FDG-PET resilience signature (Arenaza-Urquijo et al., 2019) using ASL-derived perfusion data, to enable further understanding of MoCA scores and their relationship to imaging markers of cognitive resilience.

It was hypothesised that a robust 'pattern' of PCA-derived components which explain MoCA scores would be achieved, and the pattern would include more clusters than that derived from FSL-randomise, due to the methodological differences in their computation. The resultant PCA pattern was expected to comprise regions which have been previously implicated in ageing, cognitive decline and resilience, such as the precuneus, hippocampus and anterior and posterior cingulate cortices. Perfusion in such regions was also anticipated to significantly correlate with MoCA scores. Given the MoCA is a test of global cognition, network perfusion was expected to correlate more significantly with

MoCA scores than perfusion in key standalone ROIs. It was hypothesised that there would be a significant association between the perfusion of the DMN and ECN and MoCA scores. Additionally, the ASL resilience signature (as replicated from the work of Arenaza-Urquijo et al., 2019) was expected to significantly correlate with MoCA scores. These networks were expected to show some inter-relatedness, with key nodes of the graph visualisation output anticipated to comprise hub regions of the aforementioned networks.

## 4.2. Materials and methods

The methods of this study are summarised in *Figure 4.2.1.* below, and discussed at length in subsequent sections.

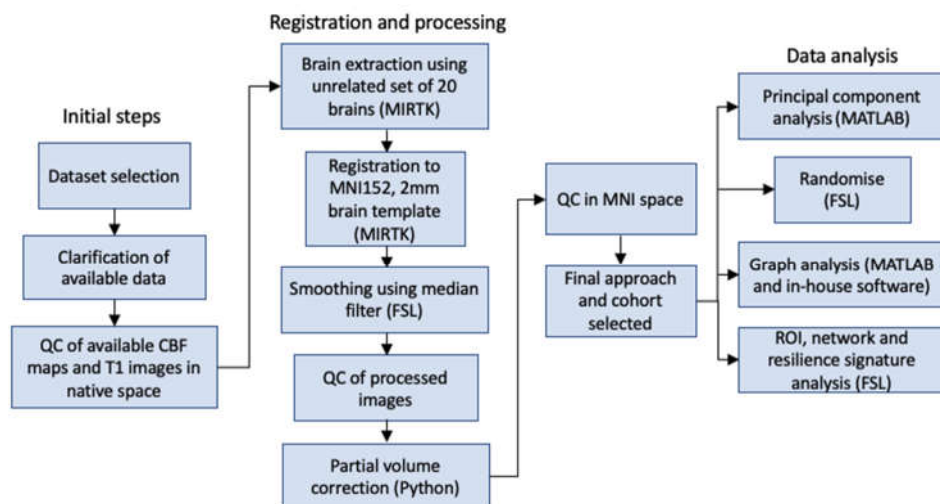


**Figure 4.2.1.:** Summary of key study steps, from conception to completion.

### 4.2.1. Dataset selection

A variety of imaging datasets exist which are available for use at request, either at no cost provided researchers are linked to an academic institution, or with an associated cost for access to the dataset. This section will provide a summary of datasets which were considered for use in this study — due to

their focus on, or inclusion of, data on ageing and cognition — and the reasons for their respective inclusion or exclusion. This is summarised in Table 4.2.1..

#### UK Biobank

The UK Biobank study ([www.ukbiobank.ac.uk](http://www.ukbiobank.ac.uk), Sudlow et al., 2015) was considered due to the expanse of the study and richness of data – it aims to investigate genetic, socio-economic and environmental factors, following 500,000 subjects for at least 30 years after their enrolment – however, at the time of dataset consideration there was no ASL data available. As such, this dataset was excluded from further consideration.

#### Open Access Series of Imaging Studies - 3 (OASIS-3)

The OASIS-3 study ([www.oasis-brains.org](http://www.oasis-brains.org), LaMontagne et al., 2019) is a retrospective study compiling data from more than 1000 subjects in various states of cognitive decline, involved in several projects across 15 years, at the Washington University Knight Alzheimer’s Disease Research Center. Whilst this dataset was of great interest due to its content, several researchers at the University of Nottingham attempted to assist with navigation of this dataset, and all found it to be challenging and time-consuming. However, the dataset was ultimately excluded due to MMSE being the only readily-available cognitive metric.

#### Alzheimer’s Disease Neuroimaging Initiative, Third Iteration

ADNI-3 (<http://adni.loni.usc.edu>, Weiner et al., 2017) is an easily-accessible dataset which contains a wealth of data on individuals who are categorised as healthy ageing, or having MCI, subjective cognitive impairment, or AD. The data is collected at over 50 sites within the United States of America and Canada, and whilst it includes data using a variety of MRI sequences, these vary depending on scanner and site. There is also a wealth of information available regarding related socio-economics, possible comorbidities, medication history, and disease development in some individuals. Resultantly, this dataset was considered appropriate for use in the study.

#### *Mayo Clinic Study of Aging*

The Mayo Clinic Study of Aging (<https://www.mayo.edu/research/centers-programs/alzheimers-disease-research-center/research-activities/mayo-clinic-study-aging/overview>, Roberts et al., 2008) focuses on vascular, psychiatric and inflammatory predictors of cognitive impairment, with a lot of work characterising the trajectory of disease, including subjects aged between 30 - 89 at the time of study enrolment, who were evaluated every 15 to 30 months. 50-60% of these subjects have MRI and PET measures, however exact demographics and availability of cognitive metrics is unclear without a data sharing agreement in place. At the time of study commencement, it was reasoned that there would not be enough time to secure a data agreement before completion of this PhD. The subsequent coronavirus pandemic extended the duration of data analysis for this PhD and would have ultimately been feasible, however initial time-constraints meant that this dataset was not considered further at this stage.

### Northwestern SuperAging Project

The Northwestern SuperAging Project ([www.brain.northwestern.edu](http://www.brain.northwestern.edu), Rogalski et al., 2013) would have provided a fascinating option for collaboration due to the vast array of clinical data available. However, ASL data was not available for this cohort.

### Lothian Birth Cohort, 1936

The Lothian Birth Cohort, 1936 ([www.ed.ac.uk/lothian-birth-cohorts](http://www.ed.ac.uk/lothian-birth-cohorts); Deary et al., 2012) contain a large amount of cognitive data, and are particularly rich in information which enables the investigation of the relationship between early- and late-life cognitive abilities. However, only structural MRI images are acquired, as part of the study of the 1936 cohort.

### The Irish Longitudinal Study on Ageing

The TILDA dataset (<https://tilda.tcd.ie>, Kearney et al., 2011) would be ideal for validation of the model described within this chapter, given the availability of structural and perfusion MRI measures in later iterations of the study, as well as MoCA scores. However, data access and collaboration requires a data sharing agreement, an application for which was approved at the very end of my PhD, and thus validation was not feasible prior to submission. This will likely be carried out by a future PhD student.

### Imaging to Understand Pain in Osteoarthritis

ImPOA is an internal cohort at the University of Nottingham, overseen by CI Professor Dorothee P. Auer. Originally collected for pain research, this

includes subjects suffering from various types of pain, as well as healthy control subjects. MRI acquisitions included ASL and structural imaging, and some subjects also underwent MoCA testing during the same visit. These subjects consented to data sharing with other researchers where necessary, meaning that no additional permissions were necessary, and data could be accessed quickly. As such, healthy control subjects from ImPOA were included as part of the study cohort for this current study.

#### *Parkinson's Magnetic Imaging Repository*

PaMIR is a multicentre study with permission for local subcohorts. The Nottingham cohort is overseen by Principal Investigator (PI) Professor Dorothee P. Auer and includes both healthy controls and Parkinson's disease patients, with ASL and structural MR images. Again, only some subjects had MoCA scores, but this data was easily accessible and could be accessed immediately due to prior consent from subjects. As such, the relevant healthy control data within this cohort was used as part of the larger cohort for this study.

**Table 4.2.1.: Summary of datasets considered for inclusion within this current study, the available data within each, and the rationale for subsequent inclusion or exclusion. Note that not all 'available' data listed within the table is available for all subjects.**

<b>Study cohort</b>	<b>URL</b>	<b>Number of subjects enrolled across study</b>	<b>Type(s) of data available</b>	<b>Data access</b>	<b>Pursued?</b>
<b>UK Biobank</b>	<a href="http://www.ukbiobank.ac.uk">www.ukbiobank.ac.uk</a>	Ongoing, ~500,000 to be enrolled	Brain, heart and full-body MRI, DEXA scan, ultrasound of carotid arteries, genotypes, biochemistry, primary care, exome sequencing, telomere data, metabolomics	Access fees (differ dependent on Tier), requires registration and review, and regular updates on study progress	No - ASL data unavailable
<b>OASIS-3</b>	<a href="http://www.oasis-brains.org">www.oasis-brains.org</a>	1,098	MRI, PET, biomarkers, cognitive assessments	Free, requires registration and updates on progress	No - difficult to navigate
<b>ADNI-3</b>	<a href="http://adni.loni.usc.edu">http://adni.loni.usc.edu</a>	Ongoing, 1,070 - 2,000 will be enrolled (some rollover from previous ADNI iterations)	T1, ASL, various clinical tests including MoCA, genetic, PET, biospecimens	Free, requires registration and regular updates on study progress	Yes
<b>Mayo Clinic Study of Aging</b>	<a href="https://www.mayo.edu/research/centers-programs/alzheimers-disease-research-center/research-">https://www.mayo.edu/research/centers-programs/alzheimers-disease-research-center/research-</a>	Ongoing, ~6,000 subjects recruited to date, aim to have an active study population	Cognitive and brain-ageing trajectories, characterisation of and outcomes for MCI and dementia, vascular, psychiatric and inflammatory predictors of	Submission and approval of data-sharing requests. Associated costs unclear.	No - time-constraints when originally considered

	<a href="https://www.mayoclinic.org/activities/mayo-clinic-study-aging/overview">activities/mayo-clinic-study-aging/overview</a>	of ~3,000 subjects	cognitive impairment, and in-vivo brain pathology		
<b>Northwestern SuperAging Project</b>	<a href="http://www.brain.northwestern.edu">www.brain.northwestern.edu</a>	Recruitment ongoing, subject number unclear	MRI, PET, longitudinal data. Available cognitive metrics unclear.	Unclear	No - ASL data unavailable
<b>Lothian Birth Cohort, 1936</b>	<a href="http://www.ed.ac.uk/lothian-birth-cohorts">www.ed.ac.uk/lothian-birth-cohorts</a>	1,091	Cognitive assessments, brain imaging, biological metrics	Requires registration, associated costs unclear	No - ASL data unavailable
<b>TILDA</b>	<a href="https://tilda.tcd.ie">https://tilda.tcd.ie</a>	~500	T1, ASL, cognitive metrics including MoCA. Lifestyle and socio-economic factors.	Submission and approval of data-sharing requests. Associated costs unclear.	No - time-constraints when originally considered. Pursued for validation beyond this thesis.
<b>ImPOA</b>	N/A	122	T1, ASL, MoCA	Data sharing allowed if subjects gave consent during original study	Yes
<b>PaMIR</b>	N/A	300	T1, ASL, MoCA	Data sharing allowed if subjects gave consent during original study	Yes

---

#### 4.2.2. Design and participants

This was a cross-sectional retrospective study of healthy subjects aged 50+ years old, including data from ADNI-3 and internal cohorts acquired at the University of Nottingham. Subject selection was limited to those with scans acquired using the General Electric (GE) Healthcare platform, to avoid possible findings which may be due to difference in vendor (see Section 4.2.2.1. for acquisition parameter details).

Data used in the preparation of this thesis were obtained from the ADNI database ([www.adni.loni.usc.edu](http://www.adni.loni.usc.edu)). As such, the investigators within the ADNI contributed to the design and implementation of ADNI and/or provided data but did not participate in analysis or writing of this report. A complete listing of ADNI investigators can be found at: [http://adni.loni.usc.edu/wp-content/uploads/how\\_to\\_apply/ADNI\\_Acknowledgement\\_List.pdf](http://adni.loni.usc.edu/wp-content/uploads/how_to_apply/ADNI_Acknowledgement_List.pdf). The ADNI was launched in 2003 as a public-private partnership, led by Principal Investigator Michael W. Weiner, MD. The primary goal of ADNI has been to test whether serial MRI, PET, other biological markers, and clinical and neuropsychological assessment can be combined to measure the progression of MCI and early AD. Further data was retrospectively collated within the University of Nottingham from healthy controls who previously took part in studies carried out between 2011-2020, and consented to their data being used for further investigation. These studies, ImPOA and PAMIR, are overseen by CI Professor Dorothee Auer. ImPOA was granted ethical approval by the Nottingham Research Ethics Committee 2 (Ref: 10/H0408/115) and funded by Versus Arthritis UK (Grant 18769). PAMIR was

granted ethical approval by the NHS Research Committee (Ref: 14/EM/0061), and funded by Parkinson's UK (Grant J-1204).

Subject recruitment criteria are summarised in Appendix D. Note that these are specific to the original study for which they were recruited as healthy controls. Data which was collected from ADNI-3 was limited to baseline scans of ADNI-3 subjects, available in December 2019, who had readily-available CBF maps and relevant cognitive metrics. The final dataset across all cohorts comprised 49 healthy control subjects (13M: 36F, mean age = 66.45 [SD = 9.023, range = 50.98 - 84]), and the MoCA assessment was administered to all participants prior to scanning. Subjects were not categorised as healthy on the basis of their MoCA score, rather by all demographic information and prior medical history collected in the respective study. Subjects categorised within ADNI-3 as having AD and MCI were also considered for inclusion in the subsequent study for the purposes of comparison, however not enough AD and MCI subjects with available MoCA data survived quality control, making meaningful comparison with healthy subjects unfeasible. Subject selection is summarised in *Figure 4.2.2.*

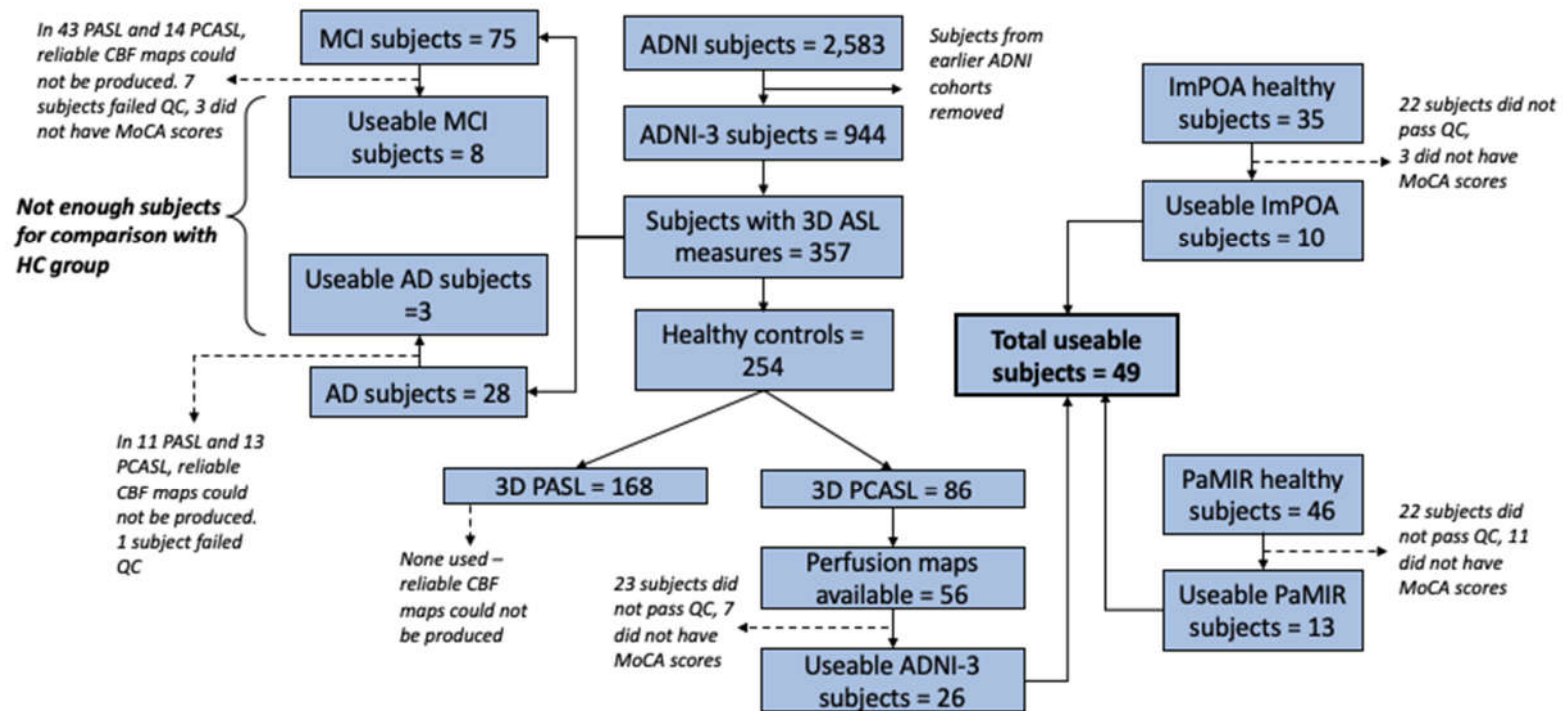


Figure 4.2.2.: Summary of the process of subject selection within ADNI-3, ImPOA, and PaMIR carried out in December 2019.

#### *4.2.2.1. MRI data acquisition*

Subjects included within this study all underwent MRI scanning at 3T. Due to the multi-site nature of ADNI-3, these subjects were scanned on various different scanners, of either a Discovery MR750 or MR750w model (GE Healthcare, Chicago, IL), with either a 32- or 8-channel head coil. Subjects who were included from internal cohorts were all imaged using a GE Discovery MR750 scanner, with 32-channel head coil (MR Instruments Inc, Hopkins, MN). Data from only one scanner manufacturer was used to reduce heterogeneity.

High-resolution T1-weighted anatomical images were acquired for the registration of perfusion maps. For ADNI-3, the associated T1 acquisition employed a sagittal fast-spoiled gradient echo sequence, with parameters as follows: TR = 7.7 ms, TE = 3.1ms, TI = 400 ms, FA = 11°, slice thickness = 1mm, and approximate acquisition time ~ 6 minutes 10 seconds. For internal cohorts, they were as follows: TE/TR = 3.164/8.132 ms, TI = 450 ms, slice gap = 1mm, FOV = 256, matrix = 256x256, FA = 12°, voxel resolution = 1mm<sup>3</sup>, acquisition time ~4 minutes 10 seconds. For all subjects, a PCASL sequence with 3D spiral readout was used to image cerebral perfusion. The internal cohorts differ only in respect of PLD, with a PLD of 2025 ms for PAMIR, and 1525 ms for ImPOA. All other parameters were as follows: repetition time = 4632 ms, TE = 10.5 ms, FA = 111 degrees, labelling duration = 1450 ms, field of view (FOV) = 240 mm, slice thickness = 4 mm, slice gap = 4 mm, number of slices = 36, echo train length = 1, number of excitations = 3, acquisition matrix = 128\*128. For the ADNI-3 cohort, parameters varied slightly depending on the scanner or the site, but were as close to the following as

possible: TR = 4885 ms, TE = 10.5, PLD = 2000 ms, FA = 111 degrees, slice thickness = 4 mm, FOV = 240 mm, acquisition matrix = 128\*128. Both PAMIR and ImPOA commenced before the release of the ASL white paper (Alsop et al., 2015) so do not follow the specific parameter recommendations, however parameters such as PLD were determined to be most suitable for the demographics of the cohort from which these subjects originate, at the time of the original studies.

### 4.3. Analysis

#### 4.3.1. Image pre-processing

Each raw perfusion map underwent quality control as described in Section 3.3.1.4. of Chapter 3. In summary, this was guided by the ASL white paper (Alsop et al., 2015) and involved visual assessment of possible motion artefacts and labelling quality, and checking the physiological plausibility of GM perfusion values. T1 images were also checked for adequate coverage of the head and any artefacts.

Brain extraction was carried out using MIRTk (Rueckert et al., 1999; <https://github.com/BioMedIA/MIRTk/>), with a dataset of 20 unrelated brain used as templates to determine brain tissue voxels ([www.brain-development.org](http://www.brain-development.org), Hammers et al., 2003; Heckemann et al., 2006; Heckemann et al., 2010) through use of a majority strategy.

Registration – linear to subject space and non-linear to 2mm isotropic MNI space (T<sub>1</sub>-weighted brain averaged over 152 subjects; Montreal Neurological Institute, Montreal, QC, Canada; Mazziotta et al., 1995; Mazziotta et al.,

2001a; Mazziotta et al., 2001b) – was carried out using MIRTk (Rueckert et al., 1999), with subsequent PVE-correction based on the mLTS method (Liang, Connelly and Calamante, 2013) using Python (Python Software Foundation, Version 3.6.; <http://www.python.org>) and run over ten iterations. The resultant perfusion maps were also smoothed, using a median filter with 3x3x3 kernel, and underwent further quality control to ensure successful processing, as defined above.

This quality control approach revealed a high attrition rate within these datasets (see *Figure 4.2.2.*), with 137 individuals prior to quality control, but only 62 of these surviving quality control, and only 49 of those suitable for use, due to the necessity of available cognitive data for later analysis.

#### 4.3.2. Covariates for inclusion in whole-brain grey matter analyses

Sex, age, and GM volume were included as nuisance covariates in certain analyses. GM volume was calculated using FSL (FSL version 6.0.4; Smith et al., 2004; Woolrich et al., 2009; Jenkinson et al., 2012) and the partial-volume estimation files that were output as part of the process of PVE-correction. These files contain the computed amount of GM within each voxel, and the sum of all PVE voxels gives the volume of GM, which was then divided by 1000 to give GM volume in cm<sup>3</sup>/mL.

#### 4.3.3. Voxel-wise analysis of cerebral blood flow data

As per Chapter 3, voxel-wise analysis of the cerebral blood flow data was carried out on the concatenated perfusion maps prior to principal component

analysis, as a comparative approach. Concatenated data was visually quality controlled to ensure each individual perfusion map was overlaid correctly. A GLM was created, and used as part of FSL-randomise (FSL version 6.0.4; Smith et al., 2004; Woolrich et al., 2009; Jenkinson et al., 2012) analysis, to carry out non-parametric permutation testing to correct for multiple comparisons (5000 permutations), defining significance as  $P < 0.05$  FWE-corrected using threshold-free cluster enhancement (Nichols and Holmes, 2002; Smith and Nichols, 2009). The inputs for FSL-randomise included MoCA score, GM CBF (as concatenated and processed perfusion maps), GM volume, sex, and age, and were all demanded prior to inclusion.

#### 4.3.4. Principal component analysis of cerebral blood flow data

A PCA-based ASL linear regression model was used to assess the relationship between the associated pattern of cerebral perfusion spatial covariance within the aforementioned dataset, and MoCA scores. The MATLAB (R2018a, The Mathworks, Inc., Natick, Massachusetts, United States) script used for PCA analysis was loosely based on the theoretical methods of Spetsieris et al. (2009) and Melzer et al. (2011), without the use of group differentiation.

The PCA analysis within this Chapter was carried out prior to that in Chapter 3, and whilst the approaches are comparable, they differ such that the inclusion of MoCA scores is additionally accounted for here. The current PCA approach does not use the Kaiser-Gutmann criterion (Jackson, 1993) for component selection. Instead, selection is based solely on the “optimal” backwards selection approach described in Section 3.6.1.2., until the residual

variance of the regression model is just above the expected error variance of the clinical score. For the MoCA, the work of Feeney et al. (2016) evidences the associated error variance to be approximately 4, and as such this value is used within this analysis.

Whilst validation was not carried out in the current study, due to the limited sample size, the process for validation described in Chapter 3, Section 3.6.1.2. could also be employed here, given a larger cohort such as TILDA.

#### 4.3.5. Thresholding of ASL data

The influence of thresholding of the imaging component of the PCA model upon the PCA-derived perfusion pattern was also investigated. It is possible to threshold  $c^{comb}$  (the vector of linearly combined voxel loadings), by setting all voxels whose absolute value is below a certain threshold to zero. The intention of such thresholding was to remove potential spurious voxels which may not substantially contribute towards the estimation of the MoCA scores. However, this results in the equality of Equation 3.10, as described in Chapter 3, Section 3.6.1.2. becoming an approximation. Therefore, the threshold value was chosen such that the variance explained ( $r^2$ ) by the thresholded combined loading is approximately a given percentage of the variance explained by the full unthresholded combined loading.

The resultant thresholded output was overlaid on an outline of the resilience signature (Arenaza-Urquijo et al., 2019) to determine similarity, which was created using a MATLAB script (R2018a, The Mathworks, Inc., Natick,

Massachusetts, United States) courtesy of the laboratory of Professor Chris Rorden (<https://github.com/rordenlab/spmScripts>).

#### 4.3.6. Understanding perfusion covariance

##### 4.3.6.1. Region of interest analysis

Brain structures of interest, defined *a priori* by a search of the literature which contributed to the introductory section of this chapter, were assessed to determine whether regional differences in absolute perfusion has a significant relationship with MoCA scores. The selected ROIs were the thalamus, PCC, precuneus and hippocampus – which were defined in MNI space using the Harvard-Oxford atlas, and thresholded at 50% using FSL (FSL version 6.0.4.; Smith et al., 2004; Woolrich et al., 2009; Jenkinson et al., 2012) for more conservative regional definition – and the dorsolateral prefrontal cortex (DLPFC) which was defined using the DLPFC region within the Stanford University Functional Imaging in Neuropsychiatric Disorders Lab (FINDLab, <https://findlab.stanford.edu/>) ECN mask (Shirer et al., 2012), from their atlas of ninety functional ROIs. How regional perfusion varies with MoCA score was assessed using linear regressions, controlling for covariates of age, sex, and GM volume, and GM CBF where appropriate. Both standard and 90th percentile means were assessed, given the work of Tong et al. (2016), which suggests that the values derived from the top most-activated voxels in a given ROI are more powerful, both in terms of resultant effect size and the reliability of detected differences.

#### 4.3.6.2. Network analyses

To further investigate the CBF data within this cohort, absolute perfusion values within various networks were calculated, to determine whether the relationship between CBF in these networks and MoCA could be explained through linear regression. Of particular interest were the ‘resilience signature’ – as described in the work of Arenaza-Urquijo et al. (2019) – which comprises the bilateral ACC and the anterior temporal pole, as well as the DMN, SN and ECN (<https://findlab.stanford.edu>; Shirer et al., 2012; see Appendix B).

A mask of the resilience signature was created using the Harvard-Oxford cortical atlas within FSL, with the aforementioned regions combined into a network mask and binarised using `fslmaths` (FSL version 6.0.4; Smith et al., 2004; Woolrich et al., 2009; Jenkinson et al., 2012). This was also thresholded at 50% due to their liberal coverage when unthresholded, and for greater similarity to the regions evidenced in the aforementioned prior work by Arenaza-Urquijo et al. (2019). The resultant mask is shown in *Figure 4.3.1.* below.

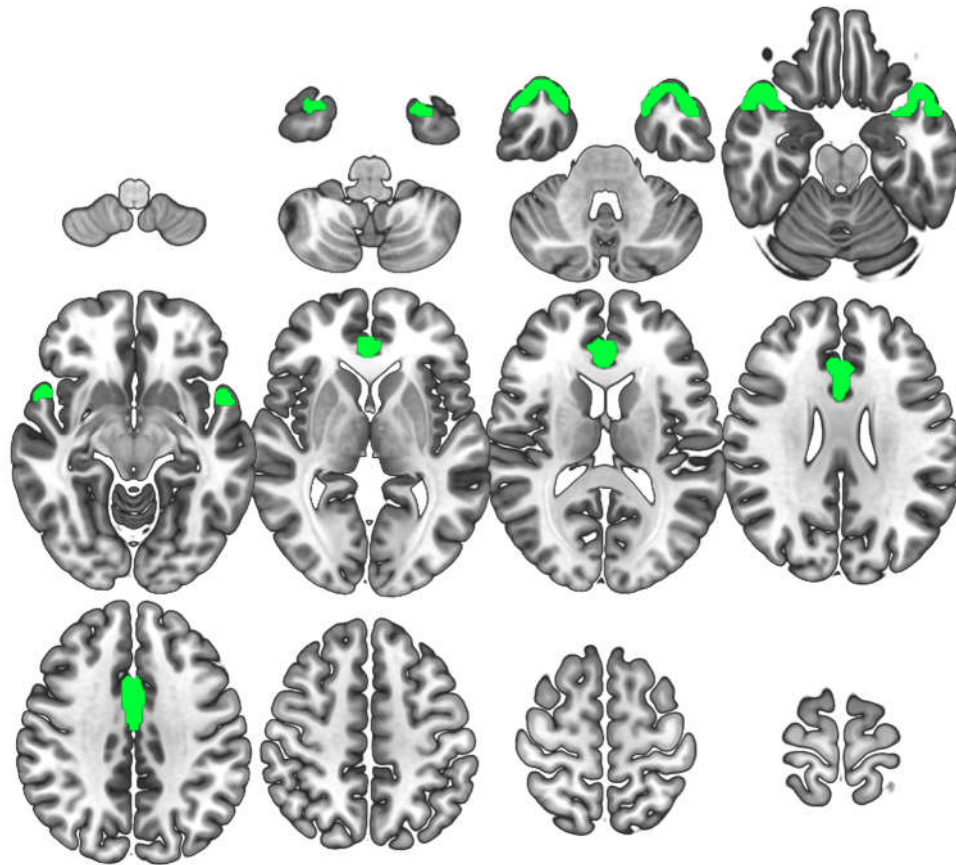


**Figure 4.3.1.:** Mask of the resilience signature (based on Arenaza-Urquijo et al., 2019), comprising the bilateral ACC and anterior temporal pole, overlaid on the 2mm MNI template.

#### 4.3.6.3. Graph visualisation

Graph visualisation was employed to enable greater understanding of the relationships between different surviving clusters resulting from PCA analysis after thresholding, by determining which of the conspicuous regions derived from the thresholded PCA spatial covariance pattern are due to true underlying biology, rather than to facilitate the PCA computation. A graph was constructed by correlating the mean vectors of each pair of regions in the covariance pattern, using the log-transformed double-demeaned CBF values, including any regions of  $\geq 0.5\text{ml}$  (63 voxels) in volume. Correlations were calculated in MATLAB (R2018a, The Mathworks, Inc., Natick, Massachusetts, United States), before being fed into in-house visualisation software. These

regions were colourised to match the nodes from the graph and overlaid on an MNI152 2mm brain template in ITK-SNAP (Yushkevich et al., 2006).

#### *4.3.6.4. Visualisation of PCA-derived covariance patterns*

To further understand the PCA-derived spatial covariance patterns, the overall thresholded spatial covariance pattern was separated into positive and negative clusters, as defined by the PCA output, and a binarised mask of each created using FSL (FSL version 6.0.4; Smith et al., 2004; Woolrich et al., 2009; Jenkinson et al., 2012). These masks were then overlaid on a concatenated file containing the perfusion maps of each subject, and `fsstats` (Jenkinson et al., 2012) used to calculate the mean perfusion values in the respective masked regions.

#### *4.3.6.5. Variance in individual subject perfusion patterns*

The individual perfusion patterns in subjects with the most commonly-occurring MoCA score were compared to assess the inter-subject perfusion pattern similarity on the basis of MoCA score. These individual pattern maps were produced during the PCA analysis.

## 4.4. Results

Summary demographic information pertaining to study site, scanner used, age, GM volume and GM perfusion are given in *Table 4.4.1.*

**Table 4.4.1.: Summary demographics of the study cohort. Standard deviations are given where appropriate.**

<b>Study cohort</b>	<b>Study site</b>	<b>Scanner</b>	<b>PLD (ms)</b>	<b>Subjects</b>	<b>Age (years)</b>	<b>GM volume (cm<sup>3</sup>)</b>	<b>GM perfusion (ml/100g/min)</b>
<b>ImPOA</b>	<b>University of Nottingham</b>	<i>GE Discovery MR750</i>	1525	10 (1M:9F)	58.7 ± 5.1	628.4 ± 87.74	63.37 ± 6.81
<b>PaMIR</b>	<b>University of Nottingham</b>	<i>GE Discovery MR750</i>	2025	13 (6M:7F)	63.5 ± 9.2	582.11 ± 99.6	59.6 ± 9.9
	<b>009</b>	<i>GE Discovery MR750w</i>	2000	2 (1M:1F)	76.7 ± 7.4	572 ± 14.5	62.3 ± 15.1
	<b>027</b>	<i>GE Discovery MR750</i>	2000	4 (2M:2F)	74.5 ± 7.5	618.7 ± 68.7	54.4 ± 8.5
<b>ADNI-3</b>	<b>029</b>	<i>GE Discovery MR750w</i>	2000	3 (1M:2F)	62.8 ± 6.1	581.6 ± 21.8	53.9 ± 4.4
	<b>098</b>	<i>GE Discovery MR750</i>	2000	1F	79.1	614.9	69.7

<b>099</b>	<i>GE Discovery MR750</i>	2000	5 (1M:4F)	72.7 ± 5.3	643.3 ± 70.5	69.5 ± 5.7
<b>128</b>	<i>GE Discovery MR750w</i>	2000	1F	62.5	620.9	43.7
<b>129</b>	<i>GE Discovery MR750</i>	2000	9 (1M:8F)	69.8 ± 8.1	592.7 ± 53.7	61.2 ± 11.5
<b>135</b>	<i>GE Discovery MR750w</i>	2000	1F	73.8	551.9	53.6

---

Biological characteristics of the cohort used as further covariates in this study – GM volume and individual cerebral perfusion values – are summarised in *Figure 4.4.1.* below. Perfusion values were calculated by overlaying the aforementioned GM mask, thresholded to exclude  $\leq 20\%$  grey matter, and  $\geq 30\%$  CSF, with GM volume calculated using partial volume estimations which were computed as part of the pre-processing pathway.

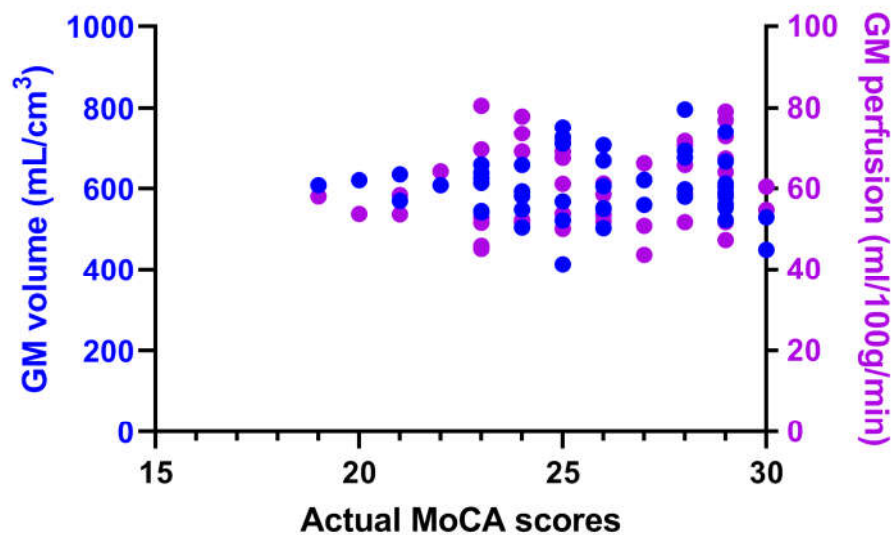


**Figure 4.4.1.:** Summary of the spread of biological covariates within the healthy control cohort used for PCA-ASL analysis. Grey matter volume is depicted in blue, and GM perfusion in purple.

The full cohort was predominantly female (13M:36F). Perfusion values in GM ranged from 43.7 - 80.6 ml/100g/min, with a mean of 60.56 ml/100g/min (SD = 9.592). The volume of the underlying GM ranged from 413.6 - 796.7 cm<sup>3</sup> (mean = 603.13 cm<sup>3</sup>, SD = 75.71).

#### 4.4.1. Voxel-wise analysis of cerebral blood flow data

The use of FSL-randomise for voxel-wise analysis for the analysis of cerebral blood flow data found no clusters of interest, when significance was defined as  $p < 0.05$  FWE-corrected, using threshold-free cluster enhancement. A *posterior* inspection at a significance threshold of  $p < 0.1$  also found no clusters of interest.

#### 4.4.2. Principal component analysis of cerebral blood flow data

The PCA model considered 48 components, of which three survived – components 1, 4 and 42. The result of the regression within the PCA was  $r^2 = 0.4944$  in the unthresholded model, suggesting variance in MoCA scoring can be moderately explained by brain perfusion within this cohort, using this model. The visual output for these combined components is exhibited below in *Figure 4.4.2.*

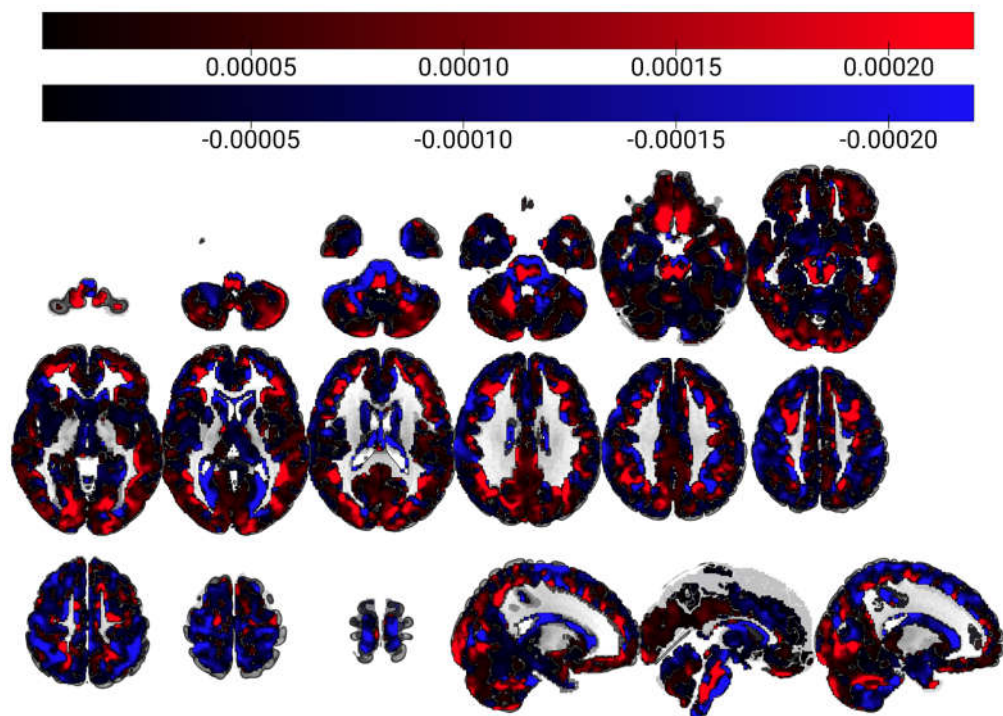


**Figure 4.4.2.:** Unthresholded combined surviving components (1, 4 and 42) for all 49 subjects, overlaid on the MNI152 template with 2mm resolution. The associated scale is in arbitrary units, but a higher perfusion value in the blue regions will reduce the estimate of MoCA scores, and higher perfusion in red areas will increase the estimate of MoCA scores.

#### 4.4.3. Thresholding

Initial thresholding was trialed for intervals of 5%  $r^2$  reduction between the fully unthresholded model (100% of model  $r^2$  retained) and 5% of  $r^2$  retained, to determine the best thresholding value, which balances the removal of spurious voxel and noise, but retains valuable imaging data. The results are summarised below in *Figure 4.4.3.*

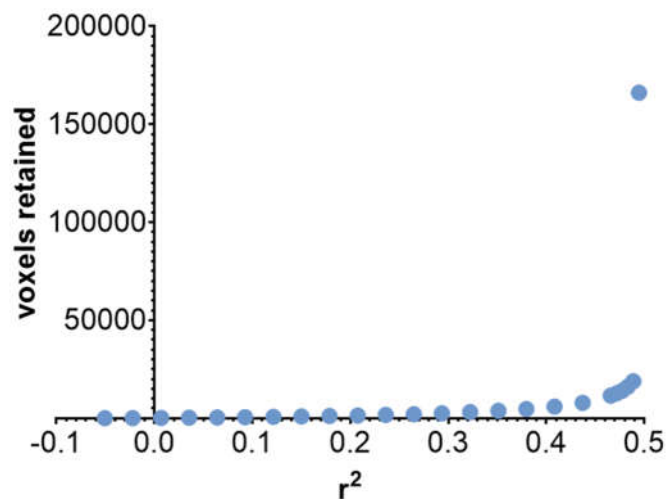


**Figure 4.4.3.:** Investigation of voxel retention with decreasing  $r^2$ , from 100% - 5% of  $r^2$  retained. 99-96% are also depicted here, in an attempt to define the drop-off between 100-95%.

The steep drop-off in  $r^2$  between 100-95% was further explored and evidenced to occur between 100-99%. As such, a more detailed investigation of the

effect of thresholding on the model quality ( $r^2$ ) and voxel retention between 100 - 98% of  $r^2$  retention was carried out, and is depicted in *Figure 4.4.4.*

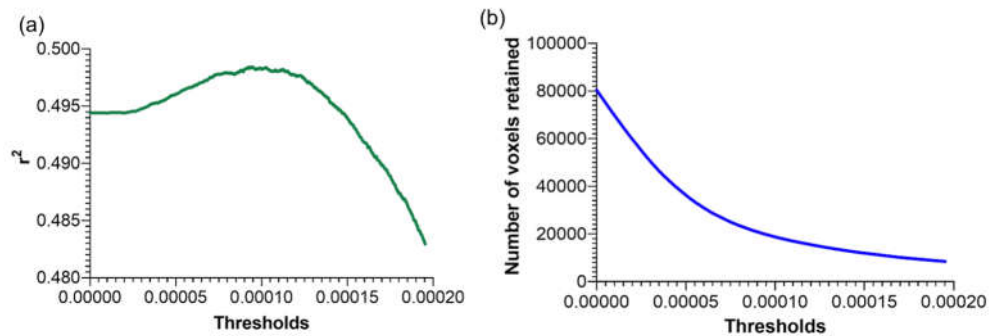


**Figure 4.4.4.:** Change in (a)  $r^2$  of the model and (b) voxel retention, by merit of threshold selection. These graphs depict the changes in these relationships between the unthresholded model, and the threshold at which 98% of the model  $r^2$  is retained.

Between the unthresholded model with an  $r^2 = 0.4944$  and a threshold with 98%  $r^2$  retention ( $r^2 = 0.4829$ ), 150,057 voxels are removed, with voxel retention starting to plateau around this stage. As such, a threshold of 98% of  $r^2$  was chosen for subsequent analyses. The difference in significant components after this thresholding is shown in *Figure 4.4.5.*, and the numbered clusters identified in Table 4.4.2..

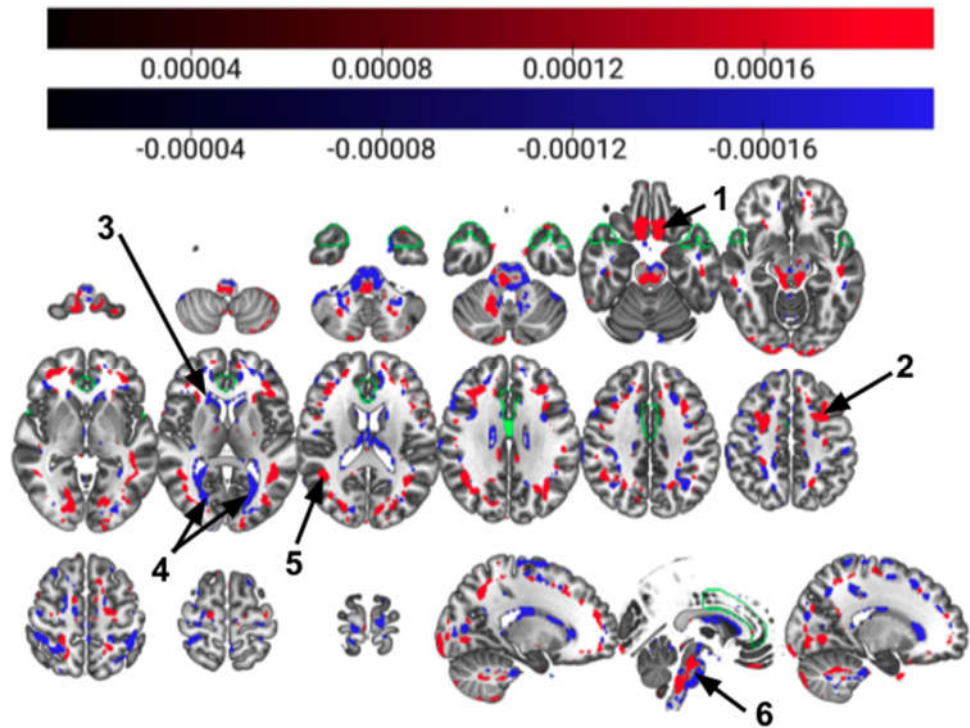


**Figure 4.4.5.:** Combined surviving components (1, 4 and 42) for all 49 subjects, thresholded at 98%  $r^2$  retention and overlaid on the MNI152 template with 2mm resolution. Higher perfusion value in the blue regions will reduce the estimate of MoCA scores, and higher perfusion in red areas will increase the estimate of the MoCA scores. The resilience signature (Arenaza-Urquijo et al., 2019) is shown in green. Numbered labels refer to key clusters identified and described within Table 4.4.2.

**Table 4.4.2.: Key clusters identified within the PCA-derived spatial covariance pattern.**

<b>Region number</b>	<b>Region name</b>	<b>Role</b>	<b>Association with MoCA score (+ or -)</b>
1	Subcallosal cortex	Inhibits motor neurone activity	+
2	Middle frontal gyrus	Convergence of dorsal and ventral attention networks	+
3	Right caudate	Learning, memory, emotion, motivation	-
4	Intra calcarine cortex	Primary visual cortex (V1) location	-
5	Angular gyrus	Attention, memory retrieval, spatial cognition, reasoning, theory of mind	+
6	Brainstem	Regulation of basic functions, information relay	+, -

#### 4.4.4. Understanding perfusion covariance

##### 4.4.4.1. Region of interest analysis

Key regions of interest were investigated to determine their mean perfusion and relationship to MoCA scoring. Cerebral blood flow within these regions is summarised in Table 4.4.3. (which contains standard mean values) and Table 4.4.4., which contains 90th percentile means (Tong et al., 2016).

**Table 4.4.3.: Unadjusted regional mean perfusion values in regions of interest within the full cohort.**

<b>Region of interest</b>	<b>Mean perfusion (ml/100g/min) [±SD]</b>	<b>Range (ml/100g/min)</b>
<b>PCC</b>	91.92 [±15.34]	63.46 - 128.93
<b>Precuneus</b>	84.39 [±13.8]	60.5 - 111.47
<b>Left hippocampus</b>	53.74 [±9.9]	38.03 - 86.38
<b>Right hippocampus</b>	52.64 [±11.27]	29.09 - 93.95
<b>Left DLPFC</b>	68.3 [±13.28]	47.67 - 95.16
<b>Right DLPFC</b>	66.27 [±13.08]	39.37 - 89.34
<b>Left thalamus</b>	64.3 [±14.26]	36.02 - 97.59
<b>Right thalamus</b>	62.52 [±14.24]	37.26 - 97.4

**Table 4.4.4.: Unadjusted regional 90th percentile mean perfusion values in regions of interest within the cohort.**

<b>Region of interest</b>	<b>Mean perfusion (ml/100g/min) [<math>\pm</math>SD]</b>	<b>Range (ml/100g/min)</b>
<b>PCC</b>	105.78 [ $\pm$ 17.38]	71 - 146
<b>Precuneus</b>	100.45 [ $\pm$ 16.61]	73 - 132
<b>Left hippocampus</b>	63.49 [ $\pm$ 13.63]	44 - 120
<b>Right hippocampus</b>	61.88 [ $\pm$ 14.84]	40 - 128
<b>Left DLPFC</b>	90.43 [ $\pm$ 17.25]	61 - 128
<b>Right DLPFC</b>	89.39 [ $\pm$ 16.31]	60 - 117
<b>Left thalamus</b>	82.35 [ $\pm$ 18.79]	50 - 124
<b>Right thalamus</b>	81.31 [ $\pm$ 18.68]	52 - 144

The relationship between perfusion of these ROIs, and actual MoCA scores, was assessed using linear regression in SPSS (*IBM SPSS Statistics for Windows*, Version 26, Armonk, NY). No significant results were found before controlling for additional covariates. When controlling for age, sex, GM volume (to address differences in total GM volume), a positive relationship approaching significance between PCC perfusion and MoCA scores was found ( $\beta = 1.652$ , 95% CI: .002 to 3.302,  $p = 0.05$ ). The results of this analysis for all ROIs is summarised in Table 4.4.5.. When GM CBF was additionally included as a covariate (to control for perfusion differences of no interest), no significant results were found. Sensitivity analysis, whereby a

subject with outlier perfusion values in the left and right hippocampus (78 year-old female) was removed from the cohort, resulted in positive trends towards significance in both ( $\beta = .920$ , 95% CI:  $-.002$  to  $1.930$ ,  $p = .051$  for the left, and  $\beta = 1.031$ , 95% CI:  $-.050$  to  $2.111$ ,  $p = .061$  for the right hippocampus, respectively) when sex, age and GM volume were controlled for. However, they were not significant when GM CBF was additionally included as a covariate.

**Table 4.4.5.: Summary of the results of linear regressions assessing the relationship between MoCA scores and mean cerebral blood flow in specific a-priori-defined regions, controlling for age, sex and GM volume.**

Region of interest	Significance (p-value)	Unstandardised $\beta$ -coefficient	95% Confidence Intervals
<b>PCC</b>	.05	1.652	.002 to 3.302
<b>precuneus</b>	.197	.990	-.534 to 2.514
<b>Left hippocampus</b>	.109	.880	-.203 to 1.964
<b>Right hippocampus</b>	.150	.920	-.344 to 2.185
<b>Left DLPFC</b>	.154	1.073	-.419 to 2.564
<b>Right DLPFC</b>	.500	.509	-1.001 to 2.020
<b>Left thalamus</b>	.340	.782	-.853 to 2.416
<b>Right thalamus</b>	.251	.938	-.686 to 2.561

When the 90th percentile mean (Tong et al., 2016) is used to determine relationships between these ROIs and MoCA scores with age, sex and GM volume as covariates, a significant positive relationship between the PCC and

MoCA scores was identified ( $\beta = 2.067$ , 95% CI: .232 to 3.902,  $p = .028$ ; see Table 4.4.6.). This significance remained when GM CBF was included as an additional covariate ( $\beta = .834$ , 95% CI: .033 to 1.635,  $p = .042$ ). Sensitivity analysis within the hippocampus was carried out, and found a significant positive relationship between left hippocampal perfusion and MoCA scoring ( $\beta = 1.344$ , 95% CI: .192 to 2.496,  $p = .023$ ), and a trending positive relationship between right hippocampal perfusion and MoCA scoring ( $\beta = 1.153$ , 95% CI: -.099 to 2.404,  $p = .070$ ) when age, sex and GM volume are included as covariates. These relationships disappear when GM CBF is additionally included as a covariate.

**Table 4.4.6.: Summary of the results of linear regressions assessing the relationship between MoCA scores and 90th percentile mean cerebral blood flow in specific a-priori-defined regions, controlling for age, sex and GM volume. Significant findings are highlighted using an asterisk.**

Region of interest	Significance ( $p$ -value)	Unstandardised $\beta$ -coefficient	95% Confidence Intervals
<b>PCC</b>	.028*	2.067	.232 to 3.902
<b>precuneus</b>	.081	.1.558	-.200 to 3.317
<b>Left hippocampus</b>	.097	1.203	-.226 to 2.633
<b>Right hippocampus</b>	.225	.985	-.628 to 2.598
<b>Left DLPFC</b>	.130	1.481	-.453 to 3.414
<b>Right DLPFC</b>	.244	1.092	-.771 to 2.956
<b>Left thalamus</b>	.161	1.445	-.598 to 3.488
<b>Right thalamus</b>	.206	1.268	-.723 to 3.260

#### 4.4.4.2. Network analysis

Various networks were also analysed, using network masks either created as part of this study based on the work of Arenaza-Urquijo et al. (2019), or provided by FINDLab (Shirer et al., 2012). The perfusion within these networks is summarised in Table 4.4.7..

**Table 4.4.7.: Summary of unadjusted mean perfusion values in selected networks.**

<b>Network of interest</b>	<b>Mean perfusion (ml/100g/min) [±SD]</b>	<b>Range (ml/100g/min)</b>
<b>Left ECN</b>	63.4 [±11.89]	47.39 - 90.79
<b>Right ECN</b>	61.88 [±10.42]	43.25 - 82.28
<b>Dorsal DMN</b>	73.37 [±12.04]	50.74 - 99.64
<b>Ventral DMN</b>	65.22 [±11.01]	46.88 - 91.75
<b>Posterior SN</b>	64.89 [±10.85]	48.32 - 93.35
<b>Anterior SN</b>	71.37 [±12.33]	46.26 - 100.43
<b>Precuneus network</b>	73.86 [±11.99]	53.75 - 100.31
<b>Resilience signature</b>	64.58 [±11.11]	44.16 - 90.7

Linear regressions were carried out in SPSS to assess the relationship between network perfusion and MoCA scores, controlling for age, sex and GM volume as covariates. Findings are summarised in Table 4.4.8., with no significant results. However, the regressions assessing perfusion of the resilience signature and anterior SN showed a trend increase which

approached significance ( $p = 0.08$  and  $p = 0.089$ , respectively; *Figure 4.4.6.*).

When GM CBF is also included as a covariate, to account for inter-subject variance in GM CBF which is not of interest to the research question, no significant relationships are found.

**Table 4.4.8.: Summary of the results of linear regressions assessing the relationship between MoCA scores and cerebral blood flow in specific a-priori-defined cognitive networks, when age, sex, and GM volume are included as additional covariates.**

<b>Network of interest</b>	<b>Significance (<math>p</math>-value)</b>	<b>Unstandardized <math>\beta</math>-coefficient</b>	<b>95% confidence intervals</b>
<b>Left ECN</b>	0.152	0.926	-0.354 to 2.205
<b>Right ECN</b>	0.376	0.531	-0.666 to 1.729
<b>Dorsal DMN</b>	0.113	1.092	-0.270 to 2.453
<b>Ventral DMN</b>	0.313	0.631	-0.615 to 1.877
<b>Posterior SN</b>	0.106	1.005	-0.223 to 2.233
<b>Anterior SN</b>	0.089	1.187	-0.191 to 2.565
<b>Precuneus network</b>	0.108	1.080	-0.247 to 2.408
<b>Resilience signature</b>	0.08	1.11	-0.136 to 2.356

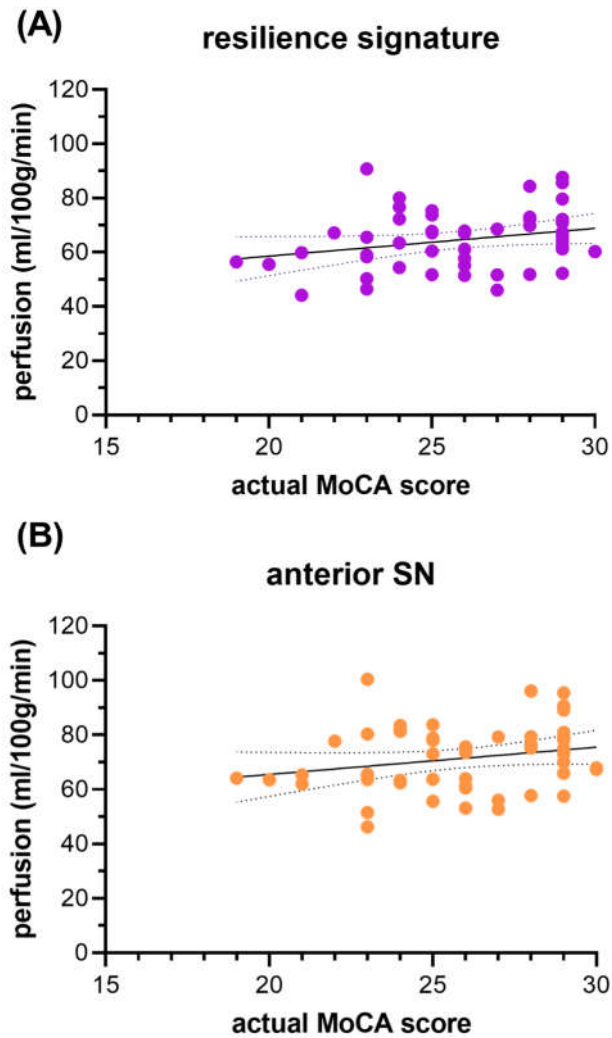


**Figure 4.4.6.:** Trending linear regressions between MoCA scores and perfusion in (A) the resilience signature and (B) the anterior SN.

#### 4.4.4.3. Graph visualisation

Graph visualisation was used to determine region inter-relatedness within the PCA-derived output, by depicting group-level correlations between any regions of  $\geq 0.5\text{ml}$  (63 voxels) in volume. The resulting graph and associated anatomical regionality is depicted in *Figures 4.4.7.* and *4.4.8.* below.

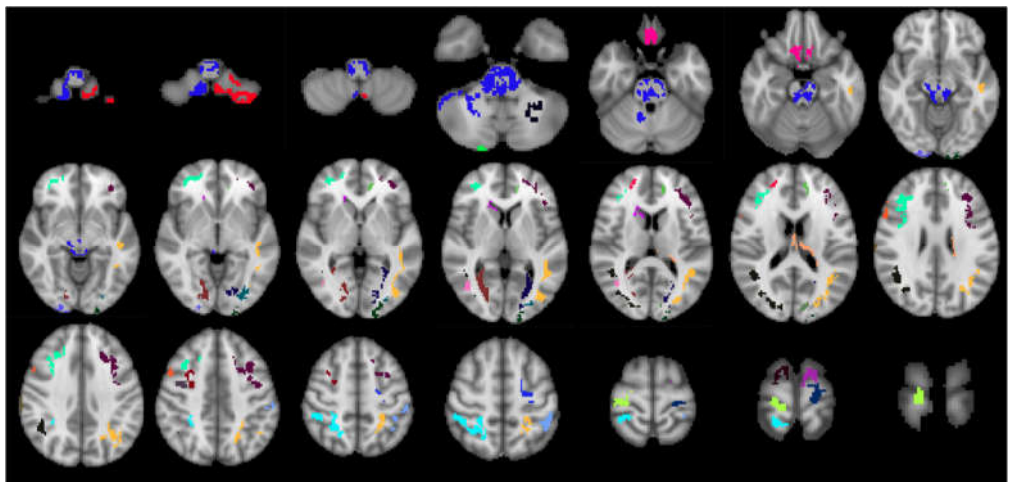
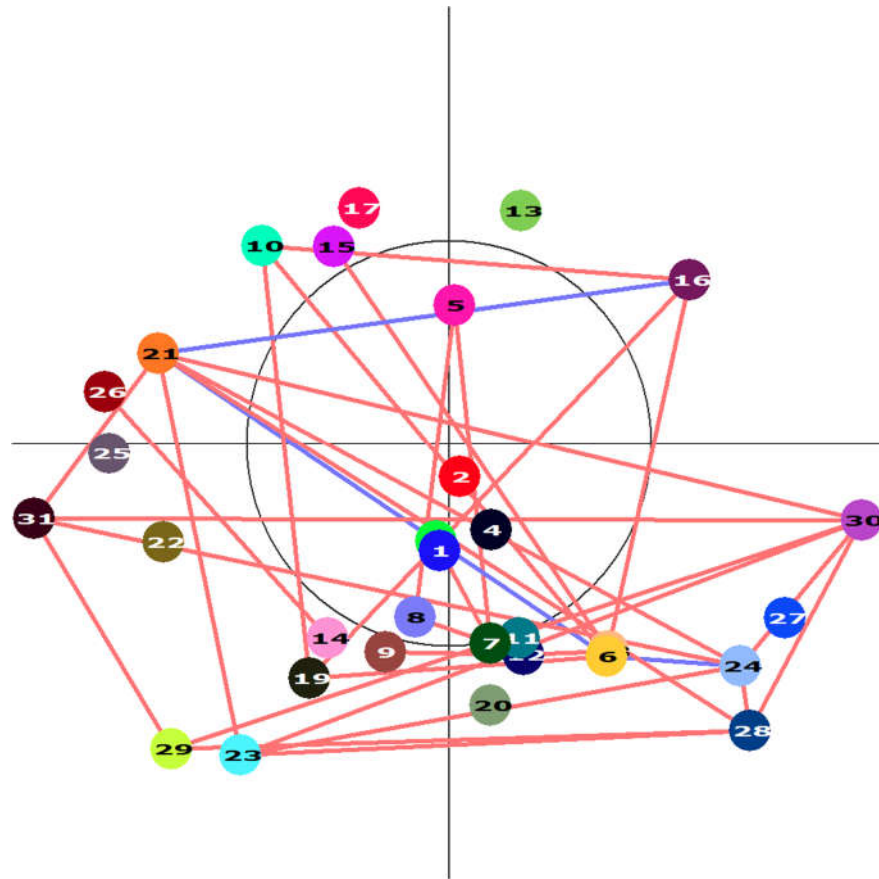


**Figure 4.4.7.:** Colour-coded graph depicting the interrelatedness of any pairs of nodes. These nodes represent regions of perfusion  $>0.5\text{ml}$  that were determined to be associated with MoCA using PCA. How these nodes correlate with one another is represented by edges, which are colour-coded as red (positive correlations) and blue (negative correlations). A positive correlation between regions suggests a regional synchrony which increases MoCA scores, and vice-versa for a negative correlation. Regionality of these nodes is depicted in the axial view, and regions named in Appendix E.

A negative correlation exists between nodes 6, 16, 21 and 24, as well as multiple positive correlations between various other nodes. These inter-correlations suggest that the respective nodes are associated with each other.

#### 4.4.4.4. Visualisation of PCA-derived covariance patterns

The surviving thresholded components (*Figure 4.4.5.*) were turned into two binary masks using FSL, one for positive voxels and one for negative. These masks were visualised in perfusion space, to determine the relationship between these components and underlying perfusion (*Figure 4.4.8.*).

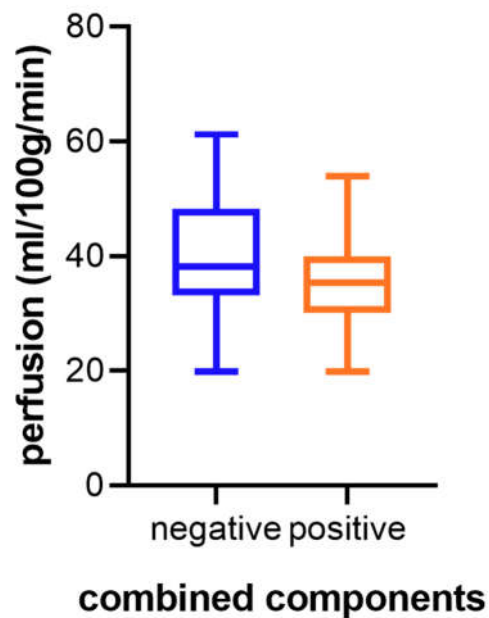


**Figure 4.4.8.:** Perfusion values associated with surviving components, visualised in perfusion space.

A two-tailed paired sample t-test showed a significant difference between negative and positive combined components, with positive components exhibiting a mean of 3.57 ml/100g/min less than negative components ( $p = 0.022$ ).

The correlation between these negative and positive clusters with MoCA scores were assessed using separate linear regressions. No significant results were found ( $p=0.46$  and  $r^2=0.012$  for negative clusters, and  $p=0.41$ ,  $r^2=0.015$  for positive clusters). Results are summarised in *Figure 4.4.9*. below.

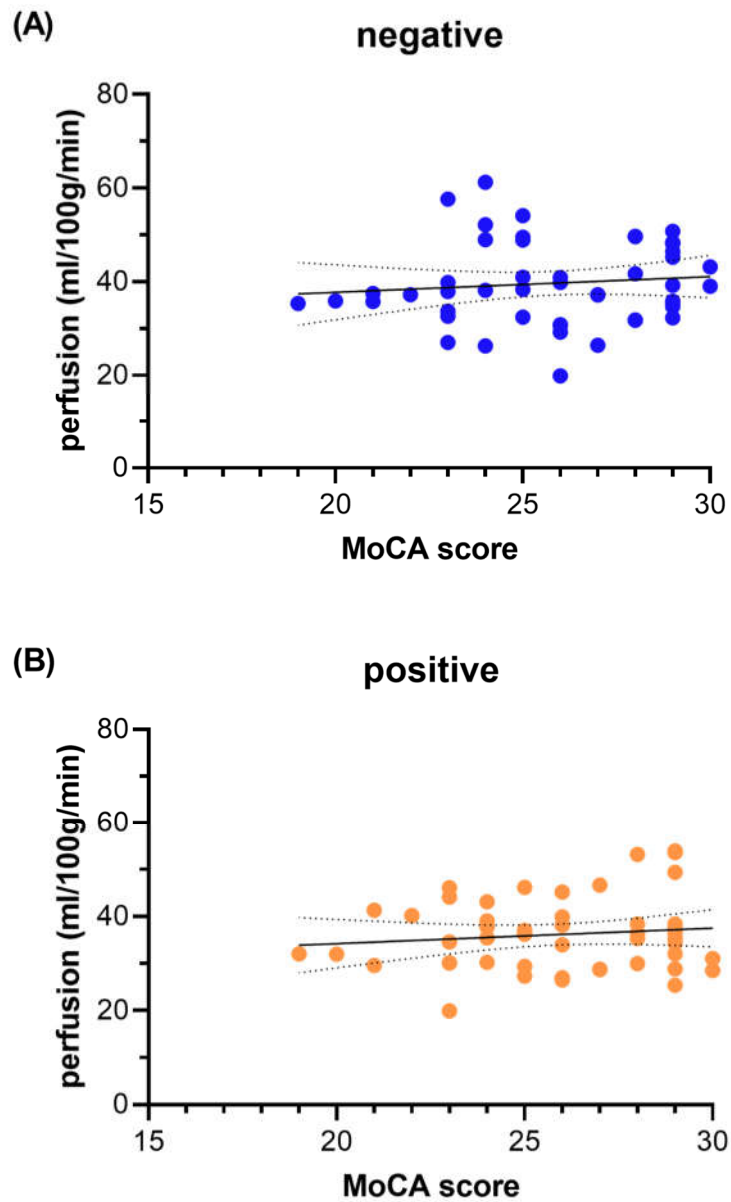


**Figure 4.4.9.:** Correlations between MoCA scores and PCA-derived clusters that are (A) negatively and (B) positively associated with these scores.

#### 4.4.4.5. Variance in individual subject perfusion patterns

The individual PCA-derived perfusion patterns in subjects with highest and lowest MoCA scores were also investigated, and shown in *Figure 4.4.10.*

Given that the subject with lowest MoCA score (19) was an 83-year-old male,

and there were no males who scored 30 in their assessment, a highest-scoring male was chosen at random, aged 69 with a score of 29. Their unadjusted mean GM perfusion values were 58.1 and 59 ml/100g/min, respectively.

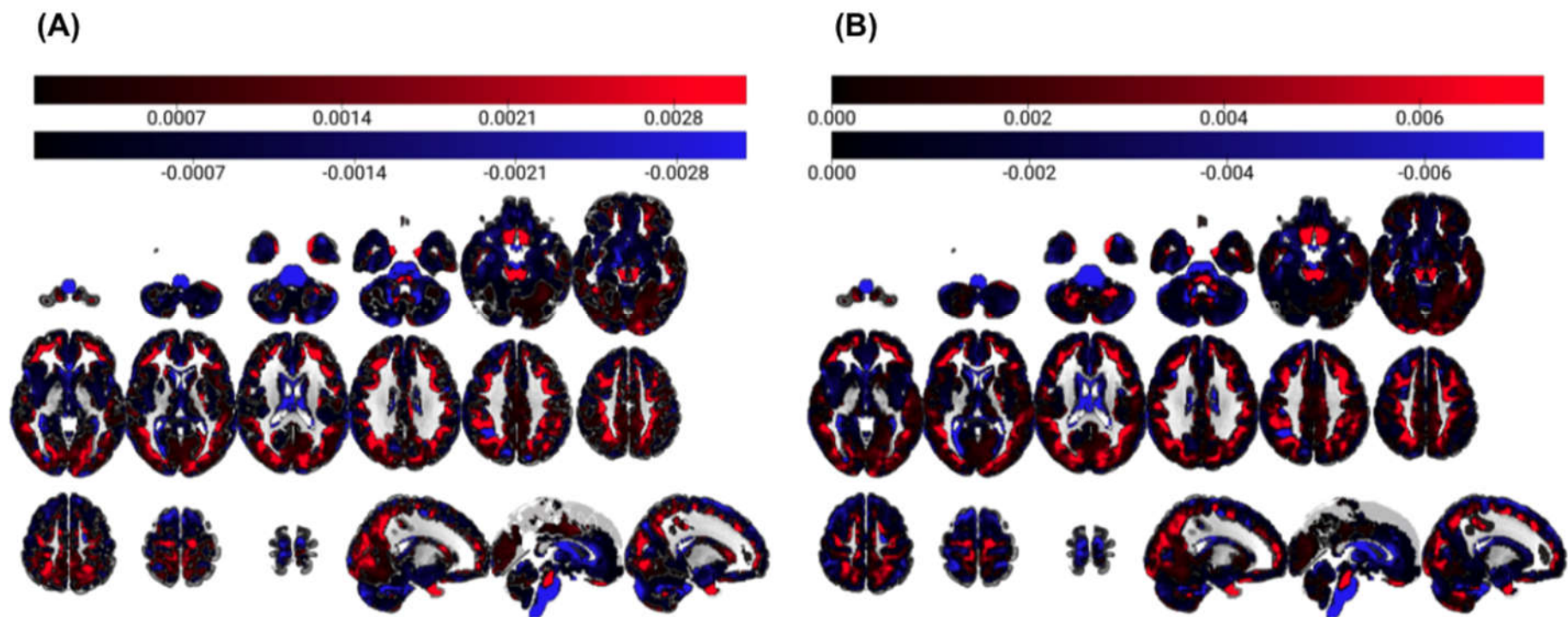


Figure 4.4.10.: Comparison of individual subject perfusion patterns in males subjects with MoCA scores of (A) 19 (n=1), and (B) 29 (n=1).

There was no apparent difference in PCA-derived perfusion pattern between these two subjects with MoCA scores of 19 and 29, respectively.

A MoCA score of 29 was the most common, and the individual perfusion patterns of all female subjects with this score were also assessed. The demographics of these subjects are summarised in Table 4.4.9., and their individual perfusion patterns in *Figure 4.4.11.*

**Table 4.4.9.: Demographics of female subjects with a MoCA score of 29.**

Subject	Age	Mean GM perfusion (ml/100g/min)	GM volume (cm <sup>3</sup> )
1	71	73.0	561.8
2	57	51.8	580.1
3	54	64.1	591.3
4	62	67.0	584.8
5	63	67.4	559.0
6	66	61.1	666.7
7	66	79.2	522.8
8	62	58.2	612.9

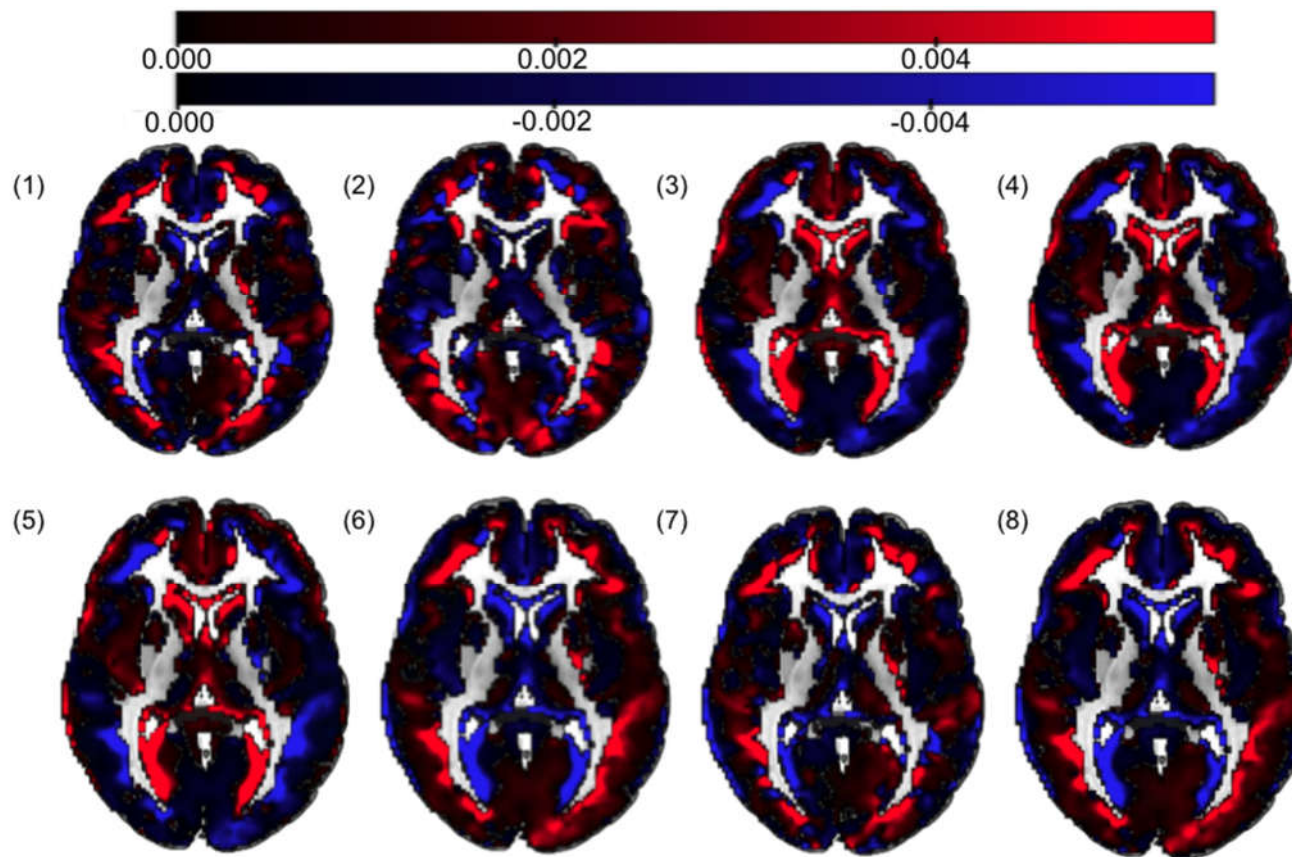


**Figure 4.4.11.:** Individual perfusion patterns, shown in the same axial brain slice of subjects 1-8, females who scored identically in the MoCA

The perfusion patterns depicted in *Figure 4.4.12.* suggest that there are two distinct patterns within this subsample of identical MoCA scores, characterised by either a preponderance of negative or positive associations with MoCA in posterior and frontal regions.

## 4.5. Discussion

### 4.5.1. General discussion

The current study used voxel-wise analysis and MVPA to characterise interrelations with cognitive performance in a healthy elderly population. The only significant finding at a voxel, predefined regional or network level with MoCA scoring in the full cohort was a positive relationship with PCC perfusion assessed using a 90th percentile mean, including covariates of age, sex and GM volume ( $p = .028$ ). Multivariate pattern analysis using PCA identified a MoCA score-related pattern which accounts for ~48% of the variance in MoCA scores, using three surviving components which contain both negative and positive weighting. This pattern points to a physiological signature which underpins the relationship between MoCA scores and brain perfusion.

After thresholding at 98% retention to remove spurious results from the computation of PCA, the PCA-derived perfusion pattern is characterised by negative clusters which include parts of the occipital, frontal, and left parietal lobes, and the right caudate, and brainstem. The frontal lobe is known to be largely involved in dementia due to its role in cognition (MacPherson and Cox, 2017) and fronto-temporal dementia (Neary et al., 1988), thereby warranting further investigation as to whether this negative correlation is driven by low

MoCA scorers. The cluster within the right caudate is also interesting, given it is part of the basal ganglia – a group of subcortical nuclei involved in various brain functions including cognition – and the caudate’s own role in goal-directed action (Grahn, Parkinson and Owen, 2008), with relative perfusion in the region shown to correlate with task complexity in the Tower of London task (Dagher et al., 1999).

Various positive correlations across much of the GM are apparent, including the middle frontal gyrus, subcallosal cortex and angular gyrus, as well as the brainstem. Interestingly, the right middle frontal gyrus is thought to be a region of network convergence for the dorsal and ventral components of the attention networks (Japee et al., 2015), and numeracy abilities (Koyama et al., 2017). However, both positive and negative component expression in such networks suggests variance in the MoCA score/cerebral perfusion relationship at a regional level, which may be missed in simpler analyses. Surprisingly, there was minimal crossover between the clusters of the resultant PCA-derived spatial covariance pattern and the networks of interest. The ECN and resilience signature were not particularly apparent, but there was slight crossover with the DMN, with positive clusters within the superior and middle frontal gyri. Additionally, there was some crossover with the SN, with negative associations within the supramarginal gyrus, and positive and negative associations within the paracingulate gyrus.

When positive and negative retained voxels were investigated separately, neither exhibited a significant relationship with actual MoCA scores when assessed using linear regressions (*Figure 4.4.10.*). These positive and

negative masks did not relate to underlying cerebral perfusion in a manner as simple as hypo- or hyper-perfusion, as evidenced in *Figure 4.4.9.*, which showed that negative components had significantly higher ml/100g/min perfusion values when back-projected into individual subject perfusion space. These additional investigations highlight the necessity to consider both positive and negative associations with MoCA scores when determining a spatial covariance pattern with potential future predictive power. The comparative FSL-randomise analysis showed no pattern, highlighting the greater power of PCA in elucidating the subtle nuances of this relationship in the current cohort.

Given the intention to further this work by using this approach across the HA-MCI-AD continuum, and in conjunction with imaging signatures of cognitive resilience, comparing the ~48% of the variance in MoCA scores explained by the PCA-derived spatial covariance pattern with imaging biomarkers is important. A review by McConathy and Sheline (2015) highlights clinical assessment accuracy of AD is ~70-80%, but as a singular diagnostic metric is sub-optimal, missing preclinical pathophysiology. Structural MRI shows high sensitivity for within-subject change, with highest sensitivity in the entorhinal cortex, with an annual percentage decrease in volume of 2.54% in MCI, compared with 0.64% in healthy controls (Holland et al., 2009). A study by Douaud et al. (2013) showed that when GM volumes were used in combination with diffusion tensor imaging (DTI) and CSF biomarkers, the MCI to AD conversion could be predicted with 96% specificity, 85% sensitivity and 91% accuracy. Mosconi (2005) has evidenced a ~90% sensitivity for early AD identification when using FDG-PET, however specificity for discrimination between different types of dementia is less (71-73%; Jagust et al., 2007). As

such, whilst this model provides moderate explanation of the perfusion/MoCA score relationship, it is less successful than many established biomarker candidates, thus utility of these findings is as a starting point for further development of a model which can fulfil the requirements of the Biomarkers Definitions Working Group (2001), who suggest a biomarker requires high sensitivity and specificity of >80%, in cases confirmed with neuropathological investigation.

Graph visualisation identified several nodes in the PCA-derived perfusion pattern, with both nodes of multiple connections, and anatomical groupings of independent regions apparent. The most connected nodes are 21, 24, and 30 – with 8, 6 and 6 connections, respectively – which include parts of regions such as the middle frontal gyrus, precentral gyrus, postcentral gyrus and the superior frontal gyrus. These regions are linked to attention (Japee et al., 2015), movement, touch and self-awareness (Goldberg, Harel and Malach, 2006) and attention shifting (Nagahama et al., 1999). Whilst it is possible that any regions which are known to have a primary movement-related role are included artefactually due to movement within the scanner, it is also feasible that they are correlated with other regions due to their role in mental imagery (Yoo et al., 2003). There is also an interesting negative connection between 6, 16, 21, 24, which suggests a synchrony between these regions which decreases MoCA score in the context of ASL-derived perfusion measures, and should be investigated further in future work. Given these nodes are derived from the PCA spatial covariance pattern, they do not comprise hub regions of key networks, in contradiction to the hypothesised finding. This is surprising, but may be due to a combination of intra-individual variance in GM perfusion (Parkes et al., 2004) and the small sample size, and thus

subsequent investigation in a larger cohort is warranted to validate or refute this finding.

Three apparent anatomical hub groupings exist between nodes 21, 25 and 26, nodes 7, 11 and 12, and nodes 27 and 28. The first of these hubs includes parts of the middle and superior frontal gyri, and the precentral gyrus. The second contains the occipital pole, much of the occipital cortex, and the occipital fusiform gyrus, and the third contains the precentral gyrus, postcentral gyrus and superior frontal gyrus. However, these are likely grouped solely due to anatomical proximity. For example, node 11 does not have any linked edges, which suggests this does not correlate with any other regions. This may be due to the region being fairly small, or possibly a region that, whilst not spurious due to its contribution to the model  $r^2$  and its size exceeding 0.5ml, is functionally spurious when considering underlying regional relatedness. Node 1 also exhibits an absence of correlations with other nodes. Given this node is comprised almost exclusively of brainstem, this suggests the possibility of an ASL acquisition-related spuriousness, warranting analysis of additional nuisance factors. The choice of 0.5ml as a cluster size threshold was somewhat arbitrary, aiming to balance inclusion of as many clusters as possible with graph comprehensibility.

The aforementioned findings of both positive and negative recruitment at a regional level, suggesting a granularity to regional functionality, is supported by the results of further ROI and network analyses. Particularly, use of a standard mean to measure regional perfusion revealed no significant relationships between any ROI and MoCA scoring when analysed using linear

regression, controlling for age, sex and GM volume, and also with the addition of GM CBF to control for perfusion variance of no interest. However, analysis using the 90th-percentile mean (see Table 4.4.4.) as recommended by Tong et al., 2016 revealed a significant positive relationship with the PCC, with the precuneus and left hippocampus approaching significance ( $p = 0.081$ , and  $p = 0.097$ , respectively). This significant relationship in the PCC is in support of both the findings of Sierra-Marcos (2017), and the HA-MCI-AD continuum, with metabolic decreases frequently present prior to clinical diagnosis of cognitive impairments (Leech and Sharp, 2014). Parts of the left and right thalami, and the left and right DLPFC, exhibit a positive relationship with MoCA scores as part of the PCA results and graph visualisation, but as whole regions, these do not show a significant relationship ( $p > 0.05$  for all). These findings are summarised in Table 4.4.3. and 4.4.4..

None of the networks investigated showed a significant linear regression with MoCA scores when the same covariates were controlled for, although the resilience signature ( $p = 0.08$ ) and anterior SN ( $p = 0.089$ ) approach significance. Considering that this resilience signature was only recently proposed by Arenaza-Urquijo et al. (2019) as a metabolic signature of cognitive resilience, this is particularly interesting, and warrants further investigation in a larger cohort. The absence of the DMN in PCA and graph visualisation results, as well as a lack of significant correlation between perfusion of both the dorsal and ventral parts of the DMN and MoCA scores, is noteworthy given its failure early in Alzheimer's disease (Greicius et al., 2004; Binnewijzend et al., 2012; Vidal-Piñeiro et al., 2014). This is in contrast to the hypothesis that DMN perfusion would increase significantly with MoCA score

increase, and the finding of a significant relationship between the PCC and MoCA scores, given that the PCC is a major node within the DMN.

Analysis comparing high- and low-scoring male subjects was limited by having only a single subject for each score, however provided some interesting tentative results, in that there were no clear regions of distinct difference between subjects. It is notable that their mean unadjusted GM perfusion values were also near-identical, 58.1 and 59 ml/100g/min, respectively. Further analysis assessing the variance in female subjects with identical MoCA scores (*Figure 4.4.12.*) suggested there were two distinct patterns, characterised by a preponderance of negative or positive relationships with MoCA scores in posterior and frontal regions. Conclusions are challenging to make here, given the limitations of sample size, but may be indicative of multiple patterns for each individual MoCA score, which may in turn be reflective of underlying confounds which were not controlled for.

#### 4.5.2. Study limitations

Whilst this study provides an interesting first step to define the relationship between MoCA scores and cerebral perfusion, there were some limitations which are important to acknowledge and further consider in future work. As in Chapter 3, the current study is limited in its cross-sectional nature, and a longitudinal cohort which followed subjects through the healthy ageing-MCI-AD continuum would greatly expand understanding of the utility and validity of the results of this study.

Attrition rate within all cohorts was high, with 137 unique 3D pCASL perfusion maps identified, of which 62 survived quality control, but only 49 had available MoCA data. This represents an attrition rate of ~54.7% which can be attributed to image quality control (further discussion pertaining to the limitations of the quality control approaches are discussed in Section 3.9.5.), and this subject loss due to image quality did not occur more commonly within a cohort acquired at a certain site or from a specific MRI scanner model. There were too few subjects from each site to explicitly control for site effects, and whilst this attrition may suggest that quality control was too strict, the recommended approach suggested by Alsop et al. (2015) was followed and any uncertain cases removed to mitigate spurious findings, which were of concern due to the highly complex methodology.

The imbalance between male and female subjects is also a key limitation, as the study findings are driven by the relationship between female brain perfusion and MoCA scores. Whilst this was included as a covariate, it is an important topic for future investigation in a larger cohort with enough power to enable the computation of independent male and female PCA-derived perfusion maps. This would also allow for further investigation of the resilience signature and its possible variance between males and females.

Notably, this whole-brain approach to PCA was necessary, given the whole-brain nature of both the ASL and cognitive components, and the lack of a robust perfusion biomarker of cognitive decline which could enable PCA to be limited to a specific area. Resultantly, this methodology does have greater elements of irrelevancy than regional PCA might. As a result of the current

approach, many of the blue and red voxels are only there to cancel each other out, as evidenced by the discrepancy between the unthresholded model and the 98% retained model (see *Figures 4.4.2. and 4.4.5.*). The presence of unconnected nodes in the graph visualisation output (*Figure 4.4.7.*), such as Node 1 which includes much of the brainstem, suggest that some regions which survived the thresholding may have been included in the final PCA-derived perfusion pattern because they are noisy, rather than physiologically relevant to the underlying relationship with MoCA scoring. This was the justification for the removal of the brainstem in the PCA analysis within Chapter 3.

The cohort used within this study was small and an independent unseen cohort is needed to enable validation, particularly due to the variance in perfusion which is exhibited even in healthy individuals (Parkes et al., 2004; Aanerud et al., 2012). Whilst this variance is core to the theoretical underpinnings of PCA, this technique is often carried out in cohorts comprising thousands of subjects, and increasing the cohort size for validation would enable the reliability of these findings to be assessed. Unfortunately, high attrition prevented the possibility of creating an unseen cohort within either local University of Nottingham data, or ADNI-3. The intention was to validate these findings within the TILDA cohort, however access to this cohort was unfortunately delayed. When feasible, this validation would involve using the PCA-derived spatial covariance pattern from the current study to predict MoCA scores within the unseen cohort, and comparing these with their actual measured scores. New PCA-derived spatial covariance patterns could also be determined within the new cohort and compared with the current cohort. A larger cohort of this scale would also enable further investigation of how the

model is affected by outlier MoCA scores, and may include additional demographic information to determine whether the subject was a true outlier or simply achieved a low score on the MoCA, for example the subject included here who had a score of 19. A validation cohort with many subjects of a given MoCA score would also allow the variance in spatial covariance pattern with subject score to be investigated, and PCA pattern to be derived for each score. Additionally, inclusion of structural brain MRI could improve the model through additional exploration of the explanatory power of perfusion alone when compared with perfusion and structural images, or structural images alone.

Direct comparison of MVPA and FSL-randomise voxel-wise analysis results to other studies in the field was not possible, as to our knowledge this is the first study which looks at the relationship between cerebral perfusion and MoCA scores in such a manner. Much of the current literature in focuses on patterns related to discrimination of healthy and disease cohorts (Spetsieris et al., 2009; Melzer et al, 2011; Ding et al., 2014), different disease states (Huang et al., 2003) or use domain-specific cognitive tests (Steffener et al., 2013; Hays et al., 2018). The lack of both positive and negative voxel-wise findings may be indicative of the inter-relatedness elucidated by MVPA, however it is possible that these findings may be specific to the current cohort and therefore warrant validation.

Using retrospective data from multiple cohorts and several sites means that some acquisition parameters vary between subjects. Whilst it was possible to achieve comparable 3D PCASL CBF maps, a single cohort using one scanner

and the same protocol for all subjects would be preferable, to avoid multi-site and multi-investigator effects (Van Horn and Toga, 2009). Unfortunately, as shown in Section 4.2.1. of this chapter, a cohort of this size and specification has proven challenging to access at this stage. It is important to acknowledge that this variance in study parameters included PLD, which likely caused the position of the label at the time of acquisition to differ. Subsequent studies should aim to use identical acquisitions, however if this is unrealistic, identical PLD should be a priority. It has been suggested that differences in acquisition parameters can affect reproducibility more than between-vendor hardware and software choices (Mutsaerts et al., 2015).

The MoCA cognitive test is also a global cognitive score metric which does not capture certain nuances that batteries focused on specific – rather than global – cerebral functionality might, and as such there may be other alternative cognitive tests which better explain the relationship between global GM cerebral perfusion and cognition. However, MoCA was chosen in large part due to its availability within possible cohorts, and its superiority to MMSE (Hsu et al., 2015), and is considered to be a gateway test to the model development, with the model designed such that it is possible to change the type of clinical score included, provided the expected error variance of the score of interest is known.

This model only partially explains MoCA scores ( $r^2$  at 98% retained = 0.4829), and whilst it does provide moderate explanation and achieving biological completeness is highly unlikely, it may be improved by consideration of further covariates which are easily measured in a future study population. Additional

covariates pertaining to both protection and risk factors could also allow for mechanistic inferences to be made regarding cognitive decline, and further understanding of cognitive resilience and resistance in a healthy cohort. Some of these covariates were already discussed in Chapter 3, however there are some additional covariates which would be of interest due to the involvement of MoCA scores and the concept of cognitive decline in this study.

A meta-analysis by Pieper et al. (2020) investigated 26 studies – including 621,548 subjects – and found that both short- and long-term use of anticholinergic medication is associated with incident dementia, and any use associated with cognitive decline. However, these studies were observational, and thus prone to a risk of bias, with causality difficult to infer. Similar conclusions pertaining to long-term use were also reached in a recent Cochrane review by Taylor-Rowan et al. (2021). Risacher et al. (2016) investigated cognitively normal individuals in the ADNI-1, ADNI-GO and ADNI-2 datasets, and found an association between use of anticholinergic medications, cerebral glucose metabolism, and brain atrophy, using FDG-PET and structural MRI. Whilst this information was limited to only the ADNI-3 cohort for this current study, some individuals were missing the associated data and thus there was not enough information provided to assess any related effect within this cohort. However, such pharmaceutical information may be pertinent to any future expansion of the model, if the data is available. Additionally, consumption of the psychostimulant caffeine is commonplace and requires additional consideration, as previously discussed in Chapter 3.

The APOE gene has been discussed previous within this thesis, however it is worth noting that it would be of particular interest here, as assessment of APOE in individuals who are currently considered to be healthy is likely to be of benefit to the model, particularly in a larger cohort which could be split into APOE sub-cohorts for further investigation.

Cerebrovascular risk factors should be considered for future inclusion, and would further inform as to the nuance of the relationship between brain perfusion and MoCA scores, and would also allow sub-division of future large cohorts based on these factors. For example, blood pressure, diabetes and obesity have all been linked to altered cerebral perfusion (Cui et al., 2017; Glodzik et al., 2019; Stillman et al., 2021). A recent study using UK Biobank data (Veldsman et al., 2020) also evidenced that such cerebrovascular risk factors were associated with decreased fronto-parietal network integrity, and executive function in a cohort of 22,059 subjects, using multivariate modelling. Systolic blood pressure was also predictive of executive function in mid-life, but not in those aged >70 years.

Inclusion of lifestyle factors is also imperative to model covariate completeness and accuracy of the resulting relationship between MoCA scores and cerebral perfusion. Exercise has been shown to have a protective effect when considering cognitive functionality (Lytle et al., 2004; Sofi et al., 2011; Tyndall et al., 2018), with a review by Balsamo et al. (2013) confirming the promise of exercise as non-pharmacological intervention in the management and prevention of cognitive decline. Larson et al. (2006) carried out a longitudinal study which showed that individuals were more likely to be

dementia-free during the six-year follow-up if they exercised three or more times per week (independent of other risk factors). As such, healthy individuals may be benefitting from current or historic exercise habits, and thus these should be considered in future iterations of the model. When considering the proposed validation of the PCA model it would also be of interest to determine whether protective factors such as exercise have an additional resilience effect which can partially explain deviations between the model-predicted MoCA scores, and actual MoCA scores.

A study by Mantri et al. (2019) highlights other factors which have an impact upon cognition in later life, with race, education level, financial status, and school district all positively associated with MoCA scores. High levels of education early in life have been shown to be protective against cognitive decline (Chen et al., 2019), although this is thought to plateau in early adulthood (Kremen et al., 2019). Koster et al. (2005) also highlight the role of low socio-economic status in predicting cognitive decline in older adults. Life stress also has a detrimental effect on the brain (Prenderville et al., 2015), and is associated with memory impairment (Lupien et al., 2009).

#### 4.6. Conclusions and future directions

Use of PCA within this specific cohort results in a model which provides a moderate explanation of the association between cerebral blood flow and MoCA scores. Interestingly, the resultant pattern showed minimal regional crossover with key networks known to be involved in cognition. However, validation is needed – ideally within a cohort acquired on a single scanner in the first instance – as this is a preliminary demonstration of the feasibility of a

very complex analysis within a small retrospective dataset comprising subjects from cohorts with differing acquisition parameters. Additionally, the model may benefit from the inclusion of further covariates, for example APOE genes and years of education, but this information was either only available for the subjects which were included from ADNI-3, or unavailable for all subjects. Such future work would enable further elucidation of this relationship, and expand understanding of moderator factors and diseases which are thought to affect perfusion and related physiology by determining how they alter PCA-derived covariance patterns. This would ultimately be valuable for the promotion of cognitive health in the elderly.

# 5. Functional $^1\text{H}$ MRS of cerebral lactate concentration changes during prolonged visual stimulation

## 5.1. Introduction

The brain relies on Glc and oxygen for its energy needs and consumes around 20% of available oxygen within the body, despite accounting for only 2% of its mass (McKenna et al., 2005; Raichle and Gusnard, 2002). Coupled with a lack of cerebral energy reserves, this results in a constant demand for both oxygen and Glc to be delivered to – and utilised by – the brain. This energy is critical for both the maintenance of specialist cerebral functions – with neuronal activity demanding around 80-90% (Attwell and Laughlin, 2001; Harris and Attwell, 2012; Howarth, Gleesan and Attwell, 2012) of the available energy – and basic metabolic function (Engl and Attwell, 2015).

Under normal, healthy conditions, the brain uses blood-borne Glc to meet its energy needs, whilst maintaining homeostasis within the related metabolic pathways (Mergenthaler et al., 2013). As seen in *Figure 5.1.1.*, Glc is converted to pyruvate, which is a key biological molecule linking the end of glycolysis to the TCA cycle and amino acid synthesis. By sitting at the entry of the TCA cycle, pyruvate metabolism is essential in generating energy in the form of ATP for brain activity. The majority of required ATP is generated via oxidative metabolism (i.e. respiration) when oxygen supply is sufficient and the mitochondria fully functional. However, a significant fraction of ATP synthesis can also be produced via non-oxidative metabolism (i.e. via

glycolysis and fermentation) when the oxygen supply is limited, or mitochondria compromised. To sustain the flux of ATP synthesis through glycolysis, lactate dehydrogenase will need to convert pyruvate to Lac via the transfer of two electrons, and nicotinamide adenine dinucleotide (NADH) will be oxidised to reform  $\text{NAD}^+$  for use in glycolysis again.

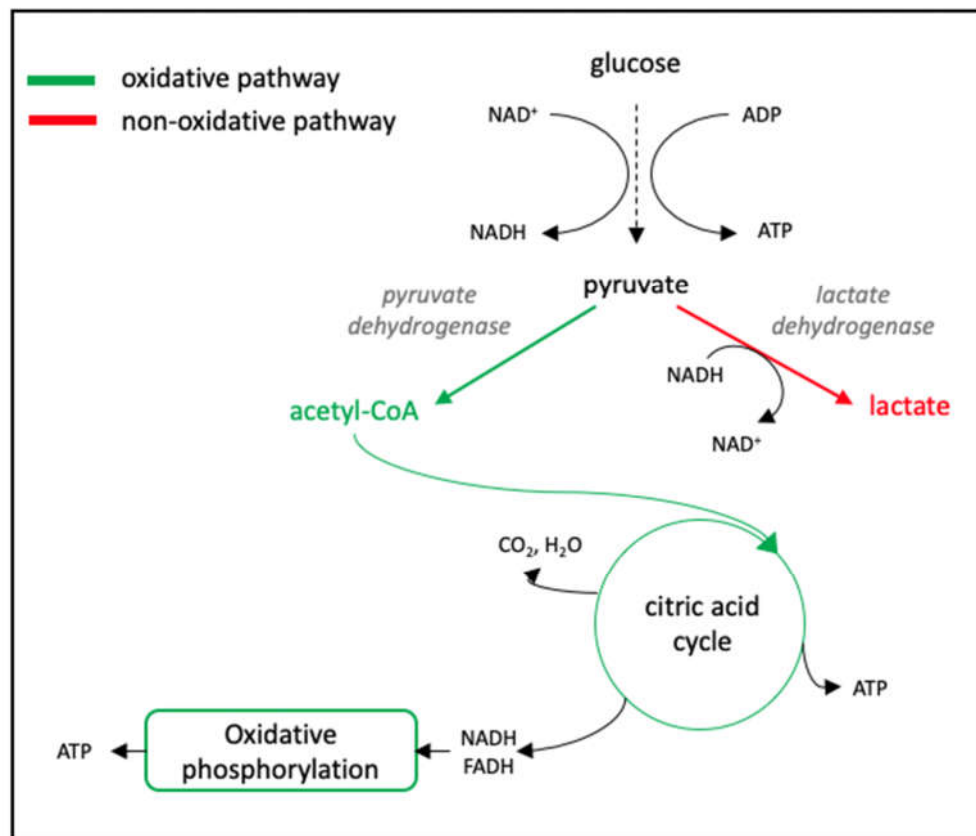


**Figure 5.1.1.:** Summary of the biochemical relationship between glucose and lactate, and their relationship to energy production.

This increased Lac production as a result of disruption to oxidative metabolism was long thought to be a metabolic dead-end, with little biochemical importance in the brain (Siesjö, 1978; Taher et al., 2016). However, in recent years the conceptual role of cerebral Lac metabolism has changed greatly,

shifting from the fuelling of development and consideration as a waste product of glycolytic metabolism, to its use as a supplemental fuel for neuroenergetics, particularly in conditions of insufficient Glc availability (Magistretti and Allaman, 2018). Despite the decreased energy efficiency of non-oxidative metabolism comparatively to glucose oxidation, temporary increases in non-oxidative reactions can be advantageous due to the faster generation of ATP by the mitochondria (Prichard et al., 1991; Schurr and Payne, 2007).

Another theory regarding the temporal relationship of this disrupted oxidative metabolism is that of uncoupling. An FDG-PET study by Fox et al. in 1988 was imperative in evidencing how Glc consumption and the cerebral metabolic rate of oxygen (CMRO<sub>2</sub>) become temporarily uncoupled during focal physiologic neural activity, a finding which has been attributed to a rise in non-oxidative metabolism during cerebral activation in response to a change in energy demand. However, such investigations only provide a cumulative measure of glucose transport and consumption, which may be partially explained by brain atrophy (Chawluk et al., 1987; Yoshii et al., 1988). In addition, FDG-PET studies have resulted in well-established evidence of cerebral glucose hypometabolism in both healthy and impaired ageing. When considering impaired ageing, the extent of such regional decreases has been shown to be related to the severity of dementia (Herholz et al., 2002), as well as suggesting that reductions in the parieto-temporal, PCC, and frontal cortices are the hallmarks of AD (Mosconi, 2005). Such characteristic findings are thought to result from the cumulative effect of impaired Glc transport and consumption, although it is important to note that large regions of the brain have been shown to also be affected by decreased Glc metabolism in healthy ageing, particularly within the frontal and temporal lobes (Bonte et al., 2017).

More specifically, Ishibashi et al. (2018) evidenced the decreasing regional uptake of fluorodeoxyglucose in elderly subjects with normal cognitive function within the ACC and PCC. However, areas of hypermetabolism have also been evidenced with age and disease through the use of ASL – namely the PCC, precuneus (Alsop, Detre and Grossman, 2000; Asllani et al., 2008) and the hippocampus (Alsop et al., 2008) – resulting in contradictory findings within the field. Given the greater complexity of cerebral energy metabolism, with tissue- and regional- specificity affecting glucose transport, glycolysis and oxidative phosphorylation (Mergenthaler et al., 2013), it is pertinent that investigation using advanced MR techniques can further elucidate the compensatory metabolism which might underpin such findings.

An alternative explanation for these changes in levels of both Glc and Lac within the brain is the astrocyte-neurone lactate shuttle model (ANLS; Pellerin and Magistretti, 1994; Pellerin et al., 1998), summarised in *Figure 5.1.2.*. The ANLS hypothesis suggests that a global increase in cerebral Glc consumption is associated with rising concentrations of Lac, whereby Glc consumption is higher in astrocytes than in neurones, thereby triggering the production of Lac in the astrocytes, which is then taken up and oxidised by neurones when they are active (Magistretti et al., 1999; Pellerin et al., 2007).

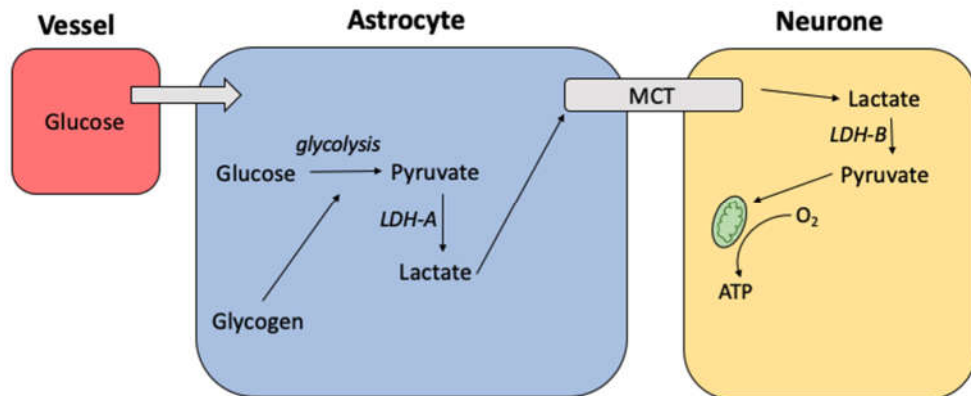


**Figure 5.1.2.:** Schematic representation of the biochemistry underlying the ANLS hypothesis. Activation of neurones causes a release of glutamate into the synapse. The reuptake of this glutamate into the astrocytes subsequently causes an increase in uptake of glucose from vessels into astrocytes. Through glycolysis (which can also be instigated by depletion of intracellular glycogen), pyruvate can be generated and then converted to lactate, by lactate dehydrogenase isoenzyme-A (LDH-A). Lactate is then transported to neurones by monocarboxylate transporters (MCT). Within the neurone, lactate dehydrogenase isoenzyme-B (LDH-B) converts lactate to pyruvate, which then fuels mitochondrial oxidative phosphorylation, generating ATP.

However, this model is highly controversial (see Chih and Roberts, 2003 for a review). Revisions by Pellerin et al. (2007) have accounted for concerns regarding the sequence of the associated metabolic pathways, but the general consensus remains that experimental observation of directional Lac transfer from astrocytes to neighbouring neurones would be required for conclusive proof in the model (Kasischke, 2009) – this model has also only been extensively trialled in immature cell cultures (Chih and Roberts, 2003; Bonvento, Herard and Voutsinos-Porche, 2005) and both *in vivo* and *ex vivo* animal models (Bouzier-Sore et al., 2003; Serres et al., 2003; Serres et al., 2004; Lee et al., 2012; Lundgaard et al., 2015; Zimmer et al., 2017), thereby necessitating further *in vivo* investigation in both animals and humans before it may be widely accepted. Investigation comparing healthy subjects and

individuals with neurodegeneration may also provide additional support (Pellerin et al., 2007).

Whilst multiple theories clearly exist within the field, the reprogramming of brain metabolism – shifting from oxidative phosphorylation to glycolysis – is still believed to be a critical component of brain ageing, and potentially a hallmark of this process (Sijens et al., 2001a; 2001b; Ross et al., 2010). Indeed, the related neuroenergetic failure also provides a mechanistic explanation of the intimate neuronal and astrocytic interactions and compensatory metabolic response evidenced in dementia, and the strong associations between age, cognitive impairment, and neurodegeneration, known as the ‘neuroenergetic hypothesis’ of dementia (Blonz, 2017). The flux of ATP through aerobic glycolysis within the healthy brain has been shown to markedly decrease with age and may be characteristic of healthy cognitive ageing (Goyal et al., 2017). However, recent work using carbon-13 MRI (<sup>13</sup>C-MRI) has shown that a pattern of Lac metabolism is preserved with age, comprising high Lac signal in the precuneus, cuneus and cingulate (Lee et al., 2020). Goyal et al. (2020) also demonstrated that the subthreshold accumulation of amyloid in young adults mirrors that seen later, and additionally corresponds to the topography of aerobic glycolysis seen in young adults. Furthermore, a recent review paper by Cunnane et al. (2020) clarified the potential of Lac as an alternative brain energy substrate when Glc metabolism is impaired and metabolic reprogramming may occur (Newington, Harris and Cumming, 2013). This is thought to occur in age-related neurodegenerative disorders, such as AD, and may precede clinical symptom onset, thus warranting further investigation (Ross et al., 2010; Cunnane et al., 2011; Zhang, Alshakhshir and Zhao, 2021).

Given the transience of Lac changes and the continued debate regarding the metabolic events of neuronal energetics during functional activity, it is important that techniques used to investigate these changes can capture them as accurately as possible.  $^1\text{H}$  MRS enables the assessment of a variety of metabolites, with increasing sensitivity provided at ultra-high field (Mangia et al., 2007; Lin et al., 2012) due to a roughly linear increase in SNR in relation to the increasing strength of  $B_0$  (Edelstein et al., 1986; Tkáč et al., 2009). Furthermore,  $^1\text{H}$  fMRS approaches provide excellent insight into the temporal behaviours of these metabolites, thereby enabling the investigation of such changes over time. Studies of particular interest within the field have previously involved utilising prolonged visual stimulation with ultra high-field MRI (Dennis et al., 2015), to measure the function of the visual pathway. The work of Bednařík et al. (2015) has also evidenced a significant, positive correlation between blood-oxygen-level-dependent functional MRI (BOLD-fMRI) and Lac changes, suggestive of an intimate relationship between these elements of brain functionality.

Reported Lac increases have varied substantially between protocols and studies. Some authors challenged the feasibility of Lac measurement, accumulation or detectable, reproducible time course during several different kinds of visual stimulation (Merboldt et al., 1992), and even failed to detect any Lac signal during prolonged stimulation (Boucard et al., 2005). However, others found significant increases in Lac during visual stimulation – ~10% (Fernandes et al., 2020), ~19% (Schaller et al., 2013), ~23% (Mangia et al., 2007), ~10-30% (Lin et al., 2012), 30% (Bednařík et al. 2015), 57% (Prichard et al., 1991), 170% (Frahm et al., 1996) and 250% (Sapèy-Marinié et al.,

1992) respectively - which returned to baseline over time after the stimulus was removed.

MRS also enables quantification of cerebral metabolic concentrations, and thus can provide information beyond their temporal dynamics. Cerebral Lac is normally present at low concentrations in the healthy adult brain, on the order of 1 mM, although this can be highly variable across individuals (Veech, 1991; Dienel, 2012). Multiple studies have attempted to quantify Lac concentrations using MRS (Mangia et al., 2007; Melke et al., 2009; Lin et al., 2012; Schaller et al., 2013; Schaller et al., 2014; Bednařík et al., 2015; Boillat et al., 2020) in young- and middle-aged healthy adults, although methodological approaches have varied. These papers are summarised in *Table 5.1.1.*

**Table 5.1.1.: Key papers which attempt to quantify “absolute” concentrations of lactate.**

Author(s)	MRI acquisition	Cohort	TR/TE (ms)	Stimulus or task	Percentage change (%)	“Absolute” concentrations	Method of conc calculation
<b>Mangia et al. (2007)</b>	7T, Magnex, STEAM	12 healthy subjects (19-26 years)	5000/6	Radial red/black checkerboard  <i>Two paradigms:</i> ON-OFF-ON-OFF, ON-OFF	23±5 ↑ during visual stimulation	↑ = 0.24±0.01 µmol/g (conc. changes ± CRLB)	Unsuppressed water signal from same VOI used as reference, assuming 80% brain water content
<b>Melke et al. (2009)</b>	7T, Siemens, SPECIAL.  Quadrature transmit/receive surface RF coil	6 healthy subjects (22-26 years old)	4000/6	<i>None - no timecourse measure</i>	-	0.7±0.1 mmol/kg (mean ± SD)	Reference to mean conc of tCr = 8 mmol/kg. LCModel.
<b>Lin et al. (2012)</b>	7T, Philips, STEAM	10 healthy subjects (3F, 25±3 years)  <b>(all mean ± s.d)</b>	3000/15	Contrast-defined wedge visual stimulus, grey background during rest  Single stimulus = OFF-ON-OFF  Double stimulus = OFF-	<b>Single stimulus</b> ↑ = 10±6  <b>Double stimulus</b> ↑ = 30±7 between first stimulation and first rest	<b>Single stimulus</b> <i>Rest</i> - 0.79±0.05 µmol/g <i>Stimulation</i> - 0.89±0.05 µmol/g  ↑ = 0.1±0.05 µmol/g <b>Double stimulus</b> ↑ = 0.21±0.05 µmol/g between first	µmol/g of wet tissue, assuming brain water content of 80%. LCModel.

				ON-OFF-ON		stimulus and first rest <b>(all mean ± s.d)</b>	
<b>Schaller et al. (2013)</b>	7T, Siemens, SPECIAL. Home-built quadrature transmit/receive coil	10 healthy subjects (1F, 20-28 years), 6 in "BOLD activated tissue", 4 outside	5000/6	Black-grey checkerboard (OFF-ON-OFF-ON-OFF), 5 periods of 5 minutes. Button press attention task - rotation of fixation cross	↑ = 19±4 (n=6, comparing activation with rest)	<i>Resting lac</i> - 0.61±0.04 μmol/g ↑ = 0.12±0.03 μmol/g  <b>(all mean ± s.e.m, n=6 [BOLD activated tissue group])</b>	LCModel
<b>Schaller et al. (2014)</b>	7T, Siemens, SPECIAL. Single-channel quadrature transmit, 32-channel receive	11 healthy subjects (2F, 18-26 years, right handed)	7500/12	Finger-thumb tapping, cued, both hands	↑ = 17±5 (comparing activation with rest)	<i>Resting lac</i> - 1.02±0.03 μmol/g <i>During activation</i> - 1.20±0.06 μmol/g <i>Absolute conc</i> ↑ = 0.17±0.05 μmol/g  <b>(all mean ± s.e.m)</b>	Summing over all rest/activation spectra. Cr conc = 8 μmol/g assumed for scaling metabolite concs from LCModel
<b>Bednařík et al. (2015)</b>	7T, semi-LASER	15 healthy subjects (8F, 33±13 years)  <b>(all mean ± s.d)</b>	5000/26	Red-black checkerboard stimulus (REST-STIM-REST-STIM-REST), black rest screen. Button press attention task - changing orientation of fixation cross	(n=12)  <i>Difference</i> [STIM-REST] no linewidth correction ↑ = 30%  After linewidth correction ↑ = 29.6%	(n=12)  <i>Baseline</i> = 1.01±0.07 μmol/g <i>Difference</i> [STIM-REST] (no linewidth correction) = 0.26±0.06 μmol/g  (After linewidth correction) = 0.26±0.06 μmol/g	From second half of period. Unsuppressed water as reference, assume 80% brain water and 9% CSF fractions in voxel. Also approx. corrected for relaxation effects.

						<b>(all mean ± s.e.m)</b>	
<b>Boillat, et al. (2020)</b>	7T, Siemens, SPECIAL	Two groups:	7500/16	<i>Positive BOLD</i> - full screen radial checkerboard, flickering at 3.3Hz	<i>Positive BOLD</i> ↑ = 20.79±27.48	<i>Positive BOLD</i> Baseline = 0.70±0.06 μmol/g	Unsuppressed water spectra used as reference.
		<i>Positive BOLD stimulus</i> - 20 subjects (5F, 21.9±1.3 years old)				<i>Negative BOLD</i> ↓ = 8.84±22.03	
		<i>Negative BOLD stimulus</i> - 21 subjects (10F, 22±3.8 years old)		<i>Negative BOLD</i> - small central checkerboard, flickering at 3.3Hz	<b>(all mean ± s.d.)</b>	<i>Negative BOLD</i> Baseline = 0.67±0.05 μmol/g	
				(REST-STIM-REST-STIM-REST)		↓ = 0.07±0.09 μmol/g	
						<b>(all mean ± s.d.)</b>	

---

Several physiological changes can result in rapidly increased Lac concentrations, including in those closely associated with neurodegeneration and limited blood flow, such as ischemic stroke (Henriksen et al., 1992). Transient physiological changes of slight hypoxia and hyperventilation (Siesjö, 1978) can also result in rapidly and significantly increased Lac concentrations (Harris et al., 2013; Anderson et al., 2013), and therefore concentration changes must be interpreted with caution. Interestingly, exogenous supplementation of Lac has also been evidenced after traumatic brain injury, suggesting it has potential as a beneficial therapeutic approach for the sparing of cerebral glucose (Bouzat et al., 2014). As such, there may also be potential for its supplementation in instances of neurodegenerative damage, such as Alzheimer's disease, in order to mitigate the decrease in glucose availability (Cunnane et al., 2020).

Most functional MRS studies of Lac in healthy brain tissue exploit short TE sequences (Schaller et al., 2014; Bednařík et al., 2015; Boillat et al., 2020), which reduce the amount of signal lost via transverse relaxation mechanisms. Unfortunately, this approach complicates accurate identification and measurement of Lac, given the overlap of its resonances with signals of higher amplitude, such as the macromolecules (MM) found at 0.89, 1.20 and 1.37ppm, respectively. Whilst attempts are made to account for the different contributions of Lac and these MM by merit of linear fitting of the model spectra, the robustness of these fits may depend on incomplete *a priori* knowledge of the degrees of freedom of the macromolecular profile – this can result in the mis-classification of these resonances as part of a noisy baseline, and can lead to over- or under-estimation of the resonances of interest, by merit of the fitting being altered incorrectly elsewhere. Additionally, inter-

subject variability in the distinct macromolecular components may not be sufficiently accounted for if spectral quantification employs a generalised measure of the macromolecular profile – an example of this can be found in the work of Schaller et al. (2014), who show that whilst general profiling of MM can accurately identify most metabolites, significant differences in the level of Lac was evidenced when acquiring spectra from tissue that is rich in white and grey matter using a Lac-specific profile for control of MM. Such a Lac-specific approach is imperative to ensure correct characterisation of metabolic time courses, given that the absolute concentration changes in Lac metabolism seen under conditions of neuronal stimulation are relatively small.

Exploitation of j-coupling effects (see Chapter 2) can help to resolve the Lac signal from the overlapping resonances – allowing the associated j-modulation to evolve, through use of a longer TE, will result in an inverted doublet signal, making Lac more visible within the spectrum. Using a longer TE for acquisition is also a promising approach which has been shown to be feasible in previous fMRS studies (Bednařík et al., 2016; Fernandes et al., 2020). Whilst this does limit the number of metabolites measurable in the resulting spectra, using TE = 144ms results in inversion of the Lac doublet at 1.31ppm, thereby also reducing the intensity of contaminant macromolecular and lipid signals, and making the small Lac peak easier to identify. This is imperative for correct metabolic characterisation throughout the time course, as this peak remains small, even during intense neuronal stimulation. Additionally, employing such approaches when investigating healthy subjects of older age is also critical, given the lack of previous investigation into fMRS measures of Lac metabolism under visual stimulation at 7T within this age group.

Investigation of such a challenging metabolite requires use of a specialised sequence. The semi-LASER sequence – with intermediate-long echo time specific to the temporal behaviour of Lac – is ideal. This sequence is discussed at length in Chapter 2, with the pulse sequence design optimised with use of paired AFP pulses (Garwood and DelaBarre, 2001). It is ideal for accurate identification of Lac, as it is less susceptible to instabilities within the MR system, and subject motion, which is particularly important in the investigation of older subjects, or those unfamiliar with the MR environment. Few published studies have been based on protocols optimised for Lac as described, however previous work recently achieved reliable serial quantification of cerebral Lac using an optimised functional MRS protocol in healthy subjects at 7T, with optimised TE and custom basis set (Fernandes et al., 2020). This protocol has only been used for the investigation of cerebral metabolism in young adults thus far, however it may provide valuable information for the study of neuroenergetics and metabolic reprogramming in the ageing brain.

This work aimed to investigate the effects of age on the temporal behaviour and quantify best-estimate absolute concentrations of Lac during visual stimulation in young healthy subjects compared with healthy subjects of older age, by employing optimised J-modulation selection using the semi-LASER sequence (Scheenen et al., 2008). This could lead to a greater understanding of the changes in the concentration of key metabolites and their role during neuronal activation, relative to age. It was hypothesised that age-related metabolic reprogramming would result in elevated cerebral Lac levels at baseline, with age-related impairments in brain energy metabolism resulting in altered stimulus-induced changes in Lac time courses in older healthy

subjects when compared with young healthy subjects. Specifically, it was hypothesised that the time course dynamics of older subjects would be characterised by a smaller increase in cerebral Lac at onset of stimulus, and a slower return to baseline after cessation of stimulus, when compared to young subjects.

## 5.2. Ethical approval and funding information

All data acquired for use within this chapter were granted ethical approval under one of two studies – MET-AGE (Metabolic Brain Ageing) and MET-AGEd (Dynamic cerebral energy metabolism in healthy older individuals: a  $^1\text{H}$ -fMRS study at 7T). Both were given ethical approval by the University of Nottingham Medicine and Health Sciences Research Ethics Committee (MET-AGE Ref: H14082014/42; MET-AGEd Ref: 1-1804 (part of umbrella ethics Ref: 162-1711)) and funded by a combination of PhD studentship allocation from the School of Medicine at the University of Nottingham, and Life Cycle 5.

## 5.3. Protocol development

### 5.3.1. Introduction

As previously mentioned, the echo time chosen for the investigation of Lac metabolism using semi-LASER at 7T is affected by other metabolites and j-coupling behaviours, and therefore selection of an appropriate TE is critical. Whilst previous work carried out at Nottingham (Fernandes et al., 2020) utilised a TE of 144ms, it was important to assess other TEs, in order to visualise the changes in j-coupling behaviours as a factor of TE. It was also pertinent to investigate the potential of a TE of 288ms to achieve the flattest baseline possible and improve peak identification, as this has been used when

employing a STEAM sequence (Frahm, Merboldt and Hänicke, 1987), as the chemical shift artefact is well controlled (Fernandes et al., 2021). This protocol development study was carried out in a phantom, and then *in vivo* in six subjects, with the aim of determining the best protocol for further *in vivo* investigation.

### 5.3.2. Echo time investigations

#### 5.3.2.1. Methods

A spherical phantom was constructed containing concentrations of metabolites similar to that of the human brain (derived from Govindaraju, Young and Maudsley, 2000; see *Figure 5.3.1.*). The phantom contained 10 mM NAA, 8 mM Cr, 3 mM choline (Cho), 1 mM Lac, 72 mM disodium phosphate ( $\text{Na}_2\text{HPO}_4$ ), 200 mM buffer solution (sodium formate), 6 mM mlns, 10 mM Glu, 5 mM Gln, 2 mM DSS, 28 mM monosodium phosphate ( $\text{NaH}_2\text{PO}_4$ ), and 1 g/l sodium azide ( $\text{NaN}_3$ ).



**Figure 5.3.1.:** Phantom used for investigation of possible echo times for semi-LASER investigation of Lac at 7T.

Four phantom MR acquisition sessions were carried out using a Philips Achieva 7T MR system (Philips Healthcare, Best, The Netherlands), a 32-channel head coil (Nova Medical, Wilmington, Massachusetts, USA) and volume transmit coil (Nova Medical) with maximum transmit  $B_1$  field of 20  $\mu$ T. The phantom was placed in the head coil, secured with foam pads, to prevent its movement during scanning. A VOI measuring 20 x 30 x 20 mm<sup>3</sup> was positioned within the phantom, avoiding the air bubble. Spectra were acquired using the semi-LASER sequence, with number of signal averages (NSA)=64 and TEs between 40 - 320ms – at intervals of 20ms – as well as 144 and 288ms, to assess the evolution of the j-coupling and the inversion of the Lac peak.

#### *5.3.2.2. Analysis*

Analysis was carried out using jMRUI v 5.2 (Naressi et al., 2001; Stefan et al., 2009) on the full spectrum. Spectra were zero filled for optimal visualisation of the peaks, as the intention of this analysis was to visually assess the evolutionary behaviour of the peak of interest, and baseline differences between 144 and 288ms TE. LCModel (Provencher, 1993) was also used for visualisation of the spectral fit at each TE.

#### *5.3.2.3. Results*

This phantom investigation of j-coupling evolution by merit of TE evidenced that the most suitable echo time using semi-LASER at 7T is 144ms (*Figure 5.3.2.*). The Lac doublet was measured at intervals of 20ms, between 40 and

320ms, and the evolution in doublet shape as a result of the interaction between j-coupling and echo time is shown below in *Figure 5.3.3.*

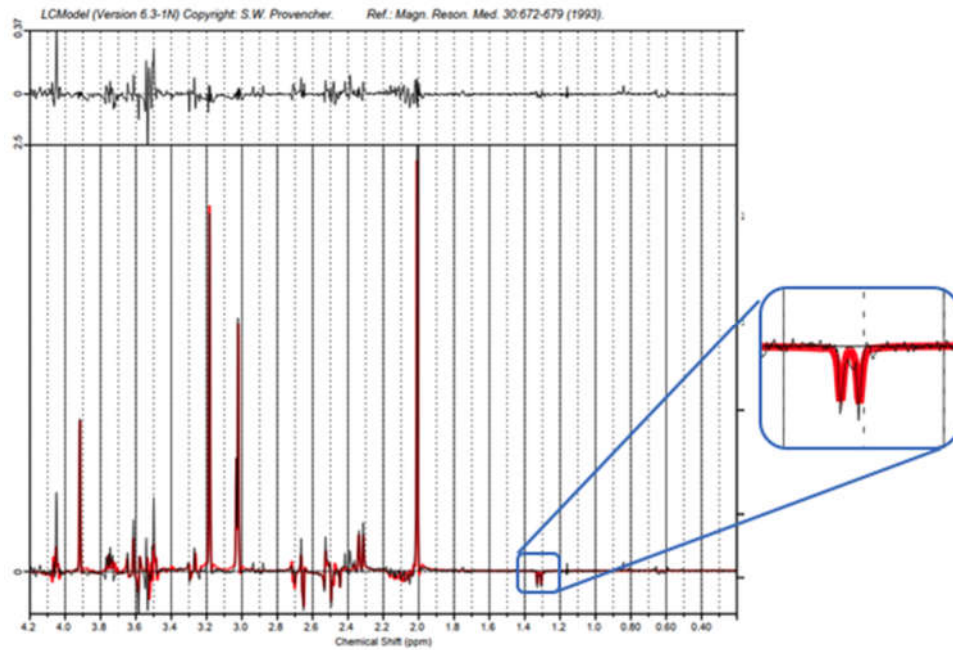


**Figure 5.3.2.:** LCMoDel fit of the Lac doublet in a phantom of the brain, using semi-LASER acquisition with 144ms TE, and 64 NSAs.

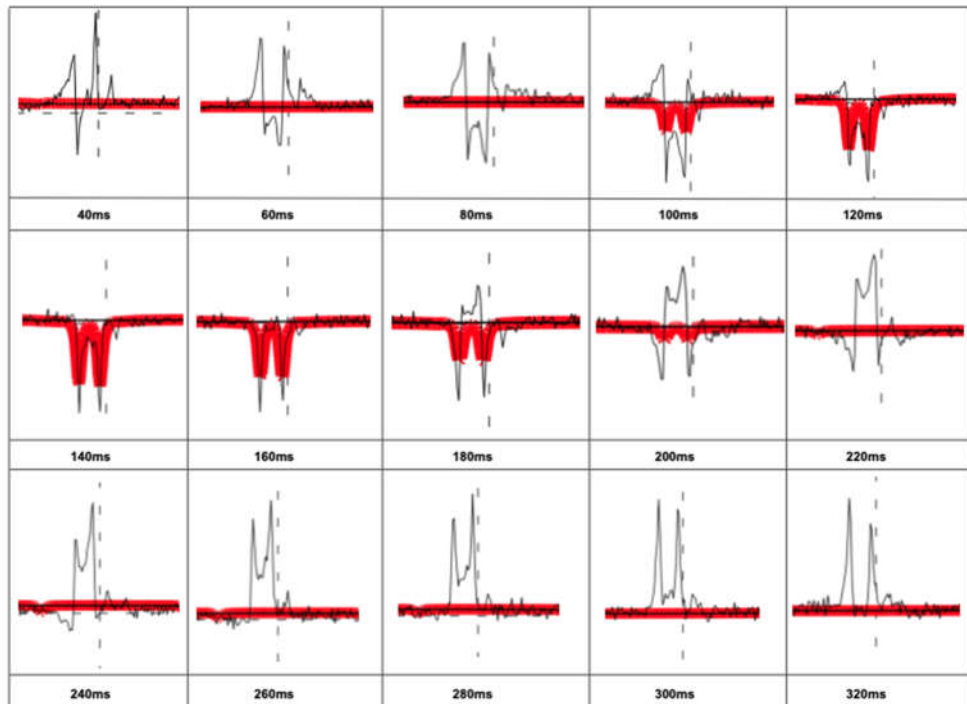
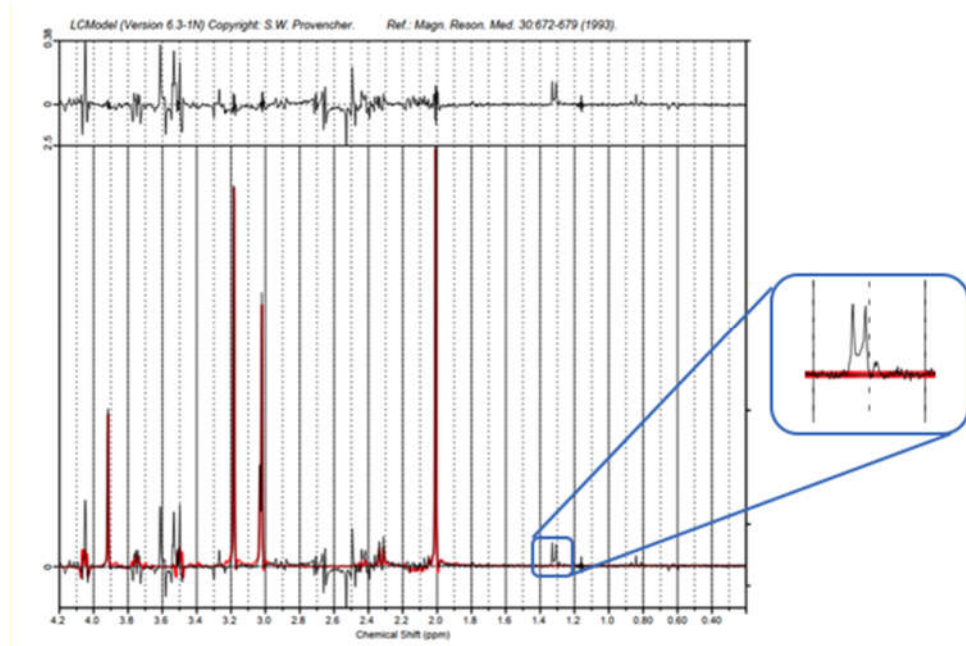


**Figure 5.3.3.:** Evolution of the Lac doublet by merit of echo time during phantom investigation with semi-LASER acquisition. LCMoDel fit is seen in red, and the vertical dashed line is at 1.3 ppm.

Whilst a TE of 288ms resulted in an easily visible Lac doublet at 1.31 ppm, due to the flattening of other metabolites by merit of a long echo time, the resultant LCMoDel fitting was poor (see *Figure 5.3.4.a* below). Investigation of TE=40ms also resulted in a poor-quality fit, with the Lac doublet not identifiable within the fit (*Figure 5.3.4.b*).

A)



B)

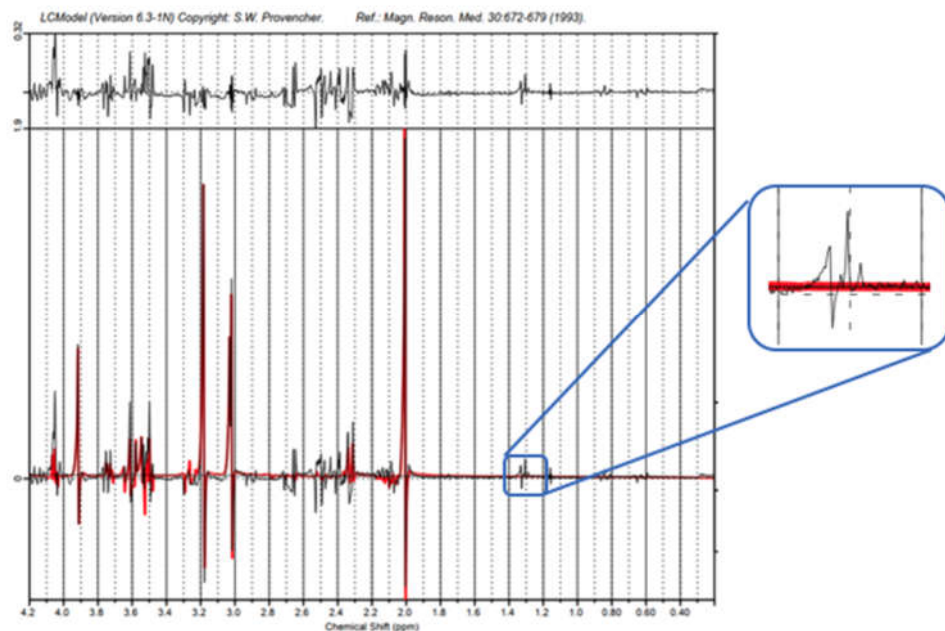


**Figure 5.3.4.:** Example outputs with TE of 288ms (A) and 40ms (B), in a phantom of the human brain, using semi-LASER acquisition at 7T. LCMoDel fits for both are shown in red.

#### 5.3.2.4. Discussion

A variety of different TEs were assessed in a phantom of a composition similar to that of the human brain using a combination of jMRUI and LCModel. Whilst certain TEs between 100 - 180ms show a partial fit to the Lac doublet, 144ms remains the TE with the tightest fit to the measured Lac peak, and thus the most suitable for further investigation.

As can be seen in *Figure 5.3.1.*, the phantom was constructed in such a way that there was an air bubble within it. Such air bubbles can sometimes result in issues with field homogeneity; however, this was not seen in this study. Voxel positioning within the phantom also carefully avoided the air bubble, and as such this was not an issue within this investigation, although is theoretically best avoided for the aforementioned potential problems.

#### 5.3.2.5. Conclusions

The results of this phantom investigation of various echo times confirmed the necessity to continue with the use of a 144ms echo time for subsequent *in vivo* studies.

### 5.3.3. Initial human studies

Given the low concentration of Lac within the brain, combined with the use of <sup>1</sup>H-fMRS, acquisition of spectra in human participants can be challenging, and thus may necessitate modification to acquisition strategies to address these difficulties. Such theoretical issues are discussed at length within this section, and practical solutions for improvement discussed and trialled.

### 5.3.3.1. Introduction

Theoretically, there are various issues which can arise during  $^1\text{H}$ -fMRS acquisition at ultra-high field strength. For example,  $B_1$  inhomogeneity can generate interference effects, given the wavelength at 7T is  $\sim 20\text{cm}$  at most ( $\sim 11\text{cm}$  in tissue), and therefore the same order of dimension as the object being imaged. This results in constructive and destructive interference patterns, which can be seen in MR images as darkened areas of signal dropout. In the brain, these can often be seen within the visual cortex, and is thus of concern to this investigation, given the necessity to position the VOI within this region.  $B_1$  homogeneity and spectral quality can be improved by the use of dielectric pads, which contain material which has a high dielectric constant (Webb, 2011; *Figure 5.3.5.*). In neuroimaging, these pads are positioned between the receive coil and the head, relative to anticipated or exhibited regions of signal dropout. Use of these pads augments the applied  $B_1$  field by creation of a secondary local RF field and can also improve geometry-related RF inhomogeneity effects (Sled and Pike, 1998). As such, use of these pads may improve spectral acquisition on a case-by-case basis.



**Figure 5.3.5.:** Calcium titanate dielectric pads, which were placed strategically on the sides of the head.

Alongside the use of such additional hardware, theoretical considerations may improve spectral quality. The choice of an appropriate shim strategy, as well as alteration of gradient direction can also be critical to the successful acquisition of an fMRS spectrum. A second-order shim approach was taken within this study, whereby spherical harmonics were fitted to best describe the magnetic field profile within the VOI. This causes a greatly diverging profile outside the voxel, which can sometimes be so divergent that it returns remote regions to resonance, an effect known as frequency folding. This can result in an associated artefact, which is thought to be a stimulated echo from water in other areas of the head such as the mouth or throat. Other shim strategies are possible, including restricting it to first-order shims and decreasing the size of the voxel. However, first-order shimming can only correct a linear field variation, and whilst this is far less likely to cause frequency folding, there is a higher risk of a poor shim, due to inadequate correction of the magnetic field. Decreasing the voxel size creates a smaller shim box, thereby reducing the number of points used for spherical harmonics, resulting in greater divergence. As such, an alternative approach was proposed for any such occurrences.

The alteration of gradient directions can also address this frequency folding, hopefully avoiding water from the mouth and throat area. This involves alteration of the position of the Lac voxel and associated water voxel, relative to each other. Standard positioning is such that it avoids pericranial fat and the ventricles of the brain, and this needs to be maintained when this change in gradient direction is selected. This is summarised in *Figure 5.3.6.* below.

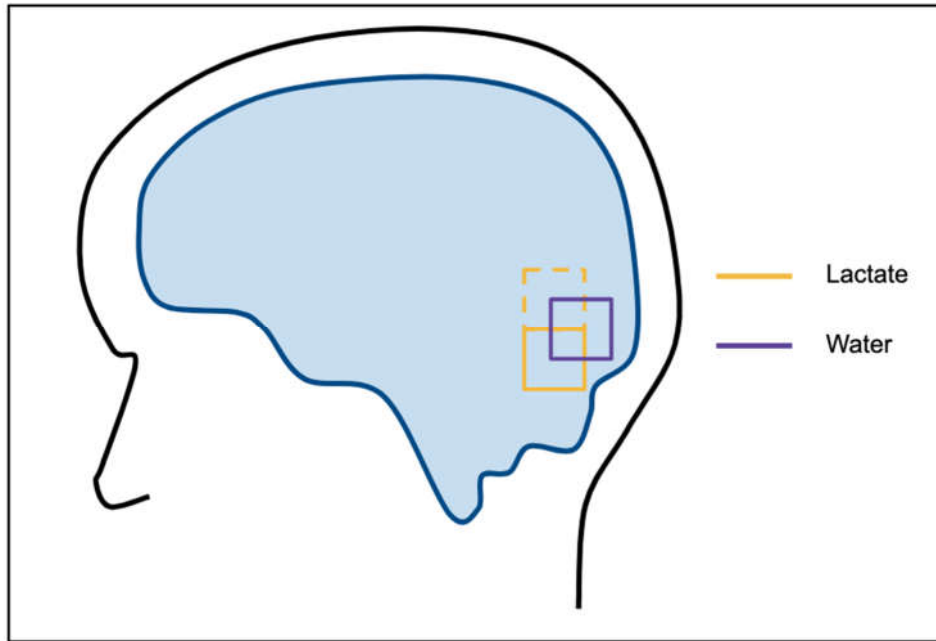


**Figure 5.3.6.:** Schematic of possible voxel positioning strategies. The shifted water voxel is represented by the purple outline, and the Lac voxel by the yellow outline. The solid yellow outline is the standard Lac positioning within the visual cortex, and the dashed yellow outline represents the proposed voxel positioning for Lac, thereby altering the gradient directions and their recombination.

Younger subjects are also known to tolerate the 7T scanner environment and the flashing checkerboard protocol, as this cohort and visual stimulus has been previously investigated at the University of Nottingham (Fernandes et al., 2020). However, older subjects are less often investigated at this field strength in Nottingham, and thus it was imperative that a representative member of this age group was invited to provide opinions as to their ability to tolerate this environment and stimulus.

In summary, this *in vivo* investigation aimed to assess the use of the protocol confirmed through phantom investigation within a group of subjects, with a focus on visual assessment of data quality, and potential theoretical issues which may need to be addressed in the main study. It was hypothesised that the spectra provided by young subjects would be of good visual quality, with a

readily identifiable and well-fitted Lac peak. However, whilst it was also hypothesised that the Lac peak would be identifiable in the older cohort, it was unclear how well the protocol would be tolerated in this group and as such this was also addressed in this *in vivo* trial study.

#### 5.3.3.2. Methods

The findings of the phantom work and the strategies described in Section 5.3.3.1. (where possible or required) were trialled in five young subjects (3M:2F, age range = 23-33 years, mean age = 27.2 years, SD = 3.633), without history of neurological disorders. Additionally, an older subject (69F) was tested, predominantly to assess tolerance of the 7T scanner environment in older subjects. This study was approved by the University of Nottingham Medical School Ethics Committee, and informed consent was also obtained from each subject prior to MR examination, in accordance with the Declaration of Helsinki.

MR acquisition was carried out using the same hardware setup as employed for the phantom investigations, with subjects provided with ear plugs and movement minimised by positioning foam pads on either side of the head within the head coil. An initial fMRI localiser (multi-slice echo-planar imaging [EPI], TR/TE = 2000/25ms, spatial resolution = 2 x 2 x 3mm<sup>3</sup>, 30 slices), was carried out to assist with positioning of the fMRS VOI (20 x 30 x 20 mm<sup>3</sup>) within activated areas of the visual cortex. A black and white checkerboard, flickering at 8Hz, was used as the visual stimulus, with a button response task employed and monitored on a computer screen in the control room, to ensure subject attention (*Figure 5.3.7.*). The activation paradigm consisted of 50

seconds of stimulation, followed by 10 seconds of rest, repeated three times (*Figure 5.3.8.*). MP-RAGE images (TR/TE = 7/3ms, 1mm<sup>3</sup> of isotropic resolution) were acquired for high-resolution anatomical confirmation of spectroscopic voxel positioning, verifying that the VOIs pertaining to water (4.7 ppm) and Lac (1.31 ppm) fit completely within the visual cortex.

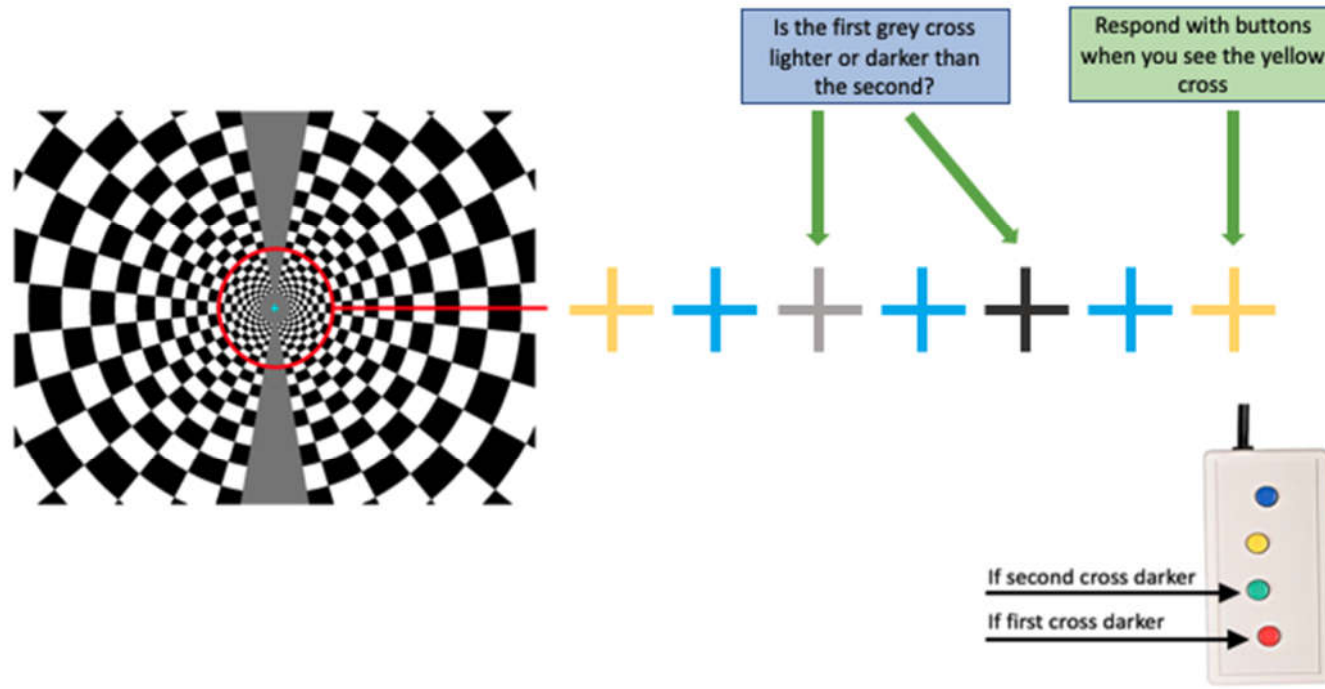


**Figure 5.3.7:** Flashing (8Hz) checkerboard used for visual stimulation during fMRS measurement of lactate. Subjects were also provided with response buttons to carry out a judgement task, to maintain subject attention.

Subsequent fMRS measures utilised the same stimulus as previously mentioned, with a 5-minute baseline measurement (OFF period, viewing a grey screen), followed by a test period of 15 minutes of stimulation, and 10 minutes of recovery. The ON period consisted of 50 seconds of stimulation, with a short 10 second resting block, repeated 15 times (*Figure 5.3.8.*). The short rest blocks were included to keep the attention of the subjects and minimise their adaptation to the stimulus.

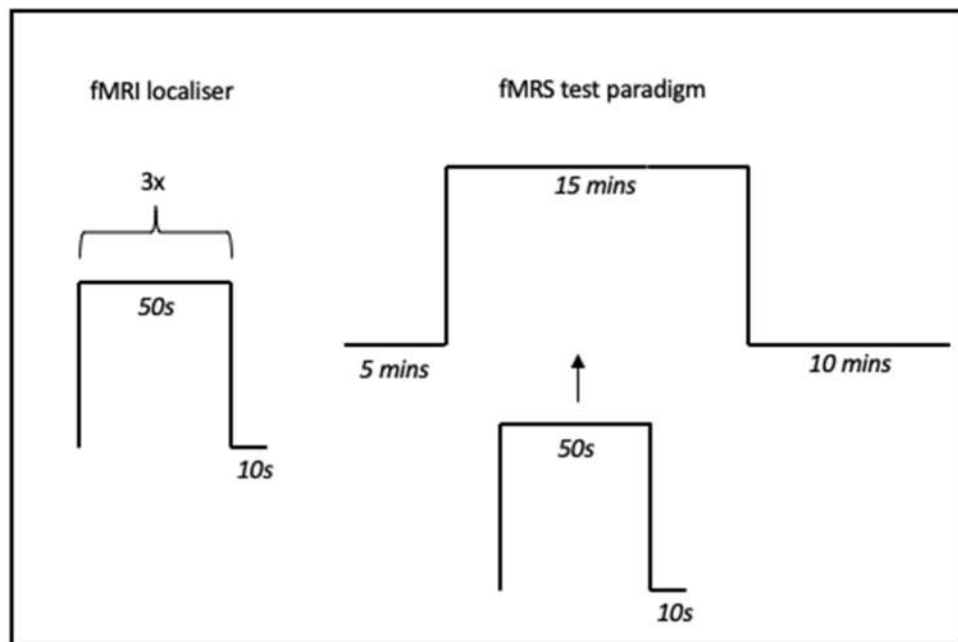


**Figure 5.3.8.:** Summary of timings used in testing of the fMRI localiser and fMRS testing paradigm.

$^1\text{H}$  MRS data were continuously acquired using a semi-LASER sequence (Scheenen et al., 2008), comprising of an adiabatic excitation pulse (bandwidth = 5372 Hz) and two pairs of AFP pulses for refocusing (bandwidths = 5424 Hz), with TR/TE = 5000/144ms. Suppression of the water resonance was performed using the variable power and optimized relaxation

delays scheme (VAPOR, Tkáč et al., 1999) scheme, with unsuppressed water spectra obtained prior to each scan. Shimming was applied, covering both water and Lac VOIs, using a second-order pencil-beam routine based on fast, automatic shimming by mapping along projections (FASTMAP, Gruetter, 1993). In order to achieve the most optimal conditions for measurement of Lac, a regional saturation technique (REST, Haase, 1986) was also employed, to minimise contaminant signal from the pericranial fat. The signal from this fat is suppressed preceding spectral acquisition with two such outer volume suppression (OVS) modules, or REST slabs, which apply a slice-selective pulse and crusher gradients in order to suppress this signal (*Figure 5.3.9.*).

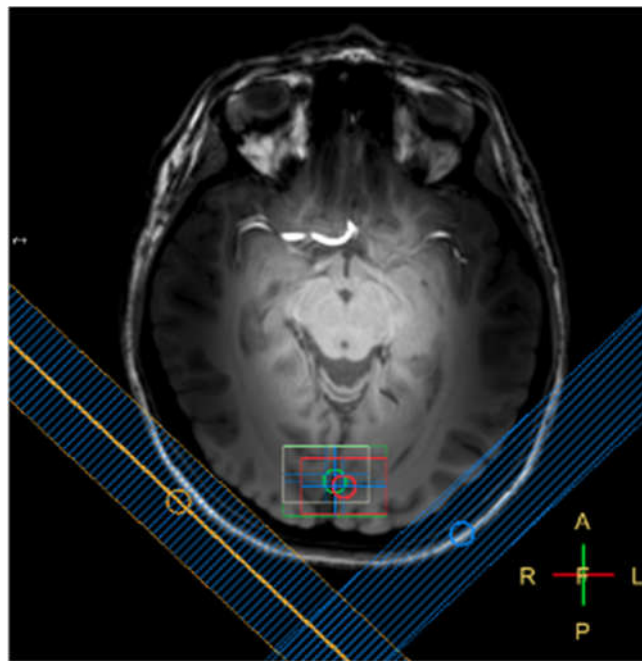


**Figure 5.3.9.** Outer volume suppression (OVS) modules shown in blue during set-up for acquisition of a spectrum in a 28-year-old female test subject.

#### 5.3.3.3. Analysis

The fMRS data independently acquired from each of the 32 channels were optimally combined and reconstructed using a method based on that of Hall et

al. (2014). Initial processing was carried out in MATLAB version 9.4.0. R2018a (The Mathworks Inc, Natick, Massachusetts, USA), with data aligned to the NAA singlet peak at 2.01 ppm, phase-corrected in MATLAB, and averaged across all NSAs.

LCModel (Provencher, 1993) was used for the quantification of all spectra over the 0.2 to 4.2 ppm range, with a basis set comprised of 19 metabolites: Asp, Cho, Cr, GABA, Glc, Glu, Gln, GSH, glycerophosphocholine (GPC), glycine (Gly), Lac, mIns, NAA, NAAG, phosphocholine (PCho), PCr, phosphorylethanolamine (PE), scyllo-inositol, and Tau. This basis set was simulated using Versatile Simulation, Pulses, and Analysis (VESPA) software (Soher et al., 2011), and for NAA, PCr and Cr, the methyl and methylene groups were separately included in the basis set, to account for differing transverse relaxation times (Marjańska et al., 2012). Residual MM resonances were simulated in MATLAB, as Lorentzian peaks of 3Hz linewidth – these were identified at 0.89 ppm (MM1), 1.20 ppm (MM2) and 1.37 ppm (MM3). Additionally, the node spacing of the spline function was set as 4ppm, to achieve tighter and flatter baseline fitting, given the full relaxation of most MM and lipid signals at an echo time of 144ms. The pilot analysis pipeline is summarised in *Figure 5.3.10*. below. Additional statistical analysis was carried out using GraphPad Prism 8.3.1 for Windows (GraphPad Software, La Jolla California, USA), and SNR and full-width at half maximum (FWHM) calculated in MATLAB using the NAA singlet peak at 2.01ppm and the water peak, respectively.

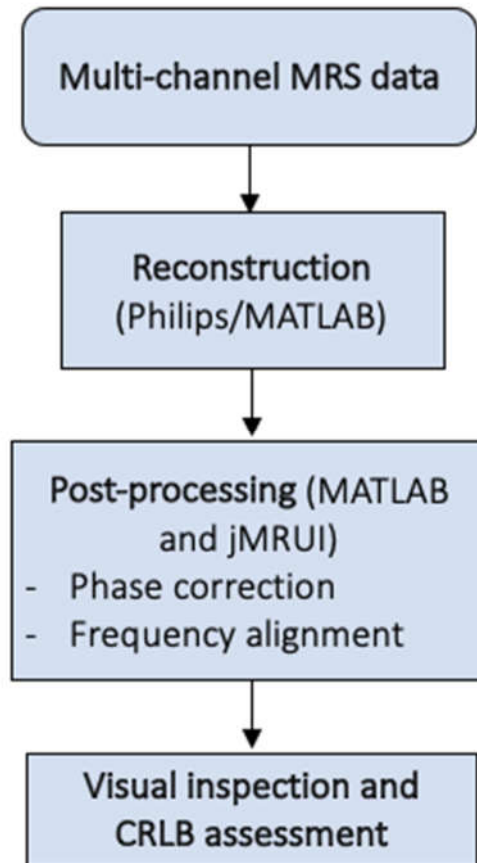


**Figure 5.3.10.:** Summary of the analysis pipeline for the pilot study.

#### 5.3.3.4. Results

##### **General findings**

Good-quality spectra – averaged across the full time course – were successfully acquired over 360 NSA in four of the young subjects (2M:2F, age range = 23 - 27 years, mean age = 25.75 years [SD = 1.893]). In these subjects, visual inspection found well-fitted Lac peaks – when quantified, CRLBs of Lac ranged from 10-21% (mean = 15% [SD = 4.967]). Average SNR of the NAA singlet within these spectra was 136.42, although this varied substantially between subjects (range = 102.1-200.6, SD=45.3, SEM=22.6).

FWHM was measured using the water peak, with a mean value of 12.6Hz (SD=1.1, SEM=0.5).

Good quality spectra were not successfully acquired in the 33-year-old male and 69-year-old female subjects, however both subjects are discussed at length in subsequent sections.

### **Use of dielectric pads for improving B<sub>1</sub> homogeneity**

A 33-year-old male test subject provided an opportunity to trial dielectric pad use, and his spectral outputs are shown in *Figure 5.3.11*.. Acquisition of his first spectrum (a) was stopped after 120 NSAs (~10 mins, 5 mins of rest and 5 mins of stimulation), due to the poor quality shown in the live monitoring, and then restarted and acquired for the same duration (b), with the addition of dielectric pads by the side of the head.

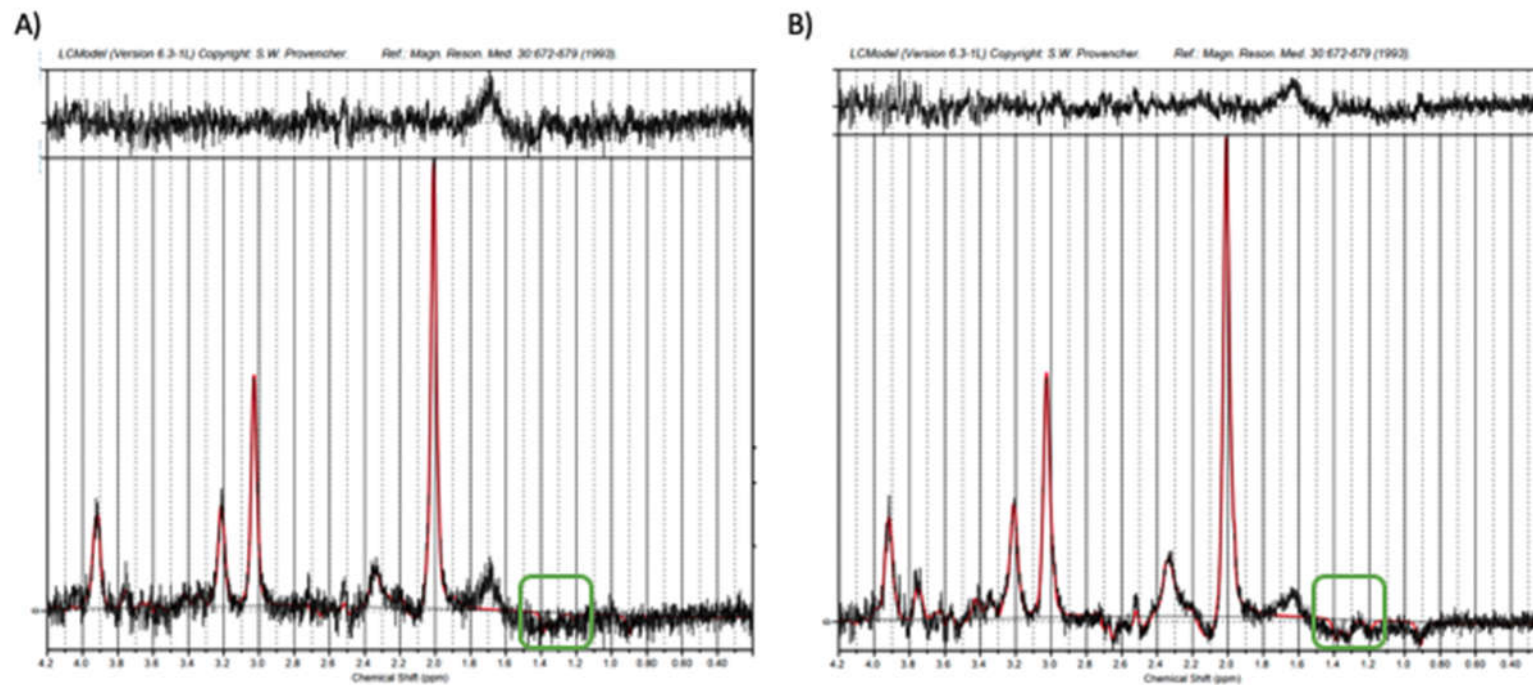


**Figure 5.3.11.:** LCMoDel fit in a representative participant (33-year-old male) with acquisition parameters of  $TE/TR/NSA = 144\text{ms}/5000\text{ms}/120$ , (A) without using dielectric pads and (B) using dielectric pads. The initial and improved fits of the Lac peak (at 1.31 ppm) are highlighted in green. The associated CRLBs of Lac were 15% without dielectric pads, and 10% when they were used.

The fit of Lac, as measured using CRLB, improved with use of dielectric pads, from 15% without dielectric pads, to 10% with the pads. Additionally, visual inspection shows an improved fit around the Lac peak, with dielectric pad use.

### **Changing voxel positioning**

Alteration of voxel positioning for the improvement of spectral quality was assessed in the same 33-year-old male during a different scanning session. The fit of Lac, as assessed using CRLBs, improved from 999% (considered not present in the spectrum and evidencing unreliable LCModel processing) when using the original voxel orientation, to 14% with altered voxel positioning (as per *Figure 5.3.12.*). 360 NSAs were acquired with original orientation and this acquisition followed the full described protocol, but only 64 NSAs of rest were acquired for comparison due to time constraints of the scanning session.

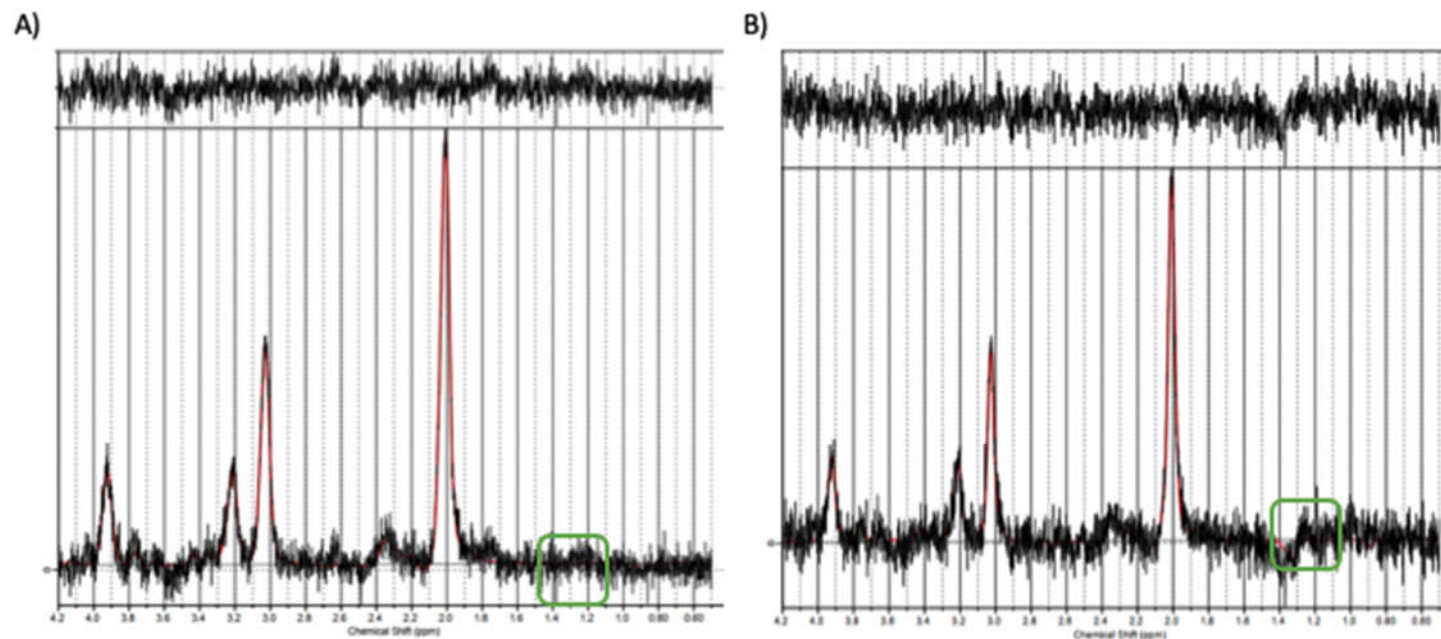


**Figure 5.3.12.:** Spectra acquired (a) before and (b) after changing the orientation of the Lac voxel in a 33-year-old male subject. Spectrum (a) was acquired with NSA = 360, whereas spectrum (b) was acquired with NSA = 64, due to time constraints of the scanning session.

### **Spectral artefacts**

A 69 year-old female test subject exhibited the artefact discussed in Section 5.3.3.1., thought to result from frequency folding due to the chosen second-order shim strategy. As shown in the associated LCModel output (*Figure 5.3.13.*), this artefact occurs around 4.2 - 3.5 ppm. This artefact was not evident during live monitoring, and the subject was unable to return to the Centre for a follow-up scan to trial alternative ordering of gradient application to avoid frequency folding, as discussed in the aforementioned section. As such, they were excluded from any further analysis, but if any subjects in the main study exhibited this artefact in live monitoring the scan would be stopped and restarted with changed gradient orientation. If the artefact was only evident at the analysis stage, they would be invited to be rescanned.

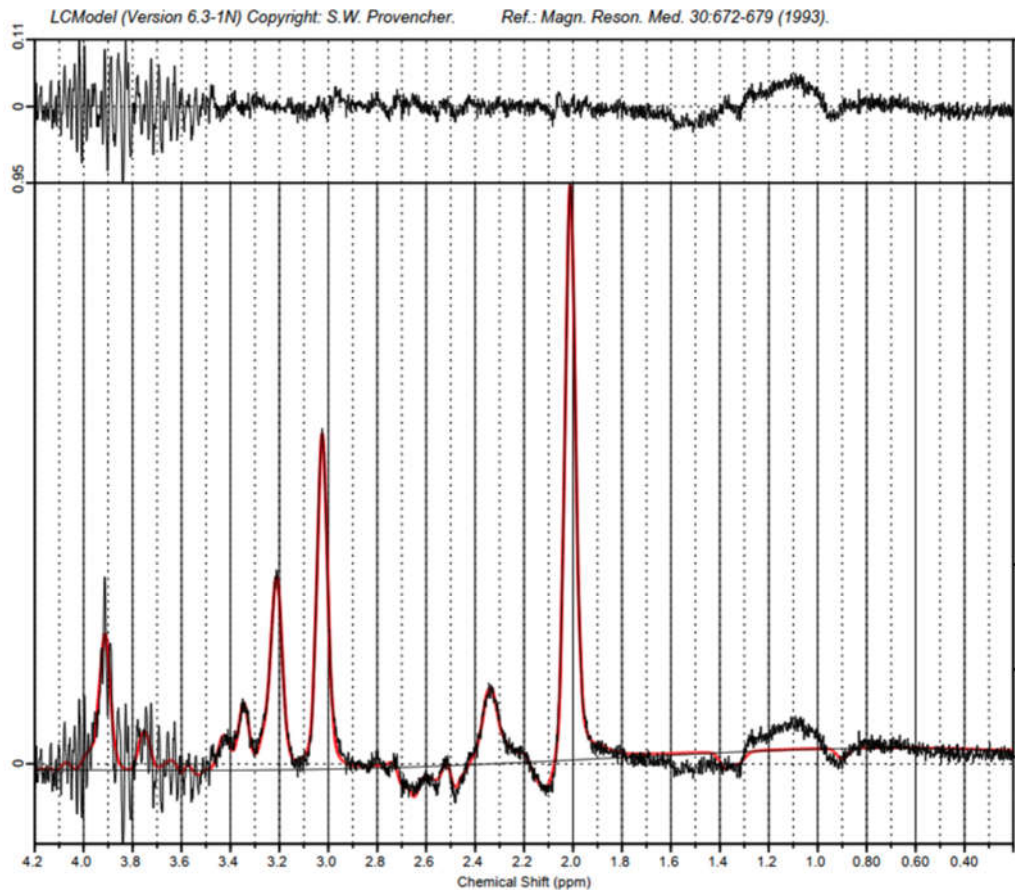


**Figure 5.3.13.:** Representative example of a spectral artefact seen in a 69-year-old female test subject between 4.2 - 3.5 ppm.

### **Tolerance of 7T scanner environment and visual stimulation protocol in an example older subject**

Tolerance of older subjects in the 7T scanner environment was an important consideration for the study protocol. A 69-year-old female was invited to discuss the experience with the research team, and highlighted several key points, which were of great importance going forwards. Whilst she found the scanning experience to be generally tolerable, she highlighted the need to carry out slower explanations of the protocol, and allocate additional time for familiarisation with the surrounding environment. She mentioned that MRI may be more unfamiliar to subjects in her age group, and as such they may have

more general queries about the technology, and that time should be provided to answer these, thereby making the participant feel more at ease. She did mention that the visual stimulus may be quite intense for some older subjects, although she found it tolerable, and helpful in keeping her awake when surrounded by the rhythmic sounds of the MRI scanner. She also highlighted possible claustrophobia concerns, however these are something which is considered for all possible MRI subjects as standard.

#### *5.3.3.5. Discussion*

Trial investigation of fMRS at 7T in six human subjects provided great insight as to the technical challenges of such acquisition. In four healthy young subjects, good-quality spectra were acquired as expected, assessed through visual assessment of peak fit and associated CRLBs. The resultant spectra varied greatly with regards to both CRLBs of Lac and SNR, highlighting the possible variance within the young cohort, and the possible complexity of the main study. In two subjects, acquisition did not go as planned but provided opportunity for further investigation and theoretical discussion.

Dielectric pads were tested in one subject where the potential for a gain in spectral quality was most evident. Whilst there was some improvement in fit when using dielectric pads (CRLB of Lac = 10%) compared with not using them (CRLB of Lac = 15%), this approach does not necessarily improve the quality of the spectrum enough for fMRS analysis, given that this necessitates high spectral quality, as spectra are averaged over fewer NSAs, rather than the full duration of the fMRS acquisition. Indeed, this subject did not pass visual assessment of Lac peak fit, even after using the dielectric pads.

Theoretically, the best shim strategy is already being employed. However, as shown in *Figure 5.3.13.*, this can still cause frequency folding, which can contaminate the part of the spectrum which is of interest, thereby making it unusable in further analysis. As evidenced in this can also occur at a ppm which is irrelevant to the study question and peak of interest, and thus the impact of the artefact can vary on a case-by-case basis. Unfortunately, the proposed strategy to mitigate this issue could not be trialled on the one subject whose spectrum showed this issue during *in vivo* testing, as it was only evident at the point of analysis, and the subject was unable to attend the MRI Centre again at a later date for further investigation. It was trialled on the 33-year-old male subject and showed improvement in spectral quality as measured with CRLBs but did not improve visual identification and assessment of the Lac peak.

#### *5.3.3.6. Implications for in vivo work*

The results of both the phantom and *in vivo* protocol development lead to the proposal of the optimal strategy for investigation of Lac at 7T, going forwards. Analysis of phantom data confirmed that an echo time of 144ms remained the most favourable for investigation of Lac at 7T, using the sLASER sequence. The pilot in-vivo work also highlighted the potential necessity for use of dielectric pads on a case-by-case basis, as well as a similar approach to a change in orientation of the voxel of interest if required. Ultimately, it is recommended that live data monitoring is employed throughout, to assess if there is a need to restart the scan with any of these strategies in place. Additionally, the 69-year-old female subject also provided great insight as to the experience of an older participant being scanned in an unfamiliar 7T environment, and these considerations were taken forwards by all team

members and employed when interacting with the older cohort in the main *in vivo* study.

#### 5.4. Assessing cerebral lactate concentrations *in vivo*

##### 5.4.1. MRI measurements

Six healthy young subjects (3M:3F; average age = 26.0 years old, range 22 - 32 years, SD = 3.5) and six healthy older (>60 years) subjects (2M:4F; average age 68.3 years old, range 63 - 75 years, SD = 5.9) without history of neurological disorders participated in this study, which was approved by the University of Nottingham Medical School Ethics Committee. Informed consent was also obtained prior to MR examination, in accordance with the Declaration of Helsinki.

MR acquisition used the same 7T MR system and 32-channel head coil as previously discussed. The scanning protocol was near-identical to that used in the *in vivo* trial subjects, with voxel positioning employing the same strategy as described in Section 5.3.3.2. and use of an identical visual stimulus (*Figure 5.3.7.*) and associated stimulus timings (*Figure 5.3.8.*), but with the addition of dynamic fMRS time course investigation. <sup>1</sup>H MRS data were continuously acquired using the semi-LASER sequence (Oz and Tkáč, 2011), with VAPOR water suppression (Tkáč et al. 1999), FASTMAP shimming (Gruetter, 1993) and use of REST slabs (Haase, 1986), as previously described in Section 5.3.3.2..

#### 5.4.2. Implementation of protocol development findings

The results of protocol development were implemented throughout the main study, with regards to TE. Whilst the intention was to take a case-by-case approach with regards to further adjustments that may be taken – as summarised in Section 5.3.3. – these were unnecessary for the subjects in this study, despite live monitoring of spectral acquisition. However, these considerations remain important for any studies of Lac at 7T using sLASER going forwards.

#### 5.4.3. Analysis

Analysis of fMRS within the main study was as before in the *in vivo* pilot trials, but with additional focus on the dynamics of the resultant spectra, and tissue segmentation to enable calculation of tissue-corrected concentration. This is summarised in *Figure 5.4.1.* below, and discussed at length in the subsequent sections.

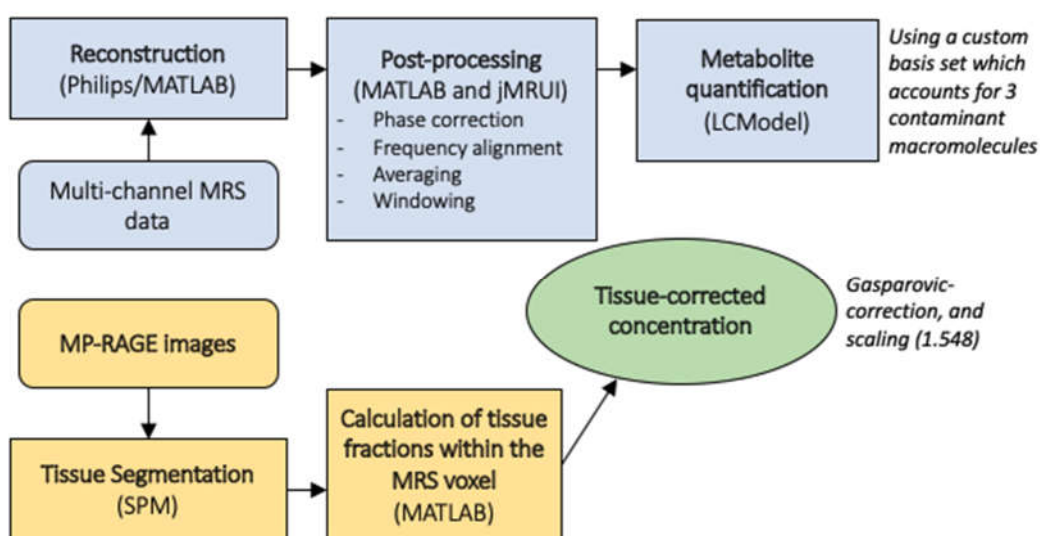


**Figure 5.4.1.:** Summary of analysis approach used for *in vivo* investigations. Custom basis sets and Gasparovic-correction (Gasparovic et al., 2006) and scaling are discussed in Section 5.3.3.3. and 5.4.3.2., respectively.

#### 5.4.3.1. Data processing

The fMRS data independently acquired from each of the 32 channels were combined and aligned using MATLAB version 9.8.0. R2020a (The Mathworks Inc, Natick, Massachusetts, USA), as previously described in Section 5.3.3.3., and phase-corrected using customised MATLAB scripts. A moving average strategy, with a kernel of three blocks, was then employed to average the data from each subject into blocks of 20 scans (60 averages each). Averages which covered the transition between ON and OFF periods were excluded from certain statistical analyses, to avoid mixing signals from different acquisition states, but are included in figures and analysis which require full understanding of the temporal activity of Lac. This strategy is summarised in *Figure 5.4.2.* below. Subsequent group analysis was carried out with frequency aligned spectra for both the young and old cohorts, resulting in a grouped time course with the same temporal resolution as the individual time courses, but each timepoint corresponding to 360 averages (6 subjects per cohort, 60 averages each).

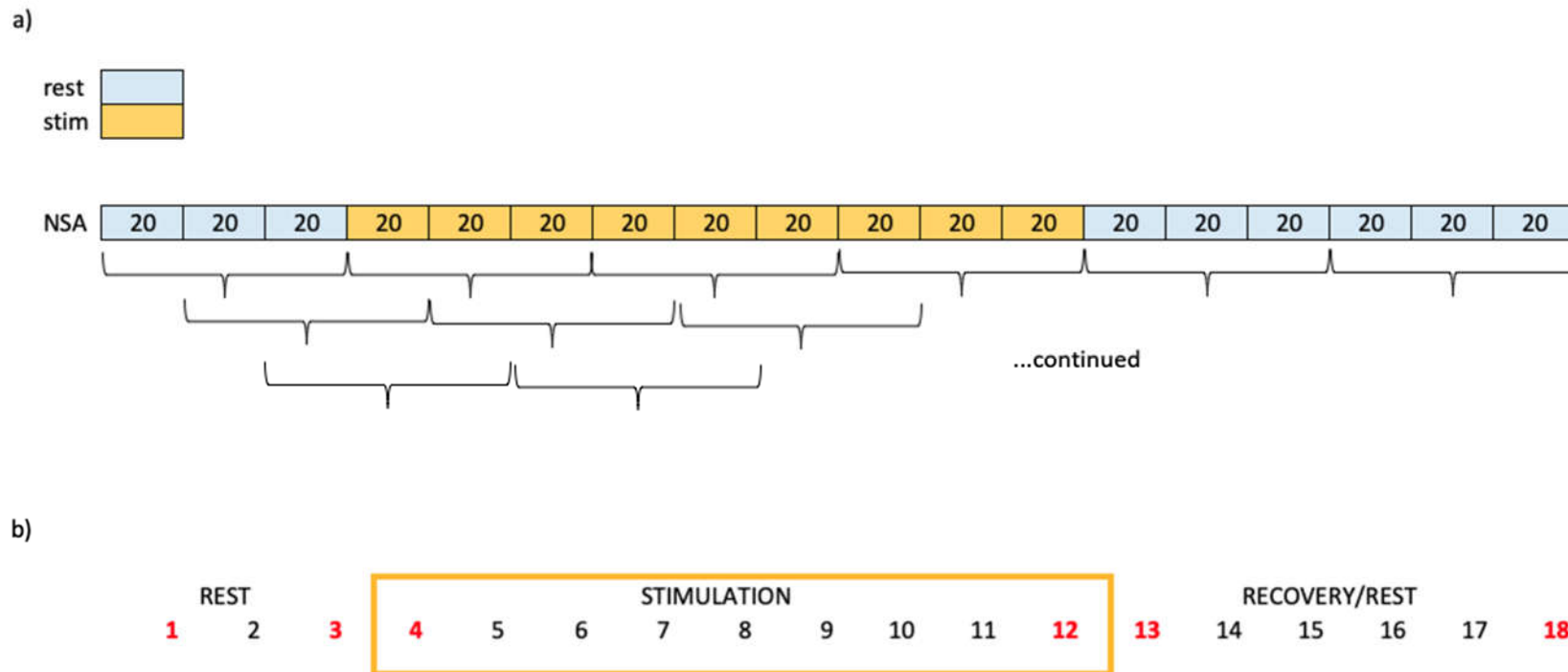


**Figure 5.4.2.:** Schematics depicting (a) the rest/stimulation timings of sLASER acquisition, consisting of 360 NSAs. Each NSA is of ~4.75 secs duration, thus each kernel of 60 NSAs equates to ~285 secs, and a moving average is then utilised to ensure most accurate characterisation of the time course, and (b) the subsequent selection of kernels for inclusion. The numbers in red refer to the blocks which are excluded from certain further analysis, due to the mixing of signals from different acquisition states. Blocks 1 and 18 are excluded due to the MATLAB analysis approach requiring looping of the moving average back to the start, to ensure that each moving average kernel is of the same duration.

LCModel (Provencher, 1993) was used as previously described, with the aforementioned custom VESPA (Soher et al., 2011) basis set with residual MM resonance inclusion also employed, with node spacing of the spline function was set as 4ppm.

MPRAGE images were segmented using statistical parametric mapping (SPM12) software (University College London, London, United Kingdom), and a VOI mask was created using spatial coordinates of the MRS voxel, and superimposed onto the MPRAGE images to determine tissue composition within the VOI using MATLAB. Analysis of the multi-slice echo-planar imaging (EPI) fMRI data used to assess the BOLD response seen during visual stimulation employed a general linear model (GLM) in combination with FSL-FLIRT (Jenkinson et al., 2002; Jenkinson and Smith, 2001; Greve and Fischl, 2009), for registration of fMRI data to MPRAGE images, and FSL-FEAT (Woolrich et al., 2001; Woolrich et al., 2004), to determine regions of activation in response to the visual stimulus, using uncorrected cluster thresholding.

#### *5.4.3.2. Calculation of lactate concentrations*

Calculation of Lac concentrations was carried out using the aforementioned calculated tissue compositions and the following saturation factors, summarised in *Table 5.4.1.*:

**Table 5.4.1.: Summary of information used for calculation of saturation factors.**  
Lactate values quoted from Dehghani et al. (2020).

	T <sub>1</sub> (ms)	1 - exp (- TR/T <sub>1</sub> )	T <sub>2</sub> (ms)	exp (- TE/T <sub>2</sub> )	Relax F (R)
<b>GM</b>	1940	0.924	45	0.0408	0.0337 R <sub>GM</sub>
<b>WM</b>	1130	0.988	45	0.0408	0.0403 R <sub>WM</sub>
<b>CSF</b>	4300	0.687	150	0.3829	0.263 R <sub>CSF</sub>
<b>Lactate (est)</b>	1900	0.928	94	0.216	0.201 R <sub>M</sub>  (N.B. - this is ~1/5 maximum possible value)

This information was then used in the following equation, as per Gasparovic et al. (2006):

$$\frac{S_{M\ obs}}{S_{H2O\ obs}} \times \left\{ \frac{f_{GM} R_{GM} + f_{WM} R_{WM} + f_{CSF} R_{CSF}}{1 - f_{CSF}} \right\} \left\{ \frac{2}{\#_M} \cdot \frac{H_2O}{R_M} \right\}$$

[5.1]

Where S<sub>M obs</sub> refers to the Lac signal, R<sub>M</sub> to the relaxation factor of the metabolite of interest, #<sub>M</sub> to the number of protons contributing to the

resonance of a given metabolite, H<sub>2</sub>O to water, and  $S_{H_2O\ obs}$  to unsuppressed water.  $f_{GM}$ ,  $f_{WM}$  and  $f_{CSF}$  are given by the following equations:

$$f_{GM} = \frac{f_{GM}^{vol} \cdot 0.78}{f_{GM}^{vol} \cdot 0.78 + f_{WM}^{vol} \cdot 0.65 + f_{CSF}^{vol} \cdot 0.97}$$

[5.2]

$$f_{WM} = \frac{f_{WM}^{vol} \cdot 0.65}{f_{GM}^{vol} \cdot 0.78 + f_{WM}^{vol} \cdot 0.65 + f_{CSF}^{vol} \cdot 0.97}$$

[5.3]

$$f_{CSF} = \frac{f_{CSF}^{vol} \cdot 0.97}{f_{GM}^{vol} \cdot 0.78 + f_{WM}^{vol} \cdot 0.65 + f_{CSF}^{vol} \cdot 0.97}$$

[5.4]

It is important to note that even though  $f_{CSF}^{vol}$  is typically  $\leq 0.1$ ,  $R_{CSF}$  is 6-7 times larger than  $R_{tissue}$ , thus CSF water signal is disproportionately large, and it is necessary to correct for this.

A scaling factor of 1.548 was also used to correct for the default WCONC value in LCModel. This is set as 35880 mM in LCModel analysis, which is the WM value, but was altered to the free water value (55556 mM) to reflect the separate correction of the different water contents of CSF and tissues, as follows:

$$SF = \frac{55556}{35880}$$

[5.5]

#### 5.4.3.3. Statistical analysis

All statistical analysis was carried out using a combination of MATLAB and GraphPad Prism 8.3.1 for Windows (GraphPad Software, San Diego, California USA, [www.graphpad.com](http://www.graphpad.com)). Statistical analysis predominantly focused on quantifying the temporal time course behaviour and the difference in this between young and old cohorts, using a combination of percentage change measures, and two-tailed paired and unpaired t-test. Sensitivity analysis was employed for possible outliers, whereby the subject was removed and relevant analysis repeated. Both SD and SEM were calculated where appropriate, to express data variability. SNR and FWHM were calculated in MATLAB, using the NAA singlet at 2.01ppm and water peak, respectively.

#### 5.4.4. Results

All spectra were visually inspected for potential artefacts, lipid contaminants, or improper shimming. The average SNR, calculated using the NAA singlet, was 195.9 (SD=59.5, SEM=24.3) for the young cohort (n=6), and 159.7 (SD=28.9, SEM=11.8) for the old cohort (n=6). A two-tailed unpaired t-test with Welch's correction for uneven group standard deviations showed there was no significant difference in SNR between these groups ( $p = 0.221$ ). The FWHM for young subjects was 11.6 Hz (SD=1.9Hz, SEM=0.8Hz), and 9.6Hz

(SD=1.6Hz, SEM=0.6Hz) for old subjects. A two-tailed unpaired t-test with Welch's correction showed the difference between FWHM in young and old cohorts was approaching significance (95% CI: -.26 to 4.19,  $p = .077$ ).

Figures 5.4.3. and 5.4.4. show the BOLD response in the older cohort, and example spectra from a single subject, respectively.

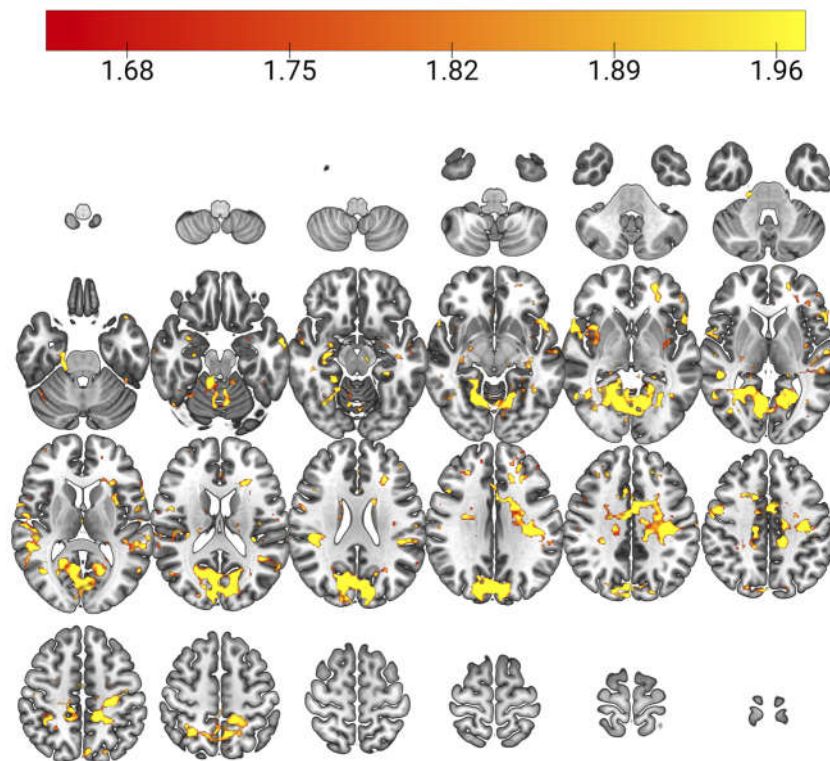


**Figure 5.4.3.:** Example averaged BOLD response (ON>OFF) of 5 older subjects during the fMRI acquisition for lactate voxel placement in the visual cortex (~3.5 minutes duration). Thresholded non-parametrically at  $P=0.05$  (uncorrected), with z-scores reflected in the colour variance of the activated regions.

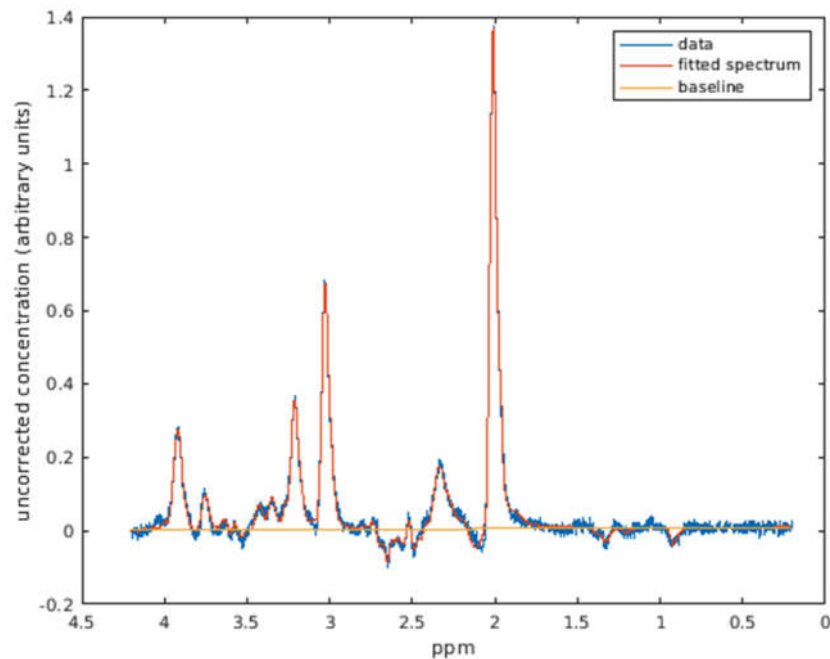


**Figure 5.4.4.:** Representative example of a spectrum averaged across the entire time course, in a 32-year-old female.

There was good agreement between subjects' spectra in the younger cohort, however, the older cohort showed greater variation in response time course upon visual inspection. Lac measures within the full averaged time course were estimated in LCMoDel with CRLB of 7% (SD = 1.41) for young subjects and 6.2% (SD = 1.47) for old subjects, thereby demonstrating the efficacy of both data acquisition and post-processing pathways, and that the addition of macromolecule resonances to the basis set ensured a well-fitted Lac peak for all subjects. In line with prior work (Fernandes et al., 2020), Glu, tCr and total NAA (tNAA) were also assessed for comparison. In young subjects, these had CRLBs of 2% (SD = 0.63), 1% (SD = 0.0) and 1% (SD = 0.0), and in old subjects CRLBs of 2% (SD = 0.0), 1% (SD = 0.0) and 1% (SD = 0.0), respectively. These findings are summarised in *Table 5.4.2.*

**Table 5.4.2.: Summary of key values in the averaged spectra.** Sub01 - 06 are the young cohort, and 07 - 12 are the old cohort. SNR was calculated using the NAA singlet, and FWHM using the water peak.

Participant	Average Cramér-Rao Lower Bounds (%)				SNR	FWHM (Hz)
	Lac	Glu	tNAA	tCr		
<b>Sub01</b>	8	2	1	1	167.7	11.4
<b>Sub02</b>	9	2	1	1	178.6	9.8
<b>Sub03</b>	7	2	1	1	178.9	12.2
<b>Sub04</b>	7	1	1	1	302.4	9.7
<b>Sub05</b>	5	3	1	1	129.0	14.8
<b>Sub06</b>	6	2	1	1	218.7	11.4
<b>Sub07</b>	6	2	1	1	189.5	10.3
<b>Sub08</b>	4	2	1	1	163.7	6.9
<b>Sub09</b>	5	2	1	1	154.2	8.8
<b>Sub10</b>	8	2	1	1	162.6	10.7
<b>Sub11</b>	7	2	1	1	107.0	9.6
<b>Sub12</b>	7	2	1	1	181.3	11.2

When considering the sliding windows of 60 NSAs as described in *Figure 5.4.2.*, these CRLB values do increase, however they are still within the bounds for which it is commonly considered that the LCModel fit is accurate (Kreis, 2016). Rather than rejecting the data outright if the %CRLB output from LCModel was >20%, the strategy described in the paper by Kreis (2016) was employed, to determine whether windowed spectra with CRLBs of 20-

30% were acceptable through visual inspection of the Lac fit. Any spectra with CRLBs of >30% were to be rejected, however no subjects were rejected within this main study cohort.

The percentage change relative to baseline was used to measure quantitative changes in Lac levels, as shown in *Figure 5.4.5*. Mean changes in percentage Lac concentration relative to the first measure were quantified at a key window central in the stimulus period (window 8), and close to the end of the recovery period (window 17). In the young cohort, Lac concentration is an average of 21.4% (SD=13.8%, SEM=5.7%) greater than the first datapoint during stimulation, and 3.2% (SD=19.2%, SEM=7.8%) higher than the first data point near the end of acquisition. In the old cohort, the mean percentage change is more difficult to discern due to the intersubject variance, but was -4.6% (SD=28.6%, SEM=11.7%) from the first measure during stimulation, and +2.4% (SD=19.6%, SEM=8%) during recovery.

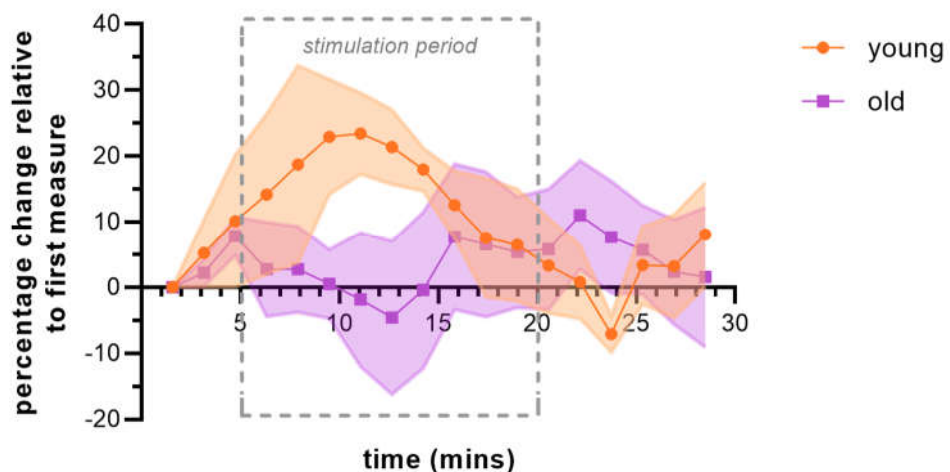


**Figure 5.4.5.** Percentage change in Lac levels relative to first baseline measure in the young (orange) and old (purple) cohorts. The traces depict the respective SEM measures for each group at each time point, and the stimulation period is shown with a dotted line.

Absolute Lac concentrations were quantified using the equations described in Section 5.4.3.2. of the Methods. This required calculation of tissue compositions, as shown in *Table 5.4.3.* below.

***Table 5.4.3.: Summary of the tissue composition of spectroscopic voxels.***

<b>Participant</b>	<b>Total tissue percentage (%)</b>	<b>GM %</b>	<b>WM %</b>	<b>CSF %</b>
<b>Sub01</b>	89.1	43.67	45.43	10.9
<b>Sub02</b>	93.48	51.5	41.97	6.52
<b>Sub03</b>	92.65	61.46	31.19	7.35
<b>Sub04</b>	94.9	68.64	26.26	5.1
<b>Sub05</b>	95.39	56.8	38.59	4.61
<b>Sub06</b>	94.29	59.54	34.75	5.71
<b>Sub07</b>	94.08	53.85	40.22	5.92
<b>Sub08</b>	82.28	52.12	30.16	17.72
<b>Sub09</b>	88.9	46.19	42.7	11.1
<b>Sub10</b>	85.94	43.26	42.68	14.06
<b>Sub11</b>	94.27	49.88	44.39	5.73
<b>Sub12</b>	95.99	38.58	57.41	4.01

Absolute values were determined by use of Gasparovic-correction and scaling to free water, resulting in all subjects being on the same scale after correction, and then plotted over the time course (*Figure 5.4.6.*). Calculation of

concentrations as per unit voxel volume and per unit brain tissue volume were also carried out and these measures are compared in *Table 5.4.4*.

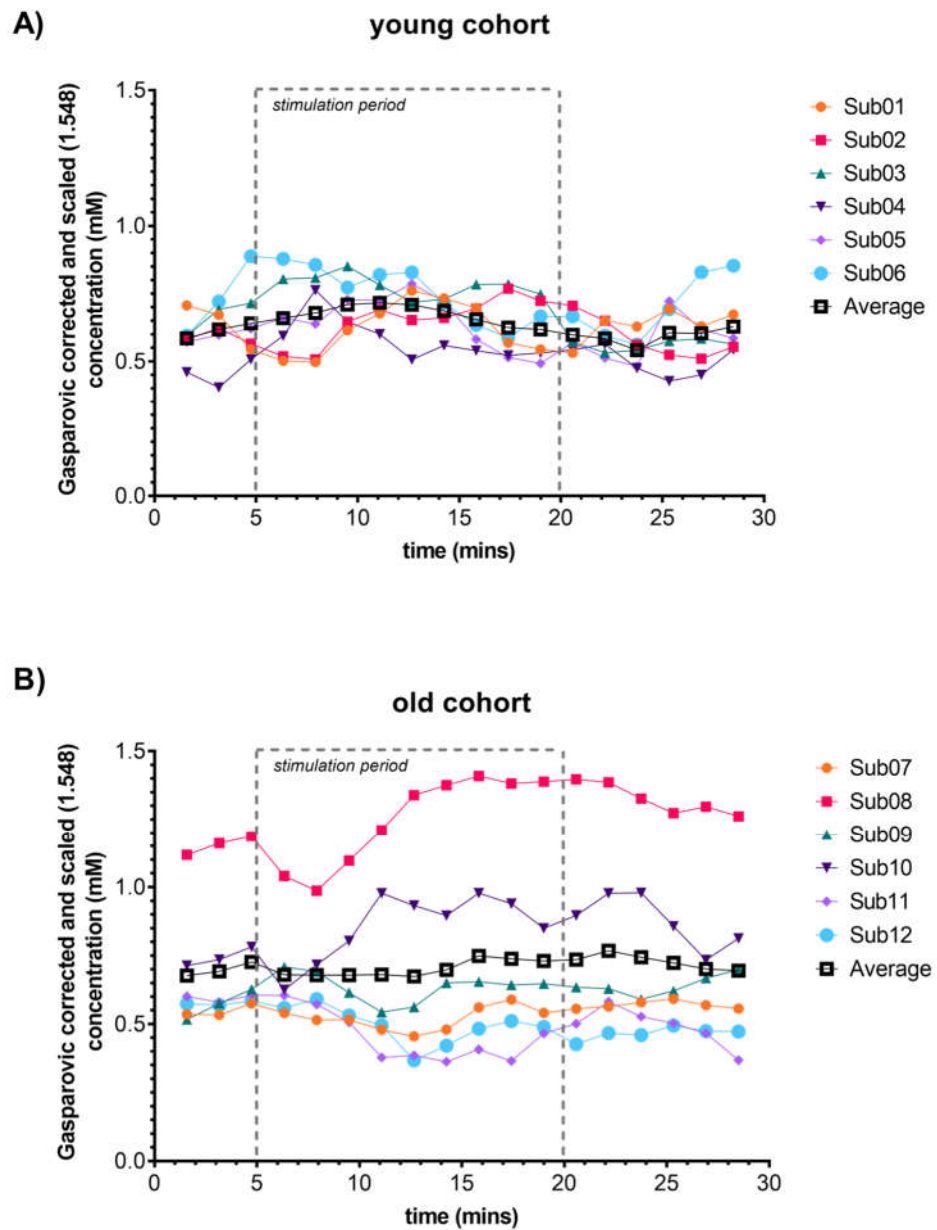


**Figure 5.4.6.:** Gasparovic-corrected (Gasparovic et al., 2006) and scaled Lac concentrations throughout the time course of fMRS acquisition in (a) the young cohort and (b) the old cohort. The stimulation period is shown with a dashed line. As a rolling window is used, some data points – 3, 4, 12 and 13 – contain data from both rest and stimulation periods. Such transition windows were not used in other analyses and are included here for visualisation. Average is depicted in black.

**Table 5.4.4.: Summary of Lac concentrations in the averaged spectra, using various concentration calculation approaches. Results are given in mM.**

	Concentration (mM) calculation approach		
	Gasparovic-correction and scaling (1.548)	Per unit voxel volume	Per unit brain tissue volume
<b>Sub01</b>	0.686	0.436	0.489
<b>Sub02</b>	0.611	0.412	0.441
<b>Sub03</b>	0.859	0.586	0.632
<b>Sub04</b>	0.648	0.457	0.482
<b>Sub05</b>	0.682	0.473	0.496
<b>Sub06</b>	0.923	0.637	0.676
<b>Sub07</b>	0.622	0.424	0.451
<b>Sub08</b>	1.458	0.879	1.068
<b>Sub09</b>	0.688	0.439	0.494
<b>Sub10</b>	0.869	0.534	0.622
<b>Sub11</b>	0.562	0.381	0.404
<b>Sub12</b>	0.551	0.371	0.387

Gasparovic-corrected and scaled values averaged 0.735 mM (SD = 0.13, SEM = 0.05) and 0.79 mM (SD = 0.35, SEM = 0.14) in young and old subjects, respectively. Given the small cohort size, tests of normality were not used, and instead the distribution of the full cohort was assessed via histogram in SPSS (*Figure 5.4.7.*). Parametric tests were initially carried out,

with non-parametric comparisons made, due to the difficulty of determining the distribution normality in this small cohort. Only parametric estimates are given, due to their comparative ease of interpretability.

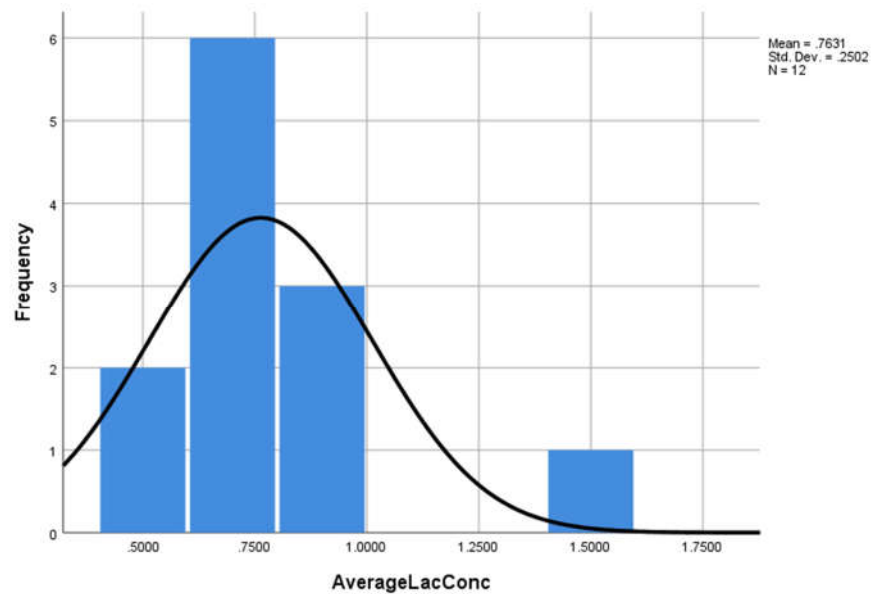


**Figure 5.4.7.:** Histogram depicting Lac concentrations in the full cohort. Sub08 has a mean Lac concentration of 1.4579 mM and is an outlier within the cohort.

This highlighted that Sub08 was an outlier, and therefore warranted subsequent additional analysis. This is addressed in sensitivity analysis in subsequent statistical tests. When Sub08 is removed, the average concentration of Lac in the old cohort is 0.66 mM (SD = 0.13, SEM = 0.058). A two-tailed unpaired t-test comparing the full young cohort with the adjusted old cohort found no significant difference in average Lac concentration, with a difference in means of 0.076 (95% CI: -0.098 to 0.25,  $p > 0.05$ ). Non-parametric Mann-Whitney U comparison also resulted in  $p > 0.05$ .

Statistical analysis was also carried out to compare concentrations between rest and stimulation, and stimulation and recovery for the subjects. A non-transitional window from each period was selected as representative for the full period. Windows 2, 8, and 17 were selected (see *Figure 5.4.2.*). For the rest window (window 2), mean Lac values were 0.62 mM (SD = 0.11, SEM = 0.05) for young subjects, and 0.69 mM (SD = 0.24, SEM = 0.1) for old subjects (when Sub08 is removed for sensitivity testing, mean Lac is 0.6 [SD = 0.08, SEM = 0.04] in the old cohort). Two-tailed unpaired t-tests with Welch's correction for uneven standard deviations found no significant difference between young and old subjects in either the original cohort comparison, or the sensitivity testing cohort comparison. In the original cohort comparison, the difference in means was -0.099 (95% CI: -0.42 to 0.22,  $p > 0.05$ ), and in the sensitivity testing cohort this was 0.02 (95% CI: -0.11 to 0.15,  $p > 0.05$ ). These results are supported by non-parametric Mann-Whitney U tests ( $p > 0.05$  for both original and sensitivity cohorts).

For the stimulation window (window 8), mean Lac values were 0.71 mM (SD = 0.12, SEM = 0.05) and 0.67 (SD = 0.39, SEM = 0.16) for young and old subjects respectively (0.54 mM [SD = 0.23, SEM = 0.1] in sensitivity testing cohort). Two-tailed unpaired t-tests with Welch's correction found no significant difference between group-averaged Lac concentrations at this stage, in either the original or sensitivity-adjusted cohorts. For the original cohorts, the difference in means was 0.035 (95% CI: -0.37 to 0.44,  $p > 0.05$ ), and for the sensitivity-adjusted cohort this mean difference was 0.168 (95% CI: -0.12 to 0.45,  $p > 0.05$ ). Non-parametric Mann-Whitney comparison tests supported these findings ( $p > 0.05$  for both).

During the recovery window (window 17), mean Lac values were 0.6 mM (SD = 0.13, SEM = 0.05) for young subjects, and 0.7 mM (SD = 0.31, SEM = 0.13) for old subjects (0.58 mM [SD = 0.12, SEM = 0.05] in the old sensitivity cohort). Two-tailed unpaired t-tests with Welch's correction found no significant differences between the young and old cohorts, in both the original (difference in means = -0.098, 95% CI: -0.43 to 0.23,  $p > 0.05$ ) and sensitivity-adjusted (difference in means = 0.021, 95% CI: -0.15 to 0.19,  $p > 0.05$ ) cohorts. Mann-Whitney U tests support these findings ( $p > 0.05$  in both).

Within-cohort differences in Lac concentrations between rest and stimulus, and stimulus and recovery periods were also analysed. In the young cohort, a two-tailed paired t-test found that Lac concentrations were significantly higher during the stimulation window when compared with the rest window (mean of differences = 0.09, 95% CI: 0.028 to 0.15,  $p = 0.014$ ). The difference between concentrations during the stimulus and recovery windows is also significant (mean of differences = 0.1055, 95% CI: 0.039 to 0.17,  $p = 0.0098$ ). These findings are also evidenced when using non-parametric Wilcoxon matched-pairs signed rank test for the comparison of rest and stimulation ( $p = 0.0313$ ), however this test did not find a significant difference between stimulation and recovery ( $p = 0.0625$ ).

In the original old cohort, the difference between rest and stimulation was not significant (mean of differences = 0.01834, 95% CI: -0.17 to 0.2,  $p > 0.05$ ) when assessed using a two-tailed paired t-test. The difference between

stimulation and recovery was also found to not be significant when using this approach (mean of differences = -0.02736, 95% CI: -0.16 to 0.1,  $p > 0.05$ ). Comparative non-parametric Wilcoxon matched-pairs signed rank tests found no significant difference between rest and stimulation ( $p > 0.05$ ), or stimulation and recovery ( $p > 0.05$ ). In the sensitivity-adjusted cohort with Sub08 removed, two-tailed paired t-tests found no significant difference in Lac concentration between rest and stimulation (mean of differences = 0.0576, 95% CI: -0.145 to 0.26,  $p > 0.05$ ), or stimulation and recovery (mean of differences = -0.04125, 95% CI: -0.21 to 0.13,  $p > 0.05$ ). Wilcoxon matched-pairs signed rank tests were carried out for non-parametric comparison. Between rest and stimulation there was no significant difference in Lac concentration ( $p > 0.05$ ). Lac concentration differences between stimulation and recovery were also not significant ( $p > 0.05$ ).

Post-hoc analysis was carried out on Sub08, Sub10, Sub11 and Sub12, to assess whether misidentification of Lac had occurred due to their outlier behaviour in the percentage change (Sub11 and Sub12) and concentration (Sub08 and Sub10) analysis. Their uncorrected Lac time courses are shown in *Figure 5.4.8.* below, alongside the time courses of MM1 (0.89 ppm), MM2 (1.20 ppm) and MM3 (1.37 ppm). The time courses were visually inspected and respective CRLBs were also assessed. Lac was determined to have been correctly identified in Sub08, Sub11 and Sub12, however in Sub10 it is possible that Lac and MM2 were incorrectly identified.

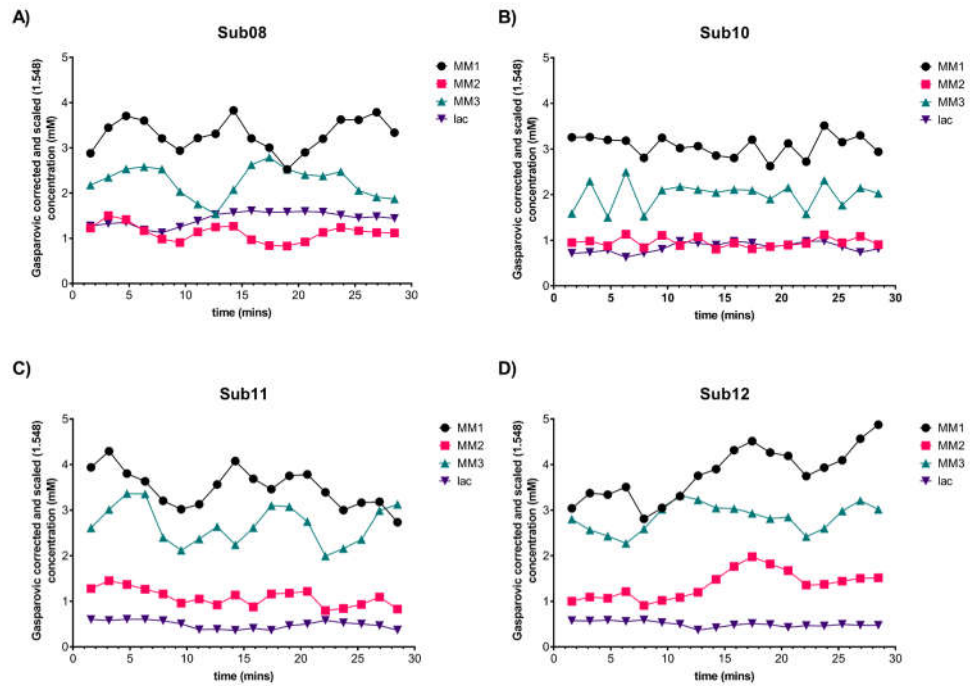


**Figure 5.4.8.**: Comparison of Gasparovic-corrected and scaled concentrations of Lac, MM1, MM2 and MM3 over the time course. (a) depicts Sub08, (b) Sub10, (c) Sub11, and (d) Sub12.

On the basis of the above analysis, sensitivity analysis was carried out, whereby Sub10 was removed from the old cohort, and between- and within-cohort differences in rest, stimulation and recovery periods assessed again. This was firstly done with an older cohort comprising 5 subjects, as Sub08 was reintroduced, and then with an older cohort of 4 subjects, with both Sub08 and Sub10 removed. When considering differences between cohorts at each window of interest, parametric two-tailed unpaired t-tests with Welch's correction were used, with subsequent non-parametric Mann-Whitney tests for comparison. For window 2, the five-subject sensitivity-adjusted cohort comparison (Sub10 removed) with the full young cohort found no significant difference between the young and old groups when using either the aforementioned t-test (difference in means of -0.065, 95% CI: -0.65 to 0.13,  $p > 0.05$ ) or Mann-Whitney U test ( $p > 0.05$ ). No significant differences between

young and old cohorts were found at window 8 when using a two-tailed unpaired t-test with Welch's correction (difference in means = 0.087, 95% CI: -0.41 to 0.59,  $p > 0.05$ ) or a Mann-Whitney test ( $p > 0.05$ ). There were also no significant differences between young and old subjects at window 17 using either test, with the results of the t-test showing a difference in means of -0.091 (95% CI: -0.51 to 0.33,  $p > 0.05$ ). This is supported by the Mann-Whitney U test ( $p > 0.05$ ). In the four-subject sensitivity-adjusted older cohort (Sub08 and Sub10 removed), differences between young and old cohorts were not significant when either parametric two-tailed unpaired t-tests with Welch's correction or non-parametric Mann-Whitney tests were used at windows 2 (t-test: difference in means = 0.054, 95% CI: -0.07 to 0.17,  $p > 0.05$ ; Mann-Whitney U:  $p > 0.05$ ), and 17 (t-test: difference in means = 0.059, 95% CI: -0.1 to 0.22; Mann-Whitney U:  $p > 0.05$ ). However, at window 8, an unpaired two-tailed t-test with Welch's correction found significantly higher Lac concentrations in the young cohort compared with the four-subject sensitivity-adjusted cohort (difference in means = 0.266, 95% CI: 0.12 to 0.42,  $p = 0.004$ ). A Mann-Whitney test for the same comparison also found a significant difference ( $p = 0.019$ ).

The evolution of the time course was then assessed in these sensitivity-adjusted cohorts. For the five-subject sensitivity-adjusted cohort, there was no significant difference found between windows 2 and 8, using either the two-tailed paired t-test or comparison Wilcoxon matched-pairs signed rank test (paired t-test: difference in means of 0.06148 [95% CI: -0.13 to 0.25,  $p > 0.05$ ]; Wilcoxon:  $p > 0.05$ ). Differences in windows 8 and 17 were approaching significance when using a two-tailed paired t-test (difference in means = -0.0726, 95% CI: -0.15 to 0.01,  $p = 0.068$ ), supported by Wilcoxon matched-

pairs signed rank test results ( $p = 0.08$ ). For the four-subject sensitivity-adjusted cohort, the results of the two-tailed paired t-test between windows 2 and 8 was approaching significance (difference in means = 0.1213, 95% CI: -0.02 to 0.27,  $p = 0.077$ ). A Wilcoxon test on the same data gave an insignificant p-value of  $p = 0.125$ . Between windows 8 and 17, a two-tailed paired t-test found a significant difference ( $p < 0.001$ ), but a Wilcoxon matched-pairs signed rank test only approached significance ( $p = 0.068$ ).

## 5.5. Discussion

The elucidation of the temporal dynamics and associated concentrations of Lac and its involvement in cerebral activation is critical to our understanding of brain functionality, and the assessment of how this differs across the healthy lifespan. However, the role of Lac in neuronal stimulation is often debated and remains unclear. Thus, proper quantification is critical for the understanding of brain activation. So far, Lac quantification has proven to be challenging for a variety of reasons, particularly the strong MM contamination, and additional lipid resonances from the pericranial fat. This is of particular concern when investigating VOIs which lie adjacent to this fat, such as the occipital cortex, as investigated here. Within this chapter, phantom studies were carried out to determine optimal protocol parameters, and these used in a pilot investigation of human subjects, which aimed to assess the selected protocol and its tolerance within subjects. This optimal protocol was then taken forward to investigate age effects on temporal Lac behaviour and quantify best-estimate absolute concentrations in young and old healthy subjects, using the semi-LASER sequence which is optimised for J-modulation selection (Scheenen et al., 2008).

Earlier work carried out prior to this study (Fernandes et al., 2020), as well as the confirmatory phantom studies discussed earlier in this chapter, confirmed the necessity for use of a long TE semi-LASER sequence (144ms). This results in an out-of-phase Lac peak, whilst also exploiting the differences in  $T_2$  relaxation time between metabolites and pericranial lipid signals, which were also controlled for using saturation slabs. Although prior work (Bednařík et al., 2016) has employed a longer TE, this included a general MM profile within the basis set, which was not done here. Given the non-negligible MM signal adjacent to the 1.31 ppm Lac peak which remains at an echo time of 144ms, it is imperative to account for their contributions independently in order to optimally account for signal contributions. Therefore, following the work of Fernandes et al. (2020), three MM signals (MM1, MM2, MM3) were individually fitted with simulated Lorentzian peaks which enabled the variability in these components to be adequately accounted for. This current study differed from this prior work by both taking this protocol into an old cohort and attempting absolute quantification of Lac concentrations.

The results of this study showed that the Lac peak is reliably identifiable in young subjects, with good SNR and spectral linewidth. However, there was large variation in response to stimulus within this cohort. Such variation is also clear in the old cohort, especially with Sub 11 and Sub 12, who exhibit a decrease in Lac relative to the first measure at the onset of the stimulus. Consideration was given to the possibility of Lac and MM2 (at 1.20 ppm) misidentification in these subjects, however as *Figure 5.4.8.* shows, this was unlikely to be the case.

When considering percentage changes seen with time (*Figure 5.4.5.*), the mean Lac time course is shown to increase upon stimulation for young subjects, declining in the later stage of stimulation. After cessation of stimulation, the response dips slightly below baseline for some young subjects and returns above baseline before the acquisition is finished. This post-stimulus undershoot has been evidenced previously using various MRI techniques (Frahm et al., 1996; Krüger, Kleinschmidt and Frahm, 1996; Lu et al., 2004; Yacoub, Ugurbil and Harel, 2006; van Zijl, Hua and Lu, 2012), and whilst the findings of the current study are tentative due to the variation in the individual responses, it warrants further investigation. The old cohort showed a different mean response, with no clear increase until halfway through stimulation, and with minimal percentage changes exhibited throughout the time course. However, there is also great variance in subject response in this cohort. Whilst percentage changes in the old cohort were too disparate between subjects to reach true conclusions, mean percentage changes in Lac concentration in the young cohort were 21.4% greater than the first data point measure during stimulation, a significant increase which is in line with some of the previous literature (Prichard et al., 1991; Sappey-Marinier et al., 1992; Frahm et al., 1996; Mangia et al., 2007; Lin et al., 2012; Schaller et al., 2013; Bednařík et al., 2015; Fernandes et al., 2020).

Tying the analysis to the first measure when assessing spectral behaviour does bias the results, as they focus on the quality of the first data point, and do not reflect the true concentration of Lac within the brain, and any changes in this. In this study, the best estimates of absolute Lac concentrations were calculated by accounting for subject-specific tissue compositions, their

associated saturation factors, and scaling to free water (see Section 5.4.3.2.). When considering both full cohorts, no significant differences were found at key points between young and old subjects. However, Lac concentrations are significantly lower in the four-subject sensitivity-adjusted old cohort compared with the full young cohort (two-tailed unpaired t-test with Welch's correction,  $p < 0.05$ ) during stimulation when Sub08 and Sub10 were removed for various reasons described previously. In this same sensitivity-adjusted cohort, comparison of within-cohort Lac concentrations during stimulus and recovery found a significant increase in concentrations after stimulus cessation (two-tailed paired t-test,  $p < 0.001$ ). In the young cohort, a two-tailed paired t-test found that Lac concentrations were significantly higher during the stimulation window when compared with the rest window ( $p < 0.05$ ). Significantly higher concentrations were also found during the stimulus period compared with recovery ( $p < 0.01$ ). Non-parametric statistical analysis was also carried out, due to the impossibility of determining the normality of distribution in such small sample sizes. Whilst concerns are noted regarding multiple comparisons here, statistical advice was sought from two independent senior statisticians within the University of Nottingham, who cautioned against the use of multiple comparison correction in this instance due to sample size and inter-individual variance in results. As such, subsequent interpretation is cautionary, and the lack of multiple comparison correction acknowledged.

Average Lac concentrations throughout the full time courses were broadly in-keeping with findings of other studies (see *Table 5.3.1.*; Mangia et al., 2007; Melke et al., 2009; Lin et al., 2012; Schaller et al., 2014; Bednařík et al., 2015; Boillat et al., 2020). However, these studies used various different stimulation approaches and imaging sequences, so drawing direct comparisons is

impossible. All of these results should be considered with caution, due to the discrepancies in cohort time courses, and small cohort sizes, particularly in the sensitivity analysis cohorts. The cohort size in the current study was guided by the work of Fernandes et al. (2020), who investigated a young cohort (age range 25-30 years, 3M) comprising six subjects. As such, the current study aimed to include at least six subjects in each cohort, however a statistical power analysis performed on the work of Lin et al. (2012) using G\*Power (version 3.1; Faul et al., 2007) predicted  $n=8$  per group. Thus, the intention was to recruit eight subjects per group, although the impact of the coronavirus pandemic lockdowns of the University of Nottingham and the SPMIC meant that only six subjects per cohort was possible, and as a result the study lacks power. Any follow-up work should aim to include at least eight subjects per cohort as a minimum, but ideally more so that any outliers such as those in the current study can be accounted for.

The younger cohort time courses are broadly comparable with each other, but interpretation is limited by cohort size. The possible misidentification of Lac and MM2 in Sub10 was surprising, and this subject was removed for sensitivity tests. It is unclear how to address this possible misidentification within the processing pathway, and as such plotting all subject Lac concentrations alongside MM1, MM2 and MM3 should be considered as an additional quality control metric in future studies (see *Figure 5.4.8.*), with subsequent removal of subjects where misidentification may have occurred. Interestingly, Sub08 exhibited higher concentrations of brain Lac but appeared to not be misidentified. The reason for this is unclear, and future investigation in a larger cohort is warranted to assess whether some older subjects naturally exhibit higher brain Lac concentrations and may separate into two

distinct groups based on Lac concentration, one which is comparable to the young cohort, and one which is significantly higher.

Statistical analysis was biased to the representative data points that were chosen, however due to the windowing process in MATLAB these contain data from neighbouring data points and were selected to ensure those adjacent data points did not include information from windows which transitioned between rest and stimulation, or stimulation and recovery. This limited the number of points which could be considered, and the windows were then chosen to be central to the stimulus, and as close to the end of the recovery period as possible. It is also important to acknowledge the issues with using CRLBs as the main output in MRS. As summarised by Kreis' 2016 paper, the commonly used threshold value of 20% is somewhat arbitrary, and additionally may result in systematic inaccuracies which are negatively contributing to the aim of having MRS viewed as a possible clinical instrument. Thus, it is critical that care is given when using CRLBs, and they should be considered to be a criterion which assesses quality, as opposed to thresholding for inclusion or exclusion of specific subjects. The field is also biased towards the use of LCModel for spectral analysis, but numerous other programmes are available, such as GANNET and TARQUIN. Whilst LCModel is likely to remain the norm, particularly due to the recent announcement that this software is now free, it would be interesting to compare results across analysis packages in future. Many in the field are keen to move away from the standard of Cr as reference metabolite, due to potential inaccuracies by merit of different Cr and PCr  $T_2$  relaxation times (Ke et al., 2002), and changing Cr levels under certain disease conditions, such as cognitive decline (Ferguson et al., 2002; Gasparovic et al., 2013; Rackayova et al., 2017; Khomenko et al.,

2019). The current study attempted to account for these by separately measuring Cr and PCr, before combining them as tCr and monitoring this throughout the acquisition time course in each subject.

The advantage of a long TE approach is also evident in these results. fMRS studies which employed short echo times to quantify metabolic changes using a difference spectrum (ON/OFF period) also require additional manipulation of the spectra, through use of a line broadening filter, to compensate for the narrowing of the spectral linewidth which occurs by merit of the BOLD-related  $T_2^*$  changes (Zhu and Chen, 2001), however this was not necessary here, given the ease of identifying the peak of interest at 1.31 ppm. The use of semi-LASER also allowed for optimal pulse application and spatial selection, thereby reducing chemical shift displacement artefacts and mitigating partial volume effects.

In the main study cohort, the visual stimulus was well-tolerated and constant monitoring of the attention task responses showed that subjects remained awake. However, alternative visual stimuli should be trialled and may be necessary in disease populations who may not be able to cope with the intensity of the current stimulus. Additionally, Wandell, Brewer and Dougherty (2005) showed that a moving wedge visual stimulus resulted in less adaptation over time than a standard checkerboard. However, attempts were made to mitigate the risk of adaptation by not using points for statistical analysis from the end of the visual stimulation period. Furthermore, subjects who were not successfully scanned in the pilot trials were not considered for re-scan and inclusion in this main study despite challenges in recruitment, in

order to avoid longer-term adaptation and effects of prior exposure. fMRS acquisition was only from a single brain region, and whilst this was determined by the stimulus of choice, it would be interesting to carry out additional investigation of multiple VOIs across the brain to determine whether time course behaviour differs significantly on the basis of regionality. This is of particular interest, as the topography of brain aerobic glycolysis has been shown to change with age in much of the brain (Goyal et al., 2017), but also shown to remain consistent across age in a reliable pattern comprising high Lac signal in the precuneus, cuneus and cingulate (Lee et al., 2020). Whilst the motor response involved in the button response task may have been responsible for some of the additional activation seen in other regions of the brain (*Figure 5.4.3.*), this was distant from the visual cortex and VOI placement.

It should be noted that a key weakness of the current study is the lack of inclusion of subjects between ~35 to 60 years old, an age range which is not bereft of age-related changes. Indeed, there is evidence to suggest that some key metabolic changes in ageing are observable during this period (Kaiser et al., 2005a;b; Gruber et al., 2008; Eylers et al., 2016; Goyal et al., 2019). A review by Cichocka and Beres (2018) looked at 82 studies which investigated metabolism across the lifespan, from foetus to older age, and found that there are characteristic brain changes at each life stage. For example, visual stimuli decrease in their sensitivity as we age (Meisami, Brown and Emerle 2007; Bi et al., 2016), which necessitates further investigation of the stimuli of choice for future fMRS studies in aged populations. During the current study, recruiting older subjects was particularly difficult due to a lack of space within the coil for MR-safe glasses, and therefore it was a requirement for subjects to

have good vision or wear contact lenses. Even in normal ageing, vision loss is common and glasses are often worn. However, for a multitude of reasons including both anatomical and physiological changes within the eye, and reduced manual dexterity (Woods, 1992; Zadnik, 1994; Benoit and Shovlin, 2003), it can be difficult for older individuals to use contact lenses, thereby reducing the number of older subjects available for the study. Whilst these were also requirements for young subjects, this population was far easier to recruit from, given the university context.

Cichocka and Beres (2018) also evidenced changes in NAA that were challenging to explain, with both a decreased concentration by merit of increasing age – supported by a 2009 systematic review by Haga et al., and a 2019 systematic review by Cleeland et al. – but also an increase with age in the white matter. This increase is likely due to a decrease in cerebral water, or the occurrence of gliosis in the brain (Schuster, Essig and Schröder, 2011; Schuff et al., 2001; Yang et al., 2015). Several studies agree that there is a negative correlation between increasing age and the ratio of metabolites relative to Cr due to increases in Cr (Chang et al., 1996; Saunders et al., 1999; Haga et al., 2009), which has also been evidenced in AD (Kantarci, 2007; Su et al., 2016). This increase in Cr may be explicable through decreasing connectivity, or axonal demyelination (Inglese et al., 2003). Whilst some changes may result from healthy brain maturation (Yang et al., 2015), MRS is well-positioned to investigate nuances of cerebral biochemistry (Lin and Rothman, 2014) at all stages, and is imperative to explicit elucidation of the metabolic underpinnings of healthy ageing and cognitive decline. It is also critical that such metabolic investigation also occurs in subjects with impaired cognition, to pinpoint metabolic changes associated with such impairment,

thereby furthering the field of knowledge and getting closer to elucidating a possible metabolic drug target. Sijens et al. (2001a;b) support the assertion in the current study that increased Lac may be linked to a metabolic shift between oxidative and non-oxidative pathways, or age-related impaired clearance mechanisms. However, to my knowledge this relationship has not yet been investigated in disease cohorts using fMRS, despite prior work evidencing a variety of metabolic changes with impaired ageing (Arneemann et al., 2018).

Whilst FDG-PET is the main metabolic brain imaging method used for the depiction of glucose hypometabolism as seen in ageing and neurodegeneration (Hoffman et al., 2000; Mosconi et al., 2008; Mosconi et al., 2009), ASL has provided an opportunity to assess this without the use of radiation. Despite this, neither of these methods allow for the assessment of associated metabolic impairments and their dynamic change, which is where fMRS provides additional complimentary information in the elucidation of age-related brain changes. Such Lac investigation is only really possible at 7T, a field strength which is not in clinical use. As such, findings from this study are not clinically translatable, however future investigation of healthy and clinical cohorts is still valid and provides metabolic information which cannot be gained at lower field strengths.  $^1\text{H}$ -MRS/fMRS is an indirect measure and as such the resultant biological inference is limited as it does not allow you to follow the metabolites of interest through their metabolic pathways or pools, which techniques such as  $^{13}\text{C}$ -MRS, or dynamic nuclear polarization of pyruvate do allow. Additionally, an increase in Lac concentration requires increased glycolytic flux, due to a lack of a pool from which it can be immediately derived for use. This will take several minutes to reach a level

observable by  $^1\text{H}$  MRS, and this is indeed what these results suggest. Furthermore, changing total concentration provides no information about the specific pathways which were up- or down-regulated during the study, as would be feasible if tracers were used. It is also important to note that – if the mass-balance is preserved – metabolic rates can change without affecting total concentrations as measured by fMRS. Whilst the current findings – when validated – may lend some support to the ANLS, *in vivo* confirmation of this hypothesis will ultimately also require support from other techniques such as those aforementioned.

When considering the different interpretations of the role of cerebral Lac and its relationship with Glc, conclusions are difficult to draw from this study, particularly given its small size and the within-subject discrepancy in the older cohort. However, this does not negate the fact that cerebral Lac metabolism plays a key role in brain functionality, and may be a critical component of brain ageing, potentially even a hallmark of this process (Ross et al., 2010; Blonz, 2017).

## 5.6. Conclusions and future directions

Elucidation of the role of cerebral Lac using 7T fMRS is still in its infancy, however can provide novel insight as to the metabolic underpinnings of healthy ageing. The use of a long-TE semi-LASER approach to the acquisition of Lac-focused spectrum during visual stimulation and subsequent calculation of ‘absolute’ Lac concentrations was evidenced to be feasible in both young and old subjects. The analysis strategy showed disparate Lac concentrations in the older group when compared with the young and highlighted the early

possibility of a subgroup defined by higher Lac concentration in older subjects. Alongside the possibility for misidentification of Lac and MM2 in older subjects, this warrants further investigation. Additionally, a more holistic understanding of the nature of these changes and confirmation of such a subgroup would only be possible with validation in a larger sample size, and future investigation of subjects experiencing impaired ageing or cognition. Given the difficulty of measuring Lac, even under resting conditions, it is imperative that optimal protocols for both acquisition and analysis are established, in order to avoid both biasing and misinterpreting results. The lack of 7T scanners available within healthcare settings would also make clinical translation challenging, and thus current findings are limited to research settings.

Future work would further the understanding of this complex metabolic pathway, and the dynamic nature of the associated metabolism. Employing methods such as carbon-13 spectroscopy (Gruetter et al., 2003; Rodrigues, Valette and Bouzier-Sore, 2013) or dynamic nuclear polarization-MRI (DNP-MRI; Grist et al., 2019) would also provide further information as to the behaviour of the related metabolic pathways which are reliant on the provision of Lac. Suggestions for further investigations are explored in Chapter 6.

## 6. General conclusions and discussion

### 6.1. Summary of results

The work within this thesis describes resting-state cerebral perfusion and functional metabolic assessments used to advance understanding of healthy brain ageing. The main goals of this thesis were to (1) further the body of knowledge around PCA-derived spatial patterns associated with age and MoCA scoring; (2) compare these PCA-derived patterns with voxel-wise approaches; (3) uncover the nature of reported perfusion changes with age, and determine whether these truly exist or are explicable by the impact of pre-processing steps or underlying confounds; (4) determine the usefulness of sCoV as a metric in understanding perfusion changes with age; (5) investigate the temporal behaviour of Lac during visual stimulation; and (6) achieve best-estimate quantification of absolute concentration of Lac. The subjects investigated within this thesis range between 22-84 years old, with all findings within this thesis derived from either ASL or (f)MRS. The findings herein expand the body of knowledge on cerebral metabolic and blood flow changes, thereby providing stimulus for future work on the use of these metrics in the study of brain ageing and associated cognitive impairment, and may have utility in supporting the assessment of preventative interventions to maintain healthy brain ageing in future.

The key findings of this thesis were:

- 1) No significant relationship was found between whole GM perfusion and age within the PVE-corrected and smoothed perfusion maps after inclusion of sex and GM volume as**

covariates, however a significant decrease ( $p < 0.001$ ) was found in the cortical GM. It is notable that whole GM perfusion significantly declined with age after sex and GM volume covariate inclusion, when assessed in the original perfusion maps which had not undergone PVE-correction or smoothing ( $p = .044$ ), highlighting the impact of processing decisions on subsequent results.

- 2) A PCA-derived spatial covariance pattern of the relationship between age and cerebral perfusion, with five-fold validation, supports the assertion that multivariate analysis techniques can elucidate more subtle changes than univariate methodology. The spatial covariance pattern within the full cohort exhibited positive associations with age in regions including parts of the cerebellum, cuneus, precuneus, occipital cortex, temporal and frontal poles, frontal, angular, postcentral, temporal cingulate, paracingulate, anterior and posterior supramarginal gyri, and superior parietal lobules. Negative associations with age were found in parts of the cerebellum, occipital cortex, frontal pole, frontal, temporal and anterior parahippocampal gyri, sub-callosal cortex, and the left and right thalami.
- 3) This thesis also evidences what is, to the best of our knowledge, the first use of sCoV across a healthy age span and found closer associations between sCoV and age than CBF and age.
- 4) PCA was also used to establish a complex relationship between MoCA scores and cerebral perfusion. The resultant pattern is characterised by positive clusters across much of the GM, and negative clusters including parts of the occipital, frontal, and left parietal lobes, and the right caudate.

- 5) **This study was the first – to our knowledge – to assess a proposed cognitive resilience signature (Arenazo-Urquijo et al., 2019) within an ASL cohort, comprising the bilateral ACC and anterior temporal poles. A trend towards a significant increase in perfusion of this signature with increasing MoCA score was found ( $p = 0.08$ ), after controlling for age, sex and GM volume.**
- 6) **Use of a long-TE semi-LASER approach to acquire Lac spectra during visual stimulation, and subsequent calculation of ‘absolute’ Lac concentration was evidenced to be feasible in old subjects.**
- 7) **Time course changes of Lac concentration were significantly higher during stimulation when compared with rest, but not significantly different between stimulation and recovery, in the young cohort. There were no significant differences in Lac concentration across the full time course within the full cohort of old subjects.**

Many of these findings are novel, and advance understanding of healthy brain ageing and the usefulness of both cerebral perfusion and fMRS metrics in this field. Additionally, this thesis provides critique of novel methodology and highlights limitations which require consideration in future work.

## 6.2. Limitations and methodological problems

There are various limitations within this thesis which should be considered.

Firstly, in both Chapters 3 and 4, PCA approaches are employed, using a script which is designed to be able to account for many additional covariates.

Unfortunately, numerous covariates of interest – for example years of education, APOE status, smoking status, body mass index (BMI) – were not available within the respective datasets. This was due to the retrospective nature of the studies, which required multiple cohorts to be pooled, with these cohorts having limited overlap of available phenotypic data. It is notable that more covariates were available within ADNI-3, but unfortunately many subjects with 3D PCASL data were missing some or all of the additional information of interest, and there were simply not enough subjects where it was available to warrant a subgroup analysis given the individual variance which can be seen in cerebral perfusion measures (Parkes, Rashid, Chard and Tofts, 2004). These additional covariates would also be relevant to the FSL-randomise and FSL-flameo analyses. Additionally, inclusion of any relevant covariate is particularly important given that it is challenging to recruit definitively healthy subjects, as they possibly have a preclinical condition which may be relevant to the variable under assessment. Regarding the ASL studies in this thesis, it is also important to note that registration, PVE-correction and smoothing are large topics in their own right, and there is no consensus approach within the field. As such, the Pearson's cross correlation method was used to attempt to quantify which of two registration approaches was more successful, and that approach used subsequently. PVE-correction was considered imperative within this work due to the investigation of ageing, where perfusion alterations are co-incident with structural changes, and evidence of significant perfusion changes disappearing after PVE-correction (see Chapter 3). The approaches used here were chosen with the intention of addressing these concerns with minimal change from the original unprocessed perfusion maps.

During the scoping phase in December 2019, it was proposed that the work in Chapter 4 also included MCI and AD cohorts to extend the analysis across the healthy ageing-MCI-AD spectrum. Unfortunately, there were not enough subjects whose data was acquired using 3D PCASL, which passed quality control, and had MoCA score information available. Whilst the sample sizes of the ASL studies within this thesis are broadly comparable to others within the field, the fMRS work in Chapter 5 would benefit greatly from the inclusion of more subjects. Particularly within the older cohort, results were very challenging to interpret due to the inter-subject variance in Lac time courses. Whilst recruitment of additional subjects was intended, this study was met with particular difficulties due to the necessity for good vision in older subjects, as well as prolonged hardware issues and the coronavirus lockdown stalling such experiments.

Generalising from studies with sample sizes comparable to those used here is impossible, making validation vital. Whilst this is proposed within this work – and actioned as five-fold validation in Chapter 3 – true validation requires an external unseen cohort. The necessity for such validation is particularly evident where the results of current work deviate from that presented in the literature. The ‘gold standard’ in ageing research remains longitudinal studies, and the cross-sectional nature of the current studies is resultantly a weakness, albeit still very informative.

Another limitation of this thesis is the lack of opportunity to compare the sCoV measures directly with ATT (Chapter 3). Given the relatively recent interest in sCoV and particularly its use as a study metric of interest as opposed to an

assessment of perfusion map quality as part of image processing, direct comparison of these measures is imperative to understand if sCoV can truly be a proxy of ATT. That is not to negate the information gained from the work within this thesis regarding spatial variance, but simply to highlight that this is required if sCoV is to become a more standardised assessment metric when only single-PLD data is available. At the time of completing the work in Chapter 4, the resilience signature proposed by Arenaza-Urquijo et al. (2019) had not yet been validated within an ASL cohort, to our knowledge. Whilst the current work highlights a potential interesting relationship between this signature and MoCA scoring, reaching strong conclusions regarding its value as a metric is therefore unwise. The results of analysis of vascular territories, and particularly watershed regions, should also be considered with caution, and either a standardised, robust atlas or an individual subject approach to defining vascular territories is necessary to begin to generalise such findings. Whilst VE-ASL provides opportunity to address the second point, this approach is far less common than the white paper-recommended single-PLD 3D PCASL approach.

When considering the Lac investigations (Chapter 5), there are also some key limitations. Possibly the most critical of these is the limitations of sample size, which have already been addressed. Potential confusion of MMs with Lac is interesting and warrants further investigation, however despite various discussions with MRS experts at the University of Nottingham, it remains unclear how best to address this whilst retaining the subject within the cohort. The field bias to the use of LCModel and reliance on CLRBS as a quality metric should also be noted, although it is doubtful that a shift away from this will be seen anytime soon, as since early 2021, LCModel software is now free.

The coronavirus pandemic had a noteworthy impact upon the work within this thesis. Much of the investigative work proposed within Section 6.3. was intended to be carried out during the time in which the UK was under strict lockdown guidelines and it was therefore unfeasible to acquire data. Whilst the University of Nottingham began to open again in mid-2020, knock-on delays and a focus on coronavirus-related MRI research continued to hold these projects back. As such, these projects are only just beginning to start back up at the time of thesis submission.

### 6.3. Future directions

A few future directions have been alluded to in this thesis, which are expanded on here, alongside some other possible directions for fruitful subsequent work. Specifically, beyond addressing the limitations and methodological problems discussed in the previous section, there are various interventional approaches which would further the understanding of the results of this thesis, particularly the fMRS work. Further investigation is pertinent to the understanding of both healthy ageing and cognitive decline, particularly given the disappointing results of many clinical trials, and the increased attention regarding breaking ground in these areas.

#### 6.3.1. Furthering ASL investigation of cerebral perfusion

When considering the studies herein, validation and additional covariates to improve model quality are the first-line developments that are required to improve this work. Furthermore, validation of the resilience signature using ASL is particularly required, ideally in direct comparison with FDG-PET.

Continuation of the ASL work within this thesis is the proposed topic for an upcoming BMedSci study, and would make use of the TILDA cohort, as was the intention as part of this thesis. Unfortunately, TILDA access was not secured until just prior to submission of this thesis, due in part to the knock-on effects of the coronavirus pandemic, and was therefore validation within this cohort was no longer a feasible part of this thesis.

ASL would be an ideal methodology for clinical uptake, given the lack of ionising radiation and ease of adding a sequence to MR protocols that are already in use to support diagnosis in dementia. However, more work is needed to determine a possible robust cerebral perfusion biomarker.

Longitudinal studies continue to be the gold-standard of elucidating predisposing or causal factors to disease progression, yet are challenging to run due to the complexity of design and the associated costs. Nevertheless, longitudinal design within very large cohorts such as UKBiobank should be strived for in subsequent ASL studies, as the additional information available with such studies over cross-sectional ones may be pertinent to the identification of a robust, related biomarker.

### 6.3.2. Furthering MRS investigation of cerebral metabolism

The use of fMRS can provide a great deal of information about metabolism underlying cerebral functionality. However, manipulation of Lac through use of an unnatural checkerboard stimulus, as per the work in Chapter 5, does not consider the potential of compensatory Lac in a real-world context, or assess metabolism adjacent to Lac metabolism. As such, two further studies into Lac and its associated metabolism are proposed. These are an exercise-based

study of Lac metabolism using fMRS, and investigation of pyruvate in healthy ageing and cognitive impairment using DNP-MRI.

#### *6.3.2.1. Investigation of lactate metabolism during exercise using fMRS at 7T*

Physical activity has been shown to have a positive effect upon general body and cognitive health (Scully et al., 1998; Saxena, Van Ommeren, Tang and Armstrong, 2005; Warburton, Nicol and Bredin, 2006; Vina, Sanchis-Gomar, Martinez-Bello and Gomez-Cabrera, 2012; Reiner, Niermann, Jekauc and Woll, 2013; Nystoriak and Bhatnagar, 2018; De la Rosa et al., 2020). As such, there is increased interest in the use of exercise as a preventative or symptom-modifying treatment of various diseases. Given that low physical activity levels are a known risk factor for AD (De la Rosa et al., 2020), greater knowledge of exercise-induced changes in cerebral metabolism would enable more informed recommendations of appropriate exercise approaches for symptom management, on a case-by-case basis. This could be assessed by performing sustained metabolic challenge tasks which aim to assess changes in cerebral Lac metabolism over time, before, during and after transient exercise.

#### **Proposed study design and analysis**

*[The subsequent study was originally designed to be part of Chapter 5 of this thesis, and the protocol has already received ethical approval from the Faculty of Medicine and Health Sciences Research Committee at the University of Nottingham (Ref: 1-1804, part of umbrella ethics Ref: 162-1711 ). However, issues with the hardware of the 7T MRI scanner arose, which were followed by the coronavirus pandemic, and prevented study commencement. My role*

*within this study was in its conception and design, and additionally in acquisition, analysis and write up, had this gone forward during my PhD].*

The aim of such a future study would be to establish whether exercise has a statistically significant restorative impact upon neuroenergetic metabolism. Two cohorts of subjects, 20 young and 20 old, as defined in the previous study (half of each cohort exercising to 40% of maximal, half at 80% of maximal (Torchi et al., 2019)) would first undergo physiological testing using standard measures of heart rate,  $VO_2$  max, and  $O_2$  consumption to determine study suitability. This would also be used to determine the intensity at which they should subsequently exercise during the main study. They would be given an assessment of their general physical activity, such as the Rapid Assessment of Physical Activity (RAPA, Topolski et al., 2006), answer questions pertaining to their general health and lifestyle, and be given a fitness tracker to monitor their physical activity for the following week, prior to an MRI session. At the MRI session, subjects would undergo MoCA testing (Nasreddine et al., 2005), and baseline T1 and fMRS measures prior to 15 minutes of sub-maximal exercise (tailored to their individual abilities) using an MR-compatible cycle ergometer (see *Figure 6.3.1.*). This would be followed by a post-exercise fMRS protocol, with heart rate monitored throughout by a researcher. During scanning, all safety procedures would be followed, including the provision of ear protection, and the subject would be able to communicate with the researchers throughout, using an intercom system. Study visits are summarised in *Figure 6.3.2.*

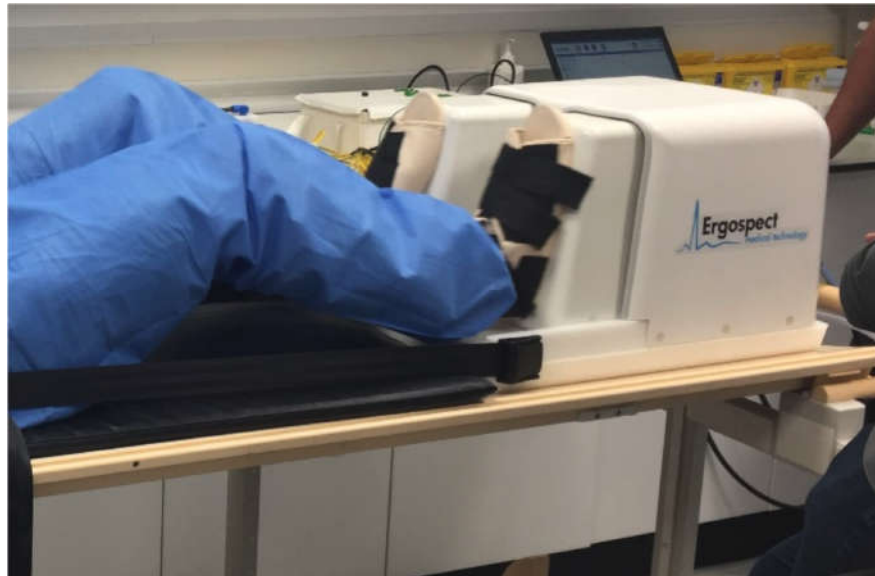


**Figure 6.3.1.:** The Ergospect pedal which would be used for sub-maximal exercise within the MRI scanner.

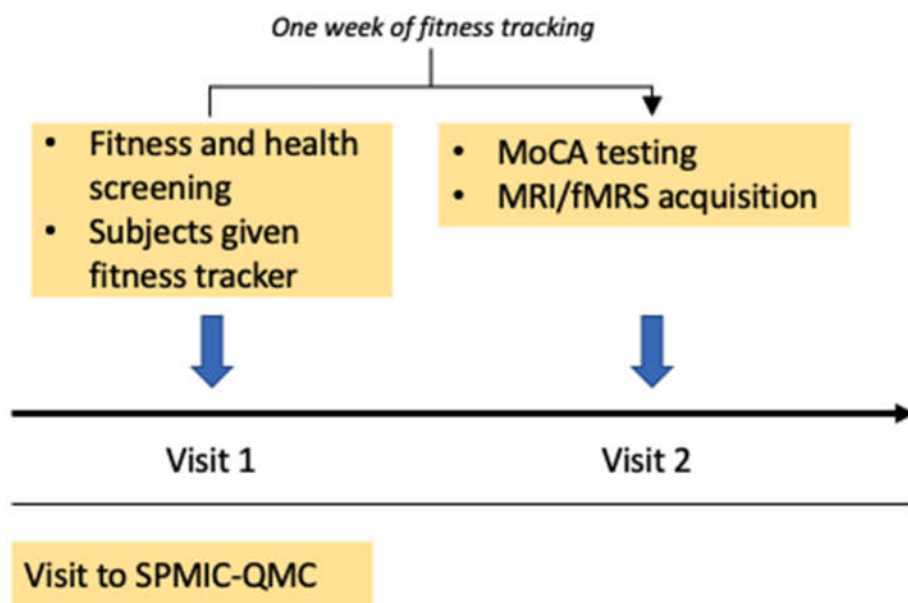


**Figure 6.3.2.:** Summary of study visit timings. Subjects would undergo fitness testing and a general health screening during Visit 1, to ensure they are able to partake safely in the study. If suitable, they would then be given a fitness tracker to monitor their activity for one week, with Visit 2 occurring at the end of that week. During Visit 2, they will undergo MoCA testing before the main MRI/fMRS study.

For fMRS acquisition, the VOI would be positioned within an appropriate motor region, as determined by fMRI investigation as part of protocol setup, and tailored to the activation pattern seen in live monitoring for each subject. Data would be processed and analysed following the same methods discussed in Chapter 5, using a combination of MATLAB, LCModel, and SPM12. The full spectral time course for each subject would be assessed as per Chapter 5, and comparisons drawn between baseline and post-exercise fMRS measures. Changes in levels of Lac, Glu, NAA and tCr relative to the onset of stimulus would also be reported, and group analysis used to confirm whether any patterns seen are representative of the cohort. The cognitive test results would be analysed to determine correlations between them and baseline/post-exercise Lac concentrations. Statistical comparisons would also be made between cerebral perfusion measures in the VOI used for Lac investigation, and the Lac concentrations within the VOI. Such an analysis approach would then allow for comparison with follow-up work on the metabolic changes in cognitively impaired individuals with exercise intervention. It should also be noted that researchers would, of course, be open to field developments in analysis approaches, and re-designing the study accordingly (if appropriate).

Outcome measures will include: (i) descriptive analysis of temporal metabolic patterns and characterisation of their properties, (ii) any significant age effects, (iii) effect of exercise on the metabolism of lactate, and (iv) correlation to cognitive performance.

### **Analysis**

Spectral quality would be evaluated in terms of CRLBs, concentrations, linewidth, signal-to-noise and the visual fit to the basis set. Data will be analysed using a variety of software including t-tests for group analysis in SPSS, and spectral analysis using MATLAB and LCModel.

### **Anticipated results**

The results of this study would be expected to show an increase in cerebral Lac after a brief period of sub-maximal exercise, with older subjects having a higher baseline Lac concentration, and taking longer to recover to baseline after exercise. Ideally, a follow-up fMRS scan would be carried out, expected to evidence that the Lac time course in older subjects would begin to follow the pattern characteristic of young subjects, if exercise interventions were continued at home over time. This would suggest an improved capacity for a Lac-focused compensatory response in conditions of decreased Glc availability.

### **Considerations**

Whilst using a pedal in the MR scanner in order to replicate cycling is an artificial approach which does not account for the weight-bearing aspect of most exercise and is unlikely to be the most common type of exercise recommended to individuals with conditions of cognitive impairment and associated symptomatology. The proposed approach would still expand the body of knowledge pertaining to the nuances of cerebral metabolic change that exercise can induce. The protocol is defined as such as the Ergospect

allows for exercise to occur without moving the subject in and out of the scanner bore, however could be modified for use in aged or cognitively impaired cohorts, for example with a pedal exerciser, although studies assessing these have shown poor results due to lack of adherence (Cancela Carral, Pallin, Orbegozo and Ayan Perez, 2017; McGowan et al., 2018). Nevertheless, explicit knowledge regarding the potential metabolic benefits of exercise could further inform public health initiatives which aim to decrease the socio-economic burden of conditions such as dementia upon global economies.

*6.3.2.2. Investigation of pyruvate metabolism in healthy ageing and cognitive impairment using dynamic nuclear polarisation magnetic resonance imaging*

Lac has an intimate relationship with pyruvate, with pyruvate undergoing conversion to Lac during anaerobic glycolysis. Investigation of pyruvate metabolism in the brain has recently been achieved with the use of DNP-MRI (Grist et al., 2019), a technique which uses an infusion of hyperpolarised [1-<sup>13</sup>C]pyruvate to increase the magnitude of its MR signal by a factor of ~10,000 (Ardenkjær-Larsen et al., 2003). DNP-MRI therefore provides a unique approach to the study of the regulation of cerebral pyruvate metabolism, whilst providing complementary information to that of the <sup>1</sup>H-fMRS acquisitions. DNP-MRI probes the metabolism at a much shorter timescale, and can provide information pertaining to the metabolism which links Glc and Lac, thereby traversing the metabolic gap that exists within this thesis due to the current methodology employed.

### **Proposed study design and analysis**

*[N.B. - This study has ethical approval from the Faculty of Medicine and Health Sciences Research Ethics Committee [Ref: 416-1911] and funding from LifeCycle 5, but has been delayed due to the coronavirus pandemic. My role within the study has been in the conception and design of the fMRS section of the study, as well as part of the team determining the visual stimulation for use in the DNP study. Prior to the pandemic, the intention was for me to also be responsible for the running of the fMRS section of the experiment, to be responsible for the visual stimulation during DNP acquisition, and subsequently collaborate on analysis and write-up alongside my DNP-focused colleagues].*

The proposed study would aim to assess the regulation of pyruvate metabolism in the brains of healthy young subjects in comparison to healthy older subjects, with scope to also investigate subjects with MCI or early dementia. Subjects would attend a screening session, at which they would complete general health questionnaires, and view the experimental setup prior to confirming their desire to take part in the study. They would then be invited to attend two further sessions, where they would undergo the DNP-MRI visual stimulation experiment, and a <sup>1</sup>H-fMRS Lac experiment as per the study in Chapter 5, for comparison. A summary of proposed experimental procedures is summarised in *Figure 6.3.3.*

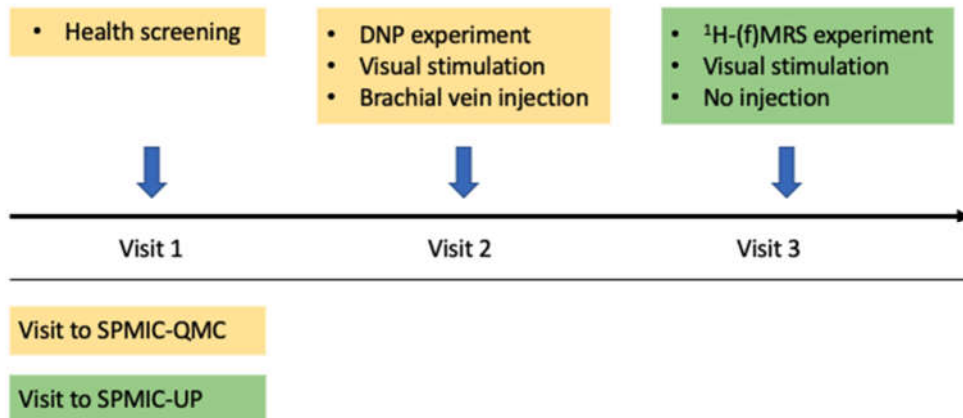


**Figure 6.3.3.:** Summary of DNP experimental protocol. A health screening visit of around 30 minutes would be required prior to the experimental study visit to the MR Centre. The DNP MRI visit would last approximately 120 minutes - the first 60 minutes for preparation, and the MR scan, and another 60 minutes for monitoring afterwards, during which drinks would be provided. The <sup>1</sup>H-fMRS visit will last approximately 60 minutes.

### **Visit 1 - Health screening**

Subjects responding to poster advertisements will be sent an information sheet with overview of the study protocol. Additional subject recruitment may also involve the use of databases of subjects who have consented to future contact for new studies, if suitable. Those expressing interest in study participation would then be invited to attend the Sir Peter Mansfield Imaging Centre in QMC (SPMIC-QMC) at a convenient time, for a medical screening visit lasting ~30 minutes. They would be asked to complete general health and MRI safety questionnaires, and consent to study participation. If they have any metallic material implanted on or in the body, suffer from claustrophobia, have a waist circumference of >150cm, or have large tattoos, they would not be suitable to participate in the study. This visit would also allow subjects to see

the laboratory and equipment which will be used during the study visits. Any questions would also be answered. If their responses to the questionnaires are satisfactory, subjects will be invited to sign a consent form and to attend two experimental visits. There would be no specific time requirement for the completion of all visits, but these would be scheduled to occur within a reasonable timeframe of no more than six months. There would be an inconvenience allowance of £200 per subject for participation in the study.

### **Visit 2 - Hyperpolarised [1-<sup>13</sup>C]pyruvate MRS study**

On the evening prior to this study, subjects would be asked to eat a standard balanced meal and abstain from alcohol. This visit would always take part in the afternoon due to the need to polarise samples in the morning (~3 hours). Subjects would then attend a thermoneutral laboratory (temperature = 22°C) at approximately 1pm at SPMIC-QMC, and a cannula inserted in the brachial vein. This would be performed by a research nurse or doctor following local anaesthetic administration. They would then be transferred to the 3T MR scanner also located in SPMIC-QMC to undergo their DNP-MRI scan, prior to which they would be given a standard MRI safety questionnaire.

After being positioned within the magnet, a pulse oximeter would be placed on subjects for monitoring oxygen saturation. Initial anatomical scans would then be carried out, before a 5-minute assessment of the response to visual stimulation. The intravenous line would then be used to administer a sterile hyperpolarised <sup>13</sup>C pyruvate solution (35ml at a rate of 5ml/sec; 0.43ml/kg at 260mM) by a designated clinician. Localised hyperpolarised <sup>13</sup>C MRS of the brain would then be performed, measuring <sup>13</sup>C-labelled metabolites (pyruvate,

lactate, alanine and bicarbonate) either during a visual stimulus, presented through MR-compatible LED goggles, or in darkness (LED goggles off).

Throughout the experiment, heart rate and oxygen saturation would be recorded. If the subject feels uncomfortable at any time, they will have a buzzer to press to alert the researchers, and the study will be terminated. Given the requirement for fasting prior to the experiment, a drink and snack will be provided after scanning. This visit would be expected to last ~120 minutes. No adverse events would be expected, as such infusions have been previously performed in healthy subjects at SPMIC-QMC, albeit in muscle (Torchi et al., 2019), and within the brain at other institutions (Grist et al., 2019).

### **Visit 3 - fMRS investigation at 7T**

The protocol employed within this visit would be as per the work in Chapter 5 of this thesis.

#### **Summary of outcome measures**

- Further establishment of DNP MRI methodology in the detection of products of pyruvate metabolism (lactate, alanine and bicarbonate) in the human brain.
- Measurement of regional differences in production rates of these metabolic products under baseline conditions and during visual stimulation.

- Assessment of relative importance of aerobic and anaerobic responses to a visual stimulus in healthy subjects
- Assessment of the suitability of the methodology developed for investigating these responses in patients with cerebrovascular and neurodegenerative disease in future studies.

### Sample size

There is very little published data on hyperpolarized  $^{13}\text{C}$  pyruvate studies in the brain upon which an accurate power analysis could be based. However, hyperpolarized  $^{13}\text{C}$  pyruvate studies generally have a coefficient of variation of about 25%. Given that the expected change in metabolic rate in the visual cortex is about 50% (Chhina et al., 2001), six subjects would be required (80% power at 5% significance using a paired t-test) to detect this. Power analysis (G\*Power version 3.1; Faul, Erdfelder, Lang and Buchner, 2007) performed on the work of Lin et al. (2012) predicted  $n=8$  per group. To account for the results of both tests, and the desire to observe regional differences in basal regional metabolic rate which are likely to be smaller, this study would aim to recruit up to 20 volunteers, 10 per group, in case of volunteer drop-out.

### 6.4. Conclusion

This thesis employed complementary resting-state cerebral perfusion and functional metabolic approaches to investigate healthy brain ageing. When considering cerebral perfusion, the use of PCA begins to define the complexity of this relationship, with a methodological advantage over voxel-wise and regional or network measures, but also highlights the necessity for additional covariates which potentially influence this relationship. Similar

conclusions are also reflected in the MoCA-PCA model within this thesis. Nevertheless, initial findings do have explanatory power, and are designed to include modified covariates and be validated in future. Additionally, the sCoV metric appears to have great future potential but requires further investigation, particularly in direct comparison to ATT, before more certain conclusions can be drawn regarding its utility. Further investigation in vascular territories would also be of interest but requires such territories to be more consistently defined. As part of this PhD, the first attempt to acquire Lac fMRS at 7T in older subjects was carried out successfully but does highlight greater variance in inter-subject temporal behaviour than the younger cohort.

Overarchingly, this thesis reveals cerebral perfusion and metabolic changes with age and supports the assertion that they may be implicated in healthy ageing. The findings herein are highly novel, and various advancements have been made. Specifically, this thesis includes the first use of PCA to derived a spatial covariance pattern between perfusion and MoCA scores, investigation of sCoV across a healthy age span, replication of a previously-defined FDG-PET resilience signature (Arenaza-Urquijo et al., 2019) within ASL data, and acquisition of Lac fMRS within an older cohort. Further study directions were also explored, but were unable to commence due to the time implications of the coronavirus pandemic. The findings of this thesis broaden the knowledge around healthy ageing, and therefore may contribute to subsequent translation efforts for both clinical diagnostics and treatment approaches.

## 7. References and appendices

### 7.1. References

- Aanerud, J., Borghammer, P., Chakravarty, M.M., Vang, K., Rodell, A.B., Jonsdottir, K.Y., Møller, A., Ashkanian, M., Vafaei, M.S., Iversen, P. and Johannsen, P., 2012. Brain energy metabolism and blood flow differences in healthy aging. *Journal of Cerebral Blood Flow & Metabolism*, 32(7), pp.1177-1187.
- Ackerman, J.J., Ewy, C.S., Kim, S.G. and Shalwitz, R.A., 1987. Deuterium magnetic resonance in vivo: the measurement of blood flow and tissue perfusion. *Annals of the New York Academy of Sciences*, 508, pp.89-98.
- Addicott, M.A., Yang, L.L., Peiffer, A.M., Burnett, L.R., Burdette, J.H., Chen, M.Y., Hayasaka, S., Kraft, R.A., Maldjian, J.A. and Laurienti, P.J., 2009. The effect of daily caffeine use on cerebral blood flow: How much caffeine can we tolerate?. *Human brain mapping*, 30(10), pp.3102-3114.
- Alber, J., Alladi, S., Bae, H.J., Barton, D.A., Beckett, L.A., Bell, J.M., Berman, S.E., Biessels, G.J., Black, S.E., Bos, I. and Bowman, G.L., 2019. White matter hyperintensities in vascular contributions to cognitive impairment and dementia (VCID): knowledge gaps and opportunities. *Alzheimer's & Dementia: Translational Research & Clinical Interventions*, 5(1), pp.107-117.
- Alexander, G.E., Chen, K., Pietrini, P., Rapoport, S.I. and Reiman, E.M., 2002. Longitudinal PET evaluation of cerebral metabolic decline in dementia: a potential outcome measure in Alzheimer's disease treatment studies. *American Journal of Psychiatry*, 159(5), pp.738-745.
- Alsaedi, A., Thomas, D., Bisdas, S. and Golay, X., 2018. Overview and critical appraisal of arterial spin labelling technique in brain perfusion imaging. *Contrast media & molecular imaging*, 2018.
- Alshuft, H.M., Condon, L.A., Dineen, R.A. and Auer, D.P., 2016. Cerebral cortical thickness in chronic pain due to knee osteoarthritis: the effect of pain duration and pain sensitization. *PloS one*, 11(9), p.e0161687.
- Alsing, K.K., Johannesen, H.H., Hansen, R.H. and Serup, J., 2020. Tattoo complications and magnetic resonance imaging: a comprehensive review of the literature. *Acta Radiologica*, 61(12), pp.1695-1700.
- Alsop, D.C., Casement, M., de Bazelaire, C., Fong, T. and Press, D.Z., 2008. Hippocampal hyperperfusion in Alzheimer's disease. *Neuroimage*, 42(4), pp.1267-1274.
- Alsop, D.C., Dai, W., Grossman, M. and Detre, J.A., 2010. Arterial spin labeling blood flow MRI: its role in the early characterization of Alzheimer's disease. *Journal of Alzheimer's Disease*, 20(3), pp.871-880.
- Alsop, D.C., Detre, J.A. and Grossman, M., 2000. Assessment of cerebral blood flow in Alzheimer's disease by spin-labeled magnetic resonance imaging. *Annals of neurology*, 47(1), pp.93-100.

Alsop, D.C., Detre, J.A., Golay, X., Günther, M., Hendrikse, J., Hernandez-Garcia, L., Lu, H., MacIntosh, B.J., Parkes, L.M., Smits, M. and Van Osch, M.J., 2015. Recommended implementation of arterial spin-labeled perfusion MRI for clinical applications: A consensus of the ISMRM perfusion study group and the European consortium for ASL in dementia. *Magnetic resonance in medicine*, 73(1), pp.102-116.

Alzheimer's Association, 2019. 2019 Alzheimer's disease facts and figures. *Alzheimer's & dementia*, 15(3), pp.321-387.

Amen, D.G., Egan, S., Meysami, S., Raji, C.A. and George, N., 2018. Patterns of regional cerebral blood flow as a function of age throughout the lifespan. *Journal of Alzheimer's Disease*, 65(4), pp.1087-1092.

Andersen, L.W., Mackenhauer, J., Roberts, J.C., Berg, K.M., Cocchi, M.N. and Donnino, M.W., 2013, October. Etiology and therapeutic approach to elevated lactate levels. In *Mayo Clinic Proceedings* (Vol. 88, No. 10, pp. 1127-1140). Elsevier.

Ardenkjær-Larsen, J.H., Fridlund, B., Gram, A., Hansson, G., Hansson, L., Lerche, M.H., Servin, R., Thaning, M. and Golman, K., 2003. Increase in signal-to-noise ratio of > 10,000 times in liquid-state NMR. *Proceedings of the National Academy of Sciences*, 100(18), pp.10158-10163.

Arenaza-Urquijo, E.M., Przybelski, S.A., Lesnick, T.L., Graff-Radford, J., Machulda, M.M., Knopman, D.S., Schwarz, C.G., Lowe, V.J., Mielke, M.M., Petersen, R.C. and Jack Jr, C.R., 2019. The metabolic brain signature of cognitive resilience in the 80+: beyond Alzheimer pathologies. *Brain*, 142(4), pp.1134-1147.

Arevalo-Rodriguez, I., Smailagic, N., i Figuls, M.R., Ciapponi, A., Sanchez-Perez, E., Giannakou, A., Pedraza, O.L., Cosp, X.B. and Cullum, S., 2015. Mini-Mental State Examination (MMSE) for the detection of Alzheimer's disease and other dementias in people with mild cognitive impairment (MCI). *Cochrane Database of Systematic Reviews*, (3).

Arnemann, K.L., Stöber, F., Narayan, S., Rabinovici, G.D. and Jagust, W.J., 2018. Metabolic brain networks in aging and preclinical Alzheimer's disease. *NeuroImage: Clinical*, 17, pp.987-999.

Asllani, I., Borogovac, A. and Brown, T.R., 2008. Regression algorithm correcting for partial volume effects in arterial spin labeling MRI. *Magnetic Resonance in Medicine: An Official Journal of the International Society for Magnetic Resonance in Medicine*, 60(6), pp.1362-1371.

Asllani, I., Habeck, C., Borogovac, A., Brown, T.R., Brickman, A.M. and Stern, Y., 2009. Separating function from structure in perfusion imaging of the aging brain. *Human brain mapping*, 30(9), pp.2927-2935.

Asllani, I., Habeck, C., Scarmeas, N., Borogovac, A., Brown, T.R. and Stern, Y., 2008. Multivariate and univariate analysis of continuous arterial spin labeling perfusion MRI in Alzheimer's disease. *Journal of Cerebral Blood Flow & Metabolism*, 28(4), pp.725-736.

Attwell, D. and Laughlin, S.B., 2001. An energy budget for signaling in the grey matter of the brain. *Journal of Cerebral Blood Flow & Metabolism*, 21(10), pp.1133-1145.

- Auer, D.P., Pütz, B., Kraft, E., Lipinski, B., Schill, J. and Holsboer, F., 2000. Reduced glutamate in the anterior cingulate cortex in depression: an in vivo proton magnetic resonance spectroscopy study. *Biological psychiatry*, 47(4), pp.305-313.
- Avants, B.B., Epstein, C.L., Grossman, M. and Gee, J.C., 2008. Symmetric diffeomorphic image registration with cross-correlation: evaluating automated labeling of elderly and neurodegenerative brain. *Medical image analysis*, 12(1), pp.26-41.
- Balsamo, S., Willardson, J.M., de Santana Frederico, S., Prestes, J. and Balsamo, D.C., 2013. Effectiveness of exercise on cognitive impairment and Alzheimer's disease. *International journal of general medicine*, 6, p.387.
- Banerjee, D., Muralidharan, A., Mohammed, A.R.H. and Malik, B.H., 2020. Neuroimaging in dementia: a brief review. *Cureus*, 12(6).
- Baranowski, B.J., Marko, D.M., Fenech, R.K., Yang, A.J. and MacPherson, R.E., 2020. Healthy brain, healthy life: A review of diet and exercise interventions to promote brain health and reduce Alzheimer's disease risk. *Applied Physiology, Nutrition, and Metabolism*, 45(10), pp.1055-1065.
- Baron, J.C., 2001. Perfusion thresholds in human cerebral ischemia: historical perspective and therapeutic implications. *Cerebrovascular Diseases*, 11(Suppl. 1), pp.2-8.
- Bartel, F., Visser, M., de Ruiter, M., Belderbos, J., Barkhof, F., Vrenken, H., de Munck, J.C., van Herk, M. and Alzheimer's Disease Neuroimaging Initiative, 2019. Non-linear registration improves statistical power to detect hippocampal atrophy in aging and dementia. *NeuroImage: Clinical*, 23, p.101902.
- Bashyam, V.M., Erus, G., Doshi, J., Habes, M., Nasrallah, I.M., Truelove-Hill, M., Srinivasan, D., Mamourian, L., Pomponio, R., Fan, Y. and Launer, L.J., 2020. MRI signatures of brain age and disease over the lifespan based on a deep brain network and 14 468 individuals worldwide. *Brain*, 143(7), pp.2312-2324.
- Béard, E. and Braissant, O., 2010. Synthesis and transport of creatine in the CNS: importance for cerebral functions. *Journal of neurochemistry*, 115(2), pp.297-313.
- Bednařík, P., Tkáč, I., Deelchand, D., Barreto, F., Eberly, L.E., Michaeli, S. and Mangia, S., 2016. Functional MRS at 7T and long TE. In *Proceedings of the International Society for Magnetic Resonance in Medicine*, 24th Scientific Meeting and Exhibition, p. 3351.
- Bednařík, P., Tkáč, I., Giove, F., DiNuzzo, M., Deelchand, D.K., Emir, U.E., Eberly, L.E. and Mangia, S., 2015. Neurochemical and BOLD responses during neuronal activation measured in the human visual cortex at 7 Tesla. *Journal of Cerebral Blood Flow & Metabolism*, 35(4), pp.601-610.
- Beer, J.S., John, O.P., Scabini, D. and Knight, R.T., 2006. Orbitofrontal cortex and social behavior: integrating self-monitoring and emotion-cognition interactions. *Journal of cognitive neuroscience*, 18(6), pp.871-879.
- Beishon, L., Clough, R.H., Kadicheeni, M., Chithiramohan, T., Panerai, R.B., Haunton, V.J., Minhas, J.S. and Robinson, T.G., 2021. Vascular and

haemodynamic issues of brain ageing. *Pflügers Archiv-European Journal of Physiology*, pp.1-17.

Belloy, M.E., Napolioni, V. and Greicius, M.D., 2019. A quarter century of APOE and Alzheimer's disease: progress to date and the path forward. *Neuron*, 101(5), pp.820-838.

Benedictus, M.R., Leeuwis, A.E., Binnewijzend, M.A., Kuijjer, J.P., Scheltens, P., Barkhof, F., van der Flier, W.M. and Prins, N.D., 2017. Lower cerebral blood flow is associated with faster cognitive decline in Alzheimer's disease. *European radiology*, 27(3), pp.1169-1175.

Benoit, D. and Shovlin, J.P., 2003. Considerations in geriatric contact lens fittings: patients over the age of 60 have very specific needs, both physically and psychologically. *Review of Optometry*, 140(7), pp.31-34.

Bentourkia, M.H., Bol, A., Ivanoiu, A., Labar, D., Sibomana, M., Coppens, A., Michel, C., Cosnard, G. and De Volder, A.G., 2000. Comparison of regional cerebral blood flow and glucose metabolism in the normal brain: effect of aging. *Journal of the neurological sciences*, 181(1-2), pp.19-28.

Bergfield, K.L., Hanson, K.D., Chen, K., Teipel, S.J., Hampel, H., Rapoport, S.I., Moeller, J.R. and Alexander, G.E., 2010. Age-related networks of regional covariance in MRI gray matter: reproducible multivariate patterns in healthy aging. *Neuroimage*, 49(2), pp.1750-1759.

Bernstein, M.A., King, K.F. and Zhou, X.J., 2004. *Handbook of MRI pulse sequences*. Elsevier.

Bherer, L., Erickson, K.I. and Liu-Ambrose, T., 2013. A review of the effects of physical activity and exercise on cognitive and brain functions in older adults. *Journal of aging research*, 2013.

Bi, W., Gillespie-Gallery, H., Binns, A. and Barbur, J.L., 2016. Flicker sensitivity in normal aging—monocular tests of retinal function at photopic and mesopic light levels. *Investigative ophthalmology & visual science*, 57(2), pp.387-395.

Biagi, L., Abbruzzese, A., Bianchi, M.C., Alsop, D.C., Del Guerra, A. and Tosetti, M., 2007. Age dependence of cerebral perfusion assessed by magnetic resonance continuous arterial spin labeling. *Journal of Magnetic Resonance Imaging: An Official Journal of the International Society for Magnetic Resonance in Medicine*, 25(4), pp.696-702.

Bibic, A., Knutsson, L., Ståhlberg, F. and Wirestam, R., 2010. Denoising of arterial spin labeling data: wavelet-domain filtering compared with Gaussian smoothing. *Magnetic Resonance Materials in Physics, Biology and Medicine*, 23(3), pp.125-137.

Binnewijzend, M.A., Schoonheim, M.M., Sanz-Arigita, E., Wink, A.M., van der Flier, W.M., Tolboom, N., Adriaanse, S.M., Damoiseaux, J.S., Scheltens, P., van Berckel, B.N. and Barkhof, F., 2012. Resting-state fMRI changes in Alzheimer's disease and mild cognitive impairment. *Neurobiology of aging*, 33(9), pp.2018-2028.

Biomarkers Definitions Working Group, Atkinson Jr, A.J., Colburn, W.A., DeGruttola, V.G., DeMets, D.L., Downing, G.J., Hoth, D.F., Oates, J.A., Peck, C.C., Schooley, R.T. and Spilker, B.A., 2001. Biomarkers and surrogate

- endpoints: preferred definitions and conceptual framework. *Clinical pharmacology & therapeutics*, 69(3), pp.89-95.
- Biswal, B.B., Mennes, M., Zuo, X.N., Gohel, S., Kelly, C., Smith, S.M., Beckmann, C.F., Adelstein, J.S., Buckner, R.L., Colcombe, S. and Dogonowski, A.M., 2010. Toward discovery science of human brain function. *Proceedings of the National Academy of Sciences*, 107(10), pp.4734-4739.
- Bliss, E.S., Wong, R.H., Howe, P.R. and Mills, D.E., 2021. Benefits of exercise training on cerebrovascular and cognitive function in ageing. *Journal of Cerebral Blood Flow & Metabolism*, 41(3), pp.447-470.
- Blonz, E.R., 2017. Alzheimer's disease as the product of a progressive energy deficiency syndrome in the central nervous system: the neuroenergetic hypothesis. *Journal of Alzheimer's Disease*, 60(4), pp.1223-1229.
- Boillat, Y., Xin, L., Van der Zwaag, W. and Gruetter, R., 2020. Metabolite concentration changes associated with positive and negative BOLD responses in the human visual cortex: a functional MRS study at 7 tesla. *Journal of Cerebral Blood Flow & Metabolism*, 40(3), pp.488-500.
- Bonte, S., Vandemaele, P., Verleden, S., Audenaert, K., Deblaere, K., Goethals, I. and Van Holen, R., 2017. Healthy brain ageing assessed with 18F-FDG PET and age-dependent recovery factors after partial volume effect correction. *European Journal of Nuclear Medicine and Molecular Imaging*, 44(5), pp.838-849.
- Bonvento, G., Herard, A.S. and Voutsinos-Porche, B., 2005. The Astrocyte—Neuron Lactate Shuttle: A Debated but still Valuable Hypothesis for Brain Imaging. *Journal of Cerebral Blood Flow & Metabolism*, 25(10), pp.1394-1399.
- Bottomley, P.A., 1987. Spatial localization in NMR spectroscopy in vivo. *Annals of the New York Academy of Sciences*, 508(1), pp.333-348.
- Boucard, C.C., Mostert, J.P., Cornelissen, F.W., De Keyser, J., Oudkerk, M. and Sijens, P.E., 2005. Visual stimulation, 1 H MR spectroscopy and fMRI of the human visual pathways. *European radiology*, 15(1), pp.47-52.
- Bouhrara, M., Alisch, J.S., Khattar, N., Kim, R.W., Rejimon, A.C., Cortina, L.E., Qian, W., Ferrucci, L., Resnick, S.M. and Spencer, R.G., 2020. Association of cerebral blood flow with myelin content in cognitively unimpaired adults. *BMJ neurology open*, 2(1).
- Bouzat, P., Sala, N., Suys, T., Zerlauth, J.B., Marques-Vidal, P., Feihl, F., Bloch, J., Messerer, M., Levivier, M., Meuli, R. and Magistretti, P.J., 2014. Cerebral metabolic effects of exogenous lactate supplementation on the injured human brain. *Intensive Care Medicine*, 40(3), pp.412-421.
- Bouzier-Sore, A.K., Serres, S., Canioni, P. and Merle, M., 2003. Lactate involvement in neuron—glia metabolic interaction: 13C-NMR spectroscopy contribution. *Biochimie*, 85(9), pp.841-848.
- Bowling, A. and Dieppe, P., 2005. What is successful ageing and who should define it?. *Bmj*, 331(7531), pp.1548-1551.

- Brayne, C., 2007. The elephant in the room—healthy brains in later life, epidemiology and public health. *Nature Reviews Neuroscience*, 8(3), pp.233-239.
- Brody, D.J., Pratt, L.A. and Hughes, J.P., 2018. Prevalence of depression among adults aged 20 and over: United States, 2013-2016.
- Brown, G.C., 2015. Living too long: the current focus of medical research on increasing the quantity, rather than the quality, of life is damaging our health and harming the economy. *EMBO reports*, 16(2), pp.137-141.
- Brown, W.R. and Thore, C.R., 2011. Cerebral microvascular pathology in ageing and neurodegeneration. *Neuropathology and applied neurobiology*, 37(1), pp.56-74.
- Buracchio, T., Dodge, H.H., Howieson, D., Wasserman, D. and Kaye, J., 2010. The trajectory of gait speed preceding mild cognitive impairment. *Archives of neurology*, 67(8), pp.980-986.
- Buxton, R.B., Frank, L.R., Wong, E.C., Siewert, B., Warach, S. and Edelman, R.R., 1998. A general kinetic model for quantitative perfusion imaging with arterial spin labeling. *Magnetic resonance in medicine*, 40(3), pp.383-396.
- Cai, S., Peng, Y., Chong, T., Zhang, Y., M von Deneen, K., Huang, L. and Alzheimer's Disease Neuroimaging Initiative, 2017. Differentiated effective connectivity patterns of the executive control network in progressive MCI: a potential biomarker for predicting AD. *Current Alzheimer Research*, 14(9), pp.937-950.
- Camargo, A., Wang, Z. and Alzheimer's Disease Neuroimaging Initiative, 2021. Longitudinal Cerebral Blood Flow Changes in Normal Aging and the Alzheimer's Disease Continuum Identified by Arterial Spin Labeling MRI. *Journal of Alzheimer's Disease*, (Preprint), pp.1-9.
- Cameron, O.G., Modell, J.G. and Hariharan, M., 1990. Caffeine and human cerebral blood flow: a positron emission tomography study. *Life sciences*, 47(13), pp.1141-1146.
- Cancela Carral, J.M., Pallin, E., Orbegozo, A. and Ayan Perez, C., 2017. Effects of three different chair-based exercise programs on people older than 80 years. *Rejuvenation research*, 20(5), pp.411-419.
- Cano, S.J., Posner, H.B., Moline, M.L., Hurt, S.W., Swartz, J., Hsu, T. and Hobart, J.C., 2010. The ADAS-cog in Alzheimer's disease clinical trials: psychometric evaluation of the sum and its parts. *Journal of Neurology, Neurosurgery & Psychiatry*, 81(12), pp.1363-1368.
- Carradus, A.J., Mouglin, O., Hunt, B.A., Tewarie, P.K., Geades, N., Morris, P.G., Brookes, M.J., Gowland, P.A. and Madan, C.R., 2020. Age-related differences in myeloarchitecture measured at 7 T. *Neurobiology of Aging*, 96, pp.246-254.
- Carson, N., Leach, L. and Murphy, K.J., 2018. A re-examination of Montreal Cognitive Assessment (MoCA) cutoff scores. *International Journal of Geriatric Psychiatry*, 33(2), pp.379-388.
- Castelli, V., Benedetti, E., Antonosante, A., Catanesi, M., Pitari, G., Ippoliti, R., Cimini, A. and d'Angelo, M., 2019. Neuronal cells rearrangement during aging

and neurodegenerative disease: metabolism, oxidative stress and organelles dynamic. *Frontiers in molecular neuroscience*, 12, p.132.

Cavanna, A.E. and Trimble, M.R., 2006. The precuneus: a review of its functional anatomy and behavioural correlates. *Brain*, 129(3), pp.564-583.

Cavassila, S., Deval, S., Huegen, C., Van Ormondt, D. and Graveron-Demilly, D., 2001. Cramér–Rao bounds: an evaluation tool for quantitation. *NMR in Biomedicine: An International Journal Devoted to the Development and Application of Magnetic Resonance In Vivo*, 14(4), pp.278-283.

Cha, Y.H.K., Jog, M.A., Kim, Y.C., Chakrapani, S., Kraman, S.M. and Wang, D.J., 2013. Regional correlation between resting state FDG PET and pCASL perfusion MRI. *Journal of Cerebral Blood Flow & Metabolism*, 33(12), pp.1909-1914.

Chalela, J.A., Alsop, D.C., Gonzalez-Atavales, J.B., Maldjian, J.A., Kasner, S.E. and Detre, J.A., 2000. Magnetic resonance perfusion imaging in acute ischemic stroke using continuous arterial spin labeling. *Stroke*, 31(3), pp.680-687.

Chand, G.B., Wu, J., Hajjar, I. and Qiu, D., 2017. Interactions of the salience network and its subsystems with the default-mode and the central-executive networks in normal aging and mild cognitive impairment. *Brain connectivity*, 7(7), pp.401-412.

Chang, D., Song, D., Zhang, J., Shang, Y., Ge, Q. and Wang, Z., 2018. Caffeine caused a widespread increase of resting brain entropy. *Scientific reports*, 8(1), pp.1-7.

Chang, L., Ernst, T., Poland, R.E. and Jenden, D.J., 1996. In vivo proton magnetic resonance spectroscopy of the normal aging human brain. *Life sciences*, 58(22), pp.2049-2056.

Chappell, M., MacIntosh, B. and Okell, T., 2018. *Introduction to perfusion quantification using arterial spin labelling*. Oxford University Press.

Chappell, M.A., MacIntosh, B.J., Donahue, M.J., Günther, M., Jezzard, P. and Woolrich, M.W., 2010. Separation of macrovascular signal in multi-inversion time arterial spin labelling MRI. *Magnetic resonance in medicine*, 63(5), pp.1357-1365.

Chappell, M.A., McConnell, F.A.K., Golay, X., Günther, M., Hernandez-Tamames, J.A., van Osch, M.J. and Asllani, I., 2021. Partial Volume Correction in Arterial Spin Labeling Perfusion MRI: A method to disentangle anatomy from physiology or an analysis step too far?. *NeuroImage*, p.118236.

Chawluk, J.B., Alavi, A., Dann, R., Hurtig, H.I., Bais, S., Kushner, M.J., Zimmerman, R.A. and Reivich, M., 1987. Positron emission tomography in aging and dementia: effect of cerebral atrophy. *Age*, 65, p.9.

Chen, J.J., 2019. Functional MRI of brain physiology in aging and neurodegenerative diseases. *Neuroimage*, 187, pp.209-225.

Chen, J.J., Rosas, H.D. and Salat, D.H., 2011. Age-associated reductions in cerebral blood flow are independent from regional atrophy. *Neuroimage*, 55(2), pp.468-478.

- Chen, Y., Lv, C., Li, X., Zhang, J., Chen, K., Liu, Z., Li, H., Fan, J., Qin, T., Luo, L. and Zhang, Z., 2019. The positive impacts of early-life education on cognition, leisure activity, and brain structure in healthy aging. *Aging (Albany NY)*, 11(14), p.4923.
- Chen, Y., Wang, D.J. and Detre, J.A., 2012. Comparison of arterial transit times estimated using arterial spin labeling. *Magnetic Resonance Materials in Physics, Biology and Medicine*, 25(2), pp.135-144.
- Chhina, N., Kuestermann, E., Halliday, J., Simpson, L.J., Macdonald, I.A., Bachelard, H.S. and Morris, P.G., 2001. Measurement of human tricarboxylic acid cycle rates during visual activation by <sup>13</sup>C magnetic resonance spectroscopy. *Journal of neuroscience research*, 66(5), pp.737-746.
- Chih, C.P. and Roberts Jr, E.L., 2003. Energy substrates for neurons during neural activity: a critical review of the astrocyte-neuron lactate shuttle hypothesis. *Journal of Cerebral Blood Flow & Metabolism*, 23(11), pp.1263-1281.
- Cho, H., Choi, J.Y., Lee, S.H., Choi, Y.S., Ryu, Y.H., Lee, M.S. and Lyoo, C.H., 2017. Principal component analysis of tau PET in Alzheimer's disease and healthy elderly. *Alzheimer's & Dementia: The Journal of the Alzheimer's Association*, 13(7), pp.P133-P134.
- Christiansen, L., Sanmartin Berglund, J., Lindberg, C., Anderberg, P. and Skär, L., 2019. Health-related quality of life and related factors among a sample of older people with cognitive impairment. *Nursing open*, 6(3), pp.849-859.
- Cichocka, M. and Bereś, A., 2018. From fetus to older age: a review of brain metabolic changes across the lifespan. *Ageing Research Reviews*, 46, pp.60-73.
- Clark, J.B., 1998. N-acetyl aspartate: a marker for neuronal loss or mitochondrial dysfunction. *Developmental neuroscience*, 20(4-5), p.271.
- Cleeland, C., Pipingas, A., Scholey, A. and White, D., 2019. Neurochemical changes in the aging brain: A systematic review. *Neuroscience & Biobehavioral Reviews*, 98, pp.306-319.
- Cohen, J.R. and D'Esposito, M., 2016. The segregation and integration of distinct brain networks and their relationship to cognition. *Journal of Neuroscience*, 36(48), pp.12083-12094.
- Cole, J.H. and Franke, K., 2017. Predicting age using neuroimaging: innovative brain ageing biomarkers. *Trends in neurosciences*, 40(12), pp.681-690.
- Cole, J.H., 2017. Neuroimaging-derived brain-age: an ageing biomarker?. *Aging (Albany NY)*, 9(8), p.1861.
- Cole, J.H., Poudel, R.P., Tsagkrasoulis, D., Caan, M.W., Steves, C., Spector, T.D. and Montana, G., 2017. Predicting brain age with deep learning from raw imaging data results in a reliable and heritable biomarker. *NeuroImage*, 163, pp.115-124.
- Collin, L., Reisner, S.L., Tangpricha, V. and Goodman, M., 2016. Prevalence of transgender depends on the "case" definition: a systematic review. *The journal of sexual medicine*, 13(4), pp.613-626.

- Connelly, A., Jackson, G.D., Duncan, J.S., King, M.D. and Gadian, D.G., 1994. Magnetic resonance spectroscopy in temporal lobe epilepsy. *Neurology*, 44(8), pp.1411-1411.
- Cottam, W.J., Condon, L., Alshuft, H., Reckziegel, D. and Auer, D.P., 2016. Associations of limbic-affective brain activity and severity of ongoing chronic arthritis pain are explained by trait anxiety. *NeuroImage: Clinical*, 12, pp.269-276.
- Cottam, W.J., Iwabuchi, S.J., Drabek, M.M., Reckziegel, D. and Auer, D.P., 2018. Altered connectivity of the right anterior insula drives the pain connectome changes in chronic knee osteoarthritis. *Pain*, 159(5), p.929.
- Cui, Y., Liang, X., Gu, H., Hu, Y., Zhao, Z., Yang, X.Y., Qian, C., Yang, Y. and Teng, G.J., 2017. Cerebral perfusion alterations in type 2 diabetes and its relation to insulin resistance and cognitive dysfunction. *Brain imaging and behavior*, 11(5), pp.1248-1257.
- Cunnane, S.C., Nugent, S., Roy, M., Courchesne-Loyer, A., Croteau, E., Tremblay, S., Castellano, A., Pifferi, F., Bocti, C., Paquet, N. and Begdouri, H., 2011. Brain fuel metabolism, aging, and Alzheimer's disease. *Nutrition*, 27(1), pp.3-20.
- Cunnane, S.C., Trushina, E., Morland, C., Prigione, A., Casadesus, G., Andrews, Z.B., Beal, M.F., Bergersen, L.H., Brinton, R.D., de la Monte, S. and Eckert, A., 2020. Brain energy rescue: an emerging therapeutic concept for neurodegenerative disorders of ageing. *Nature Reviews Drug Discovery*, 19(9), pp.609-633.
- Curiati, P.K., Tamashiro-Duran, J.H., Duran, F.L.S., Buchpiguel, C.A., Squarzonni, P., Romano, D.C., Vallada, H., Menezes, P.R., Scazufca, M., Busatto, G.F. and Alves, T.C.T.F., 2011. Age-Related Metabolic Profiles in Cognitively Healthy Elders: Results from a Voxel-Based [18F] Fluorodeoxyglucose–Positron-Emission Tomography Study with Partial Volume Effects Correction. *American journal of neuroradiology*, 32(3), pp.560-565.
- Dagher, A., Owen, A.M., Boecker, H. and Brooks, D.J., 1999. Mapping the network for planning: a correlational PET activation study with the Tower of London task. *Brain*, 122(10), pp.1973-1987.
- Dai, W., Fong, T., Jones, R.N., Marcantonio, E., Schmitt, E., Inouye, S.K. and Alsop, D.C., 2017. Effects of arterial transit delay on cerebral blood flow quantification using arterial spin labeling in an elderly cohort. *Journal of Magnetic Resonance Imaging*, 45(2), pp.472-481.
- Dai, W., Garcia, D., De Bazelaire, C. and Alsop, D.C., 2008. Continuous flow-driven inversion for arterial spin labeling using pulsed radio frequency and gradient fields. *Magnetic Resonance in Medicine: An Official Journal of the International Society for Magnetic Resonance in Medicine*, 60(6), pp.1488-1497.
- Dai, W., Lopez, O.L., Carmichael, O.T., Becker, J.T., Kuller, L.H. and Gach, H.M., 2009. Mild cognitive impairment and alzheimer disease: patterns of altered cerebral blood flow at MR imaging. *Radiology*, 250(3), pp.856-866.

- Dai, Z., Yan, C., Li, K., Wang, Z., Wang, J., Cao, M., Lin, Q., Shu, N., Xia, M., Bi, Y. and He, Y., 2015. Identifying and mapping connectivity patterns of brain network hubs in Alzheimer's disease. *Cerebral cortex*, 25(10), pp.3723-3742.
- Dalrymple-Alford, J.C., MacAskill, M.R., Nakas, C.T., Livingston, L., Graham, C., Crucian, G.P., Melzer, T.R., Kirwan, J., Keenan, R., Wells, S. and Porter, R.J., 2010. The MoCA: well-suited screen for cognitive impairment in Parkinson disease. *Neurology*, 75(19), pp.1717-1725.
- Damoiseaux, J.S., Beckmann, C.F., Arigita, E.S., Barkhof, F., Scheltens, P., Stam, C.J., Smith, S.M. and Rombouts, S.A.R.B., 2008. Reduced resting-state brain activity in the "default network" in normal aging. *Cerebral cortex*, 18(8), pp.1856-1864.
- Damoiseaux, J.S., Rombouts, S.A.R.B., Barkhof, F., Scheltens, P., Stam, C.J., Smith, S.M. and Beckmann, C.F., 2006. Consistent resting-state networks across healthy subjects. *Proceedings of the national academy of sciences*, 103(37), pp.13848-13853.
- de Graaf, R.A., 2019. *In vivo NMR spectroscopy: principles and techniques*. John Wiley & Sons.
- De la Rosa, A., Olaso-Gonzalez, G., Arc-Chagnaud, C., Millan, F., Salvador-Pascual, A., García-Lucerga, C., Blasco-Lafarga, C., Garcia-Dominguez, E., Carretero, A., Correas, A.G. and Viña, J., 2020. Physical exercise in the prevention and treatment of Alzheimer's disease. *Journal of sport and health science*, 9(5), pp.394-404.
- de la Torre, J.C., 2004. Is Alzheimer's disease a neurodegenerative or a vascular disorder? Data, dogma, and dialectics. *The Lancet Neurology*, 3(3), pp.184-190.
- de La Torre, J.C., 2012. Cardiovascular risk factors promote brain hypoperfusion leading to cognitive decline and dementia. *Cardiovascular psychiatry and neurology*, 2012.
- de la Torre, J.C., 2017. Are Major Dementias Triggered by Poor Blood Flow to the Brain? Theoretical Considerations. *Journal of Alzheimer's disease: JAD*, 57(2), pp.353-371.
- De Vis, J.B., Hendrikse, J., Bhogal, A., Adams, A., Kappelle, L.J. and Petersen, E.T., 2015. Age-related changes in brain hemodynamics; A calibrated MRI study. *Human brain mapping*, 36(10), pp.3973-3987.
- De Vis, J.B., Peng, S.L., Chen, X., Li, Y., Liu, P., Sur, S., Rodrigue, K.M., Park, D.C. and Lu, H., 2018. Arterial-spin-labeling (ASL) perfusion MRI predicts cognitive function in elderly individuals: A 4-year longitudinal study. *Journal of Magnetic Resonance Imaging*, 48(2), pp.449-458.
- Deary, I.J., Gow, A.J., Pattie, A. and Starr, J.M., 2012. Cohort profile: the Lothian Birth Cohorts of 1921 and 1936. *International journal of epidemiology*, 41(6), pp.1576-1584.
- DeBette, S. and Markus, H.S., 2010. The clinical importance of white matter hyperintensities on brain magnetic resonance imaging: systematic review and meta-analysis. *Bmj*, 341.
- Dehghani, M., Do, K.Q., Magistretti, P. and Xin, L., 2020. Lactate measurement by neurochemical profiling in the dorsolateral prefrontal cortex

at 7T: accuracy, precision, and relaxation times. *Magnetic resonance in medicine*, 83(6), pp.1895-1908.

Demeestere, J., Wouters, A., Christensen, S., Lemmens, R. and Lansberg, M.G., 2020. Review of perfusion imaging in acute ischemic stroke: from time to tissue. *Stroke*, 51(3), pp.1017-1024.

Dempsey, M.F. and Condon, B., 2001. Thermal injuries associated with MRI. *Clinical radiology*, 56(6), pp.457-465.

Dennis, A., Thomas, A.G., Rawlings, N.B., Near, J., Nichols, T.E., Clare, S., Johansen-Berg, H. and Stagg, C.J., 2015. An ultra-high field magnetic resonance spectroscopy study of post exercise lactate, glutamate and glutamine change in the human brain. *Frontiers in Physiology*, 6, p.351.

Desikan, R.S., Ségonne, F., Fischl, B., Quinn, B.T., Dickerson, B.C., Blacker, D., Buckner, R.L., Dale, A.M., Maguire, R.P., Hyman, B.T. and Albert, M.S., 2006. An automated labeling system for subdividing the human cerebral cortex on MRI scans into gyral based regions of interest. *Neuroimage*, 31(3), pp.968-980.

Detre, J.A., Leigh, J.S., Williams, D.S. and Koretsky, A.P., 1992. Perfusion imaging. *Magnetic resonance in medicine*, 23(1), pp.37-45

Dickie, D.A., Valdés Hernández, M.D.C., Makin, S.D., Staals, J., Wiseman, S.J., Bastin, M.E. and Wardlaw, J.M., 2018. The brain health index: Towards a combined measure of neurovascular and neurodegenerative structural brain injury. *International Journal of Stroke*, 13(8), pp.849-856.

Dienel, G.A., 2012. Brain lactate metabolism: the discoveries and the controversies. *Journal of Cerebral Blood Flow & Metabolism*, 32(7), pp.1107-1138.

Ding, B., Ling, H.W., Zhang, Y., Huang, J., Zhang, H., Wang, T. and Yan, F.H., 2014. Pattern of cerebral hyperperfusion in Alzheimer's disease and amnesic mild cognitive impairment using voxel-based analysis of 3D arterial spin-labeling imaging: initial experience. *Clinical interventions in aging*, 9, p.493.

Dolui, S., Li, Z., Nasrallah, I.M., Detre, J.A. and Wolk, D.A., 2020. Arterial spin labeling versus 18F-FDG-PET to identify mild cognitive impairment. *NeuroImage: Clinical*, 25, p.102146.

Douaud, G., Menke, R.A., Gass, A., Monsch, A.U., Rao, A., Whitcher, B., Zamboni, G., Matthews, P.M., Sollberger, M. and Smith, S., 2013. Brain microstructure reveals early abnormalities more than two years prior to clinical progression from mild cognitive impairment to Alzheimer's disease. *Journal of Neuroscience*, 33(5), pp.2147-2155.

Drayer, B.P., 1988. Imaging of the aging brain. Part I. Normal findings. *Radiology*, 166(3), pp.785-796.

Dringen, R., 2000. Metabolism and functions of glutathione in brain. *Progress in neurobiology*, 62(6), pp.649-671.

Dunstan, D.W., Dogra, S., Carter, S.E. and Owen, N., 2021. Sit less and move more for cardiovascular health: emerging insights and opportunities. *Nature Reviews Cardiology*, pp.1-12.

Edelman, R.R., Siewert, B., Darby, D.G., Thangaraj, V.E.N.K.E.T.A.S.E.N., Nobre, A.C., Mesulam, M.M. and Warach, S., 1994. Qualitative mapping of cerebral blood flow and functional localization with echo-planar MR imaging and signal targeting with alternating radio frequency. *Radiology*, 192(2), pp.513-520.

Edelstein, W.A., Glover, G.H., Hardy, C.J. and Redington, R.W., 1986. The intrinsic signal-to-noise ratio in NMR imaging. *Magnetic Resonance in Medicine*, 3(4), pp.604-618.

Elliott, M.L., 2020. MRI-based biomarkers of accelerated aging and dementia risk in midlife: how close are we?. *Ageing research reviews*, 61, p.101075.

Emblem, K.E., Nedregard, B., Nome, T., Due-Tonnessen, P., Hald, J.K., Scheie, D., Borota, O.C., Cvancarova, M. and Bjornerud, A., 2008. Glioma grading by using histogram analysis of blood volume heterogeneity from MR-derived cerebral blood volume maps. *Radiology*, 247(3), pp.808-817.

Engl, E. and Attwell, D., 2015. Non-signalling energy use in the brain. *The Journal of Physiology*, 593(16), pp.3417-3429.

Ernst, T., Kreis, R. and Ross, B.D., 1993. Absolute quantitation of water and metabolites in the human brain. I. Compartments and water. *Journal of magnetic resonance, Series B*, 102(1), pp.1-8.

Esposito, F., Aragri, A., Pesaresi, I., Cirillo, S., Tedeschi, G., Marciano, E., Goebel, R. and Di Salle, F., 2008. Independent component model of the default-mode brain function: combining individual-level and population-level analyses in resting-state fMRI. *Magnetic resonance imaging*, 26(7), pp.905-913.

European Commission (2012). The 2012 Ageing Report: Economic and budgetary projections for the EU-27 Member States (2010–2060).

Eylers, V.V., Maudsley, A.A., Bronzlik, P., Dellani, P.R., Lanfermann, H. and Ding, X.Q., 2016. Detection of normal aging effects on human brain metabolite concentrations and microstructure with whole-brain MR spectroscopic imaging and quantitative MR imaging. *American Journal of Neuroradiology*, 37(3), pp.447-454.

Fama, R. and Sullivan, E.V., 2015. Thalamic structures and associated cognitive functions: Relations with age and aging. *Neuroscience & Biobehavioral Reviews*, 54, pp.29-37.

Farooqui, A.A., Ong, W.Y. and Horrocks, L.A., 2008. Glutamate and aspartate in brain. In *Neurochemical Aspects of Excitotoxicity* (pp. 3-20). Springer, New York, NY.

Faul, F., Erdfelder, E., Lang, A.G. and Buchner, A., 2007. G\* Power 3: A flexible statistical power analysis program for the social, behavioral, and biomedical sciences. *Behavior research methods*, 39(2), pp.175-191.

Feeney, J., Savva, G.M., O'Regan, C., King-Kallimanis, B., Cronin, H. and Kenny, R.A., 2016. Measurement error, reliability, and minimum detectable change in the Mini-Mental State Examination, Montreal Cognitive Assessment, and Color Trails Test among community living middle-aged and older adults. *Journal of Alzheimer's Disease*, 53(3), pp.1107-1114.

Ferguson, K.J., MacLulich, A.M., Marshall, I., Deary, I.J., Starr, J.M., Seckl, J.R. and Wardlaw, J.M., 2002. Magnetic resonance spectroscopy and cognitive function in healthy elderly men. *Brain*, 125(12), pp.2743-2749.

Fernandes, C.C., Lanz, B., Chen, C. and Morris, P.G., 2020. Measurement of brain lactate during visual stimulation using a long TE semi-LASER sequence at 7 T. *NMR in Biomedicine*, 33(4), p.e4223.

Fernandes, C.C., Lanz, B., Chen, C., Morris, P.G. and Salmon, C.G., 2021. Investigating the regional effect of the chemical shift displacement artefact on the J-modulated lactate signal at ultra high-field. *NMR in Biomedicine*, 34(2), p.e4440.

Ferrando, R. and Damian, A., 2021. Brain SPECT as a Biomarker of Neurodegeneration in Dementia in the Era of Molecular Imaging: Still a Valid Option?. *Frontiers in Neurology*, 12, p.640.

Ferro, D.A., Mutsaerts, H.J., Hilal, S., Kuijf, H.J., Petersen, E.T., Petr, J., van Veluw, S.J., Venketasubramanian, N., Yeow, T.B., Biessels, G.J. and Chen, C., 2020. Cortical microinfarcts in memory clinic patients are associated with reduced cerebral perfusion. *Journal of Cerebral Blood Flow & Metabolism*, 40(9), pp.1869-1878.

Fisher, M. and Bastan, B., 2012. Identifying and utilizing the ischemic penumbra. *Neurology*, 79(13 Supplement 1), pp.S79-S85.

Fjell, A.M. and Walhovd, K.B., 2010. Structural brain changes in aging: courses, causes and cognitive consequences. *Reviews in the Neurosciences*, 21(3), pp.187-222.

Folstein, M.F., Folstein, S.E. and McHugh, P.R., 1975. "Mini-mental state": a practical method for grading the cognitive state of patients for the clinician. *Journal of psychiatric research*, 12(3), pp.189-198.

Folstein, M.F., Robins, L.N. and Helzer, J.E., 1983. The mini-mental state examination. *Archives of general psychiatry*, 40(7), pp.812-812.

Fortier, M., Castellano, C.A., St-Pierre, V., Myette-Côté, É., Langlois, F., Roy, M., Morin, M.C., Bock, C., Fulop, T., Godin, J.P. and Delannoy, C., 2021. A ketogenic drink improves cognition in mild cognitive impairment: Results of a 6-month RCT. *Alzheimer's & Dementia*, 17(3), pp.543-552.

Fox, P.T., Raichle, M.E., Mintun, M.A. and Dence, C., 1988. Nonoxidative glucose consumption during focal physiologic neural activity. *Science*, 241(4864), pp.462-464.

Frahm, J., Krüger, G., Merboldt, K.D. and Kleinschmidt, A., 1996. Dynamic uncoupling and recoupling of perfusion and oxidative metabolism during focal brain activation in man. *Magnetic resonance in medicine*, 35(2), pp.143-148.

- Frahm, J., Merboldt, K.D. and Hänicke, W., 1987. Localized proton spectroscopy using stimulated echoes. *Journal of Magnetic Resonance* (1969), 72(3), pp.502-508.
- Frahm, J.A., Bruhn, H., Gyngell, M.L., Merboldt, K.D., Hänicke, W. and Sauter, R., 1989. Localized high-resolution proton NMR spectroscopy using stimulated echoes: initial applications to human brain in vivo. *Magnetic resonance in medicine*, 9(1), pp.79-93.
- Franke, K. and Gaser, C., 2019. Ten years of brainage as a neuroimaging biomarker of brain aging: what insights have we gained?. *Frontiers in neurology*, 10, p.789.
- Franke, K., Ziegler, G., Klöppel, S., Gaser, C. and Alzheimer's Disease Neuroimaging Initiative, 2010. Estimating the age of healthy subjects from T1-weighted MRI scans using kernel methods: exploring the influence of various parameters. *Neuroimage*, 50(3), pp.883-892.
- Frazier, J.A., Chiu, S., Breeze, J.L., Makris, N., Lange, N., Kennedy, D.N., Herbert, M.R., Bent, E.K., Koneru, V.K., Dieterich, M.E. and Hodge, S.M., 2005. Structural brain magnetic resonance imaging of limbic and thalamic volumes in pediatric bipolar disorder. *American Journal of Psychiatry*, 162(7), pp.1256-1265.
- Friedman, J., 2011. Why is the nervous system vulnerable to oxidative stress?. In *Oxidative stress and free radical damage in neurology* (pp. 19-27). Humana Press.
- Fripp, J., Bourgeat, P., Acosta, O., Raniga, P., Modat, M., Pike, K.E., Jones, G., O'Keefe, G., Masters, C.L., Ames, D. and Ellis, K.A., 2008. Appearance modeling of 11C PiB PET images: characterizing amyloid deposition in Alzheimer's disease, mild cognitive impairment and healthy aging. *Neuroimage*, 43(3), pp.430-439.
- Galiano, A., Mengual, E., de Eulate, R.G., Galdeano, I., Vidorreta, M., Recio, M., Riverol, M., Zubieta, J.L. and Fernández-Seara, M.A., 2020. Coupling of cerebral blood flow and functional connectivity is decreased in healthy aging. *Brain imaging and behavior*, 14(2), pp.436-450.
- Garroway, A.N., Grannell, P.K. and Mansfield, P., 1974. Image formation in NMR by a selective irradiative process. *Journal of Physics C: Solid State Physics*, 7(24), p.L457.
- Garwood, M. and DelaBarre, L., 2001. The return of the frequency sweep: designing adiabatic pulses for contemporary NMR. *Journal of Magnetic Resonance*, 153(2), pp.155-177.
- Gaser, C., Franke, K., Klöppel, S., Koutsouleris, N., Sauer, H. and Alzheimer's Disease Neuroimaging Initiative, 2013. BrainAGE in mild cognitive impaired patients: predicting the conversion to Alzheimer's disease. *PloS one*, 8(6), p.e67346.
- Gasparovic, C., Prestopnik, J., Thompson, J., Taheri, S., Huisa, B., Schrader, R., Adair, J.C. and Rosenberg, G.A., 2013. 1H-MR spectroscopy metabolite levels correlate with executive function in vascular cognitive impairment. *Journal of Neurology, Neurosurgery & Psychiatry*, 84(7), pp.715-721.

Gasparovic, C., Song, T., Devier, D., Bockholt, H.J., Caprihan, A., Mullins, P.G., Posse, S., Jung, R.E. and Morrison, L.A., 2006. Use of tissue water as a concentration reference for proton spectroscopic imaging. *Magnetic Resonance in Medicine: An Official Journal of the International Society for Magnetic Resonance in Medicine*, 55(6), pp.1219-1226.

Gaxiola-Valdez, I., Singh, S., Perera, T., Sandy, S., Li, E. and Federico, P., 2017. Seizure onset zone localization using postictal hypoperfusion detected by arterial spin labelling MRI. *Brain*, 140(11), pp.2895-2911.

Ghandehari, K. and Ghandehari, K., 2012. Interesting basis of vertebrobasilar arterial territory. *Iranian journal of neurology*, 11(3), p.111.

Gilmore, A.W., Nelson, S.M. and McDermott, K.B., 2015. A parietal memory network revealed by multiple MRI methods. *Trends in cognitive sciences*, 19(9), pp.534-543.

Glodzik, L., Rusinek, H., Tsui, W., Pirraglia, E., Kim, H.J., Deshpande, A., Li, Y., Storey, P., Randall, C., Chen, J. and Osorio, R.S., 2019. Different relationship between systolic blood pressure and cerebral perfusion in subjects with and without hypertension. *Hypertension*, 73(1), pp.197-205.

Glover, G.H., Hayes, C.E., Pelc, N.J., Edelstein, W.A., Mueller, O.M., Hart, H.R., Hardy, C.J., O'donnell, M. and Barber, W.D., 1985. Comparison of linear and circular polarization for magnetic resonance imaging. *Journal of Magnetic Resonance (1969)*, 64(2), pp.255-270.

Godlewska, B.R., Clare, S., Cowen, P.J. and Emir, U.E., 2017. Ultra-high-field magnetic resonance spectroscopy in psychiatry. *Frontiers in psychiatry*, 8, p.123.

Godlewska, B.R., Near, J. and Cowen, P.J., 2015. Neurochemistry of major depression: a study using magnetic resonance spectroscopy. *Psychopharmacology*, 232(3), pp.501-507.

Goldberg, I.I., Harel, M. and Malach, R., 2006. When the brain loses its self: prefrontal inactivation during sensorimotor processing. *Neuron*, 50(2), pp.329-339.

Goldstein, J.M., Seidman, L.J., Makris, N., Ahern, T., O'Brien, L.M., Caviness Jr, V.S., Kennedy, D.N., Faraone, S.V. and Tsuang, M.T., 2007. Hypothalamic abnormalities in schizophrenia: sex effects and genetic vulnerability. *Biological psychiatry*, 61(8), pp.935-945.

Govindaraju, V., Young, K. and Maudsley, A.A., 2000. Proton NMR chemical shifts and coupling constants for brain metabolites. *NMR in Biomedicine: An International Journal Devoted to the Development and Application of Magnetic Resonance In Vivo*, 13(3), pp.129-153.

Goyal, M.S., Blazey, T.M., Su, Y., Couture, L.E., Durbin, T.J., Bateman, R.J., Benzinger, T.L.S., Morris, J.C., Raichle, M.E. and Vlassenko, A.G., 2019. Persistent metabolic youth in the aging female brain. *Proceedings of the National Academy of Sciences*, 116(8), pp.3251-3255.

Goyal, M.S., Gordon, B.A., Couture, L.E., Flores, S., Xiong, C., Morris, J.C., Raichle, M.E., Benzinger, T.L. and Vlassenko, A.G., 2020. Spatiotemporal

- relationship between subthreshold amyloid accumulation and aerobic glycolysis in the human brain. *Neurobiology of Aging*, 96, pp.165-175.
- Goyal, M.S., Vlassenko, A.G., Blazey, T.M., Su, Y., Couture, L.E., Durbin, T.J., Bateman, R.J., Benzinger, T.L.S., Morris, J.C. and Raichle, M.E., 2017. Loss of brain aerobic glycolysis in normal human aging. *Cell metabolism*, 26(2), pp.353-360.
- Grahn, J.A., Parkinson, J.A. and Owen, A.M., 2008. The cognitive functions of the caudate nucleus. *Progress in neurobiology*, 86(3), pp.141-155.
- Greicius, M.D. and Kimmell, D.L., 2012. Neuroimaging insights into network-based neurodegeneration. *Current opinion in neurology*, 25(6), pp.727-734.
- Greicius, M.D., Srivastava, G., Reiss, A.L. and Menon, V., 2004. Default-mode network activity distinguishes Alzheimer's disease from healthy aging: evidence from functional MRI. *Proceedings of the National Academy of Sciences*, 101(13), pp.4637-4642.
- Greve, D.N. and Fischl, B., 2009. Accurate and robust brain image alignment using boundary-based registration. *Neuroimage*, 48(1), pp.63-72.
- Grist, J.T., McLean, M.A., Riemer, F., Schulte, R.F., Deen, S.S., Zaccagna, F., Woitek, R., Daniels, C.J., Kaggie, J.D., Matys, T. and Patterson, I., 2019. Quantifying normal human brain metabolism using hyperpolarized [1-13C] pyruvate and magnetic resonance imaging. *NeuroImage*, 189, pp.171-179.
- Gruber, S., Pinker, K., Riederer, F., Chmelík, M., Stadlbauer, A., Bittšanský, M., Mlynárik, V., Frey, R., Serles, W., Bodamer, O. and Moser, E., 2008. Metabolic changes in the normal ageing brain: consistent findings from short and long echo time proton spectroscopy. *European Journal of Radiology*, 68(2), pp.320-327.
- Gruetter, R., 1993. Automatic, localized in vivo adjustment of all first-and second-order shim coils. *Magnetic Resonance in Medicine*, 29(6), pp.804-811.
- Gruetter, R., Adriany, G., Choi, I.Y., Henry, P.G., Lei, H. and Öz, G., 2003. Localized in vivo 13C NMR spectroscopy of the brain. *NMR in Biomedicine: An International Journal Devoted to the Development and Application of Magnetic Resonance In Vivo*, 16(6-7), pp.313-338.
- Grundy, E. and Sloggett, A., 2003. Health inequalities in the older population: the role of personal capital, social resources and socio-economic circumstances. *Social science & medicine*, 56(5), pp.935-947.
- Günther, M., Bock, M. and Schad, L.R., 2001. Arterial spin labeling in combination with a look-locker sampling strategy: inflow turbo-sampling EPI-FAIR (ITS-FAIR). *Magnetic Resonance in Medicine: An Official Journal of the International Society for Magnetic Resonance in Medicine*, 46(5), pp.974-984.
- Haase, A., 1986. Localization of unaffected spins in NMR imaging and spectroscopy (LOCUS spectroscopy). *Magnetic Resonance in Medicine*, 3(6), pp.963-969.
- Habeck, C. and Stern, Y., 2010. Multivariate data analysis for neuroimaging data: overview and application to Alzheimer's disease. *Cell biochemistry and biophysics*, 58(2), pp.53-67.

- Habeck, C., Foster, N.L., Perneczky, R., Kurz, A., Alexopoulos, P., Koeppe, R.A., Drzezga, A. and Stern, Y., 2008. Multivariate and univariate neuroimaging biomarkers of Alzheimer's disease. *Neuroimage*, 40(4), pp.1503-1515.
- Hachinski, V., Avan, A., Gilliland, J. and Oveisgharan, S., 2021. A new definition of brain health. *The Lancet Neurology*, 20(5), pp.335-336.
- Haga, K.K., Khor, Y.P., Farrall, A. and Wardlaw, J.M., 2009. A systematic review of brain metabolite changes, measured with <sup>1</sup>H magnetic resonance spectroscopy, in healthy aging. *Neurobiology of aging*, 30(3), pp.353-363.
- Hajjar, E.R., Cafiero, A.C. and Hanlon, J.T., 2007. Polypharmacy in elderly patients. *The American journal of geriatric pharmacotherapy*, 5(4), pp.345-351.
- Hakim, A.M., 1998. Ischemic penumbra: the therapeutic window. *Neurology*, 51(3 Suppl 3), pp.S44-S46.
- Halaweh, H., Dahlin-Ivanoff, S., Svantesson, U. and Willén, C., 2018. Perspectives of older adults on aging well: a focus group study. *Journal of aging research*, 2018.
- Hales, P.W., d'Arco, F., Cooper, J., Pfeuffer, J., Hargrave, D., Mankad, K. and Clark, C., 2019. Arterial spin labelling and diffusion-weighted imaging in paediatric brain tumours. *NeuroImage: Clinical*, 22, p.101696.
- Hall, E.L., Stephenson, M.C., Price, D. and Morris, P.G., 2014. Methodology for improved detection of low concentration metabolites in MRS: optimised combination of signals from multi-element coil arrays. *Neuroimage*, 86, pp.35-42.
- Hammen, T. and Kuzniecky, R., 2012. Magnetic resonance spectroscopy in epilepsy. In *Handbook of clinical neurology* (Vol. 107, pp. 399-408). Elsevier.
- Hammers, A., Allom, R., Koeppe, M.J., Free, S.L., Myers, R., Lemieux, L., Mitchell, T.N., Brooks, D.J. and Duncan, J.S., 2003. Three-dimensional maximum probability atlas of the human brain, with particular reference to the temporal lobe. *Human brain mapping*, 19(4), pp.224-247.
- Han, X., Jovicich, J., Salat, D., van der Kouwe, A., Quinn, B., Czanner, S., Busa, E., Pacheco, J., Albert, M., Killiany, R. and Maguire, P., 2006. Reliability of MRI-derived measurements of human cerebral cortical thickness: the effects of field strength, scanner upgrade and manufacturer. *Neuroimage*, 32(1), pp.180-194.
- Hanaoka, T., Kimura, N., Aso, Y., Takemaru, M., Kimura, Y., Ishibashi, M. and Matsubara, E., 2016. Relationship between white matter lesions and regional cerebral blood flow changes during longitudinal follow up in Alzheimer's disease. *Geriatrics & gerontology international*, 16(7), pp.836-842.
- Harris, A.D., Robertson, V.H., Huckle, D.L., Saxena, N., Evans, C.J., Murphy, K., Hall, J.E., Bailey, D.M., Mitsis, G., Edden, R.A. and Wise, R.G., 2013. Temporal dynamics of lactate concentration in the human brain during acute inspiratory hypoxia. *Journal of Magnetic Resonance Imaging*, 37(3), pp.739-745.

- Harris, J. J. & Attwell, D., 2012. The Energetics of CNS White Matter. *J. Neurosci.* **32**, 356–371.
- Harris, J.L., Choi, I.Y. and Brooks, W.M., 2015. Probing astrocyte metabolism in vivo: proton magnetic resonance spectroscopy in the injured and aging brain. *Frontiers in aging neuroscience*, *7*, p.202.
- Harris, R.K., Becker, E.D., De Menezes, S.M.C., Goodfellow, R. and Granger, P., 2001. NMR nomenclature. Nuclear spin properties and conventions for chemical shifts (IUPAC Recommendations 2001). *Pure and Applied Chemistry*, *73*(11), pp.1795-1818.
- Hasler, G., van der Veen, J.W., Tumonis, T., Meyers, N., Shen, J. and Drevets, W.C., 2007. Reduced prefrontal glutamate/glutamine and  $\gamma$ -aminobutyric acid levels in major depression determined using proton magnetic resonance spectroscopy. *Archives of general psychiatry*, *64*(2), pp.193-200.
- Hays, C.C., Zlatar, Z.Z. and Wierenga, C.E., 2016. The utility of cerebral blood flow as a biomarker of preclinical Alzheimer's disease. *Cellular and molecular neurobiology*, *36*(2), pp.167-179.
- Hays, C.C., Zlatar, Z.Z., Campbell, L., Meloy, M.J. and Wierenga, C.E., 2018. Subjective cognitive decline modifies the relationship between cerebral blood flow and memory function in cognitively normal older adults. *Journal of the International Neuropsychological Society*, *24*(3), pp.213-223.
- Heckemann, R.A., Hajnal, J.V., Aljabar, P., Rueckert, D. and Hammers, A., 2006. Automatic anatomical brain MRI segmentation combining label propagation and decision fusion. *NeuroImage*, *33*(1), pp.115-126.
- Heckemann, R.A., Keihaninejad, S., Aljabar, P., Rueckert, D., Hajnal, J.V., Hammers, A. and Alzheimer's Disease Neuroimaging Initiative, 2010. Improving intersubject image registration using tissue-class information benefits robustness and accuracy of multi-atlas based anatomical segmentation. *Neuroimage*, *51*(1), pp.221-227.
- Hendrikse, J., Petersen, E.T., Van Laar, P.J. and Golay, X., 2008. Cerebral border zones between distal end branches of intracranial arteries: MR imaging. *Radiology*, *246*(2), pp.572-580.
- Henriksen, O., Gideon, P., Sperling, B., Olsen, T.S., Jørgensen, H.S. and Arlien-Søborg, P., 1992. Cerebral lactate production and blood flow in acute stroke. *Journal of Magnetic Resonance Imaging*, *2*(5), pp.511-517.
- Herholz, K., Salmon, E., Perani, D., Baron, J.C., Holthoff, V., Frölich, L., Schönknecht, P., Ito, K., Mielke, R., Kalbe, E. and Zündorf, G., 2002. Discrimination between Alzheimer dementia and controls by automated analysis of multicenter FDG PET. *Neuroimage*, *17*(1), pp.302-316.
- Herrick, R.C., Hayman, L.A., Taber, K.H., Diaz-Marchan, P.J. and Kuo, M.D., 1997. Artifacts and pitfalls in MR imaging of the orbit: a clinical review. *Radiographics*, *17*(3), pp.707-724.
- Herscovitch, P. and Raichle, M.E., 1985. What is the correct value for the brain-blood partition coefficient for water?. *Journal of Cerebral Blood Flow & Metabolism*, *5*(1), pp.65-69.

Hoffman, J.M., Welsh-Bohmer, K.A., Hanson, M., Crain, B., Hulette, C., Earl, N. and Coleman, R.E., 2000. FDG PET imaging in patients with pathologically verified dementia. *Journal of Nuclear Medicine*, 41(11), pp.1920-1928.

Hofmann, L., Slotboom, J., Jung, B., Maloca, P., Boesch, C. and Kreis, R., 2002. Quantitative <sup>1</sup>H-magnetic resonance spectroscopy of human brain: influence of composition and parameterization of the basis set in linear combination model-fitting. *Magnetic Resonance in Medicine: An Official Journal of the International Society for Magnetic Resonance in Medicine*, 48(3), pp.440-453.

Holland, D., Brewer, J.B., Hagler, D.J., Fennema-Notestine, C., Dale, A.M. and Alzheimer's Disease Neuroimaging Initiative, 2009. Subregional neuroanatomical change as a biomarker for Alzheimer's disease. *Proceedings of the National Academy of Sciences*, 106(49), pp.20954-20959.

Hoops, S., Nazem, S., Siderowf, A.D., Duda, J.E., Xie, S.X., Stern, M.B. and Weintraub, D., 2009. Validity of the MoCA and MMSE in the detection of MCI and dementia in Parkinson disease. *Neurology*, 73(21), pp.1738-1745.

Hotelling, H., 1933. Analysis of a complex of statistical variables into principal components. *Journal of educational psychology*, 24(6), p.417.

Hou, Y., Dan, X., Babbar, M., Wei, Y., Hasselbalch, S.G., Croteau, D.L. and Bohr, V.A., 2019. Ageing as a risk factor for neurodegenerative disease. *Nature Reviews Neurology*, 15(10), pp.565-581.

Howarth, C., Gleeson, P. and Attwell, D., 2012. Updated energy budgets for neural computation in the neocortex and cerebellum. *Journal of Cerebral Blood Flow & Metabolism*, 32(7), pp.1222-1232.

Howe, F.A., Barton, S.J., Cudlip, S.A., Stubbs, M., Saunders, D.E., Murphy, M., Wilkins, P., Opstad, K.S., Doyle, V.L., McLean, M.A. and Bell, B.A., 2003. Metabolic profiles of human brain tumors using quantitative in vivo <sup>1</sup>H magnetic resonance spectroscopy. *Magnetic Resonance in Medicine: An Official Journal of the International Society for Magnetic Resonance in Medicine*, 49(2), pp.223-232.

Hsu, J.L., Fan, Y.C., Huang, Y.L., Wang, J., Chen, W.H., Chiu, H.C. and Bai, C.H., 2015. Improved predictive ability of the Montreal Cognitive Assessment for diagnosing dementia in a community-based study. *Alzheimer's Research & Therapy*, 7(1), p.69.

Hu, Y., Wang, J., Li, C., Wang, Y.S., Yang, Z. and Zuo, X.N., 2016. Segregation between the parietal memory network and the default mode network: effects of spatial smoothing and model order in ICA. *Science bulletin*, 61(24), pp.1844-1854.

Huang, C., Wahlund, L.O., Almkvist, O., Elehu, D., Svensson, L., Jonsson, T., Winblad, B. and Julin, P., 2003. Voxel-and VOI-based analysis of SPECT CBF in relation to clinical and psychological heterogeneity of mild cognitive impairment. *Neuroimage*, 19(3), pp.1137-1144.

Huang, C.W., Hsu, S.W., Chang, Y.T., Huang, S.H., Huang, Y.C., Lee, C.C., Chang, W.N., Lui, C.C., Chen, N.C. and Chang, C.C., 2018. Cerebral perfusion insufficiency and relationships with cognitive deficits in Alzheimer's

disease: A multiparametric neuroimaging study. *Scientific reports*, 8(1), pp.1-14.

Huang, S.C., Carson, R.E., Hoffman, E.J., Carson, J., MacDonald, N., Barrio, J.R. and Phelps, M.E., 1983. Quantitative measurement of local cerebral blood flow in humans by positron computed tomography and <sup>15</sup>O-water. *Journal of Cerebral Blood Flow & Metabolism*, 3(2), pp.141-153.

Hussenoeder, F.S., Conrad, I., Roehr, S., Fuchs, A., Pentzek, M., Bickel, H., Moesch, E., Weyerer, S., Werle, J., Wiese, B. and Mamone, S., 2020. Mild cognitive impairment and quality of life in the oldest old: a closer look. *Quality of Life Research*, 29(6), pp.1675-1683.

Ibáñez, V., Pietrini, P., Furey, M.L., Alexander, G.E., Millet, P., Bokde, A.L., Teichberg, D., Schapiro, M.B., Horwitz, B. and Rapoport, S.I., 2004. Resting state brain glucose metabolism is not reduced in normotensive healthy men during aging, after correction for brain atrophy. *Brain research bulletin*, 63(2), pp.147-154.

Ibaraki, M., Nakamura, K., Toyoshima, H., Takahashi, K., Matsubara, K., Umetsu, A., Pfeuffer, J., Kuribayashi, H. and Kinoshita, T., 2019. Spatial coefficient of variation in pseudo-continuous arterial spin labeling cerebral blood flow images as a hemodynamic measure for cerebrovascular stenocclusive disease: A comparative <sup>15</sup>O positron emission tomography study. *Journal of Cerebral Blood Flow & Metabolism*, 39(1), pp.173-181.

Ibaraki, M., Shinohara, Y., Nakamura, K., Miura, S., Kinoshita, F. and Kinoshita, T., 2010. Interindividual variations of cerebral blood flow, oxygen delivery, and metabolism in relation to hemoglobin concentration measured by positron emission tomography in humans. *Journal of Cerebral Blood Flow & Metabolism*, 30(7), pp.1296-1305.

Ihle-Hansen, H., Vigen, T., Berge, T., Einvik, G., Aarsland, D., Rønning, O.M., Thommessen, B., Røsjø, H., Tveit, A. and Ihle-Hansen, H., 2017. Montreal cognitive assessment in a 63- to 65-year-old norwegian cohort from the general population: Data from the Akershus Cardiac Examination 1950 study. *Dementia and geriatric cognitive disorders extra*, 7(3), pp.318-327.

Inglese, M., Li, B.S., Rusinek, H., Babb, J.S., Grossman, R.I. and Gonen, O., 2003. Diffusely elevated cerebral choline and creatine in relapsing-remitting multiple sclerosis. *Magnetic Resonance in Medicine: An Official Journal of the International Society for Magnetic Resonance in Medicine*, 50(1), pp.190-195.

Inoue, K., Ito, H., Goto, R., Nakagawa, M., Kinomura, S., Sato, T., Sato, K. and Fukuda, H., 2005. Apparent CBF decrease with normal aging due to partial volume effects: MR-based partial volume correction on CBF SPECT. *Annals of nuclear medicine*, 19(4), pp.283-290.

International Commission on Non-Ionizing Radiation Protection, 2020. Guidelines for limiting exposure to electromagnetic fields (100 kHz to 300 GHz). *Health physics*, 118(5), pp.483-524.

Iscan, Z., Jin, T.B., Kendrick, A., Szeglin, B., Lu, H., Trivedi, M., Fava, M., McGrath, P.J., Weissman, M., Kurian, B.T. and Adams, P., 2015. Test-retest reliability of freesurfer measurements within and between sites: Effects of visual approval process. *Human brain mapping*, 36(9), pp.3472-3485.

- Ishibashi, K., Onishi, A., Fujiwara, Y., Oda, K., Ishiwata, K. and Ishii, K., 2018. Longitudinal effects of aging on 18 F-FDG distribution in cognitively normal elderly individuals. *Scientific Reports*, 8(1), pp.1-8.
- Ishii, K., 2014. PET approaches for diagnosis of dementia. *American Journal of Neuroradiology*, 35(11), pp.2030-2038.
- Iturria-Medina, Y., Sotero, R.C., Toussaint, P.J., Mateos-Pérez, J.M. and Evans, A.C., 2016. Early role of vascular dysregulation on late-onset Alzheimer's disease based on multifactorial data-driven analysis. *Nature communications*, 7(1), pp.1-14.
- Jack Jr, C.R., Knopman, D.S., Jagust, W.J., Shaw, L.M., Aisen, P.S., Weiner, M.W., Petersen, R.C. and Trojanowski, J.Q., 2010. Hypothetical model of dynamic biomarkers of the Alzheimer's pathological cascade. *The Lancet Neurology*, 9(1), pp.119-128.
- Jackson, D.A., 1993. Stopping rules in principal components analysis: a comparison of heuristical and statistical approaches. *Ecology*, 74(8), pp.2204-2214.
- Jackson, P.A., Pialoux, V., Corbett, D., Drogos, L., Erickson, K.I., Eskes, G.A. and Poulin, M.J., 2016. Promoting brain health through exercise and diet in older adults: a physiological perspective. *The Journal of physiology*, 594(16), pp.4485-4498.
- Jagust, W.M.R.B., Reed, B., Mungas, D., Ellis, W. and DeCarli, C., 2007. What does fluorodeoxyglucose PET imaging add to a clinical diagnosis of dementia?. *Neurology*, 69(9), pp.871-877.
- Japee, S., Holiday, K., Satyshur, M.D., Mukai, I. and Ungerleider, L.G., 2015. A role of right middle frontal gyrus in reorienting of attention: a case study. *Frontiers in systems neuroscience*, 9, p.23.
- Järnum, H., Steffensen, E.G., Knutsson, L., Fründ, E.T., Simonsen, C.W., Lundbye-Christensen, S., Shankaranarayanan, A., Alsop, D.C., Jensen, F.T. and Larsson, E.M., 2010. Perfusion MRI of brain tumours: a comparative study of pseudo-continuous arterial spin labelling and dynamic susceptibility contrast imaging. *Neuroradiology*, 52(4), pp.307-317.
- Jenkinson, M. and Smith, S., 2001. A global optimisation method for robust affine registration of brain images. *Medical image analysis*, 5(2), pp.143-156.
- Jenkinson, M., Bannister, P., Brady, M. and Smith, S., 2002. Improved optimization for the robust and accurate linear registration and motion correction of brain images. *Neuroimage*, 17(2), pp.825-841.
- Jenkinson, M., Beckmann, C.F., Behrens, T.E., Woolrich, M.W. and Smith, S.M., 2012. Fsl. *Neuroimage*, 62(2), pp.782-790.
- Jeste, D.V., Depp, C.A. and Vahia, I.V., 2010. Successful cognitive and emotional aging. *World Psychiatry*, 9(2), p.78.
- Johnson, N.A., Jahng, G.H., Weiner, M.W., Miller, B.L., Chui, H.C., Jagust, W.J., Gorno-Tempini, M.L. and Schuff, N., 2005. Pattern of cerebral hypoperfusion in Alzheimer disease and mild cognitive impairment measured with arterial spin-labeling MR imaging: initial experience. *Radiology*, 234(3), pp.851-859.

- Jones, D.T., Knopman, D.S., Gunter, J.L., Graff-Radford, J., Vemuri, P., Boeve, B.F., Petersen, R.C., Weiner, M.W. and Jack Jr, C.R., 2016. Cascading network failure across the Alzheimer's disease spectrum. *Brain*, 139(2), pp.547-562.
- Jordan, J.D. and Powers, W.J., 2012. Cerebral autoregulation and acute ischemic stroke. *American journal of hypertension*, 25(9), pp.946-950.
- Jutten, C. and Héroult, J., 1991. Blind separation of sources, part I: An adaptive algorithm based on neuromimetic architecture. *Signal processing*, 24(1), pp.1-10.
- Juttukonda, M.R., Li, B., Alaktoum, R., Stephens, K.A., Yochim, K.M., Buckner, R.L. and Salat, D.H., 2021. Cerebral gray and white matter hemodynamic function across the adult lifespan. *NeuroImage*, p.117807.
- Kaiser, L.G., Schuff, N., Cashdollar, N. and Weiner, M.W., 2005a. Age-related glutamate and glutamine concentration changes in normal human brain: 1H MR spectroscopy study at 4 T. *Neurobiology of Aging*, 26(5), pp.665-672.
- Kaiser, L.G., Schuff, N., Cashdollar, N. and Weiner, M.W., 2005b. Scyllo-inositol in normal aging human brain: 1H magnetic resonance spectroscopy study at 4 Tesla. *NMR in Biomedicine: An International Journal Devoted to the Development and Application of Magnetic Resonance In vivo*, 18(1), pp.51-55.
- Kalback, W., Esh, C., Castaño, E.M., Rahman, A., Kokjohn, T., Luehrs, D.C., Sue, L., Cisneros, R., Gerber, F., Richardson, C. and Bohrmann, B., 2004. Atherosclerosis, vascular amyloidosis and brain hypoperfusion in the pathogenesis of sporadic Alzheimer's disease. *Neurological research*, 26(5), pp.525-539.
- Kalpouzos, G., Chételat, G., Baron, J.C., Landeau, B., Mevel, K., Godeau, C., Barré, L., Constans, J.M., Viader, F., Eustache, F. and Desgranges, B., 2009. Voxel-based mapping of brain gray matter volume and glucose metabolism profiles in normal aging. *Neurobiology of aging*, 30(1), pp.112-124.
- Kantarci, K., 2007. 1H magnetic resonance spectroscopy in dementia. *The British journal of radiology*, 80(special\_issue\_2), pp.S146-S152.
- Kantarci, K., 2013. Magnetic resonance spectroscopy in common dementias. *Neuroimaging Clinics*, 23(3), pp.393-406.
- Kasischke, K.A., 2009. Activity-dependent metabolism in glia and neurones. L.R. Squire (Ed.), *New Encyclopedia of Neuroscience*, Elsevier Ltd., Oxford, UK. pp. 53-60.
- Katz, R.C., Wilson, L. and Frazer, N., 1994. Anxiety and its determinants in patients undergoing magnetic resonance imaging. *Journal of behavior therapy and experimental psychiatry*, 25(2), pp.131-134.
- Kawas, C., Gray, S., Brookmeyer, R., Fozard, J. and Zonderman, A., 2000. Age-specific incidence rates of Alzheimer's disease: the Baltimore Longitudinal Study of Aging. *Neurology*, 54(11), pp.2072-2077.
- Ke, Y., Cohen, B.M., Lowen, S., Hirashima, F., Nassar, L. and Renshaw, P.F., 2002. Biexponential transverse relaxation (T2) of the proton MRS creatine resonance in human brain. *Magnetic Resonance in Medicine: An Official*

*Journal of the International Society for Magnetic Resonance in Medicine*, 47(2), pp.232-238.

Kearney, P.M., Cronin, H., O'Regan, C., Kamiya, Y., Savva, G.M., Whelan, B. and Kenny, R., 2011. Cohort profile: the Irish longitudinal study on ageing. *International journal of epidemiology*, 40(4), pp.877-884.

Keller, J.N., 2006. Age-related neuropathology, cognitive decline, and Alzheimer's disease. *Ageing research reviews*, 5(1), pp.1-13.

Kelly-Hayes, M., 2010. Influence of age and health behaviors on stroke risk: lessons from longitudinal studies. *Journal of the American Geriatrics Society*, 58, pp.S325-S328.

Kemp, P.M., Holmes, C., Hoffmann, S.M.A., Bolt, L., Holmes, R., Rowden, J. and Fleming, J.S., 2003. Alzheimer's disease: differences in technetium-99m HMPAO SPECT scan findings between early onset and late onset dementia. *Journal of Neurology, Neurosurgery & Psychiatry*, 74(6), pp.715-719.

Khomenko, Y.G., Kataeva, G.V., Bogdan, A.A., Chernysheva, E.M. and Susin, D.S., 2019. Cerebral Metabolism in Patients with Cognitive Disorders: a Combined Magnetic Resonance Spectroscopy and Positron Emission Tomography Study. *Neuroscience and Behavioral Physiology*, 49(9), pp.1199-1207.

Kim, S.G. and Ackerman, J.J., 1988. Quantitative determination of tumor blood flow and perfusion via deuterium nuclear magnetic resonance spectroscopy in mice. *Cancer research*, 48(12), pp.3449-3453.

Kim, S.G., 1995. Quantification of relative cerebral blood flow change by flow-sensitive alternating inversion recovery (FAIR) technique: application to functional mapping. *Magnetic resonance in medicine*, 34(3), pp.293-301.

Kong, L., Chen, H., Yang, Y. and Chen, L., 2017. A meta-analysis of arterial spin labelling perfusion values for the prediction of glioma grade. *Clinical Radiology*, 72(3), pp.255-261.

Koster, A., Penninx, B.W., Bosma, H., Kempen, G.I., Newman, A.B., Rubin, S.M., Satterfield, S., Atkinson, H.H., Ayonayon, H.N., Rosano, C. and Yaffe, K., 2005. Socioeconomic differences in cognitive decline and the role of biomedical factors. *Annals of epidemiology*, 15(8), pp.564-571.

Koyama, M.S., O'Connor, D., Shehzad, Z. and Milham, M.P., 2017. Differential contributions of the middle frontal gyrus functional connectivity to literacy and numeracy. *Scientific reports*, 7(1), pp.1-13.

Kramer, A.F., Erickson, K.I. and Colcombe, S.J., 2006. Exercise, cognition, and the aging brain. *Journal of applied physiology*, 101(4), pp.1237-1242.

Kreis, R., 2016. The trouble with quality filtering based on relative Cramér-Rao lower bounds. *Magnetic Resonance in Medicine*, 75(1), pp.15-18.

Kreis, R., Ernst, T. and Ross, B.D., 1993. Absolute quantitation of water and metabolites in the human brain. II. Metabolite concentrations. *Journal of magnetic resonance, Series B*, 102(1), pp.9-19.

- Kremen, W.S., Beck, A., Elman, J.A., Gustavson, D.E., Reynolds, C.A., Tu, X.M., Sanderson-Cimino, M.E., Panizzon, M.S., Vuoksimaa, E., Toomey, R. and Fennema-Notestine, C., 2019. Influence of young adult cognitive ability and additional education on later-life cognition. *Proceedings of the National Academy of Sciences*, 116(6), pp.2021-2026.
- Krüger, G., Kleinschmidt, A. and Frahm, J., 1996. Dynamic MRI sensitized to cerebral blood oxygenation and flow during sustained activation of human visual cortex. *Magnetic Resonance in Medicine*, 35(6), pp.797-800.
- Kueper, J.K., Speechley, M. and Montero-Odasso, M., 2018. The Alzheimer's disease assessment scale–cognitive subscale (ADAS-Cog): modifications and responsiveness in pre-dementia populations. a narrative review. *Journal of Alzheimer's Disease*, 63(2), pp.423-444.
- Kunz, A. and Iadecola, C., 2008. Cerebral vascular dysregulation in the ischemic brain. *Handbook of clinical neurology*, 92, pp.283-305.
- Kuschinsky, W., 1991. Coupling of function, metabolism, and blood flow in the brain. *Neurosurgical review*, 14(3), pp.163-168.
- LaMontagne, P.J., Benzinger, T.L., Morris, J.C., Keefe, S., Hornbeck, R., Xiong, C., Grant, E., Hassenstab, J., Moulder, K., Vlassenko, A. and Raichle, M.E., 2019. OASIS-3: longitudinal neuroimaging, clinical, and cognitive dataset for normal aging and Alzheimer disease. *MedRxiv*.
- Landheer, K., Schulte, R.F., Treacy, M.S., Swanberg, K.M. and Juchem, C., 2020. Theoretical description of modern 1H in Vivo magnetic resonance spectroscopic pulse sequences. *Journal of Magnetic Resonance Imaging*, 51(4), pp.1008-1029.
- Lara, J., Godfrey, A., Evans, E., Heaven, B., Brown, L.J., Barron, E., Rochester, L., Meyer, T.D. and Mathers, J.C., 2013. Towards measurement of the Healthy Ageing Phenotype in lifestyle-based intervention studies. *Maturitas*, 76(2), pp.189-199.
- Larson, E.B., Wang, L., Bowen, J.D., McCormick, W.C., Teri, L., Crane, P. and Kukull, W., 2006. Exercise is associated with reduced risk for incident dementia among persons 65 years of age and older. *Annals of internal medicine*, 144(2), pp.73-81.
- Launer, L.J., Andersen, K., Dewey, M., Letenneur, L., Ott, A., Amaducci, L.A., Brayne, C., Copeland, J.R.M., Dartigues, J.F., Kragh-Sorensen, P. and Lobo, A., 1999. Rates and risk factors for dementia and Alzheimer's disease: results from EURODEM pooled analyses. *Neurology*, 52(1), pp.78-78.
- Le Bihan, D., Breton, E., Lallemand, D., Grenier, P., Cabanis, E. and Laval-Jeantet, M., 1986. MR imaging of intravoxel incoherent motions: application to diffusion and perfusion in neurologic disorders. *Radiology*, 161(2), pp.401-407.
- Ledig, C., Heckemann, R.A., Hammers, A., Lopez, J.C., Newcombe, V.F., Makropoulos, A., Lötjönen, J., Menon, D.K. and Rueckert, D., 2015. Robust whole-brain segmentation: application to traumatic brain injury. *Medical image analysis*, 21(1), pp.40-58.

- Lee, C., Lopez, O.L., Becker, J.T., Raji, C., Dai, W., Kuller, L.H. and Gach, H.M., 2009. Imaging cerebral blood flow in the cognitively normal aging brain with arterial spin labeling: implications for imaging of neurodegenerative disease. *Journal of Neuroimaging*, 19(4), pp.344-352.
- Lee, C.Y., Soliman, H., Geraghty, B.J., Chen, A.P., Connelly, K.A., Endre, R., Perks, W.J., Heyn, C., Black, S.E. and Cunningham, C.H., 2020. Lactate topography of the human brain using hyperpolarized <sup>13</sup>C-MRI. *Neuroimage*, 204, p.116202.
- Lee, Y., Morrison, B.M., Li, Y., Lengacher, S., Farah, M.H., Hoffman, P.N., Liu, Y., Tsingalia, A., Jin, L., Zhang, P.W. and Pellerin, L., 2012. Oligodendroglia metabolically support axons and contribute to neurodegeneration. *Nature*, 487(7408), pp.443-448.
- Leech, R. and Sharp, D.J., 2014. The role of the posterior cingulate cortex in cognition and disease. *Brain*, 137(1), pp.12-32.
- Leenders, K.L., Perani, D., Lammertsma, A.A., Heather, J.D., Buckingham, P., Jones, T., Healy, M.J.R., Gibbs, J.M., Wise, R.J.S., Hatazawa, J. and Herold, S., 1990. Cerebral blood flow, blood volume and oxygen utilization: normal values and effect of age. *Brain*, 113(1), pp.27-47.
- Leeuwis, A.E., Benedictus, M.R., Kuijter, J.P., Binnewijzend, M.A., Hooghiemstra, A.M., Verfaillie, S.C., Koene, T., Scheltens, P., Barkhof, F., Prins, N.D. and van der Flier, W.M., 2017. Lower cerebral blood flow is associated with impairment in multiple cognitive domains in Alzheimer's disease. *Alzheimer's & Dementia*, 13(5), pp.531-540.
- Leeuwis, A.E., Smith, L.A., Melbourne, A., Hughes, A.D., Richards, M., Prins, N.D., Sokolska, M., Atkinson, D., Tillin, T., Jäger, H.R. and Chaturvedi, N., 2018. Cerebral blood flow and cognitive functioning in a community-based, multi-ethnic cohort: the SABRE Study. *Frontiers in aging neuroscience*, 10, p.279.
- Leidhin, C.N., McMorrow, J., Carey, D., Newman, L., Williamson, W., Fagan, A.J., Chappell, M.A., Kenny, R.A., Meaney, J.F. and Knight, S.P., 2021. Age-related normative changes in cerebral perfusion: data from The Irish Longitudinal Study on Ageing (TILDA). *NeuroImage*, p.117741.
- Levitt, M.H., 2013. *Spin dynamics: basics of nuclear magnetic resonance*. John Wiley & Sons.
- Lezak, M.D., Howieson, D.B., Loring, D.W. and Fischer, J.S., 2004. *Neuropsychological assessment*. Oxford University Press, USA.
- Liang, X., Connelly, A. and Calamante, F., 2013. Improved partial volume correction for single inversion time arterial spin labeling data. *Magnetic resonance in medicine*, 69(2), pp.531-537.
- Lim, Y.M., Cho, Y.W., Shamim, S., Solomon, J., Birn, R., Luh, W.M., Gaillard, W.D., Ritzl, E.K. and Theodore, W.H., 2008. Usefulness of pulsed arterial spin labeling MR imaging in mesial temporal lobe epilepsy. *Epilepsy research*, 82(2-3), pp.183-189.

- Lin, A.L. and Rothman, D.L., 2014. What have novel imaging techniques revealed about metabolism in the aging brain?. *Future neurology*, 9(3), pp.341-354.
- Lin, E.C., 2010, December. Radiation risk from medical imaging. In *Mayo Clinic Proceedings* (Vol. 85, No. 12, pp. 1142-1146). Elsevier.
- Lin, Y., Stephenson, M.C., Xin, L., Napolitano, A. and Morris, P.G., 2012. Investigating the metabolic changes due to visual stimulation using functional proton magnetic resonance spectroscopy at 7 T. *Journal of Cerebral Blood Flow & Metabolism*, 32(8), pp.1484-1495.
- Linn, K.A., Gaonkar, B., Doshi, J., Davatzikos, C. and Shinohara, R.T., 2016. Multivariate pattern analysis and confounding in neuroimaging. *The international journal of biostatistics*, 12(1), p.31.
- Liu, W., Lou, X. and Ma, L., 2016. Use of 3D pseudo-continuous arterial spin labeling to characterize sex and age differences in cerebral blood flow. *Neuroradiology*, 58(9), pp.943-948.
- Liu, Y., Zhu, X., Feinberg, D., Guenther, M., Gregori, J., Weiner, M.W. and Schuff, N., 2012. Arterial spin labeling MRI study of age and gender effects on brain perfusion hemodynamics. *Magnetic resonance in medicine*, 68(3), pp.912-922.
- Lo, E.H., Dalkara, T. and Moskowitz, M.A., 2003. Mechanisms, challenges and opportunities in stroke. *Nature reviews neuroscience*, 4(5), pp.399-414.
- López-Otín, C., Blasco, M.A., Partridge, L., Serrano, M. and Kroemer, G., 2013. The hallmarks of aging. *Cell*, 153(6), pp.1194-1217.
- Lotze, M., Domin, M., Gerlach, F.H., Gaser, C., Lueders, E., Schmidt, C.O. and Neumann, N., 2019. Novel findings from 2,838 adult brains on sex differences in gray matter brain volume. *Scientific reports*, 9(1), pp.1-7.
- Lu, H., Clingman, C., Golay, X. and Van Zijl, P.C., 2004. Determining the longitudinal relaxation time (T1) of blood at 3.0 Tesla. *Magnetic Resonance in Medicine: an Official Journal of the International Society for Magnetic Resonance in Medicine*, 52(3), pp.679-682.
- Lu, H., Golay, X., Pekar, J.J. and Van Zijl, P.C., 2004. Sustained poststimulus elevation in cerebral oxygen utilization after vascular recovery. *Journal of Cerebral Blood Flow & Metabolism*, 24(7), pp.764-770.
- Lu, H., Xu, F., Rodrigue, K.M., Kennedy, K.M., Cheng, Y., Flicker, B., Hebrank, A.C., Uh, J. and Park, D.C., 2011. Alterations in cerebral metabolic rate and blood supply across the adult lifespan. *Cerebral cortex*, 21(6), pp.1426-1434.
- Lüders, E., Gaser, C., Narr, K.L. and Toga, A.W., 2009. Why sex matters: brain size independent differences in gray matter distributions between men and women. *Journal of Neuroscience*, 29(45), pp.14265-14270.
- Lumbreras, B., Salinas, J.M. and Gonzalez-Alvarez, I., 2019. Cumulative exposure to ionising radiation from diagnostic imaging tests: a 12-year follow-up population-based analysis in Spain. *BMJ open*, 9(9), p.e030905.

Lundgaard, I., Li, B., Xie, L., Kang, H., Sanggaard, S., Haswell, J.D., Sun, W., Goldman, S., Blekot, S., Nielsen, M. and Takano, T., 2015. Direct neuronal glucose uptake heralds activity-dependent increases in cerebral metabolism. *Nature communications*, 6(1), pp.1-12.

Lupien, S.J., McEwen, B.S., Gunnar, M.R. and Heim, C., 2009. Effects of stress throughout the lifespan on the brain, behaviour and cognition. *Nature reviews neuroscience*, 10(6), pp.434-445.

Lustig, C., Shah, P., Seidler, R. and Reuter-Lorenz, P.A., 2009. Aging, training, and the brain: a review and future directions. *Neuropsychology review*, 19(4), pp.504-522.

Lytle, M.E., Vander Bilt, J., Pandav, R.S., Dodge, H.H. and Ganguli, M., 2004. Exercise level and cognitive decline: the MoVIES project. *Alzheimer Disease & Associated Disorders*, 18(2), pp.57-64.

MacDonald, M.E., Williams, R.J., Rajashekar, D., Stafford, R.B., Hanganu, A., Sun, H., Berman, A.J., McCreary, C.R., Frayne, R., Forkert, N.D. and Pike, G.B., 2020. Age-related differences in cerebral blood flow and cortical thickness with an application to age prediction. *Neurobiology of Aging*, 95, pp.131-142.

MacPherson, S. and Cox, S., 2017. The frontal ageing hypothesis: Evidence from normal ageing and dementia.

Magistretti, P.J. and Allaman, I., 2018. Lactate in the brain: from metabolic end-product to signalling molecule. *Nature Reviews Neuroscience*, 19(4), p.235.

Magistretti, P.J., Pellerin, L., Rothman, D.L. and Shulman, R.G., 1999. Energy on demand. *Science*, 283(5401), pp.496-497.

Maher, R.L., Hanlon, J. and Hajjar, E.R., 2014. Clinical consequences of polypharmacy in elderly. *Expert opinion on drug safety*, 13(1), pp.57-65.

Majós, C., Alonso, J., Aguilera, C., Serrallonga, M., Pérez-Martín, J., Acebes, J.J., Arús, C. and Gili, J., 2003. Proton magnetic resonance spectroscopy (1 H MRS) of human brain tumours: assessment of differences between tumour types and its applicability in brain tumour categorization. *European radiology*, 13(3), pp.582-591.

Mak, H.K., Chan, Q., Zhang, Z., Petersen, E.T., Qiu, D., Zhang, L., Yau, K.K., Chu, L.W. and Golay, X., 2012. Quantitative assessment of cerebral hemodynamic parameters by QUASAR arterial spin labeling in Alzheimer's disease and cognitively normal Elderly adults at 3-tesla. *Journal of Alzheimer's Disease*, 31(1), pp.33-44.

Makris, N., Goldstein, J.M., Kennedy, D., Hodge, S.M., Caviness, V.S., Faraone, S.V., Tsuang, M.T. and Seidman, L.J., 2006. Decreased volume of left and total anterior insular lobule in schizophrenia. *Schizophrenia research*, 83(2-3), pp.155-171.

Mangia, S., Tkáč, I., Gruetter, R., Van de Moortele, P.F., Maraviglia, B. and Uğurbil, K., 2007. Sustained neuronal activation raises oxidative metabolism to a new steady-state level: evidence from 1H NMR spectroscopy in the

human visual cortex. *Journal of cerebral blood flow & metabolism*, 27(5), pp.1055-1063.

Mansfield, P. and Maudsley, A.A., 1977. Medical imaging by NMR. *The British journal of radiology*, 50(591), pp.188-194.

Mantri, S., Nwadiogbu, C., Fitts, W. and Dahodwala, N., 2019. Quality of education impacts late-life cognition. *International journal of geriatric psychiatry*, 34(6), pp.855-862.

Marjańska, M., Auerbach, E.J., Valabrègue, R., Van de Moortele, P.F., Adriany, G. and Garwood, M., 2012. Localized <sup>1</sup>H NMR spectroscopy in different regions of human brain in vivo at 7 T: T2 relaxation times and concentrations of cerebral metabolites. *NMR in Biomedicine*, 25(2), pp.332-339.

Martin, A.J., Friston, K.J., Colebatch, J.G. and Frackowiak, R.S., 1991. Decreases in regional cerebral blood flow with normal aging. *Journal of Cerebral Blood Flow & Metabolism*, 11(4), pp.684-689.

Martin, W.W., 2007. MR spectroscopy in neurodegenerative disease. *Molecular imaging and biology*, 9(4), pp.196-203.

Martirosian, P., Pohmann, R., Schraml, C., Schwartz, M., Kuestner, T., Schwenzer, N.F., Scheffler, K., Nikolaou, K. and Schick, F., 2019. Spatial-temporal perfusion patterns of the human liver assessed by pseudo-continuous arterial spin labeling MRI. *Zeitschrift für Medizinische Physik*, 29(2), pp.173-183.

*MATLAB R2018a*, The Mathworks, Inc., Natick, Massachusetts, United States. Available at <http://www.mathworks.com>

Mattson, M.P. and Arumugam, T.V., 2018. Hallmarks of brain aging: adaptive and pathological modification by metabolic states. *Cell metabolism*, 27(6), pp.1176-1199.

Maudsley, A.A., Govindaraju, V., Young, K., Aygula, Z.K., Pattany, P.M., Soher, B.J. and Matson, G.B., 2005. Numerical simulation of PRESS localized MR spectroscopy. *Journal of magnetic resonance*, 173(1), pp.54-63.

Mazziotta, J., Toga, A., Evans, A., Fox, P., Lancaster, J., Zilles, K., Woods, R., Paus, T., Simpson, G., Pike, B. and Holmes, C., 2001a. A probabilistic atlas and reference system for the human brain: International Consortium for Brain Mapping (ICBM). *Philosophical Transactions of the Royal Society of London. Series B: Biological Sciences*, 356(1412), pp.1293-1322.

Mazziotta, J., Toga, A., Evans, A., Fox, P., Lancaster, J., Zilles, K., Woods, R., Paus, T., Simpson, G., Pike, B. and Holmes, C., 2001b. A four-dimensional probabilistic atlas of the human brain. *Journal of the American Medical Informatics Association*, 8(5), pp.401-430.

Mazziotta, J.C., Toga, A.W., Evans, A., Fox, P. and Lancaster, J., 1995. A probabilistic atlas of the human brain: theory and rationale for its development. *Neuroimage*, 2(2), pp.89-101.

McConathy, J. and Sheline, Y.I., 2015. Imaging biomarkers associated with cognitive decline: a review. *Biological psychiatry*, 77(8), pp.685-692.

McCreary, C.R., Salluzzi, M., Andersen, L.B., Gobbi, D., Lauzon, L., Saad, F., Smith, E.E. and Frayne, R., 2020. Calgary Normative Study: design of a prospective longitudinal study to characterise potential quantitative MR biomarkers of neurodegeneration over the adult lifespan. *BMJ open*, 10(8), p.e038120.

McGowan, T., Ong, T., Kumar, A., Lunt, E. and Sahota, O., 2018. The effect of chair-based pedal exercises for older people admitted to an acute hospital compared to standard care: a feasibility study. *Age and ageing*, 47(3), pp.483-486.

McKenna, M. C., Gruetter, R., Sonnewald, U., Waagepetersen, H. S. & Schousboe, A. in *Basic Neurochemistry : Molecular, Cellular and Medical Aspects* (eds Brady, Scott, Siegel, G. & Albers, R. W.) (Academic Press, Burlington, US, 2005).

Meisami, E., Brown, C.M. and Emerle, H.F., 2007. Sensory systems: normal aging, disorders, and treatments of vision and hearing in humans. In *Physiological basis of aging and geriatrics* (pp. 121-148). CRC Press.

Mekle, R., Mlynárik, V., Gambarota, G., Hergt, M., Krueger, G. and Gruetter, R., 2009. MR spectroscopy of the human brain with enhanced signal intensity at ultrashort echo times on a clinical platform at 3T and 7T. *Magnetic Resonance in Medicine: An Official Journal of the International Society for Magnetic Resonance in Medicine*, 61(6), pp.1279-1285.

Meltzer, C.C., Cantwell, M.N., Greer, P.J., Ben-Eliezer, D., Smith, G., Frank, G., Kaye, W.H., Houck, P.R. and Price, J.C., 2000. Does cerebral blood flow decline in healthy aging? A PET study with partial-volume correction. *Journal of Nuclear Medicine*, 41(11), pp.1842-1848.

Melzer, T.R., Watts, R., MacAskill, M.R., Pearson, J.F., Rüeger, S., Pitcher, T.L., Livingston, L., Graham, C., Keenan, R., Shankaranarayanan, A. and Alsop, D.C., 2011. Arterial spin labelling reveals an abnormal cerebral perfusion pattern in Parkinson's disease. *Brain*, 134(3), pp.845-855.

Menon, V. and Uddin, L.Q., 2010. Saliency, switching, attention and control: a network model of insula function. *Brain structure and function*, 214(5-6), pp.655-667.

Merboldt, K.D., Bruhn, H., Hanicke, W., Michaelis, T. and Frahm, J., 1992. Decrease of glucose in the human visual cortex during photic stimulation. *Magnetic Resonance in Medicine*, 25(1), pp.187-194.

Mergenthaler, P., Lindauer, U., Dienel, G.A. and Meisel, A., 2013. Sugar for the brain: the role of glucose in physiological and pathological brain function. *Trends in neurosciences*, 36(10), pp.587-597.

Mevel, K., Chételat, G., Eustache, F. and Desgranges, B., 2011. The default mode network in healthy aging and Alzheimer's disease. *International journal of Alzheimer's disease*, 2011.

Miklossy, J., 2003. Cerebral hypoperfusion induces cortical watershed microinfarcts which may further aggravate cognitive decline in Alzheimer's disease. *Neurological research*, 25(6), pp.605-610.

- Mintzer, J. and Burns, A., 2000. Anticholinergic side-effects of drugs in elderly people. *Journal of the Royal Society of Medicine*, 93(9), pp.457-462.
- Moeller, J.R., Ishikawa, T., Dhawan, V., Spetsieris, P., Mandel, F., Alexander, G.E., Grady, C., Pietrini, P. and Eidelberg, D., 1996. The metabolic topography of normal aging. *Journal of Cerebral Blood Flow & Metabolism*, 16(3), pp.385-398.
- Moeller, J.R., Strother, S.C., Sidtis, J.J. and Rottenberg, D.A., 1987. Scaled subprofile model: a statistical approach to the analysis of functional patterns in positron emission tomographic data. *Journal of Cerebral Blood Flow & Metabolism*, 7(5), pp.649-658.
- Momjian-Mayor, I. and Baron, J.C., 2005. The pathophysiology of watershed infarction in internal carotid artery disease: review of cerebral perfusion studies. *Stroke*, 36(3), pp.567-577.
- Montero-Odasso, M., Pieruccini-Faria, F., Ismail, Z., Li, K., Lim, A., Phillips, N., Kamkar, N., Sarquis-Adamson, Y., Speechley, M., Theou, O. and Verghese, J., 2020. CCCDTD5 recommendations on early non cognitive markers of dementia: A Canadian consensus. *Alzheimer's & Dementia: Translational Research & Clinical Interventions*, 6(1), p.e12068.
- Montine, T.J., Cholerton, B.A., Corrada, M.M., Edland, S.D., Flanagan, M.E., Hemmy, L.S., Kawas, C.H. and White, L.R., 2019. Concepts for brain aging: resistance, resilience, reserve, and compensation. *Alzheimer's research & therapy*, 11(1), pp.1-3.
- Morgan, J.F., 2007. p Value fetishism and use of the Bonferroni adjustment. *Evidence-based mental health*, 10(2), pp.34-35.
- Mormino, E.C. and Papp, K.V., 2018. Amyloid accumulation and cognitive decline in clinically normal older individuals: Implications for aging and early Alzheimer's disease. *Journal of Alzheimer's Disease*, 64(s1), pp.S633-S646.
- Morris, J.C., Roe, C.M., Xiong, C., Fagan, A.M., Goate, A.M., Holtzman, D.M. and Mintun, M.A., 2010. APOE predicts amyloid-beta but not tau Alzheimer pathology in cognitively normal aging. *Annals of neurology*, 67(1), pp.122-131.
- Mosconi, L., 2005. Brain glucose metabolism in the early and specific diagnosis of Alzheimer's disease. *European journal of nuclear medicine and molecular imaging*, 32(4), pp.486-510.
- Mosconi, L., Mistur, R., Switalski, R., Tsui, W.H., Glodzik, L., Li, Y., Pirraglia, E., De Santi, S., Reisberg, B., Wisniewski, T. and de Leon, M.J., 2009. FDG-PET changes in brain glucose metabolism from normal cognition to pathologically verified Alzheimer's disease. *European Journal of Nuclear Medicine and Molecular Imaging*, 36(5), pp.811-822.
- Mosconi, L., Sorbi, S., De Leon, M.J., Li, Y., Nacmias, B., Myoung, P.S., Tsui, W., Ginestroni, A., Bessi, V., Fayyazz, M. and Caffarra, P., 2006. Hypometabolism exceeds atrophy in presymptomatic early-onset familial Alzheimer's disease. *Journal of Nuclear Medicine*, 47(11), pp.1778-1786.
- Mosconi, L., Tsui, W.H., Herholz, K., Pupi, A., Drzezga, A., Lucignani, G., Reiman, E.M., Holthoff, V., Kalbe, E., Sorbi, S. and Diehl-Schmid, J., 2008. Multicenter standardized 18F-FDG PET diagnosis of mild cognitive

impairment, Alzheimer's disease, and other dementias. *Journal of nuclear medicine*, 49(3), pp.390-398.

Mugler III, J.P. and Brookeman, J.R., 1990. Three-dimensional magnetization-prepared rapid gradient-echo imaging (3D MP RAGE). *Magnetic resonance in medicine*, 15(1), pp.152-157.

Munn, Z. and Jordan, Z., 2011. The patient experience of high technology medical imaging: a systematic review of the qualitative evidence. *Radiography*, 17(4), pp.323-331.

Murphy, M., Loosemore, A., Clifton, A.G., Howe, F.A., Tate, A.R., Cudlip, S.A., Wilkins, P.R., Griffiths, J.R. and Bell, B.A., 2002. The contribution of proton magnetic resonance spectroscopy (1 HMRS) to clinical brain tumour diagnosis. *British journal of neurosurgery*, 16(4), pp.329-334.

Musiek, E.S., Chen, Y., Korczykowski, M., Saboury, B., Martinez, P.M., Reddin, J.S., Alavi, A., Kimberg, D.Y., Wolk, D.A., Julin, P. and Newberg, A.B., 2012. Direct comparison of FDG-PET and ASL-MRI in Alzheimer's disease. *Alzheimer's & dementia: the journal of the Alzheimer's Association*, 8(1), p.51.

Mutsaerts, H.J., Petr, J., Bokkers, R.P., Lazar, R.M., Marshall, R.S. and Asllani, I., 2020. Spatial coefficient of variation of arterial spin labeling MRI as a cerebrovascular correlate of carotid occlusive disease. *Plos one*, 15(2), p.e0229444.

Mutsaerts, H.J., Petr, J., Thomas, D.L., De Vita, E., Cash, D.M., Van Osch, M.J., Golay, X., Groot, P.F., Ourselin, S., van Swieten, J. and Laforce Jr, R., 2018. Comparison of arterial spin labeling registration strategies in the multi-center GENetic frontotemporal dementia initiative (GENFI). *Journal of Magnetic Resonance Imaging*, 47(1), pp.131-140.

Mutsaerts, H.J., Petr, J., Václavů, L., Van Dalen, J.W., Robertson, A.D., Caan, M.W., Masellis, M., Nederveen, A.J., Richard, E. and MacIntosh, B.J., 2017. The spatial coefficient of variation in arterial spin labeling cerebral blood flow images. *Journal of Cerebral Blood Flow & Metabolism*, 37(9), pp.3184-3192.

Mutsaerts, H.J., Van Osch, M.J., Zelaya, F.O., Wang, D.J., Nordhøy, W., Wang, Y., Wastling, S., Fernandez-Seara, M.A., Petersen, E.T., Pizzini, F.B. and Fallatah, S., 2015. Multi-vendor reliability of arterial spin labeling perfusion MRI using a near-identical sequence: implications for multi-center studies. *Neuroimage*, 113, pp.143-152.

Mutsaerts, H.J., Van Dalen, J., Heijtel, D.F.R., Groot, P.F.C., Majoie, C.B.L.M., Petersen, E.T., Richard, E. and Nederveen, A.J., 2015. Cerebral perfusion measurements in elderly with hypertension using arterial spin labeling. *PloS one*, 10(8), p.e0133717.

Nadebaum, D.P., Krishnadas, N., Poon, A.M., Kalff, V., Lichtenstein, M., Villemagne, V.L., Jones, G. and Rowe, C.C., 2020. A head-to-head comparison of cerebral blood flow SPECT and 18F-FDG PET in the diagnosis of Alzheimer's Disease. *Internal medicine journal*.

Nagahama, Y., Okada, T., Katsumi, Y., Hayashi, T., Yamauchi, H., Sawamoto, N., Toma, K., Nakamura, K., Hanakawa, T., Konishi, J. and Fukuyama, H., 1999. Transient neural activity in the medial superior frontal

gyrus and precuneus time locked with attention shift between object features. *Neuroimage*, 10(2), pp.193-199.

Nakano, S., Asada, T., Matsuda, H., Uno, M. and Takasaki, M., 2000. Effects of healthy aging on the regional cerebral blood flow measurements using 99mTc-ECD SPECT assessed with statistical parametric mapping. *Nihon Ronen Igakkai zasshi. Japanese journal of geriatrics*, 37(1), pp.49-55.

Naressi, A., Couturier, C., Devos, J.M., Janssen, M., Mangeat, C., De Beer, R. and Graveron-Demilly, D., 2001. Java-based graphical user interface for the MRUI quantitation package. *Magnetic Resonance Materials in Physics, Biology and Medicine*, 12(2-3), p.141.

Nasreddine, Z.S., Phillips, N.A., Bédirian, V., Charbonneau, S., Whitehead, V., Collin, I., Cummings, J.L. and Chertkow, H., 2005. The Montreal Cognitive Assessment, MoCA: a brief screening tool for mild cognitive impairment. *Journal of the American Geriatrics Society*, 53(4), pp.695-699.

Neary, D., Snowden, J.S., Northen, B. and Goulding, P., 1988. Dementia of frontal lobe type. *Journal of Neurology, Neurosurgery & Psychiatry*, 51(3), pp.353-361.

Newington, J.T., Harris, R.A. and Cumming, R.C., 2013. Reevaluating metabolism in Alzheimer's disease from the perspective of the astrocyte-neuron lactate shuttle model. *Journal of neurodegenerative diseases*, 2013.

Newsholme, P., Lima, M.M.R., Procopio, J., Pithon-Curi, T.C., Bazotte, R.B. and Curi, R., 2003. Glutamine and glutamate as vital metabolites. *Brazilian Journal of Medical and Biological Research*, 36(2), pp.153-163.

Ng, K.K., Lo, J.C., Lim, J.K., Chee, M.W. and Zhou, J., 2016. Reduced functional segregation between the default mode network and the executive control network in healthy older adults: a longitudinal study. *Neuroimage*, 133, pp.321-330.

Nichols, T.E. and Holmes, A.P., 2002. Nonparametric permutation tests for functional neuroimaging: a primer with examples. *Human brain mapping*, 15(1), pp.1-25.

Niu, X., Zhang, F., Kounios, J. and Liang, H., 2020. Improved prediction of brain age using multimodal neuroimaging data. *Human brain mapping*, 41(6), pp.1626-1643.

Niu, X., Zheng, S., Liu, H. and Li, S., 2018. Protective effects of taurine against inflammation, apoptosis, and oxidative stress in brain injury. *Molecular medicine reports*, 18(5), pp.4516-4522.

Nobili, F., Salmaso, D., Morbelli, S., Girtler, N., Piccardo, A., Brugnolo, A., Dessi, B., Larsson, S.A., Rodriguez, G. and Pagani, M., 2008. Principal component analysis of FDG PET in amnesic MCI. *European journal of nuclear medicine and molecular imaging*, 35(12), pp.2191-2202.

Norton, S., Matthews, F.E. and Brayne, C., 2013. A commentary on studies presenting projections of the future prevalence of dementia. *BMC Public Health*, 13(1), pp.1-5.

- Nowinski, W.L., Chua, B.C., Marchenko, Y., Puspitsari, F., Volkau, I. and Knopp, M.V., 2011. Three-dimensional reference and stereotactic atlas of human cerebrovasculature from 7 Tesla. *Neuroimage*, 55(3), pp.986-998.
- Nystoriak, M.A. and Bhatnagar, A., 2018. Cardiovascular effects and benefits of exercise. *Frontiers in cardiovascular medicine*, 5, p.135.
- O'Brien, J.T. and Thomas, A., 2015. Vascular dementia. *The Lancet*, 386(10004), pp.1698-1706.
- Odudu, A., Nery, F., Hartevelde, A.A., Evans, R.G., Pendse, D., Buchanan, C.E., Francis, S.T. and Fernández-Seara, M.A., 2018. Arterial spin labelling MRI to measure renal perfusion: a systematic review and statement paper. *Nephrology Dialysis Transplantation*, 33(suppl\_2), pp.ii15-ii21.
- Oeppen, J. and Vaupel, J.W., 2002. Broken limits to life expectancy. *Science* 296, 1029-1031.
- Okell, T.W., Chappell, M.A., Woolrich, M.W., Günther, M., Feinberg, D.A. and Jezzard, P., 2010. Vessel-encoded dynamic magnetic resonance angiography using arterial spin labeling. *Magnetic resonance in medicine*, 64(3), pp.698-706.
- Olson, R.A., Chhanabhai, T. and McKenzie, M., 2008. Feasibility study of the Montreal Cognitive Assessment (MoCA) in patients with brain metastases. *Supportive Care in Cancer*, 16(11), pp.1273-1278.
- Ordidge, R.J., Connelly, A. and Lohman, J.A., 1986. Image-selected in vivo spectroscopy (ISIS). A new technique for spatially selective NMR spectroscopy. *Journal of Magnetic Resonance (1969)*, 66(2), pp.283-294.
- Öz, G. and Tkáč, I., 2011. Short-echo, single-shot, full-intensity proton magnetic resonance spectroscopy for neurochemical profiling at 4 T: validation in the cerebellum and brainstem. *Magnetic Resonance in Medicine*, 65(4), pp.901-910.
- Pagani, M., Salmaso, D., Jonsson, C., Hatherly, R., Jacobsson, H., Larsson, S.A. and Wägner, A., 2002. Regional cerebral blood flow as assessed by principal component analysis and 99m Tc-HMPAO SPET in healthy subjects at rest: normal distribution and effect of age and gender. *European journal of nuclear medicine and molecular imaging*, 29(1), pp.67-75.
- Pagani, M., Salmaso, D., Rodriguez, G., Nardo, D. and Nobili, F., 2009. Principal component analysis in mild and moderate Alzheimer's disease—A novel approach to clinical diagnosis. *Psychiatry Research: Neuroimaging*, 173(1), pp.8-14.
- Palmqvist, S., Schöll, M., Strandberg, O., Mattsson, N., Stomrud, E., Zetterberg, H., Blennow, K., Landau, S., Jagust, W. and Hansson, O., 2017. Earliest accumulation of  $\beta$ -amyloid occurs within the default-mode network and concurrently affects brain connectivity. *Nature communications*, 8(1), pp.1-13.
- Pan, B., Jin, X., Jun, L., Qiu, S., Zheng, Q. and Pan, M., 2019. The relationship between smoking and stroke: a meta-analysis. *Medicine*, 98(12).

- Pantoni, L., 2010. Cerebral small vessel disease: from pathogenesis and clinical characteristics to therapeutic challenges. *The Lancet Neurology*, 9(7), pp.689-701.
- Papuć, E. and Rejdak, K., 2020. The role of myelin damage in Alzheimer's disease pathology. *Archives of medical science: AMS*, 16(2), p.345.
- Pardo, J.V., Lee, J.T., Sheikh, S.A., Surerus-Johnson, C., Shah, H., Munch, K.R., Carlis, J.V., Lewis, S.M., Kuskowski, M.A. and Dysken, M.W., 2007. Where the brain grows old: decline in anterior cingulate and medial prefrontal function with normal aging. *Neuroimage*, 35(3), pp.1231-1237.
- Parkes, L.M., 2003. *Measuring blood perfusion in the brain using Arterial spin labelled MRI*. University of London, University College London (United Kingdom).
- Parkes, L.M., Rashid, W., Chard, D.T. and Tofts, P.S., 2004. Normal cerebral perfusion measurements using arterial spin labeling: reproducibility, stability, and age and gender effects. *Magnetic Resonance in Medicine: An Official Journal of the International Society for Magnetic Resonance in Medicine*, 51(4), pp.736-743.
- Partington, J.E. and Leiter, R.G., 1949. Partington's Pathways Test. *Psychological Service Center Journal*.
- Paulson, O.B., 2002. Blood-brain barrier, brain metabolism and cerebral blood flow. *European Neuropsychopharmacology*, 12(6), pp.495-501.
- Pearson, K., 1901. LIII. On lines and planes of closest fit to systems of points in space. *The London, Edinburgh, and Dublin Philosophical Magazine and Journal of Science*, 2(11), pp.559-572.
- Pellerin, L. and Magistretti, P.J., 1994. Glutamate uptake into astrocytes stimulates aerobic glycolysis: a mechanism coupling neuronal activity to glucose utilization. *Proceedings of the National Academy of Sciences*, 91(22), pp.10625-10629.
- Pellerin, L., Bouzier-Sore, A.K., Aubert, A., Serres, S., Merle, M., Costalat, R. and Magistretti, P.J., 2007. Activity-dependent regulation of energy metabolism by astrocytes: an update. *Glia*, 55(12), pp.1251-1262.
- Pellerin, L., Pellegrini, G., Bittar, P.G., Charnay, Y., Bouras, C., Martin, J.L., Stella, N. and Magistretti, P.J., 1998. Evidence supporting the existence of an activity-dependent astrocyte-neuron lactate shuttle. *Developmental neuroscience*, 20(4-5), pp.291-299.
- Perneger, T.V., 1998. What's wrong with Bonferroni adjustments. *Bmj*, 316(7139), pp.1236-1238.
- Peters, R., 2006. Ageing and the brain. *Postgraduate medical journal*, 82(964), pp.84-88.
- Petit-Taboué, M.C., Landeau, B., Desson, J.F., Desgranges, B. and Baron, J.C., 1998. Effects of healthy aging on the regional cerebral metabolic rate of glucose assessed with statistical parametric mapping. *Neuroimage*, 7(3), pp.176-184.

- Pfister, H., Kaynig, V., Botha, C.P., Bruckner, S., Dercksen, V.J., Hege, H.C. and Roerdink, J.B., 2012. Visualization in connectomics. *arXiv preprint arXiv:1206.1428*.
- Pieper, N.T., Grossi, C.M., Chan, W.Y., Loke, Y.K., Savva, G.M., Haroulis, C., Steel, N., Fox, C., Maidment, I.D., Arthur, A.J. and Myint, P.K., 2020. Anticholinergic drugs and incident dementia, mild cognitive impairment and cognitive decline: a meta-analysis. *Age and ageing*, 49(6), pp.939-947.
- Pini, L., Pievani, M., Bocchetta, M., Altomare, D., Bosco, P., Cavedo, E., Galluzzi, S., Marizzoni, M. and Frisoni, G.B., 2016. Brain atrophy in Alzheimer's disease and aging. *Ageing research reviews*, 30, pp.25-48.
- Pinto, T.C., Machado, L., Bulgacov, T.M., Rodrigues-Júnior, A.L., Costa, M.L., Ximenes, R.C. and Sougey, E.B., 2019. Is the Montreal Cognitive Assessment (MoCA) screening superior to the Mini-Mental State Examination (MMSE) in the detection of mild cognitive impairment (MCI) and Alzheimer's Disease (AD) in the elderly?. *International Psychogeriatrics*, 31(4), pp.491-504.
- Pirastru, A., Pelizzari, L., Bergsland, N., Cazzoli, M., Cecconi, P., Baglio, F. and Laganà, M.M., 2020. Consistent Cerebral Blood Flow Covariance Networks across Healthy Individuals and Their Similarity with Resting State Networks and Vascular Territories. *Diagnostics*, 10(11), p.963.
- Prabhakaran, S. and Naidech, A.M., 2012. Ischemic brain injury after intracerebral hemorrhage: a critical review. *Stroke*, 43(8), pp.2258-2263.
- Pradhan, S., Bonekamp, S., Gillen, J.S., Rowland, L.M., Wijtenburg, S.A., Edden, R.A. and Barker, P.B., 2015. Comparison of single voxel brain MRS AT 3 T and 7 T using 32-channel head coils. *Magnetic resonance imaging*, 33(8), pp.1013-1018.
- Preibisch, C., Sorg, C., Förchler, A., Grimmer, T., Sax, I., Wohlschläger, A.M., Perneczky, R., Förstl, H., Kurz, A., Zimmer, C. and Alexopoulos, P., 2011. Age-related cerebral perfusion changes in the parietal and temporal lobes measured by pulsed arterial spin labeling. *Journal of Magnetic Resonance Imaging*, 34(6), pp.1295-1302.
- Prenderville, J.A., Kennedy, P.J., Dinan, T.G. and Cryan, J.F., 2015. Adding fuel to the fire: the impact of stress on the ageing brain. *Trends in neurosciences*, 38(1), pp.13-25.
- Prichard, J., Rothman, D., Novotny, E., Petroff, O., Kuwabara, T., Avison, M., Howseman, A., Hanstock, C. and Shulman, R., 1991. Lactate rise detected by <sup>1</sup>H NMR in human visual cortex during physiologic stimulation. *Proceedings of the National Academy of Sciences of the United States of America*, 88(13), p.5829.
- Prince, M., Bryce, R., Albanese, E., Wimo, A., Ribeiro, W. and Ferri, C.P., 2013. The global prevalence of dementia: a systematic review and metaanalysis. *Alzheimer's & dementia*, 9(1), pp.63-75.
- Proctor, W.G. and Yu, F.C., 1950. The dependence of a nuclear magnetic resonance frequency upon chemical compound. *Physical Review*, 77(5), p.717.

Provencher, S.W., 1993. Estimation of metabolite concentrations from localized in vivo proton NMR spectra. *Magnetic resonance in medicine*, 30(6), pp.672-679.

Quarantelli, M., Berkouk, K., Prinster, A., Landeau, B., Svarer, C., Balkay, L., Alfano, B., Brunetti, A., Baron, J.C. and Salvatore, M., 2004. Integrated software for the analysis of brain PET/SPECT studies with partial-volume-effect correction. *Journal of Nuclear Medicine*, 45(2), pp.192-201.

Qureshi, A.I., Hanel, R.A., Kirmani, J.F., Yahia, A.M. and Hopkins, L.N., 2002. Cerebral blood flow changes associated with intracerebral hemorrhage. *Neurosurgery Clinics*, 13(3), pp.355-370.

Rabi, I.I., Ramsey, N.F. and Schwinger, J., 1954. Use of rotating coordinates in magnetic resonance problems. *Reviews of Modern Physics*, 26(2), p.167.

Rackayova, V., Cudalbu, C., Pouwels, P.J. and Braissant, O., 2017. Creatine in the central nervous system: From magnetic resonance spectroscopy to creatine deficiencies. *Analytical biochemistry*, 529, pp.144-157.

Raichle, M.E. and Gusnard, D.A., 2002. Appraising the brain's energy budget. *Proceedings of the National Academy of Sciences*, 99(16), pp.10237-10239.

Reckziegel, D., Raschke, F., Cottam, W.J. and Auer, D.P., 2016. Cingulate GABA levels inversely correlate with the intensity of ongoing chronic knee osteoarthritis pain. *Molecular pain*, 12, p.1744806916650690.

Reichstadt, J., Sengupta, G., Depp, C.A., Palinkas, L.A. and Jeste, D.V., 2010. Older adults' perspectives on successful aging: Qualitative interviews. *The American Journal of Geriatric Psychiatry*, 18(7), pp.567-575.

Reiner, M., Niermann, C., Jekauc, D. and Woll, A., 2013. Long-term health benefits of physical activity—a systematic review of longitudinal studies. *BMC public health*, 13(1), pp.1-9.

Reisberg, B., Franssen, E.H., Hasan, S.M., Monteiro, I., Boksay, I., Souren, L.E., Kenowsky, S., Auer, S.R., Elahi, S. and Kluger, A., 1999. Retrogenesis: clinical, physiologic, and pathologic mechanisms in brain aging, Alzheimer's and other dementing processes. *European Archives of Psychiatry and Clinical Neuroscience*, 249(3), pp.S28-S36.

Reisberg, B., Franssen, E.H., Souren, L.E., Auer, S.R., Akram, I. and Kenowsky, S., 2002. Evidence and mechanisms of retrogenesis in Alzheimer's and other dementias: management and treatment import. *American Journal of Alzheimer's Disease & Other Dementias*®, 17(4), pp.202-212.

Respino, M., Jaywant, A., Kuceyeski, A., Victoria, L.W., Hoptman, M.J., Scult, M.A., Sankin, L., Pimontel, M., Liston, C., Murri, M.B. and Alexopoulos, G.S., 2019. The impact of white matter hyperintensities on the structural connectome in late-life depression: relationship to executive functions. *NeuroImage: Clinical*, 23, p.101852.

Rex, D.E., Ma, J.Q. and Toga, A.W., 2003. The LONI pipeline processing environment. *Neuroimage*, 19(3), pp.1033-1048.

- Ribeiro, A., Husson, O., Drey, N., Murray, I., May, K., Thurston, J. and Oyen, W., 2020. Ionising radiation exposure from medical imaging—a review of Patient's (un) awareness. *Radiography*, 26(2), pp.e25-e30.
- Risacher, S.L., McDonald, B.C., Tallman, E.F., West, J.D., Farlow, M.R., Unverzagt, F.W., Gao, S., Boustani, M., Crane, P.K., Petersen, R.C. and Jack, C.R., 2016. Association between anticholinergic medication use and cognition, brain metabolism, and brain atrophy in cognitively normal older adults. *JAMA neurology*, 73(6), pp.721-732.
- Ritchie, S.J., Cox, S.R., Shen, X., Lombardo, M.V., Reus, L.M., Alloza, C., Harris, M.A., Alderson, H.L., Hunter, S., Neilson, E. and Liewald, D.C., 2018. Sex differences in the adult human brain: evidence from 5216 UK biobank participants. *Cerebral cortex*, 28(8), pp.2959-2975.
- Roberts, R.O., Geda, Y.E., Knopman, D.S., Cha, R.H., Pankratz, V.S., Boeve, B.F., Ivnik, R.J., Tangalos, E.G., Petersen, R.C. and Rocca, W.A., 2008. The Mayo Clinic Study of Aging: design and sampling, participation, baseline measures and sample characteristics. *Neuroepidemiology*, 30(1), pp.58-69.
- Rodrigues, T.B., Valette, J. and Bouzier-Sore, A.K., 2013. <sup>13</sup>C NMR spectroscopy applications to brain energy metabolism. *Frontiers in neuroenergetics*, 5, p.9.
- Rogalski, E.J., Gefen, T., Shi, J., Samimi, M., Bigio, E., Weintraub, S., Geula, C. and Mesulam, M.M., 2013. Youthful memory capacity in old brains: anatomic and genetic clues from the Northwestern SuperAging Project. *Journal of cognitive neuroscience*, 25(1), pp.29-36.
- Rohlfing, T., 2011. Image similarity and tissue overlaps as surrogates for image registration accuracy: widely used but unreliable. *IEEE transactions on medical imaging*, 31(2), pp.153-163.
- Rokicki, J., Wolfers, T., Nordhøy, W., Tesli, N., Quintana, D.S., Alnæs, D., Richard, G., de Lange, A.M.G., Lund, M.J., Norbom, L. and Agartz, I., 2021. Multimodal imaging improves brain age prediction and reveals distinct abnormalities in patients with psychiatric and neurological disorders. *Human brain mapping*, 42(6), pp.1714-1726.
- Román, G.C., 2004. Brain hypoperfusion: a critical factor in vascular dementia. *Neurological research*, 26(5), pp.454-458.
- Romanowski, C.A. and Wilkinson, I.D., 2011. Atrophy: when too much atrophy is too little brain. *Neuroradiology*, 53(1), pp.133-139.
- Romeo, B., Petillion, A., Martelli, C. and Benyamina, A., 2020. Magnetic resonance spectroscopy studies in subjects with high risk for psychosis: A meta-analysis and review. *Journal of psychiatric research*, 125, pp.52-65.
- Rosen, W.G., Mohs, R.C. and Davis, K.L., 1984. A new rating scale for Alzheimer's disease. *The American journal of psychiatry*.
- Ross, J.M., Öberg, J., Brené, S., Coppotelli, G., Terzioglu, M., Pernold, K., Goiny, M., Sitnikov, R., Kehr, J., Trifunovic, A. and Larsson, N.G., 2010. High brain lactate is a hallmark of aging and caused by a shift in the lactate dehydrogenase A/B ratio. *Proceedings of the National Academy of Sciences*, 107(46), pp.20087-20092.

- Rossini, F., Zauner, H., Bergmann, J., Kronbichler, M., Spindler, I., Golaszewski, S., Trinka, E. and Staffen, W., 2019. HMPAO-SPECT can discriminate between patients with subjective cognitive complaints with and without cognitive deficits and those with mild cognitive impairment. *Current Alzheimer Research*, 16(9), pp.843-851.
- Rothman, K.J., 1990. No adjustments are needed for multiple comparisons. *Epidemiology*, pp.43-46.
- Rueckert, D., Sonoda, L.I., Hayes, C., Hill, D.L., Leach, M.O. and Hawkes, D.J., 1999. Nonrigid registration using free-form deformations: application to breast MR images. *IEEE transactions on medical imaging*, 18(8), pp.712-721.
- Rusinek, H., Brys, M., Glodzik, L., Switalski, R., Tsui, W.H., Haas, F., McGorty, K., Chen, Q. and de Leon, M.J., 2011. Hippocampal blood flow in normal aging measured with arterial spin labeling at 3T. *Magnetic resonance in medicine*, 65(1), pp.128-137.
- Sadigh-Eteghad, S., Talebi, M. and Farhoudi, M., 2012. Association of apolipoprotein E epsilon 4 allele with sporadic late onset Alzheimer's disease. *A meta-analysis. Neurosciences (Riyadh)*, 17(4), pp.321-326.
- Salvadores, N., Sanhueza, M. and Manque, P., 2017. Axonal degeneration during aging and its functional role in neurodegenerative disorders. *Frontiers in neuroscience*, 11, p.451.
- Sanchis-Segura, C., Ibañez-Gual, M.V., Adrián-Ventura, J., Aguirre, N., Gómez-Cruz, Á.J., Avila, C. and Forn, C., 2019. Sex differences in gray matter volume: how many and how large are they really?. *Biology of sex Differences*, 10(1), pp.1-19.
- Sandson, T.A., O'Connor, M., Sperling, R.A., Edelman, R.R. and Warach, S., 1996. Noninvasive perfusion MRI in Alzheimer's disease: a preliminary report. *Neurology*, 47(5), pp.1339-1342.
- Sappey-Marinié, D., Calabrese, G., Fein, G., Hugg, J.W., Biggins, C. and Weiner, M.W., 1992. Effect of photic stimulation on human visual cortex lactate and phosphates using <sup>1</sup>H and <sup>31</sup>P magnetic resonance spectroscopy. *Journal of Cerebral Blood Flow & Metabolism*, 12(4), pp.584-592.
- Saunders, D.E., Howe, F.A., van den Boogaart, A., Griffiths, J.R. and Brown, M.M., 1999. Aging of the adult human brain: in vivo quantitation of metabolite content with proton magnetic resonance spectroscopy. *Journal of Magnetic Resonance Imaging: An Official Journal of the International Society for Magnetic Resonance in Medicine*, 9(5), pp.711-716.
- Saxena, S., Van Ommeren, M., Tang, K.C. and Armstrong, T.P., 2005. Mental health benefits of physical activity. *Journal of Mental Health*, 14(5), pp.445-451.
- Scarmeas, N., Habeck, C.G., Zarahn, E., Anderson, K.E., Park, A., Hilton, J., Pelton, G.H., Tabert, M.H., Honig, L.S., Moeller, J.R. and Devanand, D.P., 2004. Covariance PET patterns in early Alzheimer's disease and subjects with cognitive impairment but no dementia: utility in group discrimination and correlations with functional performance. *Neuroimage*, 23(1), pp.35-45.
- Schaller, B., Mекle, R., Xin, L., Kunz, N. and Gruetter, R., 2013. Net increase of lactate and glutamate concentration in activated human visual cortex

detected with magnetic resonance spectroscopy at 7 tesla. *Journal of neuroscience research*, 91(8), pp.1076-1083.

Schaller, B., Xin, L., O'Brien, K., Magill, A.W. and Gruetter, R., 2014. Are glutamate and lactate increases ubiquitous to physiological activation? A 1H functional MR spectroscopy study during motor activation in human brain at 7 Tesla. *NeuroImage*, 93, pp.138-145.

Scheenen, T.W., Klomp, D.W., Wijnen, J.P. and Heerschap, A., 2008. Short echo time 1H-MRSI of the human brain at 3T with minimal chemical shift displacement errors using adiabatic refocusing pulses. *Magnetic Resonance in Medicine: An Official Journal of the International Society for Magnetic Resonance in Medicine*, 59(1), pp.1-6.

Schmidt, R., Schmidt, H., Haybaeck, J., Loitfelder, M., Weis, S., Cavalieri, M., Seiler, S., Enzinger, C., Ropele, S., Erkinjuntti, T. and Pantoni, L., 2011. Heterogeneity in age-related white matter changes. *Acta neuropathologica*, 122(2), pp.171-185.

Schuff, N., Ezekiel, F., Gamst, A.C., Amend, D.L., Capizzano, A.A., Maudsley, A.A. and Weiner, M.W., 2001. Region and tissue differences of metabolites in normally aged brain using multislice 1H magnetic resonance spectroscopic imaging. *Magnetic Resonance in Medicine: An Official Journal of the International Society for Magnetic Resonance in Medicine*, 45(5), pp.899-907.

Schurr, A. and Payne, R.S., 2007. Lactate, not pyruvate, is neuronal aerobic glycolysis end product: an in vitro electrophysiological study. *Neuroscience*, 147(3), pp.613-619.

Schuster, L., Essig, M. and Schröder, J., 2011. Normal aging and imaging correlations. *Der Radiologe*, 51(4), pp.266-272.

Scully, D., Kremer, J., Meade, M.M., Graham, R. and Dudgeon, K., 1998. Physical exercise and psychological well being: a critical review. *British journal of sports medicine*, 32(2), pp.111-120.

Seeley, W.W., Menon, V., Schatzberg, A.F., Keller, J., Glover, G.H., Kenna, H., Reiss, A.L. and Greicius, M.D., 2007. Dissociable intrinsic connectivity networks for salience processing and executive control. *Journal of Neuroscience*, 27(9), pp.2349-2356.

Serres, S., Bezancon, E., Franconi, J.M. and Merle, M., 2004. Ex vivo analysis of lactate and glucose metabolism in the rat brain under different states of depressed activity. *Journal of Biological Chemistry*, 279(46), pp.47881-47889.

Serres, S., Bouyer, J.J., Bezancon, E., Canioni, P. and Merle, M., 2003. Involvement of brain lactate in neuronal metabolism. *NMR in Biomedicine: An International Journal Devoted to the Development and Application of Magnetic Resonance In Vivo*, 16(6-7), pp.430-439.

Shi, S.K., 2016. An unusual variation of carotid-vertebrobasilar arteries: An anatomical case report. *The neuroradiology journal*, 29(4), pp.277-279.

Shirer, W.R., Ryali, S., Rykhlevskaia, E., Menon, V. and Greicius, M.D., 2012. Decoding subject-driven cognitive states with whole-brain connectivity patterns. *Cerebral cortex*, 22(1), pp.158-165.

Shirzadi, Z., Stefanovic, B., Mutsaerts, H.J., Masellis, M., MacIntosh, B.J. and Alzheimer's Disease Neuroimaging Initiative, 2019. Classifying cognitive

impairment based on the spatial heterogeneity of cerebral blood flow images. *Journal of Magnetic Resonance Imaging*, 50(3), pp.858-867.

Siedlecki, K.L., Habeck, C.G., Brickman, A.M., Gazes, Y. and Stern, Y., 2009. Examining the multifactorial nature of cognitive aging with covariance analysis of PET data. *Journal of the International Neuropsychological Society: JINS*, 15(6), p.973.

Sierra-Marcos, A., 2017. Regional cerebral blood flow in mild cognitive impairment and Alzheimer's disease measured with arterial spin labeling magnetic resonance imaging. *International journal of Alzheimer's disease*, 2017.

Siesjö, B.K., 1978. *Brain energy metabolism* (pp. 101-130). New York: Wiley.

Sijens, P., Den Heijer, T., de Leeuw, F., de Groot, J., Achten, E., Heijboer, R., Hofman, A., Breteler, M. and Oudkerk, M., 2001b. MR spectroscopy detection of lactate and lipid signals in the brains of healthy elderly people. *European radiology*, 11(8), pp.1495-1501.

Sijens, P.E., Den Heijer, T., De Leeuw, F.E., De Groot, J.C., Achten, E., Heijboer, R.J., Hofman, A., Breteler, M.M. and Oudkerk, M., 2001a. Human brain chemical shift imaging at age 60 to 90: analysis of the causes of the observed sex differences in brain metabolites. *Investigative Radiology*, 36(10), pp.597-603.

Silverman, D.H., 2004. Brain 18F-FDG PET in the diagnosis of neurodegenerative dementias: comparison with perfusion SPECT and with clinical evaluations lacking nuclear imaging. *Journal of Nuclear Medicine*, 45(4), pp.594-607.

Simic, G., Babic, M., Borovecki, F. and Hof, P.R., 2014. Early failure of the default-mode network and the pathogenesis of Alzheimer's disease. *CNS neuroscience & therapeutics*, 20(7), p.692.

Skinner, J., Carvalho, J.O., Potter, G.G., Thames, A., Zelinski, E., Crane, P.K., Gibbons, L.E. and Alzheimer's Disease Neuroimaging Initiative, 2012. The Alzheimer's disease assessment scale-cognitive-plus (ADAS-Cog-Plus): an expansion of the ADAS-Cog to improve responsiveness in MCI. *Brain imaging and behavior*, 6(4), pp.489-501.

Skurdal, M.J., Bjørnerud, A., Van Osch, M.J., Nordhøy, W., Lagopoulos, J. and Groote, I.R., 2015. Voxel-wise perfusion assessment in cerebral white matter with PCASL at 3T; Is it possible and how long does it take?. *PloS one*, 10(8), p.e0135596.

Sled, J.G. and Pike, G.B., 1998. Standing-wave and RF penetration artifacts caused by elliptic geometry: an electrodynamic analysis of MRI. *IEEE transactions on medical imaging*, 17(4), pp.653-662.

Smallwood, J., Bernhardt, B.C., Leech, R., Bzdok, D., Jefferies, E. and Margulies, D.S., 2021. The default mode network in cognition: a topographical perspective. *Nature Reviews Neuroscience*, pp.1-11.

Smith, L.A., Melbourne, A., Owen, D., Cardoso, M.J., Sudre, C.H., Tillin, T., Sokolska, M., Atkinson, D., Chaturvedi, N., Ourselin, S. and Hughes, A.D.,

2019. Cortical cerebral blood flow in ageing: effects of haematocrit, sex, ethnicity and diabetes. *European radiology*, 29(10), pp.5549-5558.
- Smith, S.M. and Nichols, T.E., 2009. Threshold-free cluster enhancement: addressing problems of smoothing, threshold dependence and localisation in cluster inference. *Neuroimage*, 44(1), pp.83-98.
- Smith, S.M., Jenkinson, M., Woolrich, M.W., Beckmann, C.F., Behrens, T.E., Johansen-Berg, H., Bannister, P.R., De Luca, M., Drobnjak, I., Flitney, D.E. and Niazy, R.K., 2004. Advances in functional and structural MR image analysis and implementation as FSL. *Neuroimage*, 23, pp.S208-S219.
- Smith, S.M., Vidaurre, D., Alfaro-Almagro, F., Nichols, T.E. and Miller, K.L., 2019. Estimation of brain age delta from brain imaging. *Neuroimage*, 200, pp.528-539.
- Sofi, F., Valecchi, D., Bacci, D., Abbate, R., Gensini, G.F., Casini, A. and Macchi, C., 2011. Physical activity and risk of cognitive decline: a meta-analysis of prospective studies. *Journal of internal medicine*, 269(1), pp.107-117.
- Soher, B.J., Semanchuk, P., Todd, D., Steinberg, J. and Young, K., 2011. VeSPA: integrated applications for RF pulse design, spectral simulation and MRS data analysis. In *Proc Int Soc Magn Reson Med* (Vol. 19, No. 19, p. 1410).
- Soni, N, Jain, A, Kumar, S., 2016. Arterial spin labeling magnetic resonance perfusion study to evaluate the effects of age and gender on normal cerebral blood flow. *Neurol India*; 64 (Suppl): S32–S38.
- Sperling, R.A., Aisen, P.S., Beckett, L.A., Bennett, D.A., Craft, S., Fagan, A.M., Iwatsubo, T., Jack Jr, C.R., Kaye, J., Montine, T.J. and Park, D.C., 2011. Toward defining the preclinical stages of Alzheimer's disease: recommendations from the National Institute on Aging-Alzheimer's Association workgroups on diagnostic guidelines for Alzheimer's disease. *Alzheimer's & dementia*, 7(3), pp.280-292.
- Spetsieris, P.G., Ma, Y., Dhawan, V. and Eidelberg, D., 2009. Differential diagnosis of parkinsonian syndromes using PCA-based functional imaging features. *Neuroimage*, 45(4), pp.1241-1252.
- Spisák, T., Spisák, Z., Zunhammer, M., Bingel, U., Smith, S., Nichols, T. and Kincses, T., 2019. Probabilistic TFCE: a generalized combination of cluster size and voxel intensity to increase statistical power. *Neuroimage*, 185, pp.12-26.
- Staal, M.A. and Bolton, A.E., 2008. Cognitive Performance and Resilience to Stress RITA A. YAROUGH, AND LYLE E. BOURNE Jr. In *Biobehavioral resilience to stress* (pp. 281-322). Routledge.
- Staffaroni, A.M., Cobigo, Y., Elahi, F.M., Casaletto, K.B., Walters, S.M., Wolf, A., Lindbergh, C.A., Rosen, H.J. and Kramer, J.H., 2019. A longitudinal characterization of perfusion in the aging brain and associations with cognition and neural structure. *Human brain mapping*, 40(12), pp.3522-3533.
- Stefan, D.D.C.F., Di Cesare, F., Andrasescu, A., Popa, E., Lazariev, A., Vescovo, E., Strbak, O., Williams, S., Starcuk, Z., Cabanas, M. and Van Ormondt, D., 2009. Quantitation of magnetic resonance spectroscopy signals:

the jMRUI software package. *Measurement Science and Technology*, 20(10), p.104035.

Steffener, J., Brickman, A.M., Habeck, C.G., Salthouse, T.A. and Stern, Y., 2013. Cerebral blood flow and gray matter volume covariance patterns of cognition in aging. *Human brain mapping*, 34(12), pp.3267-3279.

Stern, Y., Arenaza-Urquijo, E.M., Bartrés-Faz, D., Belleville, S., Cantilon, M., Chetelat, G., Ewers, M., Franzmeier, N., Kempermann, G., Kremen, W.S. and Okonkwo, O., 2020. Whitepaper: Defining and investigating cognitive reserve, brain reserve, and brain maintenance. *Alzheimer's & Dementia*, 16(9), pp.1305-1311.

Stillman, C.M., Jakicic, J., Rogers, R., Alfini, A.J., Smith, J.C., Watt, J., Kang, C. and Erickson, K.I., 2021. Changes in cerebral perfusion following a 12-month exercise and diet intervention. *Psychophysiology*, 58(7), p.e13589.

Stites, S.D., Harkins, K., Rubright, J.D. and Karlawish, J., 2018. Relationships between Cognitive Complaints and Quality of Life in Older Adults with Mild Cognitive Impairment, Mild Alzheimer's Disease Dementia, and Normal Cognition. *Alzheimer disease and associated disorders*, 32(4), p.276.

Su, L., Blamire, A.M., Watson, R., He, J., Hayes, L. and O'brien, J.T., 2016. Whole-brain patterns of 1 H-magnetic resonance spectroscopy imaging in Alzheimer's disease and dementia with Lewy bodies. *Translational psychiatry*, 6(8), pp.e877-e877.

Sudlow, C., Gallacher, J., Allen, N., Beral, V., Burton, P., Danesh, J., Downey, P., Elliott, P., Green, J., Landray, M. and Liu, B., 2015. UK biobank: an open access resource for identifying the causes of a wide range of complex diseases of middle and old age. *Plos med*, 12(3), p.e1001779.

Sugawara, J., Tomoto, T., Repshas, J., Zhang, R. and Tarumi, T., 2020. Middle-aged endurance athletes exhibit lower cerebrovascular impedance than sedentary peers. *Journal of Applied Physiology*, 129(2), pp.335-342.

Suter, O.C., Sunthorn, T., Kraftsik, R., Straubel, J., Darekar, P., Khalili, K. and Miklossy, J., 2002. Cerebral hypoperfusion generates cortical watershed microinfarcts in Alzheimer disease. *Stroke*, 33(8), pp.1986-1992.

Taher, M., Leen, W.G., Wevers, R.A. and Willemsen, M.A., 2016. Lactate and its many faces. *European Journal of Paediatric Neurology*, 20(1), pp.3-10.

Takahashi, H., Ishii, K., Hosokawa, C., Hyodo, T., Kashiwagi, N., Matsuki, M., Ashikaga, R. and Murakami, T., 2014. Clinical application of 3D arterial spin-labeled brain perfusion imaging for Alzheimer disease: comparison with brain perfusion SPECT. *American Journal of Neuroradiology*, 35(5), pp.906-911.

Tartaglia, M.C., Rosen, H.J. and Miller, B.L., 2011. Neuroimaging in dementia. *Neurotherapeutics*, 8(1), pp.82-92.

Tatu, L., Moulin, T., Bogousslavsky, J. and Duvernoy, H., 1998. Arterial territories of the human brain: cerebral hemispheres. *Neurology*, 50(6), pp.1699-1708.

Taylor, R., Neufeld, R.W., Schaefer, B., Densmore, M., Rajakumar, N., Osuch, E.A., Williamson, P.C. and Théberge, J., 2015. Functional magnetic resonance spectroscopy of glutamate in schizophrenia and major depressive

- disorder: anterior cingulate activity during a color-word Stroop task. *NPJ schizophrenia*, 1(1), pp.1-8.
- Taylor, W.D., Aizenstein, H.J. and Alexopoulos, G.S., 2013. The vascular depression hypothesis: mechanisms linking vascular disease with depression. *Molecular psychiatry*, 18(9), pp.963-974.
- Taylor-Rowan, M., Edwards, S., Noel-Storr, A.H., McCleery, J., Myint, P.K., Soiza, R., Stewart, C., Loke, Y.K. and Quinn, T.J., 2021. Anticholinergic burden (prognostic factor) for prediction of dementia or cognitive decline in older adults with no known cognitive syndrome. *Cochrane Database of Systematic Reviews*, (4).
- Tazegul, G., Etcioğlu, E., Yildiz, F., Yildiz, R. and Tuney, D., 2015. Can MRI related patient anxiety be prevented?. *Magnetic resonance imaging*, 33(1), pp.180-183.
- Terribilli, D., Schaufelberger, M.S., Duran, F.L., Zanetti, M.V., Curiati, P.K., Menezes, P.R., Scazufca, M., Amaro Jr, E., Leite, C.C. and Busatto, G.F., 2011. Age-related gray matter volume changes in the brain during non-elderly adulthood. *Neurobiology of aging*, 32(2), pp.354-368.
- Teune, L.K., Renken, R.J., de Jong, B.M., Willemsen, A.T., van Osch, M.J., Roerdink, J.B., Dierckx, R.A. and Leenders, K.L., 2014. Parkinson's disease-related perfusion and glucose metabolic brain patterns identified with PCASL-MRI and FDG-PET imaging. *NeuroImage: Clinical*, 5, pp.240-244.
- Thakkar, K.N., Rösler, L., Wijnen, J.P., Boer, V.O., Klomp, D.W., Cahn, W., Kahn, R.S. and Neggers, S.F., 2017. 7T proton magnetic resonance spectroscopy of gamma-aminobutyric acid, glutamate, and glutamine reveals altered concentrations in patients with schizophrenia and healthy siblings. *Biological psychiatry*, 81(6), pp.525-535.
- Tkáč, I., Öz, G., Adriany, G., Uğurbil, K. and Gruetter, R., 2009. In vivo 1H NMR spectroscopy of the human brain at high magnetic fields: metabolite quantification at 4T vs. 7T. *Magnetic Resonance in Medicine: An Official Journal of the International Society for Magnetic Resonance in Medicine*, 62(4), pp.868-879.
- Tkáč, I., Starčuk, Z., Choi, I.Y. and Gruetter, R., 1999. In vivo 1H NMR spectroscopy of rat brain at 1 ms echo time. *Magnetic Resonance in Medicine: An Official Journal of the International Society for Magnetic Resonance in Medicine*, 41(4), pp.649-656.
- Tombaugh, T.N. and McIntyre, N.J., 1992. The mini-mental state examination: a comprehensive review. *Journal of the American Geriatrics Society*, 40(9), pp.922-935.
- Tombaugh, T.N., McDowell, I., Kristjansson, B. and Hubley, A.M., 1996. Mini-Mental State Examination (MMSE) and the Modified MMSE (3MS): a psychometric comparison and normative data. *Psychological Assessment*, 8(1), p.48.
- Tong, Y., Chen, Q., Nichols, T.E., Rasetti, R., Callicott, J.H., Berman, K.F., Weinberger, D.R. and Mattay, V.S., 2016. Seeking optimal region-of-interest

(ROI) single-value summary measures for fMRI studies in imaging genetics. *PLoS one*, 11(3), p.e0151391.

Topiwala, A., Ebmeier, K.P., Maullin-Sapey, T. and Nichols, T.E., 2021. No safe level of alcohol consumption for brain health: observational cohort study of 25,378 UK Biobank participants. *medRxiv*.

Topolski, T.D., LoGerfo, J., Patrick, D.L., Williams, B., Walwick, J. and Patrick, M.M.B., 2006. Peer reviewed: the Rapid Assessment of Physical Activity (RAPA) among older adults. *Preventing chronic disease*, 3(4).

Torchi, A., Serres, S. Cooper, A., Mallinson, J., McGing, J., Lobo, D.N., Awais, R., Årstad, E., Glaser, M., Twyman, F., Gowland, P., Greenhaff, P., Auer, D.P., Faas, H. and Morris, P.G., 2019. 'Monitoring muscle metabolism non-invasively with dynamic nuclear polarisation magnetic resonance.' *World Molecular Imaging Congress 2019*, Montréal, Québec, Canada, 4-7 September.

Torvik, A.N.S.G.A.R., 1984. The pathogenesis of watershed infarcts in the brain. *Stroke*, 15(2), pp.221-223.

Toth, P., Tarantini, S., Csiszar, A. and Ungvari, Z., 2017. Functional vascular contributions to cognitive impairment and dementia: mechanisms and consequences of cerebral autoregulatory dysfunction, endothelial impairment, and neurovascular uncoupling in aging. *American Journal of Physiology-Heart and Circulatory Physiology*, 312(1), pp.H1-H20.

Toussaint, P.J., Maiz, S., Coynel, D., Doyon, J., Messé, A., de Souza, L.C., Sarazin, M., Perlberg, V., Habert, M.O. and Benali, H., 2014. Characteristics of the default mode functional connectivity in normal ageing and Alzheimer's disease using resting state fMRI with a combined approach of entropy-based and graph theoretical measurements. *Neuroimage*, 101, pp.778-786.

Turner, G.R. and Spreng, R.N., 2015. Prefrontal engagement and reduced default network suppression co-occur and are dynamically coupled in older adults: the default-executive coupling hypothesis of aging. *Journal of cognitive neuroscience*, 27(12), pp.2462-2476.

Tyndall, A.V., Clark, C.M., Anderson, T.J., Hogan, D.B., Hill, M.D., Longman, R.S. and Poulin, M.J., 2018. Protective effects of exercise on cognition and brain health in older adults. *Exercise and sport sciences reviews*, 46(4), pp.215-223.

United Nations Population Division. World Population Prospects: The 2017 Revision—Key Findings and Advance Tables. United Nations Population Division; New York, NY, USA: 2017. Working Paper No. ESA/P/WP/248.

Urenjak, J., Williams, S.R., Gadian, D.G. and Noble, M., 1993. Proton nuclear magnetic resonance spectroscopy unambiguously identifies different neural cell types. *Journal of Neuroscience*, 13(3), pp.981-989.

Valotassiou, V., Malamitsi, J., Papatriantafyllou, J., Dardiotis, E., Tsougos, I., Psimadas, D., Alexiou, S., Hadjigeorgiou, G. and Georgoulas, P., 2018. SPECT and PET imaging in Alzheimer's disease. *Annals of nuclear medicine*, 32(9), pp.583-593.

Van Horn, J.D. and Toga, A.W., 2009. Multi-site neuroimaging trials. *Current opinion in neurology*, 22(4), p.370.

- Van Laere, K.J. and Dierckx, R.A., 2001. Brain perfusion SPECT: age-and sex-related effects correlated with voxel-based morphometric findings in healthy adults. *Radiology*, 221(3), pp.810-817.
- van Minde, D., Klaming, L. and Weda, H., 2014. Pinpointing moments of high anxiety during an MRI examination. *International journal of behavioral medicine*, 21(3), pp.487-495.
- van Zijl, P.C., Hua, J. and Lu, H., 2012. The BOLD post-stimulus undershoot, one of the most debated issues in fMRI. *Neuroimage*, 62(2), pp.1092-1102.
- Vatner, S.F., Zhang, J., Oydanich, M., Berkman, T., Naftalovich, R. and Vatner, D.E., 2020. Healthful aging mediated by inhibition of oxidative stress. *Ageing Research Reviews*, p.101194.
- Veech, R.L., 1991. The metabolism of lactate. *NMR in Biomedicine*, 4(2), pp.53-58.
- Veehof, L.J.G., Stewart, R.E., Haaijer-Ruskamp, F.M. and Jong, B.M.D., 2000. The development of polypharmacy. A longitudinal study. *Family practice*, 17(3), pp.261-267.
- Veldsman, M., Tai, X.Y., Nichols, T., Smith, S., Peixoto, J., Manohar, S. and Husain, M., 2020. Cerebrovascular risk factors impact frontoparietal network integrity and executive function in healthy ageing. *Nature communications*, 11(1), pp.1-10.
- Vemuri, P., Lesnick, T.G., Przybelski, S.A., Graff-Radford, J., Reid, R.I., Lowe, V.J., Zuk, S.M., Senjem, M.L., Schwarz, C.G., Gunter, J.L. and Kantarci, K., 2018. Development of a cerebrovascular magnetic resonance imaging biomarker for cognitive aging. *Annals of neurology*, 84(5), pp.705-716.
- Vernooij, M.W., Van der Lugt, A., Ikram, M.A., Wielopolski, P.A., Vrooman, H.A., Hofman, A., Krestin, G.P. and Breteler, M.M., 2008. Total cerebral blood flow and total brain perfusion in the general population: the Rotterdam Scan Study. *Journal of Cerebral Blood Flow & Metabolism*, 28(2), pp.412-419.
- Versluis, M.J., Teeuwisse, W.M., Kan, H.E., van Buchem, M.A., Webb, A.G. and van Osch, M.J., 2013. Subject tolerance of 7 T MRI examinations. *Journal of Magnetic Resonance Imaging*, 38(3), pp.722-725.
- Vidal-Piñeiro, D., Valls-Pedret, C., Fernández-Cabello, S., Arenaza-Urquijo, E.M., Sala-Llonch, R., Solana, E., Bargalló, N., Junqué, C., Ros, E. and Bartrés-Faz, D., 2014. Decreased default mode network connectivity correlates with age-associated structural and cognitive changes. *Frontiers in aging neuroscience*, 6, p.256.
- Vidyasagar, R., Greyling, A., Draijer, R., Corfield, D.R. and Parkes, L.M., 2013. The effect of black tea and caffeine on regional cerebral blood flow measured with arterial spin labeling. *Journal of Cerebral Blood Flow & Metabolism*, 33(6), pp.963-968.
- Vijayakumari, A.A., Menon, R.N., Thomas, B., Arun, T.M., Nandini, M. and Kesavadas, C., 2020. Glutamatergic response to a low load working memory paradigm in the left dorsolateral prefrontal cortex in patients with mild cognitive impairment: a functional magnetic resonance spectroscopy study. *Brain imaging and behavior*, 14(2), pp.451-459.

- Vina, J., Sanchis-Gomar, F., Martinez-Bello, V. and Gomez-Cabrera, M.C., 2012. Exercise acts as a drug; the pharmacological benefits of exercise. *British journal of pharmacology*, 167(1), pp.1-12.
- Vion-Dury, J., Meyerhoff, D.J., Cozzone, P.J. and Weiner, M.W., 1994. What might be the impact on neurology of the analysis of brain metabolism by in vivo magnetic resonance spectroscopy?. *Journal of neurology*, 241(6), pp.354-371.
- Vollmar, C., O'Muircheartaigh, J., Barker, G.J., Symms, M.R., Thompson, P., Kumari, V., Duncan, J.S., Richardson, M.P. and Koepp, M.J., 2010. Identical, but not the same: intra-site and inter-site reproducibility of fractional anisotropy measures on two 3.0 T scanners. *Neuroimage*, 51(4), pp.1384-1394.
- Walhovd, K.B., Fjell, A.M., Reinvang, I., Lundervold, A., Dale, A.M., Quinn, B.T., Salat, D., Makris, N. and Fischl, B., 2005. Neuroanatomical aging: Universal but not uniform. *Neurobiology of Aging*, 26(9), pp.1279-1282.
- Wandell, B.A., Brewer, A.A. and Dougherty, R.F., 2005. Visual field map clusters in human cortex. *Philosophical Transactions of the Royal Society B: Biological Sciences*, 360(1456), pp.693-707.
- Wang, R., Liu, M., Cheng, X., Wu, Y., Hildebrandt, A. and Zhou, C., 2021. Segregation, integration, and balance of large-scale resting brain networks configure different cognitive abilities. *Proceedings of the National Academy of Sciences*, 118(23).
- Wang, X. and Michaelis, E.K., 2010. Selective neuronal vulnerability to oxidative stress in the brain. *Frontiers in aging neuroscience*, 2, p.12.
- Wang, Y., Pan, Y. and Li, H., 2020. What is brain health and why is it important?. *bmj*, 371.
- Warburton, D.E., Nicol, C.W. and Bredin, S.S., 2006. Health benefits of physical activity: the evidence. *Cmaj*, 174(6), pp.801-809.
- Watts, M.E., Pocock, R. and Claudianos, C., 2018. Brain energy and oxygen metabolism: emerging role in normal function and disease. *Frontiers in molecular neuroscience*, 11, p.216.
- Weaverdyck, M.E., Lieberman, M.D. and Parkinson, C., 2020. Tools of the Trade Multivoxel pattern analysis in fMRI: a practical introduction for social and affective neuroscientists. *Social cognitive and affective neuroscience*, 15(4), pp.487-509.
- Webb, A.G., 2011. Dielectric materials in magnetic resonance. *Concepts in magnetic resonance part A*, 38(4), pp.148-184.
- Wei, W., Karim, H.T., Lin, C., Mizuno, A., Andreescu, C., Karp, J.F., Reynolds III, C.F. and Aizenstein, H.J., 2018. Trajectories in cerebral blood flow following antidepressant treatment in late-life depression: support for the vascular depression hypothesis. *The Journal of clinical psychiatry*, 79(6), pp.0-0.
- Weiner, M.W., Veitch, D.P., Aisen, P.S., Beckett, L.A., Cairns, N.J., Green, R.C., Harvey, D., Jack Jr, C.R., Jagust, W., Morris, J.C. and Petersen, R.C., 2017. The Alzheimer's Disease Neuroimaging Initiative 3: Continued

innovation for clinical trial improvement. *Alzheimer's & Dementia*, 13(5), pp.561-571.

Weyts, K., Vernooij, M., Steketee, R., Valkema, R. and Smits, M., 2017. Qualitative agreement and diagnostic performance of arterial spin labelling MRI and FDG PET-CT in suspected early-stage dementia: Comparison of arterial spin labelling MRI and FDG PET-CT in suspected dementia. *Clinical Imaging*, 45, pp.1-7.

Whitwell, J.L., Przybelski, S.A., Weigand, S.D., Knopman, D.S., Boeve, B.F., Petersen, R.C. and Jack Jr, C.R., 2007. 3D maps from multiple MRI illustrate changing atrophy patterns as subjects progress from mild cognitive impairment to Alzheimer's disease. *Brain*, 130(7), pp.1777-1786.

Wierenga, C.E., Clark, L.R., Dev, S.I., Shin, D.D., Jurick, S.M., Rissman, R.A., Liu, T.T. and Bondi, M.W., 2013. Interaction of age and APOE genotype on cerebral blood flow at rest. *Journal of Alzheimer's Disease*, 34(4), pp.921-935.

Williams, D.S., Detre, J.A., Leigh, J.S. and Koretsky, A.P., 1992. Magnetic resonance imaging of perfusion using spin inversion of arterial water. *Proceedings of the National Academy of Sciences*, 89(1), pp.212-216.

Willis, M.W., Ketter, T.A., Kimbrell, T.A., George, M.S., Herscovitch, P., Danielson, A.L., Benson, B.E. and Post, R.M., 2002. Age, sex and laterality effects on cerebral glucose metabolism in healthy adults. *Psychiatry Research: Neuroimaging*, 114(1), pp.23-37.

Wilson, M., Cummins, C.L., MacPherson, L., Sun, Y., Natarajan, K., Grundy, R.G., Arvanitis, T.N., Kauppinen, R.A. and Peet, A.C., 2013. Magnetic resonance spectroscopy metabolite profiles predict survival in paediatric brain tumours. *European Journal of Cancer*, 49(2), pp.457-464.

Wimo, A., Guerchet, M., Ali, G.C., Wu, Y.T., Prina, A.M., Winblad, B., Jönsson, L., Liu, Z. and Prince, M., 2017. The worldwide costs of dementia 2015 and comparisons with 2010. *Alzheimer's & Dementia*, 13(1), pp.1-7.

Winkler, A.M., Ridgway, G.R., Webster, M.A., Smith, S.M. and Nichols, T.E., 2014. Permutation inference for the general linear model. *Neuroimage*, 92, pp.381-397.

Wintermark, M., Sesay, M., Barbier, E., Borbély, K., Dillon, W.P., Eastwood, J.D., Glenn, T.C., Grandin, C.B., Pedraza, S., Soustiel, J.F. and Narai, T., 2005. Comparative overview of brain perfusion imaging techniques. *Stroke*, 36(9), pp.e83-e99.

Wishart, D.S., Bigam, C.G., Yao, J., Abildgaard, F., Dyson, H.J., Oldfield, E., Markley, J.L. and Sykes, B.D., 1995. <sup>1</sup>H, <sup>13</sup>C and <sup>15</sup>N chemical shift referencing in biomolecular NMR. *Journal of biomolecular NMR*, 6(2), pp.135-140.

Wolff, M. and Vann, S.D., 2019. The cognitive thalamus as a gateway to mental representations. *Journal of Neuroscience*, 39(1), pp.3-14.

Wolters, F.J., Zonneveld, H.I., Hofman, A., van der Lugt, A., Koudstaal, P.J., Vernooij, M.W. and Ikram, M.A., 2017. Cerebral perfusion and the risk of dementia: a population-based study. *Circulation*, 136(8), pp.719-728.

- Wong, A., Xiong, Y.Y., Kwan, P.W., Chan, A.Y., Lam, W.W., Wang, K., Chu, W.C., Nyenhuis, D.L., Nasreddine, Z., Wong, L.K. and Mok, V.C., 2009. The validity, reliability and clinical utility of the Hong Kong Montreal Cognitive Assessment (HK-MoCA) in patients with cerebral small vessel disease. *Dementia and geriatric cognitive disorders*, 28(1), pp.81-87.
- Wong, E.C., 2007. Vessel-encoded arterial spin-labeling using pseudocontinuous tagging. *Magnetic Resonance in Medicine: An Official Journal of the International Society for Magnetic Resonance in Medicine*, 58(6), pp.1086-1091.
- Wong, E.C., Buxton, R.B. and Frank, L.R., 1997. Implementation of quantitative perfusion imaging techniques for functional brain mapping using pulsed arterial spin labeling. *NMR in Biomedicine: An International Journal Devoted to the Development and Application of Magnetic Resonance In Vivo*, 10(4-5), pp.237-249.
- Woods, R.L., 1992. The aging eye and contact lenses—A review of visual performance. *Journal of the British Contact Lens Association*, 15(1), pp.31-43.
- Woolrich, M.W., Behrens, T.E., Beckmann, C.F., Jenkinson, M. and Smith, S.M., 2004. Multilevel linear modelling for fMRI group analysis using Bayesian inference. *NeuroImage*, 21(4), pp.1732-1747.
- Woolrich, M.W., Jbabdi, S., Patenaude, B., Chappell, M., Makni, S., Behrens, T., Beckmann, C., Jenkinson, M. and Smith, S.M., 2009. Bayesian analysis of neuroimaging data in FSL. *Neuroimage*, 45(1), pp.S173-S186.
- Woolrich, M.W., Ripley, B.D., Brady, M. and Smith, S.M., 2001. Temporal autocorrelation in univariate linear modeling of fMRI data. *Neuroimage*, 14(6), pp.1370-1386.
- Xu, G., Rowley, H.A., Wu, G., Alsop, D.C., Shankaranarayanan, A., Dowling, M., Christian, B.T., Oakes, T.R. and Johnson, S.C., 2010. Reliability and precision of pseudo-continuous arterial spin labeling perfusion MRI on 3.0 T and comparison with 15O-water PET in elderly subjects at risk for Alzheimer's disease. *NMR in Biomedicine*, 23(3), pp.286-293.
- Yacoub, E., Ugurbil, K. and Harel, N., 2006. The spatial dependence of the poststimulus undershoot as revealed by high-resolution BOLD-and CBV-weighted fMRI. *Journal of Cerebral Blood Flow & Metabolism*, 26(5), pp.634-644.
- Yamashita, K., Kobayashi, S. and Yamaguchi, S., 2000. Cerebral blood flow and cessation of cigarette smoking in healthy volunteers. *Internal medicine*, 39(11), pp.891-893.
- Yang, Z., Chang, C., Xu, T., Jiang, L., Handwerker, D.A., Castellanos, F.X., Milham, M.P., Bandettini, P.A. and Zuo, X.N., 2014. Connectivity trajectory across lifespan differentiates the precuneus from the default network. *Neuroimage*, 89, pp.45-56.
- Yang, Z.Y., Yue, Q., Xing, H.Y., Tan, Q.Y., Sun, H.Q., Gong, Q.Y., Tan, Z.J. and Quan, H., 2015. A quantitative analysis of 1H-MR spectroscopy at 3.0 T of three brain regions from childhood to middle age. *The British Journal of Radiology*, 88(1052), p.20140693.

- Yeo, J.M., Lim, X., Khan, Z. and Pal, S., 2013. Systematic review of the diagnostic utility of SPECT imaging in dementia. *European archives of psychiatry and clinical neuroscience*, 263(7), pp.539-552.
- Yiannopoulou, K.G., Anastasiou, A.I., Zachariou, V. and Pelidou, S.H., 2019. Reasons for failed trials of disease-modifying treatments for Alzheimer disease and their contribution in recent research. *Biomedicines*, 7(4), p.97.
- Yoo, S.S., Freeman, D.K., McCarthy III, J.J. and Jolesz, F.A., 2003. Neural substrates of tactile imagery: a functional MRI study. *Neuroreport*, 14(4), pp.581-585.
- Yoshii, F., Barker, W.W., Chang, J.Y., Loewenstein, D., Apicella, A., Smith, D., Boothe, T., Ginsberg, M.D., Pascal, S. and Duara, R., 1988. Sensitivity of cerebral glucose metabolism to age, gender, brain volume, brain atrophy, and cerebrovascular risk factors. *Journal of Cerebral Blood Flow & Metabolism*, 8(5), pp.654-661.
- Yoshiura, T., Hiwatashi, A., Noguchi, T., Yamashita, K., Ohyagi, Y., Monji, A., Nagao, E., Kamano, H., Togao, O. and Honda, H., 2009. Arterial spin labelling at 3-T MR imaging for detection of individuals with Alzheimer's disease. *European radiology*, 19(12), p.2819.
- Yushkevich, P.A., Piven, J., Hazlett, H.C., Smith, R.G., Ho, S., Gee, J.C. and Gerig, G., 2006. User-guided 3D active contour segmentation of anatomical structures: significantly improved efficiency and reliability. *Neuroimage*, 31(3), pp.1116-1128.
- Zadnik, K., 1994. Contact lenses in the geriatric patient. *Journal of the American Optometric Association*, 65(3), pp.193-197.
- Zaharchuk, G., 2014. Arterial spin-labeled perfusion imaging in acute ischemic stroke. *Stroke*, 45(4), pp.1202-1207.
- Zaharchuk, G., Straka, M., Marks, M.P., Albers, G.W., Moseley, M.E. and Bammer, R., 2010. Combined arterial spin label and dynamic susceptibility contrast measurement of cerebral blood flow. *Magnetic Resonance in Medicine: An Official Journal of the International Society for Magnetic Resonance in Medicine*, 63(6), pp.1548-1556.
- Zhang, J., 2016. How far is arterial spin labeling MRI from a clinical reality? Insights from arterial spin labeling comparative studies in Alzheimer's disease and other neurological disorders. *Journal of Magnetic Resonance Imaging*, 43(5), pp.1020-1045.
- Zhang, N., Gordon, M.L. and Goldberg, T.E., 2017. Cerebral blood flow measured by arterial spin labeling MRI at resting state in normal aging and Alzheimer's disease. *Neuroscience & Biobehavioral Reviews*, 72, pp.168-175.
- Zhang, N., Gordon, M.L., Ma, Y., Chi, B., Gomar, J.J., Peng, S., Kingsley, P.B., Eidelberg, D. and Goldberg, T.E., 2018. The age-related perfusion pattern measured with arterial spin labeling MRI in healthy subjects. *Frontiers in aging neuroscience*, 10, p.214.
- Zhang, X., Alshakhshir, N. and Zhao, L., 2021. Glycolytic Metabolism, Brain Resilience, and Alzheimer's Disease. *Frontiers in Neuroscience*, 15, p.476.

Zhao, M.Y., Mezue, M., Segerdahl, A.R., Okell, T.W., Tracey, I., Xiao, Y. and Chappell, M.A., 2017. A systematic study of the sensitivity of partial volume correction methods for the quantification of perfusion from pseudo-continuous arterial spin labeling MRI. *NeuroImage*, 162, pp.384-397.

Zhao, Q., Lu, H., Metmer, H., Li, W.X. and Lu, J., 2018. Evaluating functional connectivity of executive control network and frontoparietal network in Alzheimer's disease. *Brain research*, 1678, pp.262-272.

Zhu, X.H. and Chen, W., 2001. Observed BOLD effects on cerebral metabolite resonances in human visual cortex during visual stimulation: a functional <sup>1</sup>H MRS study at 4 T. *Magnetic Resonance in Medicine: An Official Journal of the International Society for Magnetic Resonance in Medicine*, 46(5), pp.841-847.

Zimmer, E.R., Parent, M.J., Souza, D.G., Leuzy, A., Lecrux, C., Kim, H.I., Gauthier, S., Pellerin, L., Hamel, E. and Rosa-Neto, P., 2017. [<sup>18</sup>F] FDG PET signal is driven by astroglial glutamate transport. *Nature neuroscience*, 20(3), pp.393-395.

Zonneveld, H.I., Loehrer, E.A., Hofman, A., Niessen, W.J., Lugt, A.V.D., Krestin, G.P., Ikram, M.A. and Vernooij, M.W., 2015. The bidirectional association between reduced cerebral blood flow and brain atrophy in the general population. *Journal of Cerebral Blood Flow & Metabolism*, 35(11), pp.1882-1887.

Zuendorf, G., Kerrouche, N., Herholz, K. and Baron, J.C., 2003. Efficient principal component analysis for multivariate 3D voxel-based mapping of brain functional imaging data sets as applied to FDG-PET and normal aging. *Human brain mapping*, 18(1), pp.13-21.

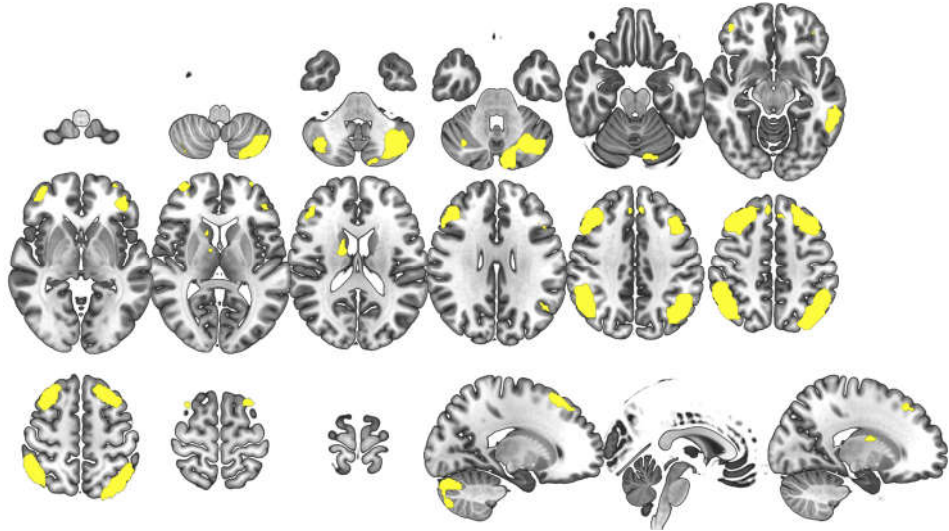
7.2. Appendices

**Appendix A: Inclusion and exclusion criteria for the retrospective studies used in Chapter 3.**

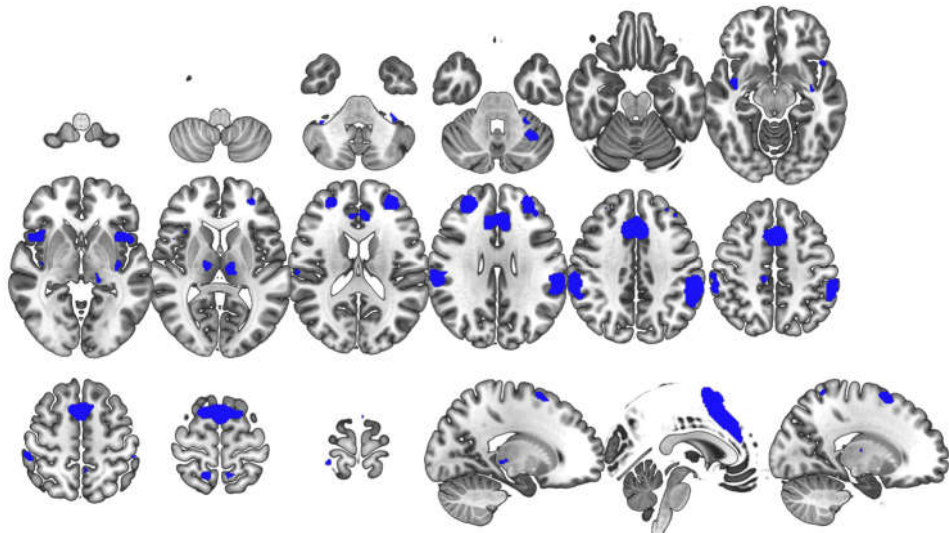
	Study enrollment criteria	
Study	Inclusion	Exclusion
<b>ImPOA</b>	<ul style="list-style-type: none"> <li>+ Aged 18+ years old</li> <li>+ Good comprehension of English</li> <li>+ Able to give informed consent</li> </ul>	<ul style="list-style-type: none"> <li>- Below 18 years old</li> <li>- Any major medical, neurological and psychiatric co-morbidities known to affect neural processing of pain</li> <li>- Currently pregnant</li> <li>- Any contraindications to MRI, such as a pacemaker, replacement heart valve, or claustrophobia</li> </ul>
<b>INCOPE</b>		
<b>PaMIR</b>	<ul style="list-style-type: none"> <li>+ Aged 18-90 years old</li> <li>+ No significant past medical history</li> <li>+ Very good comprehension of written English and fluent in spoken English</li> <li>+ Able to give informed consent</li> </ul>	<ul style="list-style-type: none"> <li>- Had a diagnosis of any major neurological, neurosurgical or psychiatric condition</li> <li>- Currently taking medications known to have a dopaminergic effect</li> <li>- Currently pregnant (may be asked to take pregnancy test)</li> <li>- Any contraindications to MRI</li> </ul>
<b>GSH-MRS</b>	<ul style="list-style-type: none"> <li>+ Aged 60+ years old</li> <li>+ Good comprehension of written English and fluent in spoken English</li> <li>+ Able to give informed consent</li> </ul>	<ul style="list-style-type: none"> <li>- Below 60 years old</li> <li>- Any major medical, neurological, neurological or psychiatric conditions</li> <li>- Any contraindications to MRI</li> </ul>
<b>BraNDy-MS</b>	<ul style="list-style-type: none"> <li>+ Aged 18-65 years</li> <li>+ Good comprehension of written English and fluent in spoken English</li> <li>+ Able to give informed consent</li> </ul>	<ul style="list-style-type: none"> <li>- Aged below 18 or above 66 years</li> <li>- Currently pregnant</li> <li>- Any contraindications to MRI</li> </ul>
<b>VeSPA-MS</b>		

**Appendix B: Network masks as provided by FINDLab.**

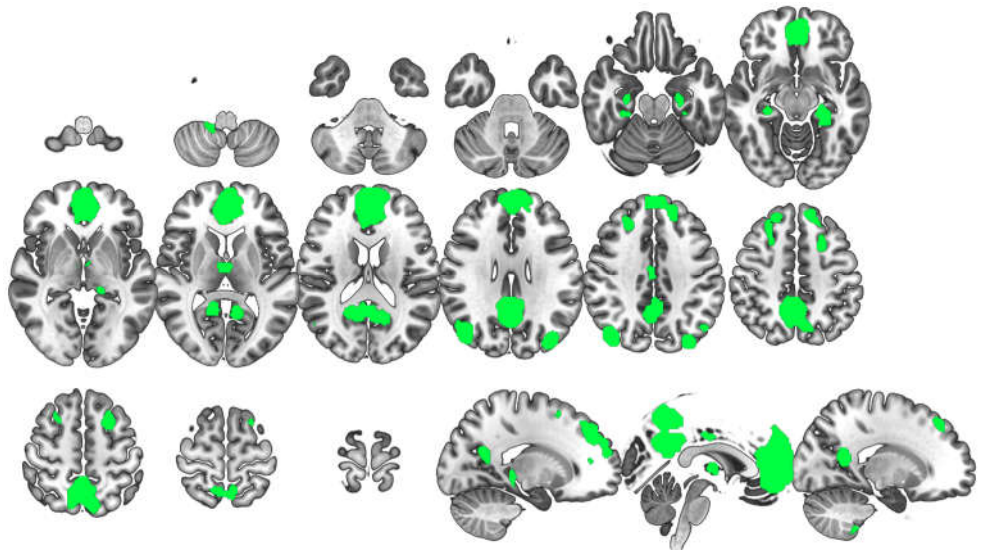
**(A) ECN**



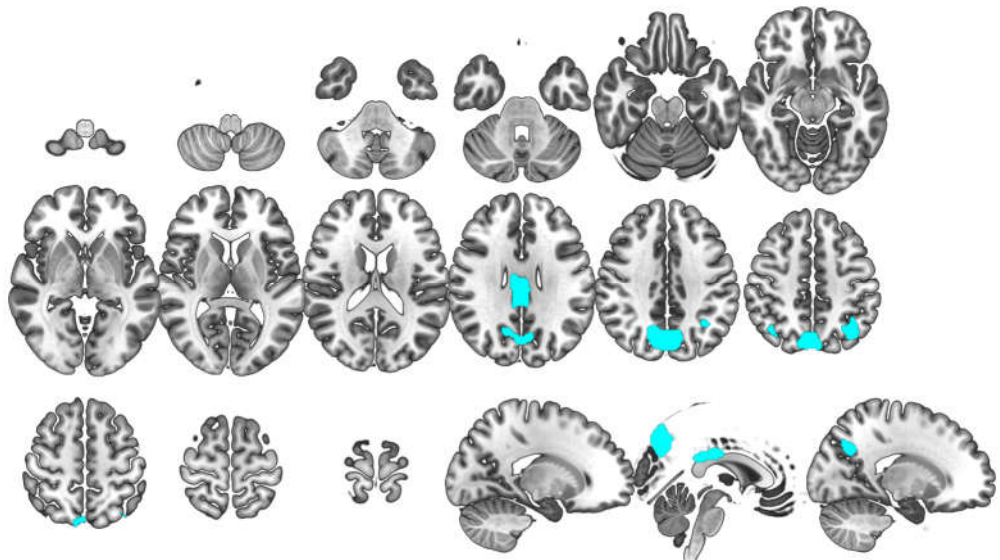
**(B) SN**



**(C) DMN**



**(D) Precuneus network**



**Appendix C: Comparison of standardised beta values from linear regressions of perfusion and sCoV with age in investigated regions, with sex and GM volume as covariates.**

	Standardised beta	
	Perfusion	sCoV
<b>Whole GM</b>	-.137	.490
<b>Cortical GM</b>	-.205	.643
<b>Subcortical GM</b>	-.218	.274
<b>ECN</b>	-.231	.621
<b>SN</b>	-.128	.363
<b>DMN</b>	-.133	.337
<b>Precuneus network</b>	-.184	.597
<b>LICA</b>	-.132	.495
<b>RICA</b>	-.051	.328
<b>VBA</b>	-.242	.618
<b>Left watershed</b>	.021	.178
<b>Right watershed</b>	.043	.014

**Appendix D: Inclusion and exclusion criteria for the studies used in Chapter 4.**

	<b>Study enrollment criteria</b>	
<b>Study</b>	<b>Inclusion</b>	<b>Exclusion</b>
<b>ImPOA</b>	<ul style="list-style-type: none"> <li>+ Aged 18+ years old</li> <li>+ Good comprehension of English</li> <li>+ Able to give informed consent</li> <li>+ MoCA data available</li> </ul>	<ul style="list-style-type: none"> <li>- Below 18 years old</li> <li>- Any major medical, neurological and psychiatric co-morbidities known to affect neural processing of pain</li> <li>- Currently pregnant</li> <li>- Any contraindications to MRI, such as a pacemaker, replacement heart valve, or claustrophobia</li> </ul>
<b>PAMIR</b>	<ul style="list-style-type: none"> <li>+ Aged 18-90 years old</li> <li>+ No significant past medical history</li> <li>+ Very good comprehension of written English and fluent in spoken English</li> <li>+ Able to give informed consent</li> <li>+ MoCA data available</li> </ul>	<ul style="list-style-type: none"> <li>- Had a diagnosis of any major neurological, neurosurgical or psychiatric condition</li> <li>- Currently taking medications known to have a dopaminergic effect</li> <li>- Currently pregnant (may be asked to take pregnancy test)</li> <li>- Any contraindications to MRI</li> </ul>
<b>ADNI-3</b>	<ul style="list-style-type: none"> <li>+ Aged 55-90 years old</li> <li>+ Able to give informed consent</li> <li>+ MMSE score of <math>\geq 24</math></li> </ul>	<ul style="list-style-type: none"> <li>- Any history of brain injury or cerebral infarction</li> <li>- Any neurological disease which may affect cognition, including (but not limited to) brain tumour, Parkinson's disease, normal pressure hydrocephalus, and brain trauma</li> <li>- Any systemic disease which may lead to cognitive impairment, including impaired liver or kidney function, thyroid dysfunction, and specific infections such as syphilis and HIV.</li> </ul>

**Appendix E: Key nodes and associated regions identified by graph visualisation.**

<b>Node number</b>	<b>Anatomical region</b>
<b>1</b>	brainstem
<b>5</b>	includes subcallosal cortex, frontal medial cortex, frontal orbital cortex
<b>7</b>	includes occipital pole, inferior and superior lateral occipital cortex
<b>11</b>	lateral occipital cortex
<b>12</b>	lingual gyrus, occipital fusiform gyrus
<b>13</b>	includes paracingulate gyrus, anterior cingulate gyrus
<b>15</b>	includes right caudate
<b>16</b>	includes inferior frontal gyrus, middle frontal gyrus, frontal pole, par triangularis
<b>18</b>	includes left thalamus
<b>21</b>	includes middle frontal gyrus, precentral gyrus
<b>24</b>	includes superior parietal lobule, postcentral gyrus, supramarginal gyrus, slight angular gyrus
<b>25</b>	includes precentral gyrus, middle frontal gyrus, superior frontal gyrus
<b>26</b>	includes precentral gyrus, middle frontal gyrus, superior frontal gyrus
<b>27</b>	includes precentral gyrus, superior frontal gyrus
<b>28</b>	includes precentral gyrus, postcentral gyrus
<b>29</b>	includes precentral gyrus, postcentral gyrus, slight superior frontal gyrus
<b>30</b>	includes superior frontal gyrus, precentral gyrus
<b>31</b>	includes superior frontal gyrus, precentral gyrus, supplementary motor area